

Hybrid nanosystems fabricated by molecular recognition

Inauguraldissertation

Zur

Erlangung der Würde eines Doktors der Philosophie

Vorgelegt der

Philosophische-Naturwissenschaftlichen Fakultät

Der Universität Basel

Von

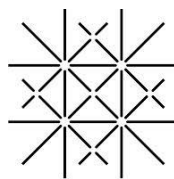
Juan Liu

Von China

Basel 2015

Originaldokument gespeichert auf dem Dokumentenserver der Universität

Basel edoc.unibas.ch



UNI
BASEL

Genehmigt von der Philosophisch-Naturwissenschaftlichen Fakultät

auf Antrag von

Prof. Dr. Wolfgang Meier

Prof. Dr. Corinne Nardin

Basel, 24.03.2015

Prof. Dr. Jörg Schibler

The Dean of Faculty

Abstract

The cell can be viewed as a miniature factory run by a large collection of molecular machines such as proteins and DNA that works together to perform complicated tasks, such as cell division, response to environmental stimuli, and energy production. Currently, nanotechnology research aims at reconstructing a fraction of complex functionality that exists in cell by designing novel systems to mimic cell properties and functions. The design of hybrid nanosystems based on biomacromolecules such as proteins, DNA, and synthetic molecules (polymers), brings science closer to achieving this target. The adaptability and mechanical properties of polymers allow for tailored designs that include various scaffolds for improved spatial-temporal connections to specific proteins, and DNA.

In this thesis, two hybrid systems were established. First, tris-nitrilotriacetic acid (trisNTA) functionalized polymers (PNTs) for the specific conjugation of his-tagged molecules was designed and synthesized. For efficient binding to the His-tagged molecules, a chelating metal (Me^{2+}) is introduced in the trisNTA site. The binding affinity of His-tagged molecules for the trisNTA- Me^{2+} , and their interactions when bound were analyzed. These characteristics were dependent on the distance between the trisNTA binding sites and the size of his-tagged molecules. In addition to the distance between trisNTA binding sites on PNTs, the nature of the selected Me^{2+} , connecting trisNTA and His tag, offers a way to tune the binding affinity of the protein for the polymer, and in this way the protein-protein interactions can also be modified to further tune the stability of the conjugates and their susceptibility to release under changing pH. The concept of polymers serving as models for combined geometric topology with size requirements is expected to show the real binding capacity of molecules to a complex targeting configuration, mimicking biological systems in details. In addition, PNTs fulfill the requirements as a great nanocarrier for protein delivery and can contribute to the development of protein therapy and other protein-related applications.

Second, we applied DNA as the algorithm to regulate the self-organization of binary polymersomes to construct multicompartmentalized structures with spatial organization and connections. Polymersomes supply a robust and shielded encapsulation of active

entities, while DNA is capable to control the spatial organization and the spatial distance between compartments due to the rigid nature of double-strand DNA (<50 nm). The size of polymersomes as the second algorithm plays an important role in the assembly behavior and results in different architectures, including linear and satellite structures. The compartmentalized polymer network system described in this work offers a new perspective into the evolution from unitary (one component) to binary (two components) or polyphyletic (multiple components) systems with properties greater than the individual building blocks.

Contents

1. Introduction	1
1.1. Hybrid nanosystems based on polymers and proteins	2
1.1.1. Protein-polymer conjugates	3
1.1.2. Proteins in polymer self-assembled structures	13
1.2. Hybrid nanosystems based on polymers and DNA.....	17
1.2.1. DNA-polymer conjugates.....	18
1.3. Molecular recognition.....	29
1.3.1. Mechanism.....	29
1.3.2. From molecular recognition to self-organization.....	31
1.4. Motivation and concept.....	32
1.5. References	34
2. Polymer design and synthesis towards molecular recognition of his-tagged molecules	43
2.1. Introduction	43
2.2. Results and discussion	45
2.2.1. Synthesis and characterization	45
2.2.2. Temperature and pH responsiveness	47
2.2.3. Coordination of Cu ²⁺ to PNT copolymers.....	49
2.2.4. Binding of His ₆ to PNT copolymers	51
2.3. Conclusion.....	57
2.4. Experiment section	58
2.5. References	64
3. Combined study of molecular recognition and spatial constraints in protein binding and interactions using a polymer module	67
3.1. Introduction	67

3.2. Results and Discussion	69
3.2.1. Influences to the protein binding ability	71
3.2.2. Influences to the protein binding affinity	76
3.2.3. Spatial Constraints induce protein-protein interactions	77
3.3. Conclusion	79
3.4. Experiment section	80
3.5. References	82
4. A single polymer chain as a nanocarrier for multiple protein delivery with regulated pH responsiveness	87
4.1. Introduction	87
4.2. Results and Discussion	90
4.2.1. Binding stoichiometry of His ₆ -eYFP to PNTs coordinated with different metal cations.....	90
4.2.2. Binding affinity of His ₆ -eYFP to PNT-Me ²⁺ copolymers	91
4.2.3. Structure of PNT-Me ²⁺ -His ₆ -eYFP conjugates and protein stability	92
4.2.4. PNT-Me ²⁺ -His ₆ -eYFP stability in varying pH	94
4.2.5. Delivery of PNT-Zn ²⁺ -His ₆ -tagged molecules conjugates into living cells	98
4.3. Conclusion.....	101
4.4. Experimental section	102
4.5. References	104
5. Design and construct of DNA-functionalized polymersomes.....	108
5.1. Introduction	108
5.2. Results and discussion	109
5.2.1. Coupling DNA to the end of triblock copolymer by solid support synthesis.....	109
5.2.2. Coupling DNA to the end of triblock copolymer in solution.....	112
5.2.3. Self-assembly of blended triblock copolymers with DNA-polymer conjugates	114

5.2.4. Construction of DNA-functionalized polymersomes by in situ modification	116
5.3. Conclusion.....	121
5.4. Experimental section	121
5.5. References	126
6. Spatially organizing polymersomes into multicompartmental systems	128
6.1. Introduction	128
6.2. Results and discussions.....	130
6.2.1. Controllable self-assembly of DNA-functionalized polymeric nanocompartments	130
6.2.2. Spatial organization of DNA-functionalized polymeric nanocompartments.....	132
6.2.3. Cellular internalization of polymersome network.....	137
6.3. Conclusion.....	141
6.4. Experimental section	142
6.5. References	146
7. Summary and perspectives.....	149
8. Acknowledgements.....	150
9. Curriculum Vitae, List of Contributions	151
10. Abbreviations.....	154

1. Introduction

In Nature, two or more constituents are often combined and organized at the nanometer or molecular level to create various elaborate hybrid systems with remarkable functions and features. One of the most well-known examples is the cell. Lipids self-assemble to form a closed boundary separating the interior and exterior cellular environments. A large number of proteins, DNA and other molecules hosted inside of cells fulfill different functions, such as catalyzing metabolic reactions, DNA replication and transcription, signal transduction, etc, to implement the cell growth and division. The combination of dissimilar components has the opportunity to collect the characteristic properties for both components, and create complex systems with new functions and properties. This principle plays a major role in the development of advanced functional materials especially nanomaterials.

Biomacromolecules, such as proteins, DNA, and synthetic polymers, are highly attractive for the design of smart and functional hybrid materials. Proteins and DNA are highly evolved biopolymers with remarkable properties and functions. Proteins are involved in many functions within living organisms, including catalyzing metabolic reactions, responding to stimuli, DNA replication, and transporting molecules from one location to another. DNA encodes the genetic information for the development and function of all known living organisms and many viruses. The powerful molecular recognition between DNA molecules makes them excellent candidates for the design of new materials for nanosciences.[1] Synthetic polymers offer many advantages compared to proteins and DNA, as the possibility to design the appropriate chemical structure with specific functional groups, length and physicochemical properties. The ideal hybrid systems would be to combine of the best of both worlds: the adaptability of synthetic polymers with the structural and the functional control ensured by biopolymers such as DNA or proteins.

In addition, nature addresses the question how to organize dissimilar components to a whole structure. By elaborate design of the chemical structures in molecules such as ion coordination sites and hydrogen bond assays, it's able to direct and drive the self-organization of molecules to form complex structures and systems by the molecular

recognition events based on well-defined interaction patterns. It provides an approach to design diverse and elaborate hybrid systems based on proteins, DNA, and synthetic polymers by their self-organization through molecular recognition. The following sections provide an overview about the approaches for the construction of protein-polymer and DNA-polymer hybrid systems, their applications, and the nanofabrication based on molecular recognition.

1.1. Hybrid nanosystems based on polymers and proteins

Proteins keep their irreplaceable role as new-emerging materials for applications in various domains, including catalysis, medicine, environmental science, electronics, nanodevices, etc. Proteins catalyze a vast array of metabolic reactions. They act as transport molecules, respond to specific stimuli, and convert ATP to thermal energy and mechanical energy. Protein-based therapeutics is highly successful in clinic and their potentials are well recognized. More than 100 modified therapeutic proteins are approved for clinical use in the European Union and the USA with 2010 sales of \$108 billion.[2] The best example of therapeutic protein application in clinics is perhaps insulin, which has already been the major therapy for diabetes mellitus type I and type II.[3] Protein therapeutics have several advantages over small-molecule drugs, such as their high specificity, which reduces the interference with normal biological processes and side effects.[3] Because the body naturally produces many of the proteins that are used as therapeutics, these agents are well tolerated and are less likely to elicit immune responses. All of these features are hard to be reproduced by simple small molecular weight drugs. In addition, due to the development of chemical modification and site-directed mutagenesis techniques for proteins, they are able to be modified with diverse functional groups and act as the selective connectors for the conjugation of various components while preserving their own functions, which is highly promising for nanoscale engineering and nanofabrication.[154] For example, biotinylated F_1 -ATPase with his tag (His_6) has been immobilized on the Ni substrate by the specific interactions between His_6 and Ni^{2+} , and sequentially connected with streptavidin functionalized inorganic propeller by biotin-streptavidin interactions.[155] F_1 -ATPase preserved its functions during the engineering process and acted as the bimolecular motor, which initiates and maintains the rotation of the conjugated inorganic propeller (Figure 1-1).

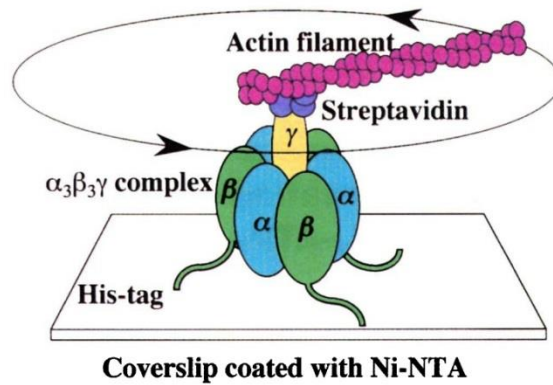


Figure 1-1. Schematic of F₁-ATPase-power nanopropeller.[155] Reproduced with permission from ref. 155. Copyright 1997 Rights Managed by Nature Publishing Group.

On the other hand, proteins have their limitations for applications. First, proteins are macromolecules that fold into unique 3-dimensional structures by covalent and non-covalent interactions. Therefore, proteins are intrinsically unstable and highly influenced by the environments such as buffer concentration and working temperature. Another main drawback of proteins for *in-vivo* applications is their rapid clearance from the systemic circulation. They can be rapidly degraded by various proteolytic enzymes. Even though protein therapy has already been applied in clinic by injecting the proteins directly to the body, which is able to avoid the digestion by alimentary system. But the activity of proteins is still decreased in most of the cases and their efficacy is strongly reduced.[3] Therefore, engineering or protecting proteins to increase their stability is strongly demanded for different applications. In the following sections, we overviewed the approaches of protein engineering with polymers, targeting to stabilize the structures for the protein therapy and nanostructure fabrication.

1.1.1. Protein-polymer conjugates

Conjugates are generally formed by either covalent or non-covalent bond between polymers and proteins. The highly flexible polymer chains generate a “conformational cloud” around the proteins, which prevents interactions with blood components and avoiding enzymatic degradation and opsonization (macrophage uptake) followed by uptake by the endothelial system.[6] The diminished interactions with the body result in protein-polymer conjugate showing less immunogenicity and antigenicity.

Conjugating polymers to proteins is the most used approach for the stabilization of proteins.[7, 153] The first protein-polymer conjugate brought to the market was SMANCS (Zinostatin stimalamer) in 1990. The conjugate contains two polymer chains of styrene-*co*-maleic anhydride (SMA) covalently bound to the anti-tumor protein neocarzinostatin (NCS).[7] The conjugation with polymers increases the lipid-solubility of NCS and enables the administration of SMANCS in the phase-contrast agent Lipiodol, increasing plasma half-life, allowing tumor visualization and improving the degree of tumor targeting. A remarkable tumor to blood ratio of >2500 was recorded using SMANCS. Furthermore, the treatment with SMANCS resulted in dramatic tumor shrinkage (95%) and decreased α -fetoprotein levels (86%), which is used as a tumor marker to detect and diagnose cancers. [7]

Protein-polymer conjugates must be carefully designed for individual applications. They have a common tripartite structure, represented by the protein, the polymer and the linker, which connects them (Figure 1-2).

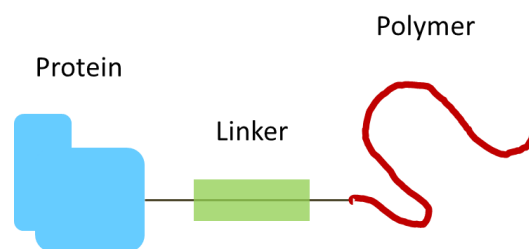


Figure 1-2. Schematic representation of tripartite structure of protein-polymer conjugates.

Proteins. Proteins are large biological macromolecules built from a series of up to 20 different L- α -amino acids. Some of the amino acids such as lysine and cysteine have active groups, which are available for the polymer conjugation. A common approach to fabricate protein-polymer conjugates is to target the lysine or cysteine residues from protein structures by the polymers with either an amino group or a maleimide group. This approach generally results in a random modification of proteins with polymer and the reduction of enzymatic or receptor-binding activity of the protein.[8] Unnatural amino acid mutagenesis enables the incorporation of site-specific linkers into both synthetic and recombinant proteins, and allow for complete control over the resulting

protein-polymer structures.[9, 10] More details are presented in the section describing site-specific protein-polymer conjugation.

Polymers. It has been well accepted that the molecular weight and physico-chemical properties of polymer play a critical role for governing biodistribution, elimination, and metabolism of the conjugates.[11, 12] Therefore, the choice of a suitable polymer is crucial. In general, the polymer should be water-soluble, non-toxic, non-immunogenic, and biodegradable. The elimination of polymers can be done by choosing biodegradable polymers. For the non-biodegradable polymers, the molecular weight (MW) must be lower than 40kDa to avoid its accumulation in the body after repeated administrations.[12] In order to take full advantage of the enhanced permeability and retention effect (EPR effect) and increase retention into the tumor tissue, the polymers should have a MW ranging between 20-40 kDa.[12] The most widely tested polymers for protein conjugation include poly(ethyleneglycol) (PEG), poly(*N*-(2-hydroxypropyl)methacrylamide) (PHPMA) and its copolymers, and poly(glutamic acid) (PGA).[6, 13] The structures of the commonly used polymers for protein conjugation are shown in Figure 1-3.

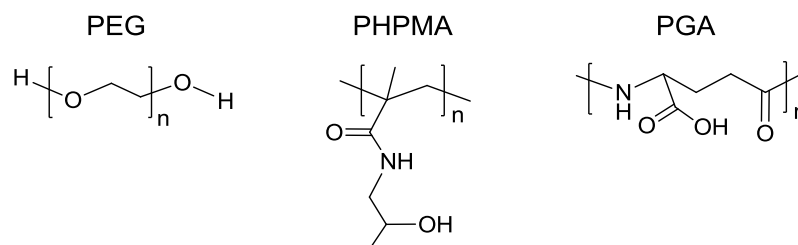


Figure 1-3. Chemical structure of PEG, PHPMA and PGA.

Linkers. The linker is the part connecting polymers and proteins. The design of the linker is dependent on the specific requirements of the application. Basically, the linker between polymers and proteins must be stable in bloodstream and non-toxic. In addition, because the conjugation of polymers can influence the function of proteins or even cause the total loss of its activity,[4] the ideal linker needs to be chemically or enzymatically cleavable in specific environments such as tumor tissue to avoid decreasing the activity of proteins by conjugation with polymers.[14, 15] More details about how to connect polymers with proteins are presented in the section describing the fabrication approaches for protein-polymer conjugation.

1.1.1.1. Methods to achieve protein-polymer conjugation

Protein-polymer conjugates are obtained by two main methods (Figure 1-4): “grafting to” and “grafting from”. The “Grafting to” approach is achieved by the active functional groups of polymers covalently or non-covalently conjugating to the corresponding amino acid side chains of proteins. “Grafting from” is to use proteins as the macro-initiator to process the polymerization. In this case, polymer chains can be grown directly from proteins.

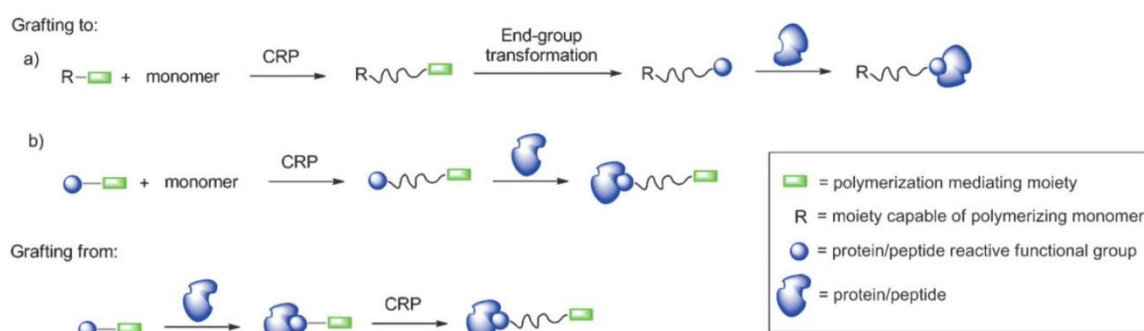


Figure 1-4. Methods to prepare protein-polymer conjugates.[16] Reproduced with permission from ref. 16. Copyright 2011 Royal Society of Chemistry.

“Grafting to” is the first approach developed for the production of protein-polymer conjugates. The polymer generally has only one terminal end active group for the simplification of the system. The active end group from the structure of polymers is able to target active sites on the proteins and accomplish the conjugation with them.

- **Amino reactive polymers.** Amino side chains of lysine residues and the N-terminus amino acids are the most common sites for polymer conjugations. This approach is desirable for conjugate formation because these residues react with a variety of functional groups, including activated esters, thioimido esters, aldehydes, ketones, isocyanates and dichlorotriazines.[17-19] A disadvantage to this approach is that lysine residues are quite numerous on the proteins, rendering the conjugation between proteins and polymers uncontrollable and reducing the protein activity due to the hindrance of active sites and/or the denaturation of proteins. However, due to the facile synthesis, this approach is still extensively applied and results in materials with improved pharmacokinetics

over unmodified proteins. Some of commercial PEGylated protein drugs obtained by this approach have been previously reviewed .[127]

- Thiol-reactive polymers.** Cysteine residues are attractive targets for polymer conjugation to proteins, because surface-exposed, free cysteines are rare in native proteins. A large number of cysteine-reactive functional groups have been introduced into polymers (e.g. activated disulfides, maleimides, and vinyl sulfones).[21-23] Polymers with activated disulfides link to cysteine residues on proteins by thiol-disulfide exchange and the linker of disulfides between polymers and proteins is cleavable by reducing agents such as dithiothreitol (DTT) and 2-mercaptoethanol (BME). The linker formed between cysteine and maleimide/vinyl sulfones are much more stable in different environments. For example, Poly(ϵ -caprolactone)s functionalized with thioester end groups have been conjugated to bovine serum albumin (BSA) by simple thiol-disulfide exchange without the need of further reaction or activation steps (Figure 1-5).[22] The polymer can be cleaved by adding DTT or excess amount of cysteine. Poly(N-isopropylacrylamide) (PolyNIPAM) with a single maleimide end group was attached to the cysteine residue on a T8C protein.[128] The obtained polymer-protein conjugate allows selective precipitation above certain temperature due to the thermo-responsive property of conjugated PolyNIPAM.

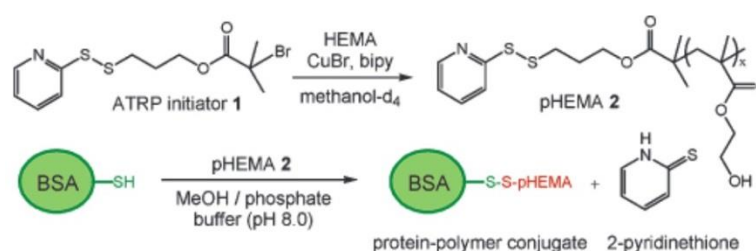


Figure 1-5. Polymer-protein conjugates obtained by thiol-disulfide exchange reaction.[22] Reproduced with permission from ref. 22. Copyright 2004 American Chemical Society.

- Ligand binding polymers.** Another route to produce well-defined protein-polymer conjugates is to use polymers with specific ligands. The binding affinity between polymers and proteins is crucial for the stability of conjugates. Biotin and streptavidin with high binding affinity ($K_a \approx 10^{15} \text{ M}^{-1}$) are most exploited to prepare numerous conjugates.[21, 26] PolyNIPAM, PEG, PHEMA, and other

polymers have been conjugated to various proteins and substrates by the interactions between biotin and streptavidin.[129-131] As non-covalent interaction between biotin and streptavidin is highly stable and resistant to organic solvents, denaturants (e.g. guanidinium chloride), detergents (e.g. sodium dodecyl sulfate, Triton), proteolytic enzymes, and extreme temperature and pH, they have been used extensively. Streptavidin covalently bound with PolyNIPAM was shown to co-precipitate biotinylated immunoglobulin G (IgG) above 37 °C and used for the purification of biotinylated proteins.[30] Biotinylated poly(L-lysine)-*graft*-poly(ethylene glycol) was absorbed on the negatively charged surface and sequentially immobilized streptavidin and biotinylated goat antirabbit immunoglobulin (α RlgG-biotin) for the sensing of rabbit IgG target molecule.[132] Other non-covalent interactions are much less reported for protein-polymer conjugation. One of the example is to obtain PEGylated BSA protein-polymer conjugate by host-guest interaction between the macrocycle cucurbit[8]uri (CB[8]), viologen (MV7) and naphthalene (Np8), which form the CB[8] ternary complex with a good binding affinity (overall binding constant, K_a , of $1.5 \times 10^9 \text{ M}^{-2}$, Figure 1-6).[133] The interaction between NTA and His₆ was used for the PEGylation of his-tagged tumor necrosis factor-related apoptosis inducing ligand (TRAIL) while it failed to reach complete complexation of PEG and his-tagged TRAIL at any ratio. Charged polymers such as poly(amidoamine)s[134] and PEG with oligo-lysine or oligo-arginine side groups[135] were used for the conjugation of negatively charged proteins such as β -galactosidase[134] and insulin[135], while large excess of polymers are required for a full and stable complexation with targeted proteins and the binding between polymers and proteins is always poorly defined. Weak interactions between ligands on both polymers and proteins cause the instability of the protein polymer conjugates, which restricts the application of non-covalent interactions for the construction of protein-polymer conjugates.

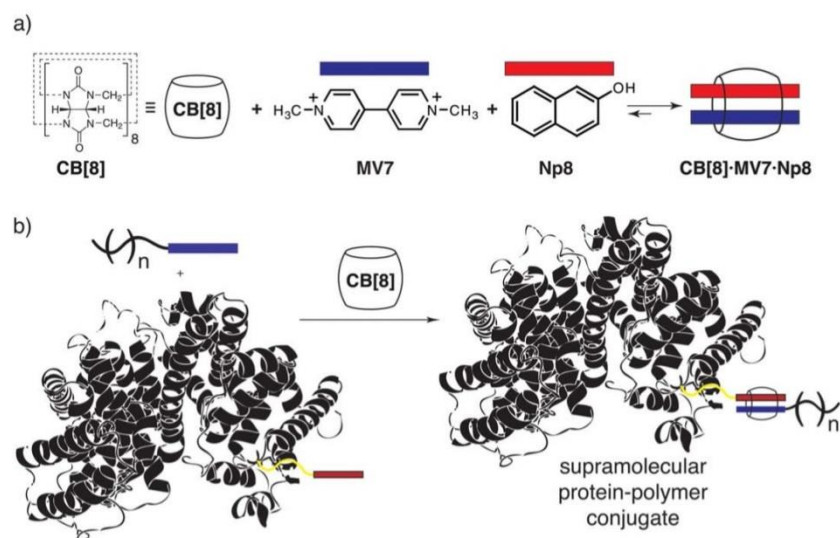


Figure 1-6. Polymer-protein conjugates obtained by the host-guest interaction between CB[8], MV7 and Np8.[133] Reproduced with permission from ref. 133. Copyright 2011 Royal Society of Chemistry.

“**Grafting from**” strategy was first reported by the group of Prof. Heather D. Maynard’, and the general idea is to grow the polymer directly from the proteins.[35, 36] The advantage of “grafting from” comparing to “grafting to” is that no purification of excess polymers is required and the polymer location can be easily identified. The “grafting from” involves two steps: the synthesis of protein macroinitiators and polymerization. Protein macroinitiators are obtained by the covalent binding of maleimide and pyridyl disulfide initiators to the cysteine residues on the proteins or coupling initiators on the protein through molecular recognition.[36] For example, BSA and lysozyme were modified with pyridyl disulfide- and maleimide-functionalized initiators for atom transfer radical polymerization (ATRP). Polymerization of NIPAM from the protein macroinitiators resulted in thermosensitive BSA-PolyNIPAM and lysozyme-PolyNIPAM in greater than 65% yield.[36] Streptavidin was coupled with a biotinylated initiator for ATRP. Various polymers including PNIPAM and poly(ethylene glycol) methyl ether methacrylate (PEGMA) were grown directly from modified streptavidin.[35] Narrow polydispersities (PDIs) of polymers can be obtained by using the grafting from approach and the proteins remain active after ATRP or (reversible addition-fragmentation chain-transfer) RAFT polymerization.[35-38] The disadvantage of the “grafting from” strategy is that it involves two step reactions and the steric hindrance of proteins will

dramatically influence the polymerization and the final conjugation efficiency. Both “grafting from” and “grafting to” approaches require a careful determination of the suitable polymers with proper physico-chemical properties and the precise location on the proteins for the polymer conjugation, to maximally preserve the native structures of proteins and their activity.

1.1.1.2. Site-specific protein-polymer conjugation

As discussed above, the non-specific reaction of polymers with the lysine or cysteine residues on the proteins provide a heterogeneous mixture of proteins modified to a different extent and at variable location. Many PEGylated protein products are produced using this type of chemistry. The negative impact brought by the polymer conjugation can't be underestimated. For example, the attachment of polymers induced an alteration of the protein structure and converted human growth hormone into a growth hormone receptor antagonist.[39] The development of unnatural amino acid mutagenesis and enzymatic catalysis enables the incorporation of unique functional groups, that are not found in natural amino acids, into intended modification sites. The protein-polymer conjugates produced by site-specific conjugation are well-characterized, homogenous and show high reproducibility.[8]

There are two strategies for the site-specific polymer conjugation. One strategy is to mutate residues bearing an active group such as lysines into less reactive residues. For example, all the lysine residues of tumor necrosis factor- α (TNF- α) were replaced with other amino acids with the preservation of full bioactivity.[40] The resultant mutant was then site-specifically PEGylated at the N terminus. This mono-PEGylated TNF- α mutant showed higher bioactivity *in vitro* and greater antitumor therapeutic potency than non-specifically mono-PEGylated wild-type TNF- α .

Another strategy is to incorporate unique functional groups or linkers into intended modification sites for the polymer conjugation. The incorporation is mainly achieved by two approaches: chemical modification and unnatural amino acid mutagenesis.

Chemical modification. The unique reactive properties of the N terminus have led to several strategies dedicating this location for site-selective protein modification.[41] N-terminal amino groups have lower pK_a values compared to that of lysine side chains, and

can be used for direct acylation reactions by selecting the appropriate pH value.[42] However, in most cases the selectivity of this reaction is limited due to the presence of the large number of competing lysine residues (10–40 on most proteins). Alternative strategies have targeted the N terminus in combination with specific amino acid side chains such as N-terminal cysteine, N-terminal aspartic acid, and other residues. In particular, the reaction of N-terminal cysteine residues with thioesters has shown a great success for site-specific protein conjugation.[43] N-terminal cysteine residues can be modified through thiazolidine formation by using aldehyde reagents (Figure 1-7).[44] Reactive aldehydes can be formed through periodate oxidation of N-terminal serine and threonine residues,[45] or through N-terminal aspartic acid residues reacted with glyoxylic acid and O-benzylhydroxylamine. N-terminal tryptophan residues can be modified through Pictet–Spengler reactions to get reactive aldehydes.[46]

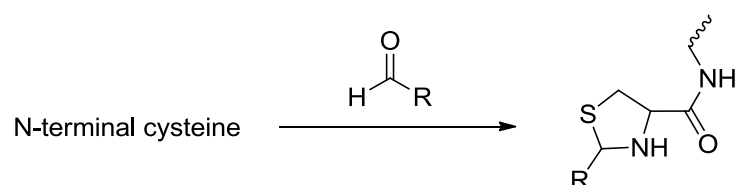


Figure 1-7. Conjugation of Polymer (R) with aldehyde group to N-terminal cysteine on the protein.

An alternative strategy that does not depend on the nature of the amino acid side chain can be envisioned through the oxidation of the N-terminal amino group to an imine, followed by hydrolysis to a ketone or an aldehyde. However, reaction conditions are too harsh to maintain the folded structure of most proteins.[47]

Unnatural amino acid mutagenesis. A variety of *in vitro* (cell-free) methods have been developed to incorporate unnatural amino acids into proteins by using the existing protein biosynthetic machinery of the cell with excellent translational fidelity.[10] As they do not represent the topic of this thesis, more details about this process will not be given.

Another promising approach to fabricate protein-polymer conjugation is the recognition between certain ligands on the polymers and the existing tags on the proteins.[5] In general, recombinant proteins contain tags so that they can be purified from their crude biological source using an affinity technique. The location of the affinity tag on the

proteins is well known. They are therefore great candidates for site-specific protein-polymer conjugation. However, up to now the application of affinity tags on the proteins is restricted to small molecular modification, such as site-specific fluorescent or radioactive labelling,[48-50] and very few publications are reported for the protein-polymer conjugation.[5, 51] The problem is that most affinity tags recognize specific antibodies, which increases the difficulty of the synthesis. His₆, which is the most used affinity tag for the protein purification, specifically binds nitrilotriacetic acid-Me²⁺ chelator (NTA-Me²⁺). However, relative low binding affinity between NTA-Me²⁺ and His₆ hinders the application as a linker for protein-polymer conjugation.[52]

1.1.1.3. Conjugation of multiple proteins to polymers

The polymers for protein conjugation are mostly end group active, therefore, the current protein-polymer conjugates have mainly two types of structures: one protein bearing a single polymer chain by site-specific protein-polymer conjugates, and one protein randomly bearing multiple polymer chains produced by non-specific protein-polymer conjugation. However, polymers are able to build up more complicated structures with proteins, and one possibility is to conjugate multiple proteins on a single polymer chain. This strategy is inspired from viruses, with which interactions between multiple trimers of the hemagglutinin on the virus surface and multiple moieties of N-acetylneuraminic acid on the surface of the target cell occurs.[53, 54] Now, polymers are designed with multiple ligands for the binding of viral surface proteins, which can inhibit the interaction of virus with healthy cells and consequently stop the virus infection.[55] However, the conjugation of polymers with multiple free proteins was rarely reported. Two publications from Prof. Laura L. Kiessling used polymers as scaffolds for protein oligomerization (Figure 1-8).[56, 57] Even though polymer-protein conjugates have been developed for more than 40 years, only few investigations have been dedicated to the conjugation of multiple proteins to a polymer, although previous studies already proved that the formation of protein cluster on polymers can enhance the protein activity.[57]

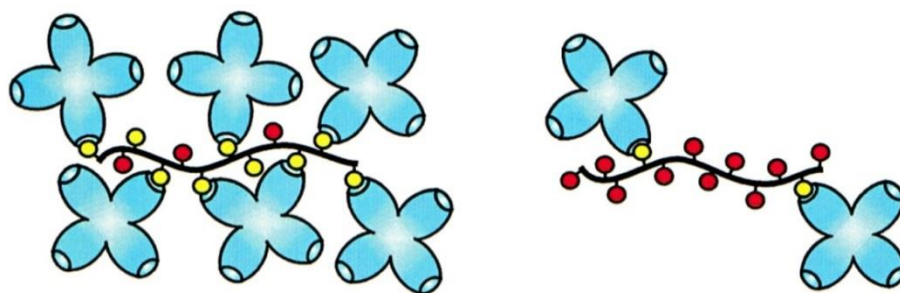


Figure 1-8. Schematic representation of concanavalin A clustering by multivalent ligands on polymers.[56] Reproduced with permission from ref. 56. Copyright 2002 American Chemical Society.

1.1.2. Proteins in polymer self-assembled structures

Polymer-protein conjugates have been largely used for various applications especially as therapeutics, which have been approved by the Food and Drug Administration (FDA).[136] However, the limitations of polymer conjugation as an approach for protein protection have also been described.[6] The polymers are able to efficiently protect proteins against the proteolysis in the body, but cannot stop the permeation of small molecules through the polymer shield and protect proteins from the change of conditions which can induce the inactivity of proteins, such as pH, ions strength, and solvents.[137, 138] In addition, targeting molecules are required on the polymer shield for targeted delivery, but the modification of polymers with targeting molecules such as antibodies can be problematic and the reaction process has the risk to inactivate the proteins. To avoid all of these problems, polymer supramolecular structures with specific sealed reaction spaces at the nanoscale level were described for proteins.[61-63, 66] The selective transport of molecules across the membrane can be achieved by the insertion of membrane proteins.[68, 69, 139, 140] Elaborate designs of polymer properties provide different physicochemical environments for the accommodation of proteins and preserves the characteristic of synthetic materials such as stability and mechanical robustness. The proteins can be encapsulated, inserted, or attached to the self-assembled structures based on the physicochemical properties of both proteins and polymers without affecting their functions.[67, 68, 70-72] For example, the water-channel protein Aquaporin Z (AqpZ) was incorporated into the membrane of polymeric vesicles self-assembled by poly(2-methyloxazoline)-*block*-poly(dimethylsiloxane)-*block*-

poly(2-methyloxazoline) (PMOXA-*b*-PDMS-*b*-PMOXA). A large enhancement in water productivity, up to 800 times compared with the one of vesicles without AqpZ, was observed.[69] Superoxide dismutase (SOD) and lactoperoxidase (LPO) were coencapsulated in polymeric vesicles formed by the self-assembly of PMOXA-*b*-PDMS-*b*-PMOXA. The enzymes acted in tandem inside the polymeric cavities and converted reactive oxygen species O_2^- to H_2O_2 , which can further react with amplex red and produce fluorescent resorufin. In addition, the reconstituted outer membrane protein F (OmpF) in the polymer membrane allowed the passive diffusion of resorufin outside of the cavities (Figure 1-9).[68] The combination of proteins and amphiphilic block polymers (ABPs) will be further discussed.

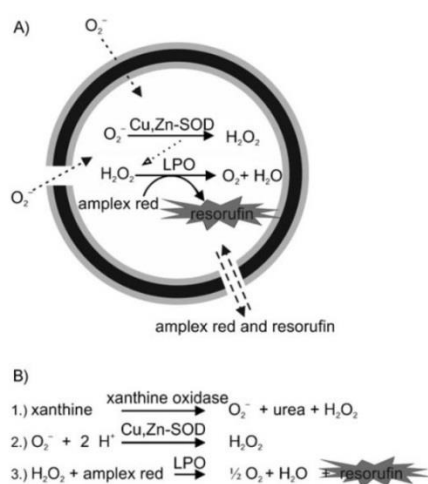


Figure 1-9. Enzymatic cascade reaction inside polymeric vesicles for detection and superoxide radical detoxification.[68] Copyright 2011 WILEY-VCH Verlag GmbH & Co. KGaA.

ABPs are composed by a hydrophilic block (water-loving) and hydrophobic block (water-repellent). Due to the dual affinity of the blocks, the polymers self-assemble into different morphologies in solution depending on molecular parameters (hydrophilic-to-hydrophobic block length ratios, molecular weight, etc.) and external factors (preparation methods, concentration, buffer, etc.).[65,73] Spherical structures including micelles and vesicles are mostly used and investigated. In the following sessions, the combination of proteins with polymeric micelles and polymeric vesicles will be reviewed.

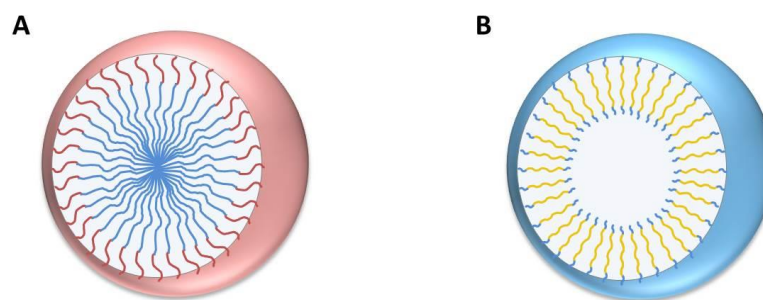


Figure 1-10. Schematic presentation of the structure of micelles (A) and vesicles (B).

1.1.2.1. Proteins in polymeric micelles

Polymeric micelles are obtained by self-assembly of ABPs in aqueous solutions at concentrations above the critical micelle concentration (cmc).[141] The hydrophilic block will orient towards aqueous environment while the hydrophobic block orients inward to shield it forming a core-shell structure. Compared with small molecular weight surfactant micelles, the cmc of polymeric micelles is much lower, resulting in a slower rate of dissociation. Therefore, polymeric micelles are more stable than surfactant micelles in different environments.[142]

The size of polymeric micelles is usually in the range of 10-100 nm. In addition, the structures and physicochemical properties of polymeric micelles can be modulated by changing the internal factors (such as chemical nature of polymers, molecular weight, or hydrophilic-to-hydrophobic block length ratios) or external factors (such as temperature, ionic strength, solvents or preparation methods).[144] Increasing the temperature reduces the size of polymeric micelles due to the improved polymer solubility and raised CMC value.[144, 145] Even though polymeric micelles have proven their adaptabilities for different environments and applications, their combination with proteins is still challenging. Only hydrophobic cargo can be loaded into the polymeric micelles, while most proteins are hydrophilic and functional only in aqueous environments. To overcome this limitation, Khmel'nitsky introduced polymeric reversed micelles, in which hydrophilic blocks aggregate to form the core while hydrophobic blocks extend away from the core.[146] Different enzymes such as laccase and α -chymotrypsin have been loaded into the micelles and used for synthetic, non-aqueous enzymology.[146-148] There are two main problems with this strategy: (1) enzymes are denatured and their specific activity is extremely low when working in organic solutions; (2) the restricted

working conditions (non-aqueous environment) limits the applications of protein-loaded polymeric reversed micelles *in vitro* or *in vivo*.

1.1.2.2. Proteins in polymeric vesicles

Polymeric vesicles are microscopic sacs formed by the self-assembly of ABPs in aqueous solution due to their amphiphilic nature.[64] The formation of either vesicular or micellar structures by ABPs is decided by internal and external factors as mentioned above.[64, 65, 73] A hydrophilic/hydrophobic ratio between 16% and 27% is desirable to obtain vesicular structures.[65] Increasing molecular weight of ABPs promotes the vesicle formation and enhances the stability of structures attributed to the increase of membrane thickness.[65]

Polymeric vesicles can be regarded as higher molar mass homologues of conventional lipids, which are the basic components forming cell membranes of bilayer structure. The polymer membrane in vesicle structures plays the role to partition aqueous volumes of different compositions and concentrations. Therefore, vesicle structures are able to provide customized and isolated environments for the proteins and maximally preserve their activities.[70, 80] In addition, due to the presence of hydrophobic domain inside the membrane, hydrophobic proteins such as membrane proteins are able to insert into polymer membranes and maintain their functions such as active or passive transport of molecules.[69, 140]

Various enzymes have been encapsulated in polymeric vesicles, acting as nanometer-sized reaction compartments. By encapsulating enzymes inside polymer vesicles, enzymes preserve their activity, while being protected from the inhibition and the degradation induced by denaturing agents such as ethylenediaminetetraacetic acid (EDTA) and proteases. Due to the high thickness of polymer membranes and their low membrane fluidity compared with lipid membranes, generally only gases and oxidant species can pass through the membrane by passive diffusion. To achieve *in situ* reactions, selectively permeable polymer membranes capable of exchanging substrates and products are required to maintain the reactions. Principally, it is possible to create, by an elaborate design, block copolymers that form porous membranes,[149, 150] but high selectivity is rarely achieved. A more elegant approach is to induce the selectivity of

membranes by the insertion of membrane proteins. Selective transport of water and protons have been performed by the insertion of aquaporin[69] and gramicidin in polymeric membrane composed by PMOXA-*b*-PDMS-*b*-PMOXA triblock copolymer. The combination of polymeric vesicles with proteins including both enzymes and hydrophobic membrane proteins generate new complex nanosystems, such as nanoreactors,[63, 68, 80, 81] used for biosensor development, or as new therapeutic and theragnostic agents.

1.2. Hybrid nanosystems based on polymers and DNA

DNA is a highly specific macromolecule that can be programmed to self-assemble into complex structures due to the free energy of base pair formation.[82, 83] The current technology is already able to virtually synthesize any DNA sequence, and amplify any DNA sequence from microscopic to macroscopic quantities by polymerase chain reaction (PCR). Another attractive feature of DNA is its 'stiffness' feature (length < 50 nm), which corresponds to 150 base pairs in the double helix. Double-stranded DNA (dsDNA) behaves as a rather rigid and straight polymer chain below this size, and can be used as a rigid spacer between two tethered functional molecular components at each end.[84] In addition, the physicochemical stability of DNA is much higher than that of proteins. Hence, nanostructured materials constructed from DNA can be synthesized, processed, and stored under a broad range of environmental conditions without the requirements of special precautions to avoid decomposition of DNA materials. Moreover, nature provides a variety of highly specific enzymes which allow the processing of DNA materials with atomic precision.[85] The DNA molecules can be either cleaved specifically at a known site by restriction endonucleases, glued together by the sticky ends on each DNA to make one molecule, specifically modified to either 3'- or 5'-terminus by terminal deoxynucleotidyl transferase (TdT), and amplified from microscopic to macroscopic quantities by polymerase. For example, high molecular-weight circular plasmid NA (pBR322, 4361 bp) was digested by a DNA restriction enzyme (Alw26I) into three dsDNA segments. The dsDNA segments could be ligated with dsDNA-polymer conjugates by DNA ligase (Figure 1-11).[74]

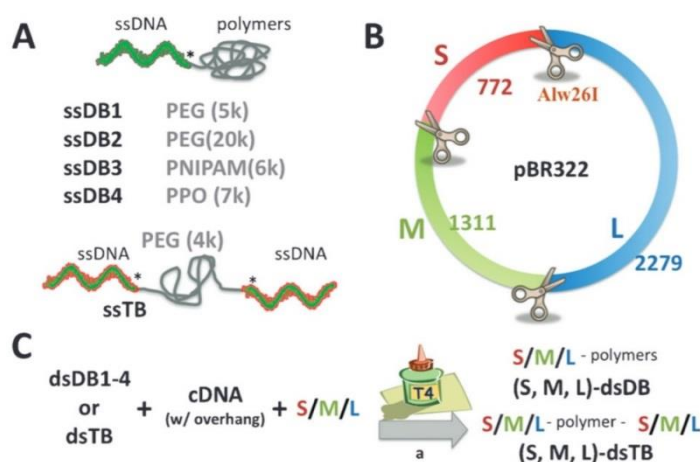


Figure 1-11. Schematic representation of the extension of dsDNA-polymer conjugates by DNA ligase. [74] Reproduced with permission from ref. 74. Copyright 2011 Royal Society of Chemistry.

DNA has been combined with inorganic materials like gold nanoparticles[25, 87, 88] and small organic moieties like fluorescent dyes[89] for various applications, such as cancer detection and gene therapy.[82, 90-95, 152] In recent years, a new type of nucleic acid hybrid has emerged, which consists of synthetic oligonucleotides and organic polymers.[24, 75, 96] As a consequence of joining these two classes of materials in DNA-polymer conjugates (DPCs), new materials preserving the features of DNA and exhibiting additional ones due to the presence of polymers are obtained. As various interactions existing in DPCs such as hydrophobic and electrostatic interactions, and the helix features of double strand DNA, nanostructures based on DPCs are able to self-assemble into diverse nanostructures including micelles and vesicular structures. These nano-scaled DNA hybrid materials hold the promise for the programmable construction of functional materials and gene relative therapies, such as nanodevices, antisense, and aptamer therapeutic strategies.

1.2.1. DNA-polymer conjugates

Existing chemistry routes allow the versatile synthesis of DNA-polymers conjugates with a large choice from the composition, property, length, and architecture from both DNA and polymer point of view. A general approach to ligate DNA and polymers is by the reactions at the 5'- or 3'- terminus, due to the higher accessibility of these positions. In general, DNA used for the polymer conjugation is represented by synthetic

oligonucleotides (ODNs). ODNs are linked to either hydrophilic polymers or hydrophobic polymers depending on the desired application. The linkage of hydrophilic polymers to ODNs improves their aqueous stability and decrease immunogenicity, resulting in a reduction of the toxicity and the prolongation of *in vivo* circulation times. The most used hydrophilic polymer is PEG due to the uncharged, water-soluble, non-toxic, and non-immunogenic nature.[97, 98] The combination of hydrophobic polymers with ODNs in general leads to self-assembly in aqueous solutions.[24, 96] The increase of size of ODN-bearing structures is able to take full advantage of the EPR effect for passive DNA delivery.

1.2.1.1. Synthesis for DNA-polymer conjugation

Polymers are commonly connected to ODN sequences either in solution or on a solid support. The coupling reaction on a solid support can be used for achieving both water-soluble and amphiphilic DNA–polymer conjugates (ADPCs) with relatively high yields.[20, 99, 100] However, carrying out the coupling reaction between ODN sequence and hydrophobic polymer segments in solution results in low yields, because of the incompatibility between the two components. Recently, new approaches such as enzymatic reactions have been performed to obtain DPCs, especially for the ones with high DNA molecular weight.[74, 101] The pros and cons of different methods are discussed in the following sections.

Solution Coupling. Solution coupling is the first approach for DNA-polymer conjugation. Four main coupling reactions in solution have been reported: amide bond formation, disulfide bond formation, Michael addition and click reaction (Figure 1-12).[99] In the first approach, the amino group of the ODN fragment reacts with the activated carboxyl group of the polymer and these two parts are linked by amide bond formation. The reaction conditions and activating agents are similar with that for peptide synthesis. *N,N'*-diisopropylcarbodiimide (DIC), *N,N'*-dicyclohexylcarbodiimide (DCC), *N*-hydroxysuccinimide (NHS), and 1-ethyl-3-(3-dimethylaminopropyl) carbodiimide (EDC) are the most used activating agents. In order to bind an ODN with a polymer by a disulfide linkage, both components are required to undergo a terminal thiol-modification and the reaction is carried out in slightly alkaline conditions in an aqueous phase. In the case of Michael addition reaction, thiol-functionalized ODNs react with the

polymers containing maleimide or acrylic acid functional group at neutral pH. High yields of DNA–polymer conjugates can be obtained by using the approaches discussed above. But these approaches are only restricted for the coupling between ODNs and hydrophilic polymers, such as poly (ethylene oxide) (PEO)[76, 77] and PolyNIPAM[102, 103] due to poor solubility of DNA in organic solvents. In addition, the yield of the coupling reaction in solution is generally low due to the random coil feature of both single stranded DNA (ssDNA) and polymers in the solution, which leads to a low exposure of the end group for coupling reactions.[20] Moreover, the purification of DPCs from non-reacted DNA and polymers can be problematic due to the comparable molecular weight and hydrodynamic size of DNA-polymer conjugates compared with free DNA and polymers.

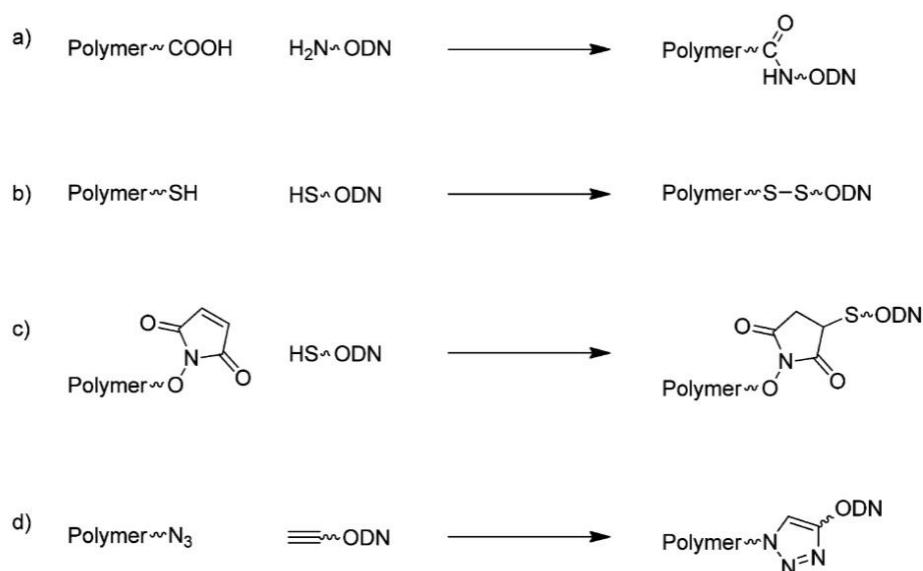


Figure 1-12. Coupling methods for DPCs synthesis in solution.[99]

Solid-phase synthesis. It has been mentioned above that the preparation of ADPCs by solution coupling is still not proficient due to the poor yields and the problematic purification. To overcome these synthetic difficulties, solid-phase synthesis has been employed and shows a higher yield comparing to solution coupling approach.[20, 99] ODNs are manufactured almost exclusively using automated solid-phase synthesis. All the potential reactive groups along the ODN fragment are protected during the synthesis. Therefore the ODN fragment immobilized on the bead is soluble in organic solvent. This feature helps the compatibility of ODNs and polymers in organic solvent. The protection of potentially reactive groups along the ODNs limits the side reactions,

improving the yield as well. In addition, the automation of solid-phase synthesis avoids performing tedious chemistry and purification steps.

The coupling between ODNs and polymers by a solid-phase synthesis approach can be done by the three reactions mentioned above, as well. In addition, the polymers with phosphoramidite groups are able to couple to the detritylated 5'-hydroxyl-end of the ODN on the solid support using a DNA synthesizer directly and no modification of DNA is needed.[104] Phosphoramidite-polymer derivatives are synthesized by reacting hydroxyl-terminated polymers with phosphoramidite chloride. After cleavage from the resin and deprotection with a concentrated ammonia solution, ODN-based copolymers can be obtained. Several ADPCs such as DNA-*block*-polypropylene (DNA-*b*-PPO),[96] DNA-*block*-poly(2-alkyl-2-oxazoline),[75] poly(2-oxazoline)-*graft*-DNA[143] have been synthesized by solid-phase synthesis approach with high yields. For example, the synthesis of DNA-*block*-poly(2-alkyl-2-oxazoline) is shown in Figure 1-13.[75] However, the main drawback of ADPCs is that it is very hard to find a good solvent for both DNA and hydrophobic polymers due to the huge difference in polarity between the two components. Therefore, a successful synthesis of ADPCs cannot guarantee that they can dissolve or self-assemble in aqueous solution after deprotection. A latest study found that the complexation of hydrophobic contracts such as surfactants elevate the solubility of DNA in organic phase.[105] However, a careful design of the hydrophilic/hydrophobic ratios is still crucial for the preparation of ADPCs.

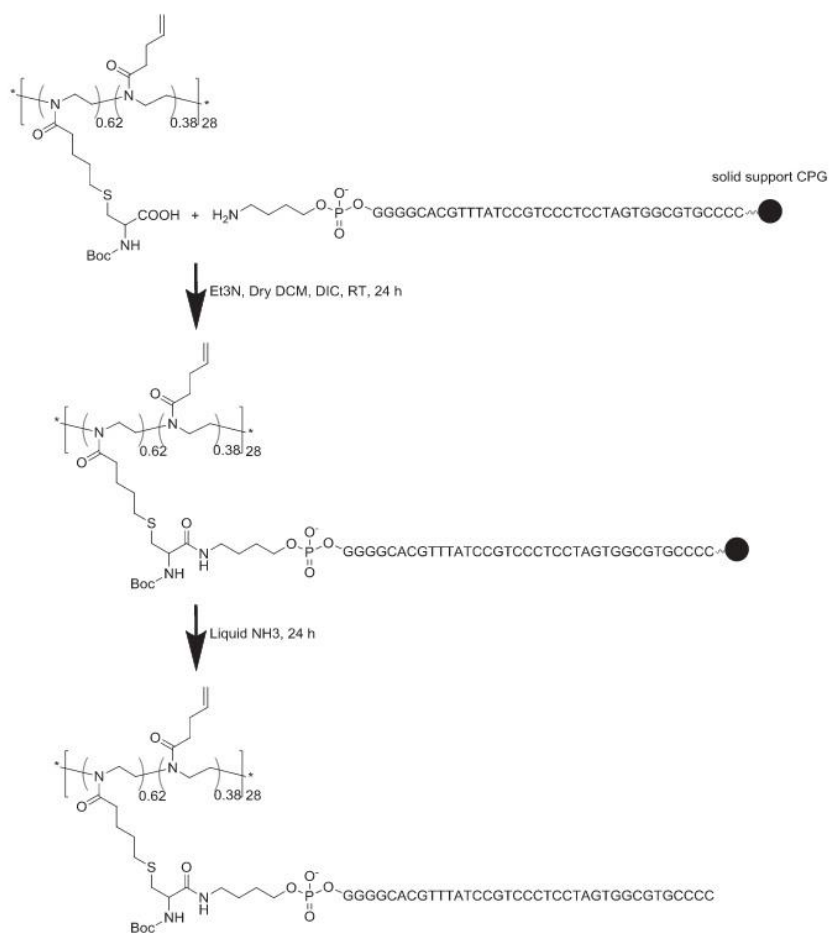


Figure 1-13. DNA-block-poly(2-alkyl-2-oxazoline) synthesized by solid-phase synthesis.[75] Reproduced with permission from ref. 75. Copyright 2013 WILEY-VCH Verlag GmbH & Co. KGaA.

Enzymatic Reactions. The greatest disadvantage of the solid-phase synthesis approach is that it is only available for short length ODNs and polymer segments due to the limited diffusion of the reactants through the pores of the solid support and the exposure of the terminal groups. Recently, elegant molecular biology methods have been adapted to the synthesis of DNA-polymer conjugates in order to overcome this impediment. Herrmann and coworkers applied DNA PCR to synthesize DNA-polymers conjugates with longer DNA fragments (Figure 1-14).[101] The ODN-polymer conjugates acted as a primer and the plasmid pBR322 was used as a template for the PCR reaction to generate double-stranded (ds) diblock copolymers with DNA fragments of extended length up to 1,578 bp. A total average molecular weight greater than 1,000 kDa and monodisperse nucleic acid chains could be achieved. The prolongation of DNA fragments on the conjugates can be done by the DNA polymerization catalyzed by TdT as well.[106] The DPCs with extremely

long DNA blocks were synthesized as well, based on the enzymatic restriction and ligation.[74] Large DNA fragments were obtained by the digestion of a circular plasmid DNA executed by a DNA restriction enzyme (Alw26I) and ligated to dsDNA-polymers conjugates with sticky ends by enzyme ligation.

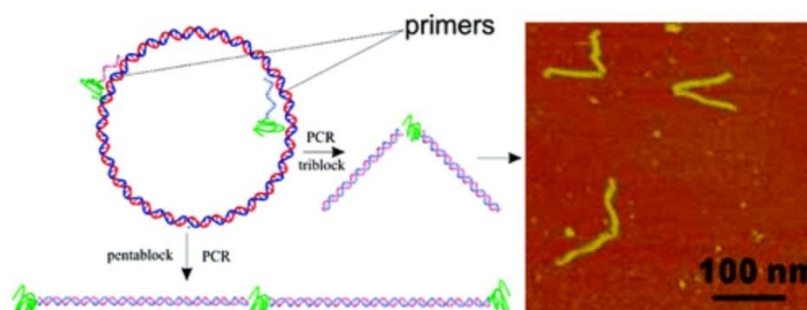


Figure 1-14. Schematic representation of the generation of DNA pentablock copolymers by PCR.[101] Reproduced with permission from ref. 101. Copyright 2009 American Chemical Society.

1.2.1.2. Supramolecular assemblies of DNA-polymer conjugate

It has already been mentioned above that ABPs containing both hydrophilic and hydrophobic segments self-assemble into various supramolecular structures such as micelles, vesicles, worms, and monolayers. Such superstructures can be used as delivery vehicles for therapeutic molecules, or act as the containers for catalytically active species. The ADPCs bring opportunities serving as containers or delivery vehicles for different applications. Besides the automated and straightforward synthesis, DNA based self-assembled structures allow a convenient functionalization by the hybridization with complementary ssDNA.[107] In addition, dynamic assemblies can be obtained by the hybridization or enzymatic catalysis,[108, 109] which changes the balance between hydrophilicity and hydrophobicity in the structure and leads to a different morphology of the self-assembled structures. Moreover, DNA composing self-assembled structures exhibit high cellular uptake by different cell lines, and some ODN's such as nucleic acid aptamers are able to specific bind to DNA and RNA, which make ADPCs highly promising for drug delivery, gene antisense and other gene therapy.[110, 111]

A simple example of such supramolecular assemblies is the one-dimensional extension of DPCs. Triblock copolymer structures of the type polymer-*block*-DNA-*block*-polymer

are able to be formed by hybridization of two DNA-*block*-polymer with complementary sequences.[112] Large one-dimensional polymer assemblies were achieved by employing two DNA-*block*-polymer-*block*-DNA triblock polymers with complementary single strands.[113] The molecular weight could be easily controlled by the ratio of DNA-hybrid monomers because the access of monomer efficiently induced chain termination.

Besides extended one-dimensional assemblies, micellar morphologies have been obtained by DPCs. The first strategy is to form micellar structures led by the complexation between DNA and positively charged species. This approach is mainly adopted by DNA- hydrophilic polymer conjugates. For example, DNA-*block*-poly(ethylene glycol) (DNA-*b*-PEG) self-assembled to micellar structures by the complexation with positively charged peptide KALA.[114] The inner polyelectrolyte complex core is surrounded by the PEG chains constituting the corona, protecting the ODN from enzymatic degradation. Another strategy is to build micellar structures by ADPCs. In this case, the assembly of the DPCs is driven by the polymer segments, which forms the hydrophobic core, while the DNA is present in the corona. Polystyrene (PS) and PPO have been used to conjugate with DNA and these ADPCs form homogeneous micelles.[115, 116] Recently, vesicular structures assembled by ADPCs have been reported, as hydrophobic poly (butadiene) (PB) or poly (isobutylene) (PIB) coupled with a 12 nucleotide sequence.[117] Compared to the conventional block polymers, the self-assembly of ADPCs is more complicated because different non-covalent interactions including hydrophobic, electrostatic interactions, and hydrogen bond formation are involved. A simpler way is assembling the structures based on the ABPs, and further modifying the surface of the structure by post functionalization. DNA with dibenzocyclooctyl group (DBCO) has been coupled to the chitosan nanoparticles with an azide group on the surface by a Cu-free click reaction.[118] The advantage of this strategy is DNA exposure to the environment, with no further influences on the self-assembly behavior.

Various morphologies assembled by DPCs have already been reported. Organic block polymers were combined with DPCs, which allows the combination of properties from both parts. Poly(polyethylene glycol)-*block*-poly (propylene)-*block*-poly(ethylene glycol) (PEG-*b*-PPO-*b*-PEG) composited with DNA-*b*-PPO formed a similar micellar structures to

DNA-*block*-poly (propylene) (DNA-*b*-PPO) alone (Figure 1-15).[119] The micelles can be cross-linked either at the periphery of the corona or within the core to protect them against disaggregation upon dilution and precipitation at low temperatures. In addition, mixed micelles formed by PEG-*b*-PPO-*b*-PEG and DNA-*b*-PPO provided the sequence specific recognition at the same time due to the DNA block.

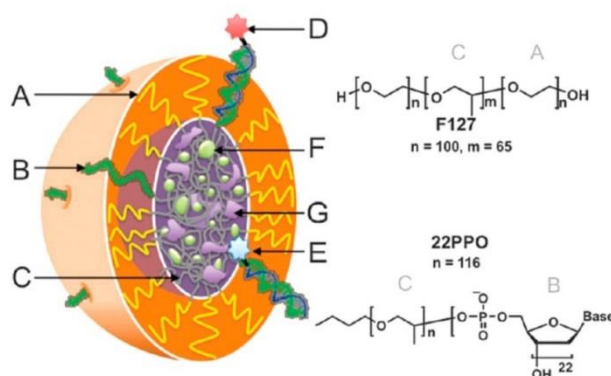


Figure 1-15. Schematic presentation of the mixed micelle architecture self-assembled by PEG-*b*-PPO-*b*-PEG and DNA-*b*-PPO.[119] Reproduced with permission from ref. 119. Copyright 2010 Royal Society of Chemistry.

An advantage of assembled structures formed by DPCs is the ability to induce a specific morphology by the hybridization. It has been reported that micelles composed by DNA-*b*-PPO can undergo a morphological transition from spherical to rod-like structures upon hybridization with long DNA sequences, while no effects on the micellar morphology was observed after hybridization with small single-stranded complementary sequences.[96] The application of DNAzyme and polymerases trigger the morphological transition of such assembled structures due to the change of DNA length and consequently the hydrophilic/hydrophobic ratio.[108]

1.2.1.3. Applications of self-assembled structures based on DPCs

Drug delivery vehicles. ADPC structures can be used for drug delivery due to the presence of their hydrophobic cores. Pyrene and anticancer drugs such as doxorubicin (Dox) have been successfully loaded into the micelles composed by ADPCs.[116, 120] ADPC-composed structures are superior due to the easy conjugation of different targeting moieties on the surface by simple hybridization. The “clicked” moieties allow a perfect control of the location depending on the conjugation of either 3'- or 5'-end of

ODNs. If a targeting moiety is connected to the 5'-end of ODN, it is present on the surface of micelles. If the conjugation is towards to the 3'-end of ODN, the targeting moiety is located inside of the DBC aggregates (Figure 1-16).[107] Folate has been conjugated to the micelle surface by the hybridization and high cellular uptake of folate modified micelles was observed.[120] The synthetic ODN corona has great biocompatibility and biodegradability, and also avoids immunological responses compared to plasmid DNA.[121] No toxicity of delivery vehicles composed by ADPCs was reported.[120]

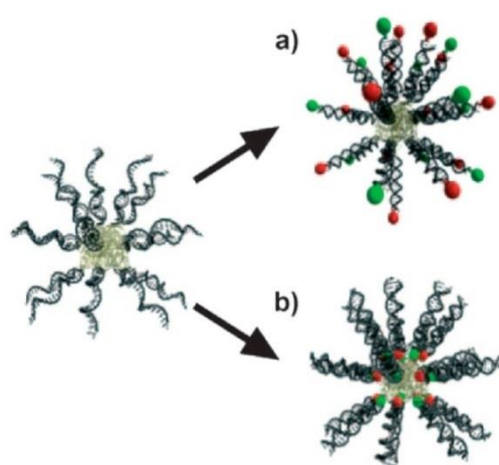


Figure 1-16. Modification of DPC micelles by hybridization with complementary ssDNA equipped with functional group either at the 5'- or at the 3'-ends.[107] Reproduced with permission from ref. 107. Copyright 2006 WILEY-VCH Verlag GmbH & Co. KgaA.

ADPCs allow for control of the ratio between hydrophilic and hydrophobic blocks by enzymes, and the hybridization due to the DNA block, which results in the formation of diverse nanostructures, and facilitates the investigation of the relationship between geometry of nanostructures and cellular uptake. DNA-*b*-PPO micelles are able to form both spherical and rod-like nanostructures depending on the length of hybridized DNA.[109] The hybridization of DNA-*b*-PPO micelles with short complementary strands keeps the overall spherical shape of the aggregation, while rod-like micelles consisting of two parallel aligned double helices result when base pairing with long complementary strands are used. The rod-like aggregates show a higher extent of uptake than both ss and ds spherical micelles.

Nanostructures self-assembled by ADPCs show the same main drawbacks as other self-assembled structures for *in vivo* applications, as they disassemble due to the dilution upon administration. For this reason, DNA-*b*-PPO system was blended with Pluronics, PEG-*b*-PPO-*b*-PEG, to stabilize the aggregation by crosslinking the hydrophobic cores.[119] The cross-linked nanostructures are much stable comparing to the one without crosslinking. Another approach to stabilize ADPC aggregates is to encapsulate the whole nanostructures in other nanocapsules. Micelles of DNA-*b*-PPO successfully act as the template for the formation of virus-like particles (Figure 1-17).[116] The Cowpea Chlorotic Mottle Virus (CCMV) coat protein dimers are able to attach and self-assemble into particles consisting of 90 and 120 proteins, respectively. Different hydrophilic and hydrophobic compounds have been loaded in the CCMV particle protected micelles.

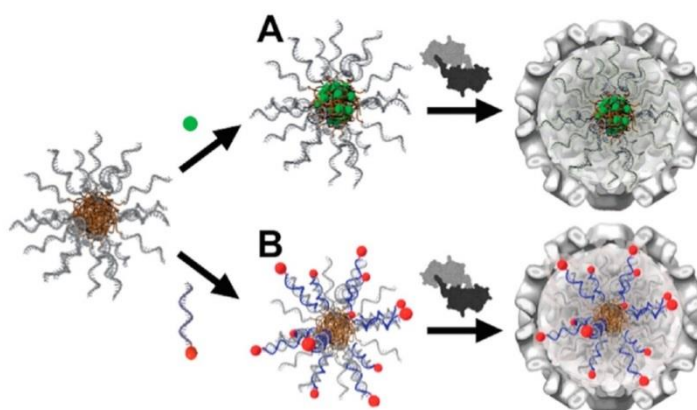


Figure 1-17. DPC micelles as the template for the formation of virus-like capsules and using for drug delivery.[116] Reproduced with permission from ref. 116. Copyright 2010 American Chemical Society.

Antisense therapy. Antisense ODNs are an important class of therapeutic molecules due to their ability to interact with their complementary target mRNA with high selectivity. The specific binding of ODN to target mRNA is able to block their expression and the production of undesirable proteins. To protect antisense ODNs against enzymatic degradation by cellular nucleases and promote their cellular uptake, antisense ODNs have been linked to polymers such as PEG and complexed with cationic molecules including KALA peptides, poly(l-lysine), polyethylenimine (PEI), and protamine to form complex micelles.[76, 114, 122] ODNs locate inside of the nanostructure to avoid the digestion by cellular nucleases. For example, antisense *c-raf* oligonucleotide-PEG

conjugates were complexed with PEI and self-assembled to form polyelectrolyte complex micelles with a diameter of approximately 70 nm in aqueous solution.[76] The complex micelles show a higher cellular uptake by A2780 cells than that of ODN alone and superior antiproliferative activity against ovarian cancer cells both *in vitro* and *in vivo*.

Hydrophobic polymers have been conjugated to antisense ODNs to avoid the usage of cationic molecules, which have potential cell toxicity. Hydrophobic polymers drive the self-assembly of DPCs and form a hydrophobic core while hydrophilic antisense ODNs are exposed outside for the binding to mRNA. It has been observed that the dense packing of DNA in the micelle corona allows for hybridization of complementary oligonucleotides, while keeping the DNA protected from enzymatic degradation (Figure 1-18).[24] Steric hindrance and the high local salt concentration surrounding the ODN corona, which prohibits the approach of cellular nucleases, are possible explanations of this behavior.[24, 25] Locked nucleic acids (LNAs) have been conjugated with a hydrophobic polymer and resulted in ADPCs that assemble into spherical micellar nanoparticles (LPA nanoparticles). LPA nanoparticles exhibit rapid uptake within 10 min across five different cell lines including human embryonic kidney cells. Treatment with antisense LPA nanoparticles significantly diminishes mRNA levels relative to endogenous glyceraldehyde 3-phosphate dehydrogenase (GAPDH) mRNA transcripts, which suggests efficient, sequence-specific binding of LPA nanoparticles with mRNA.

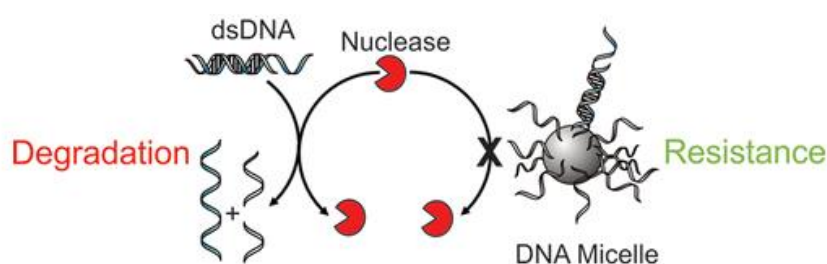


Figure 1-18. Schematic of exonuclease resistance of DPC micelles.[24] Reproduced with permission from ref. 24. Copyright 2013 American Chemical Society.

The unique self-recognition properties of DNA indicate DPCs are superior to other kinds of block copolymer assemblies, even though the studies and the developments of DPCs are still just beginning. DPCs form diverse architectures and the hybridization with complementary strands allows for easy modification and morphology transformation

under physiological conditions. In addition, high-density packing of ODNs in the nanoparticle shell renders DNA resistant to degradation by cellular nucleases. All these outstanding properties make DPCs ideal candidates for a new generation of smart biomaterials, capable of recognizing and responding to particular gene expression features. Multidisciplinary approaches from different fields will drive further evolution and realization of innovative concepts taking advantage of the unique properties of DPCs.

1.3. Molecular recognition

Molecular recognition drives highly specific interactions between molecules, and consequently contributes to biological recognition at the molecular level and the precise proceeding of numerous biological processes at the same time without any interruptions. In fact, molecular recognition is central to all biological processes including DNA replication and transcription, cellular signaling, enzyme catalysis, and so on.[123] Therefore, the understanding of the fundamental mechanisms of molecular recognition is crucial to understanding biology including the functions of proteins and DNA at the molecular level.

1.3.1. Mechanism

The highly specific interactions between substrates, which can be proteins, DNA, ligands, or many other molecules, rely on the perfect geometric fit between the “lock” molecule and “key” molecule, and the precise locational match for the formation of non-covalent bonds including hydrogen bonding, van der Waals forces, hydrophobic interactions, π - π stacking, metal coordination, electrostatic effects, and so on. The mechanism of molecular recognition was first suggested by Emil Fischer in 1894 and named the “lock-and-key” model.[124] However, while this model explains the specificity of interaction between biomolecules, it neglects the fact that biomolecules, especially proteins, are inherently dynamic with a vast ensemble of conformations and fails to explain the stabilization of the transition state of substrates that enzymes achieve or enzymatic catalysis.

A more favorable model for molecular recognition is the induced fit model suggested by Koshland, which considers biomolecules as flexible rather than geometrical rigid

structures.[27] Induced fit model suggests that the initial interaction between substrates is relatively weak, and the substrates undergo a continuous change the conformation until the substrates are completely bound to each other (Figure 1-19, P_1 transforms to P_2L).[29] Here we use enzymes as examples. The binding of substrates to enzymes induce a conformational change of the enzymes and free energy is released from the formation of many weak interactions between the enzyme-substrate complexes. To maximize the release of free energy, the substrate has to be in its transition state to favor binding which lowers the activation energy and allows the reactants to proceed towards the product at a faster rate. This explains why enzymes have high catalytic performances.

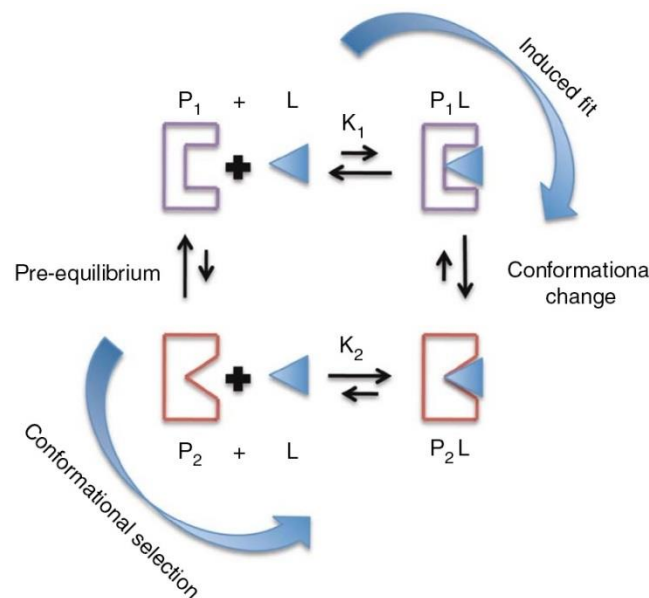


Figure 1-19. Thermodynamic cycle for molecular recognition involving induced fit or conformational selection.[29] Reproduced with permission from ref. 29. Copyright 2009 Rights Managed by Nature Publishing Group.

In 1999, Frauenfelder, Sligar and Wolynes first described the energy landscape of proteins, which led to the generation of the conformational selection model.[28] The energy landscape is a map of all possible conformations of a molecular entity in dynamic equilibrium. Therefore, in the conformational selection model, the conformation of molecules are dynamically fluctuating (P_1 and P_2) and the compatible conformation (P_2) for the binding with substrate L pre-exists,[29] which has a constitutional difference with the induced fit model (Figure 1-19). The binding of substrate L to P_2 induces the shift of

the equilibrium towards this state and consequently results in the “population shift”. Even though lots of efforts have been made to understand the mechanism of molecular recognition, so far no final conclusion, especially for proteins, has been reached.[125] The studies are also mainly restricted to binary systems, and very few expansions have been developed for polyphyletic systems.

1.3.2. From molecular recognition to self-organization

Molecular recognition relies on the molecular information stored in the interacting partners, such as hydrogen bonding arrays, sequences of donor and acceptor groups, ion coordination sites, etc. Each specific interaction occurring between partners is an intermolecular algorithm, directing the self-organization of molecules into complex matters. The specificity and the stability of the self-organization are based on the robustness of the molecular recognition. When the molecular recognition is sufficiently strong, more or less strict programming of the output species and “correct” constructions can be achieved. Biotin and streptavidin possess one of the strongest non-covalent interactions in nature and have been used for the fabrication of various nano devices and sensors based on this strict recognition. Carbon nanotubes modified with biotin have been used as a nano detector for the binding of streptavidin.[31] The binding of streptavidin to the carbon nanotubes induces a charge-transfer reaction between them and the change of device characteristic. This nanodetector is extremely sensitive and promising for in-vivo applications (studying cell physiology, medical screening and diagnosis).[31] Different inorganic nanoparticles such as gold nanorods and iron oxide nanoparticles are also organized by Biotin-streptavidin interactions targeting the applications for nanodevices.[32, 33, 151] By inspiration from nature, synthetic binding pairs such as NTA and His₆, cyclodextrin and adamantine are also frequently adopted for the nanofabrication of diverse architectures and nanodevices. Self-assembly is considered as a simple collection and aggregation of components into a confined entity by non-covalent interactions, while self-organization is information-directed organization of specific molecules into certain structures under equilibrium conditions. The selectivity and robustness of the interactions ensure the correct expression and precise output of the structural instruments stored in molecules.

When several structural instructions (specific binding pairs) exist at the same time, multiple subroutine self-organizations are displayed: (i) it may be that each instruction generates its own encoded output and directs one subprogram independently; (ii) it may present crossover and the subprograms operate in a combined fashion; (iii) it can also be that one of the instructions is dominant and impose its own output over the other one(s). The process of multiple well-defined supramolecular interactions in molecular-level is crucial for the development of complex chemical systems, as known by the execution of highly integrated functions taking place side by side in the assembly and operation of living cells.

When the molecular recognition occurs only in a narrow range of conditions and are highly sensitive to internal factors (such as pK_a) or external factors (such as concentrations and stoichiometries of the components), the system is unstable and may display a switching point between different assemblies. For example, pH can induce a morphology-shifting of DNA-b-poly(propylene oxide) assemblies from spherical micelles to nanofibers.[126] However, due to this sensitivity to the perturbations, the diversity and the adaptability are attributed into the self-organization process.

1.4. Motivation and concept

In this respect, we aim at the design and the construction of different hybrid nanosystems based on polymer/protein, polymer/DNA, and polymer/DNA/protein to understand biological interactions such as distance-dependent protein-protein interactions, mimic cell's organization, such as multicompartmentalization, and achieve novel functionalities such as signal transduction. We designed polymers with specific structures and aim to control the self-organization of polymers and protein/DNA, or nanostructures such as DNA-functionalized polymersomes. To generate systems with higher complexity, diversity, and programmability, several algorithms (influence factors) are imputed in the systems and operated in a combined fashion within the self-organization process. Molecular recognition acts as the main algorithm for the self-organization. Internal factors such as the size and external factors such as pH and temperature as the co-algorithm are read and expressed within the same process in order to programmably control the architectures, interactions, functionalities, and so on.

Two hybrid systems are established in this thesis. First, we design and synthesize tris-nitrilotriacetic acid (trisNTA) functionalized polymers (PNTs) and use as polymeric scaffold for the binding of multiple his-tagged proteins. The molecular recognition between trisNTA on polymers and his tag on proteins ensures the specific connection between polymers and proteins with high stability under different conditions (pH 4). In addition, the distance between trisNTA binding sites on polymers and the size of his-tagged molecules regulates the binding ability, the binding affinity, and protein-protein interactions of bound proteins in a combined manner. Moreover, the nature of the selected Me^{2+} connecting trisNTA and His tag and the distance between trisNTA binding sites on PNTs can influence the binding affinity between trisNTA on polymers and his-tagged proteins, which can result in the switching of polymer-protein conjugates from static (stable) to dynamic (pH-responsive) state. PNT copolymers can serve as models for combining geometric topology with size requirements and mimicking biological systems. They are also promising as protein nanocarriers for protein therapy and other protein-related applications.

In the second system, we apply DNA as the algorithm to program the self-organization of binary polymersomes (compartments) to create multi-compartmentalized system. DNA is capable of controlling the spatial organization and the spatial distance between compartments due to the rigid nature of double-strand (<50 nm), while polymersomes as nano-scale cavities supply a robust and shielded encapsulation method of the active entities. The extension of the polymersome network can be programmably controlled by the average DNA coverage on vesicle surface, concentration and temperature. In addition, the size of polymersomes plays an important role in the assembly behavior and results in different architectures. The polymeric compartmentalized network system offers a new perspective onto evolution from unitary to binary/polyphyletic systems, with collective specific properties greater than of the individual building blocks, and serve as a platform for the generation of novel multi-functional, intelligent and complex systems and bio-devices.

1.5. References

- [1] Seeman NC. DNA in a material world. *Nature*. 2003;421:427-31.
- [2] Dimitrov D. Therapeutic proteins. In: Voynov V, Caravella JA, editors. *Therapeutic proteins*: Humana Press; 2012;1-26.
- [3] Leader B, Baca QJ, Golan DE. Protein therapeutics: a summary and pharmacological classification. *Nature Reviews Drug Discovery*. 2008;7:21-39.
- [4] Gauthier MA, Klok H-A. Polymer-protein conjugates: an enzymatic activity perspective. *Polymer Chemistry*. 2010;1:1352-73.
- [5] Cong Y, Pawlisch E, Bryant P, Balan S, Laurine E, Tommasi R, et al. Site-specific PEGylation at histidine tags. *Bioconjugate Chemistry*. 2012;23:248-63.
- [6] Knop K, Hoogenboom R, Fischer D, Schubert US. Poly(ethylene glycol) in drug delivery: pros and cons as well as potential alternatives. *Angewandte Chemie International Edition*. 2010;49:6288-308.
- [7] Duncan R. Polymer conjugates as anticancer nanomedicines. *Nature reviews cancer*. 2006;6:688-701.
- [8] Kochendoerfer GG. Site-specific polymer modification of therapeutic proteins. *Current Opinion in Chemical Biology*. 2005;9:555-60.
- [9] Wang L, Xie J, Schultz PG. Expanding the genetic code. *Annual Review of Biophysics and Biomolecular Structure*. 2006;35:225-49.
- [10] Wang L, Schultz PG. Expanding the genetic code. *Angewandte Chemie International Edition*. 2005;44:34-66.
- [11] Duncan R. The dawning era of polymer therapeutics. *Nature Reviews Drug Discovery*. 2003;2:347-60.
- [12] Haag R, Kratz F. Polymer therapeutics: concepts and applications. *Angewandte Chemie International Edition*. 2006;45:1198-215.
- [13] Vicent MJ, Duncan R. Polymer conjugates: nanosized medicines for treating cancer. *Trends in Biotechnology*. 2006;24:39-47.
- [14] Kedracki D, Safir I, Gour N, Ngo K, Vebert-Nardin C. DNA-polymer conjugates: from synthesis, through complex formation and self-assembly to applications. In: Schlaad H, editor. *Bio-synthetic Polymer Conjugates*: Springer Berlin Heidelberg; 2013. p. 115-49.
- [15] Tao L, Liu J, Xu J, Davis TP. Bio-reversible polyPEGylation. *Chemical Communications*. 2009:6560-2.
- [16] Broyer RM, Grover GN, Maynard HD. Emerging synthetic approaches for protein-polymer conjugations. *Chemical Communications*. 2011;47:2212-26.
- [17] Hermanson GT. Chapter 2 - The Chemistry of Reactive Groups. In: Hermanson GT, editor. *Bioconjugate Techniques (Second Edition)*. New York: Academic Press; 2008. p. 169-212.
- [18] Pasut G, Veronese F. PEGylation of Proteins as Tailored Chemistry for Optimized Bioconjugates. In: Satchi-Fainaro R, Duncan R, editors. *Polymer Therapeutics I*: Springer Berlin Heidelberg; 2006;95-134.
- [19] Roberts MJ, Bentley MD, Harris JM. Chemistry for peptide and protein PEGylation. *Advanced Drug Delivery Reviews*. 2002;54:459-76.
- [20] Kwak M, Herrmann A. Nucleic acid amphiphiles: synthesis and self-assembled nanostructures. *Chemical Society Reviews*. 2011;40:5745-55.
- [21] Le Droumaguet B, Nicolas J. Recent advances in the design of bioconjugates from controlled/living radical polymerization. *Polymer Chemistry*. 2010;1:563-98.

- [22] Bontempo D, Heredia KL, Fish BA, Maynard HD. Cysteine-reactive polymers synthesized by atom transfer radical polymerization for conjugation to proteins. *Journal of the American Chemical Society*. 2004;126:15372-3.
- [23] Liu J, Bulmus V, Barner-Kowollik C, Stenzel MH, Davis TP. Direct synthesis of pyridyl disulfide-terminated polymers by RAFT polymerization. *Macromolecular Rapid Communications*. 2007;28:305-14.
- [24] Rush AM, Thompson MP, Tatro ET, Gianneschi NC. Nuclease-resistant DNA via high-density packing in polymeric micellar nanoparticle coronas. *ACS Nano*. 2013;7:1379-87.
- [25] Seferos DS, Prigodich AE, Giljohann DA, Patel PC, Mirkin CA. Polyvalent DNA nanoparticle conjugates stabilize nucleic acids. *Nano Letters*. 2008;9:308-11.
- [26] Heredia KL, Maynard HD. Synthesis of protein-polymer conjugates. *Organic & Biomolecular Chemistry*. 2007;5:45-53.
- [27] Koshland DE. Application of a theory of enzyme specificity to protein synthesis. *Proceedings of the National Academy of Sciences*. 1958;44:98-104.
- [28] Frauenfelder H, Sligar SG, Wolynes PG. The energy landscapes and motions of proteins. *Science*. 1991;254:1598-603.
- [29] Boehr DD, Nussinov R, Wright PE. The role of dynamic conformational ensembles in biomolecular recognition. *Nature Chemical Biology*. 2009;5:789-96.
- [30] Malmstadt N, Hyre DE, Ding Z, Hoffman AS, Stayton PS. Affinity thermoprecipitation and recovery of biotinylated biomolecules via a mutant streptavidin-smart polymer conjugate. *Bioconjugate Chemistry*. 2003;14:575-80.
- [31] Star A, Gabriel J-CP, Bradley K, Grüner G. Electronic detection of specific protein binding using nanotube FET devices. *Nano Letters*. 2003;3:459-63.
- [32] Li M, Wong KKW, Mann S. Organization of inorganic nanoparticles using biotin-streptavidin connectors. *Chemistry of Materials*. 1998;11:23-6.
- [33] Caswell KK, Wilson JN, Bunz UHF, Murphy CJ. Preferential end-to-end assembly of gold nanorods by biotin-streptavidin connectors. *Journal of the American Chemical Society*. 2003;125:13914-5.
- [34] Soong RK, Bachand GD, Neves HP, Olkhovets AG, Craighead HG, Montemagno CD. Powering an inorganic nanodevice with a biomolecular motor. *Science*. 2000;290:1555-8.
- [35] Bontempo D, Maynard HD. Streptavidin as a macroinitiator for polymerization: in situ protein-polymer conjugate formation. *Journal of the American Chemical Society*. 2005;127:6508-9.
- [36] Heredia KL, Bontempo D, Ly T, Byers JT, Halstenberg S, Maynard HD. In situ preparation of protein-“smart” polymer conjugates with retention of bioactivity. *Journal of the American Chemical Society*. 2005;127:16955-60.
- [37] Gao W, Liu W, Mackay JA, Zalutsky MR, Toone EJ, Chilkoti A. In situ growth of a stoichiometric PEG-like conjugate at a protein's N-terminus with significantly improved pharmacokinetics. *Proceedings of the National Academy of Sciences*. 2009;106:15231-6.
- [38] Boyer C, Bulmus V, Liu J, Davis TP, Stenzel MH, Barner-Kowollik C. Well-defined protein-polymer conjugates via in situ RAFT polymerization. *Journal of the American Chemical Society*. 2007;129:7145-54.
- [39] Goffin V, Touraine P. Pegvisomant. *Pharmacia. Current opinion in investigational drugs* (London, England: 2000). 2002;3:752-7.
- [40] Yamamoto Y, Tsutsumi Y, Yoshioka Y, Nishibata T, Kobayashi K, Okamoto T, et al. Site-specific PEGylation of a lysine-deficient TNF-[alpha] with full bioactivity. *Nature Biotechnology*. 2003;21:546-52.

- [41] Gilmore JM, Scheck RA, Esser-Kahn AP, Joshi NS, Francis MB. N-terminal protein modification through a biomimetic transamination reaction. *Angewandte Chemie International Edition*. 2006;45:5307-11.
- [42] Baker DP, Lin EY, Lin K, Pellegrini M, Petter RC, Chen LL, et al. N-Terminally PEGylated human interferon- β -1a with improved pharmacokinetic properties and in vivo efficacy in a melanoma angiogenesis Model. *Bioconjugate Chemistry*. 2005;17:179-88.
- [43] Muir TW. Semisynthesis of proteins by expressed protein ligation. *Annual Review of Biochemistry*. 2003;72:249-89.
- [44] Tam JP, Yu Q, Miao Z. Orthogonal ligation strategies for peptide and protein. *Peptide Science*. 1999;51:311-32.
- [45] Chen JK, Lane WS, Brauer AW, Tanaka A, Schreiber SL. Biased combinatorial libraries: novel ligands for the SH3 domain of phosphatidylinositol 3-kinase. *Journal of the American Chemical Society*. 1993;115:12591-2.
- [46] Li X, Zhang L, Hall SE, Tam * JP. A new ligation method for N-terminal tryptophan-containing peptides using the Pictet–Spengler reaction. *Tetrahedron Letters*. 2000;41:4069-73.
- [47] Dixon HBF. N-terminal modification of proteins—a review. *Journal of Protein Chemistry*. 1984;3:99-108.
- [48] Wu P, Shui W, Carlson BL, Hu N, Rabuka D, Lee J, et al. Site-specific chemical modification of recombinant proteins produced in mammalian cells by using the genetically encoded aldehyde tag. *Proceedings of the National Academy of Sciences*. 2009;106:3000-5.
- [49] Lata S, Gavutis M, Tampé R, Piehler J. Specific and stable fluorescence labeling of histidine-tagged proteins for dissecting multi-Protein complex formation. *Journal of the American Chemical Society*. 2006;128:2365-72.
- [50] You C, Wilmes S, Beutel O, Löchte S, Podoplelowa Y, Roder F, et al. Self-controlled monofunctionalization of quantum dots for multiplexed protein tracking in live cells. *Angewandte Chemie International Edition*. 2010;49:4108-12.
- [51] Kim TH, Swierczewska M, Oh Y, Kim A, Jo DG, Park JH, et al. Mix to validate: a facile, reversible PEGylation for fast screening of potential therapeutic proteins in vivo. *Angewandte Chemie International Edition*. 2013;52:6880-4.
- [52] Lata S, Reichel A, Brock R, Tampé R, Piehler J. High-affinity adaptors for switchable recognition of histidine-tagged proteins. *Journal of the American Chemical Society*. 2005;127:10205-15.
- [53] Lees WJ, Spaltenstein A, Kingery-Wood JE, Whitesides GM. Polyacrylamides bearing pendant. α -sialoside groups strongly inhibit agglutination of erythrocytes by influenza a virus: multivalency and steric stabilization of particulate biological systems. *Journal of Medicinal Chemistry*. 1994;37:3419-33.
- [54] Mammen M, Dahmann G, Whitesides GM. Effective inhibitors of hemagglutination by influenza virus synthesized from polymers having active ester groups. insight into mechanism of inhibition. *Journal of Medicinal Chemistry*. 1995;38:4179-90.
- [55] Mammen M, Choi S-K, Whitesides GM. Polyvalent interactions in biological systems: implications for design and use of multivalent ligands and inhibitors. *Angewandte Chemie International Edition*. 1998;37:2754-94.
- [56] Cairo CW, Gestwicki JE, Kanai M, Kiessling LL. Control of multivalent interactions by binding epitope density. *Journal of the American Chemical Society*. 2002;124:1615-9.

- [57] Griffith BR, Allen BL, Rapraeger AC, Kiessling LL. A polymer scaffold for protein oligomerization. *Journal of the American Chemical Society*. 2004;126:1608-9.
- [58] Ballico M, Drioli S, Morvan F, Xodo L, Bonora GM. Triple, MPEG-Conjugated, Helix-Forming Oligonucleotides (TRIPEGXs): Liquid-phase synthesis of natural and chimeric "all-purine" sequences linked to high molecular weight poly(ethylene glycols). *Bioconjugate Chemistry*. 2001;12:719-25.
- [59] Wilner OI, Weizmann Y, Gill R, Lioubashevski O, Freeman R, Willner I. Enzyme cascades activated on topologically programmed DNA scaffolds. *Nature Nanotechnology*. 2009;4:249-54.
- [60] Fu J, Yang YR, Johnson-Buck A, Liu M, Liu Y, Walter NG, et al. Multi-enzyme complexes on DNA scaffolds capable of substrate channelling with an artificial swinging arm. *Nature Nanotechnology*. 2014;9:531-6.
- [61] Langowska K, Palivan CG, Meier W. Polymer nanoreactors shown to produce and release antibiotics locally. *Chemical Communications*. 2013;49:128-30.
- [62] Palivan CG, Fischer-Onaca O, Delcea M, Itef F, Meier W. Protein-polymer nanoreactors for medical applications. *Chemical Society Reviews*. 2012;41:2800-23.
- [63] Broz P, Driamov S, Ziegler J, Ben-Haim N, Marsch S, Meier W, et al. Toward intelligent nanosize bioreactors: a pH-switchable, channel-equipped, functional polymer nanocontainer. *Nano Letters*. 2006;6:2349-53.
- [64] Discher DE, Eisenberg A. Polymer vesicles. *Science*. 2002;297:967-73.
- [65] Wu D, Spulber M, Itef F, Chami M, Pfohl T, Palivan CG, et al. Effect of molecular parameters on the architecture and membrane properties of 3D assemblies of amphiphilic copolymers. *Macromolecules*. 2014;47:5060-9.
- [66] Nardin C, Thoeni S, Widmer J, Winterhalter M, Meier W. Nanoreactors based on (polymerized) ABA-triblock copolymer vesicles. *Chemical Communications*. 2000:1433-4.
- [67] van Dongen SFM, Nallani M, Cornelissen JJLM, Nolte RJM, van Hest JCM. A three-enzyme cascade reaction through positional assembly of enzymes in a polymersome nanoreactor. *Chemistry – A European Journal*. 2009;15:1107-14.
- [68] Tanner P, Onaca O, Balasubramanian V, Meier W, Palivan CG. Enzymatic cascade reactions inside polymeric nanocontainers: a means to combat oxidative stress. *Chemistry – A European Journal*. 2011;17:4552-60.
- [69] Xie W, He F, Wang B, Chung T-S, Jeyaseelan K, Armugam A, et al. An aquaporin-based vesicle-embedded polymeric membrane for low energy water filtration. *Journal of Materials Chemistry A*. 2013;1:7592-600.
- [70] Peters RJRW, Louzao I, van Hest JCM. From polymeric nanoreactors to artificial organelles. *Chemical Science*. 2012;3:335-42.
- [71] Choi H-J, Montemagno CD. Artificial Organelle: ATP synthesis from cellular mimetic polymersomes. *Nano Letters*. 2005;5:2538-42.
- [72] Tanner P, Balasubramanian V, Palivan CG. Aiding nature's organelles: artificial peroxisomes play their role. *Nano Letters*. 2013;13:2875-83.
- [73] Blanz A, Armes SP, Ryan AJ. Self-assembled block copolymer aggregates: from micelles to vesicles and their biological applications. *Macromolecular Rapid Communications*. 2009;30:267-77.
- [74] Ayaz MS, Kwak M, Alemdaroglu FE, Wang J, Berger R, Herrmann A. Synthesis of DNA block copolymers with extended nucleic acid segments by enzymatic ligation: cut and paste large hybrid architectures. *Chemical Communications*. 2011;47:2243-5.

- [75] Kedracki D, Maroni P, Schlaad H, Vebert-Nardin C. Polymer–aptamer hybrid emulsion templating yields bioresponsive nanocapsules. *Advanced Functional Materials*. 2014;24:1133-9.
- [76] Jeong JH, Kim SW, Park TG. A new antisense oligonucleotide delivery system based on self-assembled ODN–PEG hybrid conjugate micelles. *Journal of Controlled Release*. 2003;93:183-91.
- [77] Oishi M, Sasaki S, Nagasaki Y, Kataoka K. pH-responsive oligodeoxynucleotide (ODN)–poly(Ethylene Glycol) conjugate through acid-labile β -thiopropionate linkage: preparation and polyion complex micelle formation. *Biomacromolecules*. 2003;4:1426-32.
- [78] Baumann P, Balasubramanian V, Onaca-Fischer O, Sienkiewicz A, Palivan CG. Light-responsive polymer nanoreactors: a source of reactive oxygen species on demand. *Nanoscale*. 2013;5:217-24.
- [79] Lee JS, Feijen J. Polymersomes for drug delivery: design, formation and characterization. *Journal of Controlled Release*. 2012;161:473-83.
- [80] Kim KT, Meeuwissen SA, Nolte RJM, van Hest JCM. Smart nanocontainers and nanoreactors. *Nanoscale*. 2010;2:844-58.
- [81] Nallani M, de Hoog H-PM, Cornelissen JJLM, Palmans ARA, van Hest JCM, Nolte RJM. Polymersome nanoreactors for enzymatic ring-opening polymerization. *Biomacromolecules*. 2007;8:3723-8.
- [82] Roh YH, Ruiz RCH, Peng S, Lee JB, Luo D. Engineering DNA-based functional materials. *Chemical Society Reviews*. 2011;40:5730-44.
- [83] Zhang G, Surwade SP, Zhou F, Liu H. DNA nanostructure meets nanofabrication. *Chemical Society Reviews*. 2013;42:2488-96.
- [84] Paar JM, Harris NT, Holowka D, Baird B. Bivalent ligands with rigid double-stranded DNA spacers reveal structural constraints on signaling by RI. *The Journal of Immunology*. 2002;169:856-64.
- [85] Keller S, Marx A. The use of enzymes for construction of DNA-based objects and assemblies. *Chemical Society Reviews*. 2011;40:5690-7.
- [86] Petros RA, DeSimone JM. Strategies in the design of nanoparticles for therapeutic applications. *Nature Reviews Drug Discovery*. 2010;9:615-27.
- [87] Park SY, Lytton-Jean AKR, Lee B, Weigand S, Schatz GC, Mirkin CA. DNA-programmable nanoparticle crystallization. *Nature*. 2008;451:553-6.
- [88] Cao YC, Jin R, Mirkin CA. Nanoparticles with raman spectroscopic fingerprints for DNA and RNA detection. *Science*. 2002;297:1536-40.
- [89] Loyer A, Scangos GA, Ruddle FH. Mechanisms of DNA uptake by mammalian cells: fate of exogenously added DNA monitored by the use of fluorescent dyes. *Proceedings of the National Academy of Sciences*. 1982;79:422-6.
- [90] Kim D, Jeong YY, Jon S. A drug-loaded aptamer–gold nanoparticle bioconjugate for combined CT imaging and therapy of prostate cancer. *ACS Nano*. 2010;4:3689-96.
- [91] Storhoff JJ, Lucas AD, Garimella V, Bao YP, Muller UR. Homogeneous detection of unamplified genomic DNA sequences based on colorimetric scatter of gold nanoparticle probes. *Nature Biotechnology*. 2004;22:883-7.
- [92] Lee K, Drachev VP, Irudayaraj J. DNA–gold nanoparticle reversible networks grown on cell surface marker sites: application in diagnostics. *ACS Nano*. 2011;5:2109-17.

- [93] Oh J-H, Lee J-S. Designed hybridization properties of DNA–gold nanoparticle conjugates for the ultrasensitive detection of a single-base mutation in the breast cancer gene BRCA1. *Analytical Chemistry*. 2011;83:7364-70.
- [94] Ogris M, Walker G, Blessing T, Kircheis R, Wolschek M, Wagner E. Tumor-targeted gene therapy: strategies for the preparation of ligand–polyethylene glycol–polyethylenimine/DNA complexes. *Journal of Controlled Release*. 2003;91:173-81.
- [95] Mansouri S, Cuie Y, Winnik F, Shi Q, Lavigne P, Benderdour M, et al. Characterization of folate-chitosan-DNA nanoparticles for gene therapy. *Biomaterials*. 2006;27:2060-5.
- [96] Ding K, Alemdaroglu FE, Börsch M, Berger R, Herrmann A. Engineering the structural properties of DNA block copolymer micelles by molecular recognition. *Angewandte Chemie International Edition*. 2007;46:1172-5.
- [97] Bonora G, Tocco G, Zaramella S, Veronese F, Pliasunova O, Pokrovsky A, et al. Antisense activity of an anti-HIV oligonucleotide conjugated to linear and branched high molecular weight polyethylene glycols. *Il Farmaco*. 1998;53:634-7.
- [98] Immoos CE, Lee SJ, Grinstaff MW. DNA-PEG-DNA triblock macromolecules for reagentless DNA detection. *Journal of the American Chemical Society*. 2004;126:10814-5.
- [99] Schnitzler T, Herrmann A. DNA block copolymers: functional materials for nanoscience and biomedicine. *Accounts of Chemical Research*. 2012;45:1419-30.
- [100] Alemdaroglu FE, Herrmann A. DNA meets synthetic polymers-highly versatile hybrid materials. *Organic & Biomolecular Chemistry*. 2007;5:1311-20.
- [101] Alemdaroglu FE, Zhuang W, Zöphel L, Wang J, Berger R, Rabe JP, et al. Generation of multiblock copolymers by PCR: synthesis, visualization and nanomechanical properties. *Nano Letters*. 2009;9:3658-62.
- [102] Fong RB, Ding Z, Long CJ, Hoffman AS, Stayton PS. Thermoprecipitation of streptavidin via oligonucleotide-mediated self-assembly with poly(N-isopropylacrylamide). *Bioconjugate Chemistry*. 1999;10:720-5.
- [103] Umeno D, Maeda M. Single stranded DNA-poly(N-isopropylacrylamide) conjugate for affinity precipitation separation of oligonucleotides. *Chemical Communications*. 1998:1433-4.
- [104] Rodríguez-Pulido A, Kondrachuk AI, Prusty DK, Gao J, Loi MA, Herrmann A. Light-triggered sequence-specific cargo release from DNA block copolymer–lipid vesicles. *Angewandte Chemie International Edition*. 2013;125:1042-6.
- [105] Liu K, Zheng L, Liu Q, de Vries JW, Gerasimov JY, Herrmann A. Nucleic acid chemistry in the organic phase: from functionalized oligonucleotides to DNA side chain polymers. *Journal of the American Chemical Society*. 2014;136:14255-62.
- [106] Alemdaroglu FE, Wang J, Börsch M, Berger R, Herrmann A. Enzymatic control of the size of DNA block copolymer nanoparticles. *Angewandte Chemie International Edition*. 2008;47:974-6.
- [107] Alemdaroglu FE, Ding K, Berger R, Herrmann A. DNA-templated synthesis in three dimensions: introducing a micellar scaffold for organic reactions. *Angewandte Chemie International Edition*. 2006;45:4206-10.
- [108] Chien M-P, Rush AM, Thompson MP, Gianneschi NC. Programmable shape-shifting micelles. *Angewandte Chemie International Edition*. 2010;49:5076-80.
- [109] Alemdaroglu FE, Alemdaroglu NC, Langguth P, Herrmann A. Cellular uptake of DNA block copolymer micelles with different shapes. *Macromolecular Rapid Communications*. 2008;29:326-9.

- [110] Rush AM, Nelles DA, Blum AP, Barnhill SA, Tatro ET, Yeo GW, et al. Intracellular mRNA regulation with self-Assembled locked nucleic acid polymer nanoparticles. *Journal of the American Chemical Society*. 2014;136:7615-8.
- [111] Banga RJ, Chernyak N, Narayan SP, Nguyen ST, Mirkin CA. Liposomal spherical nucleic acids. *Journal of the American Chemical Society*. 2014;136:9866-9.
- [112] Alemdaroglu FE, Safak M, Wang J, Berger R, Herrmann A. DNA multiblock copolymers. *Chemical Communications*. 2007:1358-9.
- [113] Fogleman EA, Yount WC, Xu J, Craig SL. Modular, Well-behaved reversible polymers from DNA-based monomers. *Angewandte Chemie International Edition*. 2002;41:4026-8.
- [114] Jeong JH, Kim SW, Park TG. Novel intracellular delivery system of antisense oligonucleotide by self-Assembled hybrid micelles composed of DNA/PEG conjugate and cationic fusogenic peptide. *Bioconjugate Chemistry*. 2003;14:473-9.
- [115] Li Z, Zhang Y, Fullhart P, Mirkin CA. Reversible and chemically programmable micelle assembly with DNA block-copolymer amphiphiles. *Nano Letters*. 2004;4:1055-8.
- [116] Kwak M, Minten IJ, Anaya D-M, Musser AJ, Brasch M, Nolte RJM, et al. Virus-like particles templated by DNA micelles: a general method for loading virus nanocarriers. *Journal of the American Chemical Society*. 2010;132:7834-5.
- [117] Cottenye N, Syga M-I, Nosov S, Muller AHE, Ploux L, Vebert-Nardin C. Biological-like vesicular structures self-assembled from DNA-block copolymers. *Chemical Communications*. 2012;48:2615-7.
- [118] Lee D-E, Na JH, Lee S, Kang CM, Kim HN, Han SJ, et al. Facile method To radiolabel glycol chitosan nanoparticles with ^{64}Cu via copper-free click chemistry for microPET imaging. *Molecular Pharmaceutics*. 2013;10:2190-8.
- [119] Kwak M, Musser AJ, Lee J, Herrmann A. DNA-functionalised blend micelles: mix and fix polymeric hybrid nanostructures. *Chemical Communications*. 2010;46:4935-7.
- [120] Alemdaroglu FE, Alemdaroglu NC, Langguth P, Herrmann A. DNA block copolymer micelles – a combinatorial tool for cancer nanotechnology. *Advanced Materials*. 2008;20:899-902.
- [121] Hornung V, Latz E. Intracellular DNA recognition. *Nature Reviews Immunology*. 2010;10:123-30.
- [122] Jeong JH, Kim SH, Kim SW, Park TG. Polyelectrolyte complex micelles composed of c-raf antisense oligodeoxynucleotide–poly(ethylene glycol) conjugate and poly(ethylenimine): effect of systemic administration on tumor growth. *Bioconjugate Chemistry*. 2005;16:1034-7.
- [123] Baron R, McCammon JA. Molecular recognition and ligand association. *Annual Review of Physical Chemistry*. 2013;64:151-75.
- [124] Fischer E. Ueber den einfluss der konfiguration auf die wirkung der enzyme III. *Berichte der deutschen chemischen Gesellschaft*. 1895;28:1429-38.
- [125] Csermely P, Palotai R, Nussinov R. Induced fit, conformational selection and independent dynamic segments: an extended view of binding events. *Trends in biochemical sciences*. 2010;35:539-46.
- [126] Zhao Z, Wang L, Liu Y, Yang Z, He Y-M, Li Z, et al. pH-induced morphology-shifting of DNA-b-poly(propylene oxide) assemblies. *Chemical Communications*. 2012;48:9753-5.
- [127] Alconcel SNS, Baas AS, Maynard HD. FDA-approved poly(ethylene glycol)-protein conjugate drugs. *Polymer Chemistry*. 2011;2:1442-8.

- [128] Chilkoti A, Chen G, Stayton PS, Hoffman AS. Site-specific conjugation of a temperature-sensitive polymer to a genetically engineered protein. *Bioconjugate Chemistry*. 1994;5:504-7.
- [129] Malmstadt N, Hyre DE, Ding Z, Hoffman AS, Stayton PS. Affinity thermoprecipitation and recovery of biotinylated biomolecules via a mutant streptavidin-smart polymer conjugate. *Bioconjugate Chemistry*. 2003;14:575-80.
- [130] Jeppesen C, Wong JY, Kuhl TL, Israelachvili JN, Mullah N, Zalipsky S, et al. Impact of polymer tether length on multiple ligand-receptor bond formation. *Science*. 2001;293:465-8.
- [131] Colonne M, Chen Y, Wu K, Freiberg S, Giasson S, Zhu XX. Binding of streptavidin with biotinylated thermosensitive nanospheres based on poly(N,N-diethylacrylamide-co-2-hydroxyethyl methacrylate). *Bioconjugate Chemistry*. 2007;18:999-1003.
- [132] Huang N-P, Vörös J, De Paul SM, Textor M, Spencer ND. Biotin-derivatized poly(l-lysine)-g-poly(ethylene glycol): a novel polymeric interface for bioaffinity sensing. *Langmuir*. 2001;18:220-30.
- [133] Biedermann F, Rauwald U, Zayed JM, Scherman OA. A supramolecular route for reversible protein-polymer conjugation. *Chemical Science*. 2011;2:279-86.
- [134] Coué G, Engbersen JFJ. Functionalized linear poly(amidoamine)s are efficient vectors for intracellular protein delivery. *Journal of Controlled Release*. 2011;152:90-8.
- [135] Tsiourvas D, Sideratou Z, Sterioti N, Papadopoulos A, Nounesis G, Paleos CM. Insulin complexes with PEGylated basic oligopeptides. *Journal of Colloid and Interface Science*. 2012;384:61-72.
- [136] Pelegri-O'Day EM, Lin E-W, Maynard HD. Therapeutic protein-polymer conjugates: advancing beyond PEGylation. *Journal of the American Chemical Society*. 2014;136:14323-32.
- [137] Hsu S-TD, Blaser G, Behrens C, Cabrita LD, Dobson CM, Jackson SE. Folding study of venus reveals a strong ion dependence of its yellow fluorescence under mildly acidic conditions. *Journal of Biological Chemistry*. 2010;285:4859-69.
- [138] Anderson DE, Bechtel WJ, Dahlquist FW. pH-Induced denaturation of proteins: a single salt bridge contributes 3-5 kcal/mol to the free energy of folding of T4 lysozyme. *Biochemistry*. 1990;29:2403-8.
- [139] Graff A, Sauer M, Van Gelder P, Meier W. Virus-assisted loading of polymer nanocontainer. *Proceedings of the National Academy of Sciences*. 2002;99:5064-8.
- [140] Meier W, Nardin C, Winterhalter M. Reconstitution of channel proteins in (polymerized) ABA triblock copolymer membranes. *Angewandte Chemie International Edition*. 2000;39:4599-602.
- [141] Jones M-C, Leroux J-C. Polymeric micelles – a new generation of colloidal drug carriers. *European Journal of Pharmaceutics and Biopharmaceutics*. 1999;48:101-11.
- [142] Kwon GS, Okano T. Polymeric micelles as new drug carriers. *Advanced Drug Delivery Reviews*. 1996;21:107-16.
- [143] Kedracki D, Chekini M, Maroni P, Schlaad H, Nardin C. Synthesis and self-Assembly of a DNA molecular brush. *Biomacromolecules*. 2014;15:3375-82.
- [144] Gaucher G, Dufresne M-H, Sant VP, Kang N, Maysinger D, Leroux J-C. Block copolymer micelles: preparation, characterization and application in drug delivery. *Journal of Controlled Release*. 2005;109:169-88.

- [145] Kedar U, Phutane P, Shidhaye S, Kadam V. Advances in polymeric micelles for drug delivery and tumor targeting. *Nanomedicine: Nanotechnology, Biology and Medicine*. 2010;6:714-29.
- [146] Levashov AV, Khmel'nitsky YL, Klyachko NL, Chernyak VY, Martinek K. Enzymes entrapped into reversed micelles in organic solvents: Sedimentation analysis of the protein—aerosol OT-H₂O-Octane system. *Journal of Colloid and Interface Science*. 1982;88:444-57.
- [147] Jolivalt C, Minier M, Renon H. Extraction of α -chymotrypsin using reversed micelles. *Journal of Colloid and Interface Science*. 1990;135:85-96.
- [148] Khmel'nitsky YL, Gladilin AK, Roubailo VL, Martinek K, Levashov AV. Reversed micelles of polymeric surfactants in nonpolar organic solvents. *European Journal of Biochemistry*. 1992;206:737-45.
- [149] Wang X, Liu G, Hu J, Zhang G, Liu S. Concurrent block copolymer polymersome stabilization and bilayer permeabilization by stimuli-regulated “traceless” crosslinking. *Angewandte Chemie International Edition*. 2014;53:3138-42.
- [150] Spulber M, Najer A, Winkelbach K, Glaied O, Waser M, Pieleš U, et al. Photoreaction of a hydroxyalkylphenone with the membrane of polymersomes: A versatile method to generate semipermeable nanoreactors. *Journal of the American Chemical Society*. 2013;135:9204-12.
- [151] Moll D, Huber C, Schlegel B, Pum D, Sleytr UB, Sára M. S-layer-streptavidin fusion proteins as template for nanopatterned molecular arrays. *Proceedings of the National Academy of Sciences*. 2002;99:14646-51.
- [152] Rosi NL, Giljohann DA, Thaxton CS, Lytton-Jean AKR, Han MS, Mirkin CA. Oligonucleotide-modified gold nanoparticles for intracellular gene regulation. *Science*. 2006;312:1027-30.
- [153] Pelegri-O'Day EM, Lin E-W, Maynard HD. Therapeutic protein—polymer conjugates: advancing beyond PEGylation. *Journal of the American Chemical Society*. 2014;136:14323-32.
- [154] Jutz G, Böker A. Bionanoparticles as functional macromolecular building blocks – A new class of nanomaterials. *Polymer*. 2011;52:211-32.
- [155] Noji H, Yasuda R, Yoshida M, Kinosita K. Direct observation of the rotation of F₁-ATPase. *Nature*. 1997;386:299-302.

2. Polymer design and synthesis towards molecular recognition of his-tagged molecules

Adapted with permission from *J. Am. Chem. Soc.*, 2014, 136 (36), 12607–12614.

Copyright 2014 American Chemical Society.

2.1. Introduction

A key challenge in life science research and protein engineering is to modify, conjugate, immobilize and label the proteins selectively, while preserving their specificity and activity.[1-4] Because the random conjugation might lead to a significant decrease of the proteins activity due to the blocking of the access to the active site and the alternation of the structure, specific binding is highly desired.[5, 6] One of the most commonly employed approach for site-specific protein modification targets the cysteine residues from protein structures, because it is less frequent in the structure of various proteins.[7-9] Nevertheless, very few proteins present only one cysteine residue. Besides, the insertion of free cysteins by genetic engineering increases the risk of incorrect disulfide formation and protein dimerization.[10] Specific binding based on the molecular recognition represents an alternative for protein modification. Various specific binders, including natural binders such as biotin,[11] antibodies,[12] and synthesized chelators such as NTA,[13] iminodiacetic acid (IDA),[14] are commonly applied for the protein labeling, modification and immobilization. NTA and its derivatives gained more interest due to their ability to bond specifically only to his tag, which commonly exists on the proteins for the binding affinity purification.[15, 16] The interaction between metal-ion-chelating NTA (NTA-Me²⁺), such as NTA-Cu²⁺ and NTA-Ni²⁺, and his tag is stable, selective and switchable by competing agents such as imidazole and EDTA.[15, 17] The chelators containing multi-NTA exhibit an increased binding affinity towards his tag, especially trisNTA that shows the highest selectivity and affinity, 4 orders of magnitude higher comparing with NTA.[18] Moreover the interaction between trisNTA and His-tagged proteins is reversible in the presence of different agents. The presence of imidazole or EDTA can easily separate the His-tagged

proteins from trisNTA-Me²⁺ without disturbing the structure and activity of proteins.[18, 19] Therefore, trisNTA is an ideal candidate for the binding of his-tagged proteins. Fluorescent-labeled trisNTA and trisNTA quantum dot conjugates have been already used for the labeling and tracking of individual his-tagged proteins in live cells.[20-22] TrisNTA functionalized poly(butadiene)-*block*-poly(ethylene oxide) binds to His₆-eGFP without affecting its fluorescence.[23] However, to the best of our knowledge, the functionalization of polymers by trisNTA is limited to the terminal ends of the polymers and the applications of trisNTA-modified polymers remains at the simple conjugation between polymers and proteins.[23]

Here, we have synthesized a library of novel poly (N-isopropylacrylamide-*co*-trisnitrilotriacetic acid acrylamide)s polymers (PNTs), and complexed them with Cu²⁺ to serve for conjugation of his-tagged molecules. The target is to create a flexible polymer based model and apply it for the investigation of protein-protein interactions as a function of intermolecular distance. More details are presented in Chapter 3. First, the polymers were fully characterized by ¹H NMR and gel permeation chromatography (GPC). The amount of trisNTA in polymers was evaluated by ¹H NMR and acid-base titration. The coordination of copper to the trisNTA pockets was characterized by fourier transform infrared spectroscopy (FTIR), UV-vis spectroscopy, and electron paramagnetic resonance (EPR). Then, the binding of His₆ to trisNTA was proved and quantified by fast protein liquid chromatography (FPLC), FTIR, isothermal titration calorimetry (ITC) and EPR.

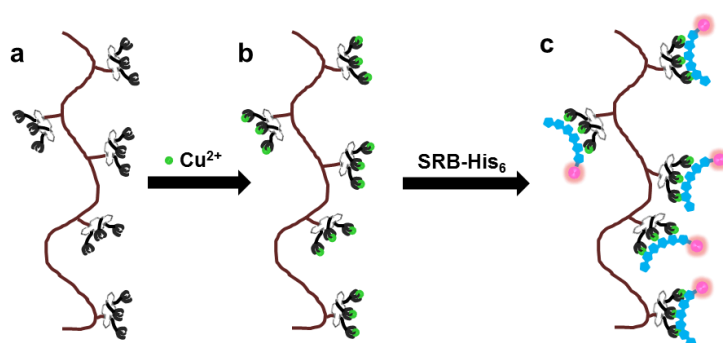


Figure 2-1. Schematic representation of PNTs, which coordinate Cu²⁺, and further bind to sulforhodamine B labelled His₆ (SRB-His₆).

2.2. Results and discussion

2.2.1. Synthesis and characterization

Tert-butyl ester protected PNTs (**3**) were synthesized by free radical polymerization of N-isopropylacrylamide (NIPAM) and *t*-butyl ester protected tris-nitrilotriacetic acid acrylate (prot-trisNTA) (**2**) using azobisisobutyronitrile (AIBN) as initiator (Scheme 2-1). PolyNIPAM was chosen due to its high hydrophilicity and biocompatibility. Molar ratios of prot-trisNTA and NIPAM in the range 1:99 and 10:90 were used for the polymerization in order to obtain polymers with different average distances between trisNTA binding sites (Table 2-1).

Scheme 2-1. Synthesis of prot-trisNTA and PNT copolymers.

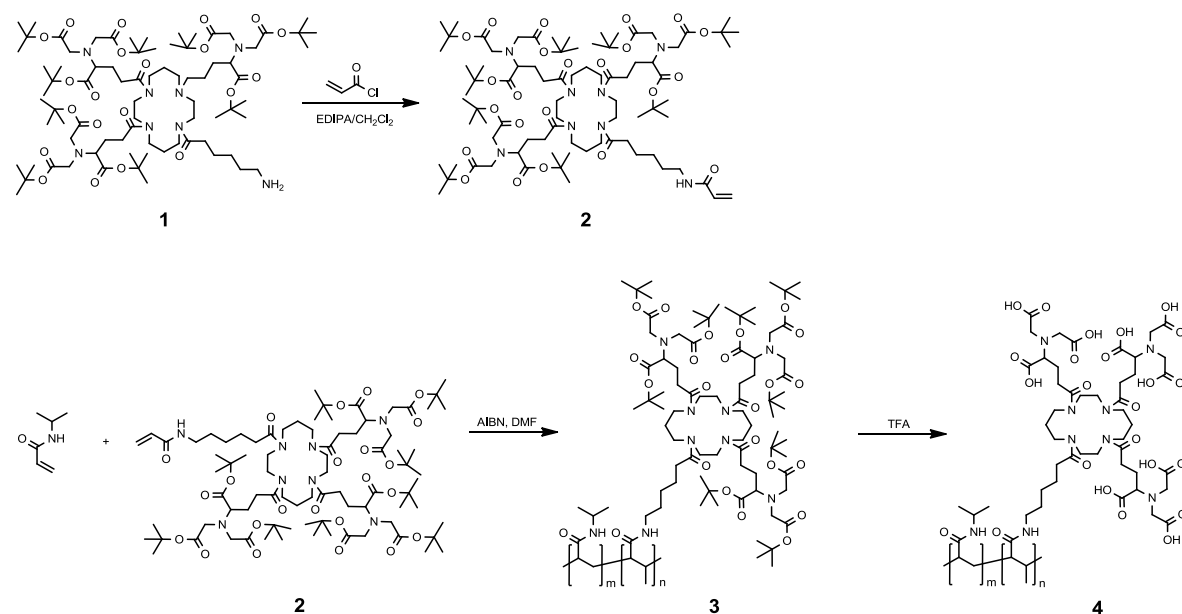


Table 2-1. Polymerization of PNTs. Molecular mass and polydispersity.

polymer code	Polymerization of protected PNTs						deprotection	
	prot-trisNTA (mol%)			Yield (%)	GPC results		Yield (%)	Mn ^c (×10 ⁴)
	in feed	in polymer ^a	In polymer ^b		Mn (×10 ⁴)	Mw/Mn		
PNT7	10.0	8.3	6.8	60	3.00	1.8	95	2.47
PNT4	5.0	4.2	4.1	63	2.95	1.8	69	2.59
PNT2	3.0	2.3	1.9	56	2.68	1.7	96	2.47
PNT1	1.0	0.8	0.8	55	3.45	1.7	94	3.34
PolyNIPAM	0	0	-	62	2.48	1.7	-	-

^a Calculated based on integration of the ¹H NMR spectrum. ^b Evaluated by acid-base titration. ^c The values were calculated based on the molecular mass, and polymer degree of protected PNTs obtained by GPC and ¹H NMR results, respectively.

The structure of prot-trisNTA was first confirmed by ¹H NMR (Figure 2-2). The peaks between $\delta=5.53$ ppm and $\delta=6.26$ ppm correspond to protons from acrylic groups. The peaks at $\delta=3.48$, $\delta=3.43$ and $\delta=3.38$ ppm correspond to protons from cyclam and NTA scaffolds. The large peak at $\delta=1.42$ and $\delta=1.38$ ppm correspond to protons from *tert*-butyl esters. The observed mass of 1630.1 for [MNa]⁺ by ESI-MS spectra was in agreement with the theoretical value of 1630.0. The formation of PNT copolymers with different trisNTA mol% was established by ¹H NMR (Figure 2-3). The characteristic peaks of prot-trisNTA appear at $\delta=3.44$ ppm, $\delta=3.50$ ppm, $\delta=1.48$ ppm and $\delta=1.45$ ppm, while the NIPAM peaks at $\delta=4.00$ ppm and $\delta=1.16$ ppm correspond to protons on –CH– and methyl groups. trisNTA contents of 0.8 - 8.3 in all copolymers was calculated from the ratios between the integrals of the peaks at $\delta=3.44$ ppm and $\delta=3.50$ ppm (from trisNTA), and the peak at $\delta=4.00$ ppm (from –CH– of NIPAM) (Figure 2-3).

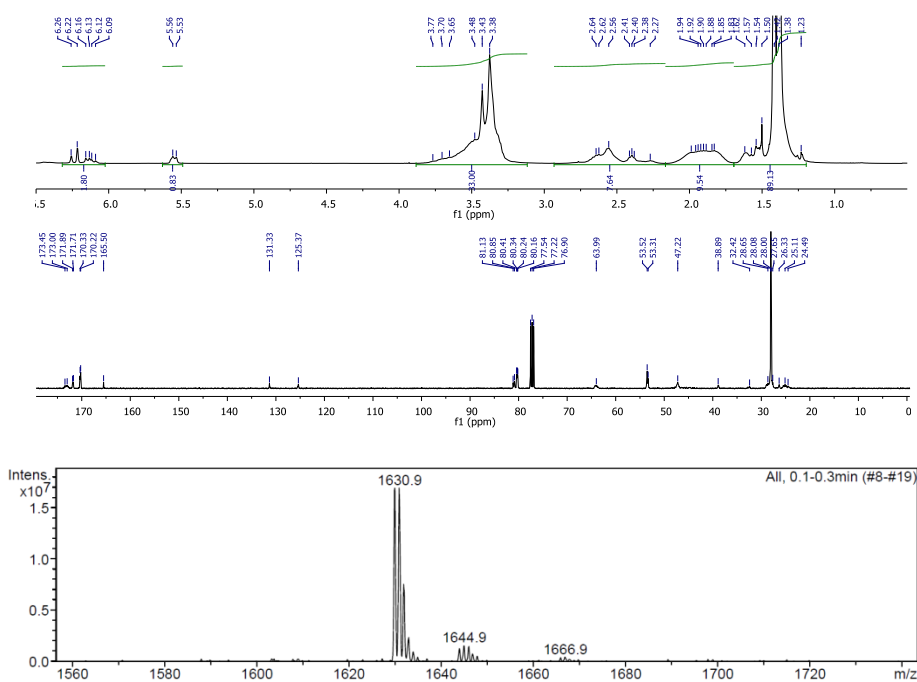


Figure 2-2. ¹H NMR, ¹³C NMR and ESI-MS of *prot*-trisNTA.

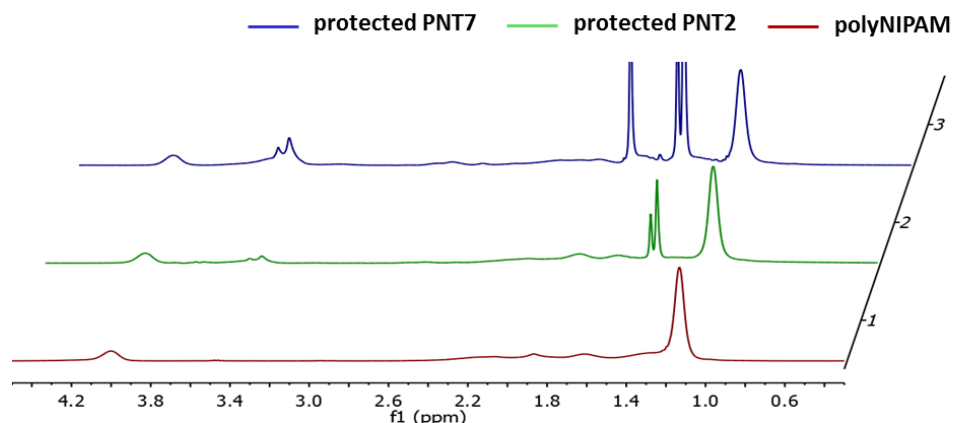


Figure 2-3. ^1H NMR spectra of PolyNIPAM and PNTs containing 2 mol% and 7 mol% of *prot*-trisNTA.

^1H NMR peaks at $\delta=1.43$ ppm and $\delta=1.40$ ppm (characteristic of *tert*-butyl ester groups) disappeared after the deprotection of the polymers, indicating a total deprotection (Figure 2-4). We used an acid-base titration to estimate the total trisNTA content (Table 2-1). These values were slightly lower than those obtained from ^1H NMR, because ^1H NMR can induce some systematic errors in the estimation of the molar ratio of trisNTA/NIPAM repeating units in polymers, due to baseline distortion. Thus we used the trisNTA mol% values obtained from acid-base titration for subsequent calculations.

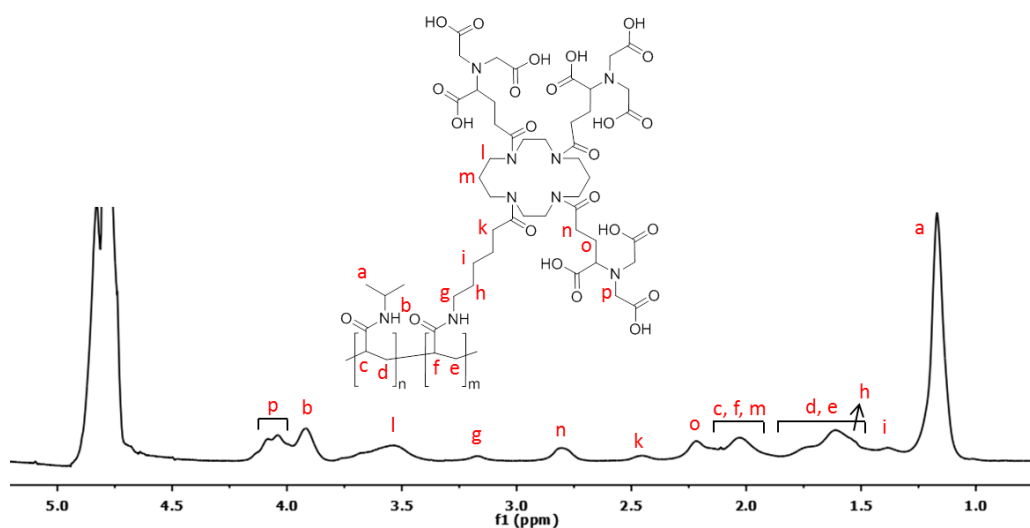


Figure 2-4. ^1H NMR spectrum of PNT7 after deprotection.

2.2.2. Temperature and pH responsiveness

It is important to understand the factors which might affect the binding ability, such as the stimuli-responsiveness of PNT copolymers. It's already been well-known that

PolyNIPAM undergoes phase transition around 32 °C. Copolymerization of NIPAM with hydrophilic or hydrophobic monomers changes the hydrophilic/hydrophobic balance and results in a shift of phase transition temperature to a higher or lower temperature, respectively [24, 25]. The thermo-responsiveness of PolyNIPAM also becomes pH-dependent after copolymerization with acrylic acid derivatives. Therefore, the phase transition of the library of PNT copolymers at different pH was assessed by UV-vis spectroscopy (Figure 2-5). In contrast to PolyNIPAM and copolymers composed of NIPAM and acrylic acid derivatives, such as poly (NIPAM-co-acrylic acid) ($pK_a=4.5$), [26] all PNT polymers showed no phase transition at $pH > 3$, because of the low pK_a values of NTA (1.9, 2.5 and 9.7). [27] 67% trisNTA units are ionized at $pH > 3$, resulting in a significant increase in hydrophilicity of the PNTs. At pH values < 2.3 , below the pK_{a2} of NTA, tris-NTA is partly protonated and exhibits hydrophobicity, resulting in a phase transition for PNT2 and PNT4. PNT7 with 6.8 mol% trisNTA only showed thermoresponsive behavior at pH values < 1.8 . A sharp phase transition for all five PNT copolymers was observed at $pH 1.0$. As the experiments were conducted in PBS buffer at room temperature, there was likely no aggregation of the PNTs copolymers.

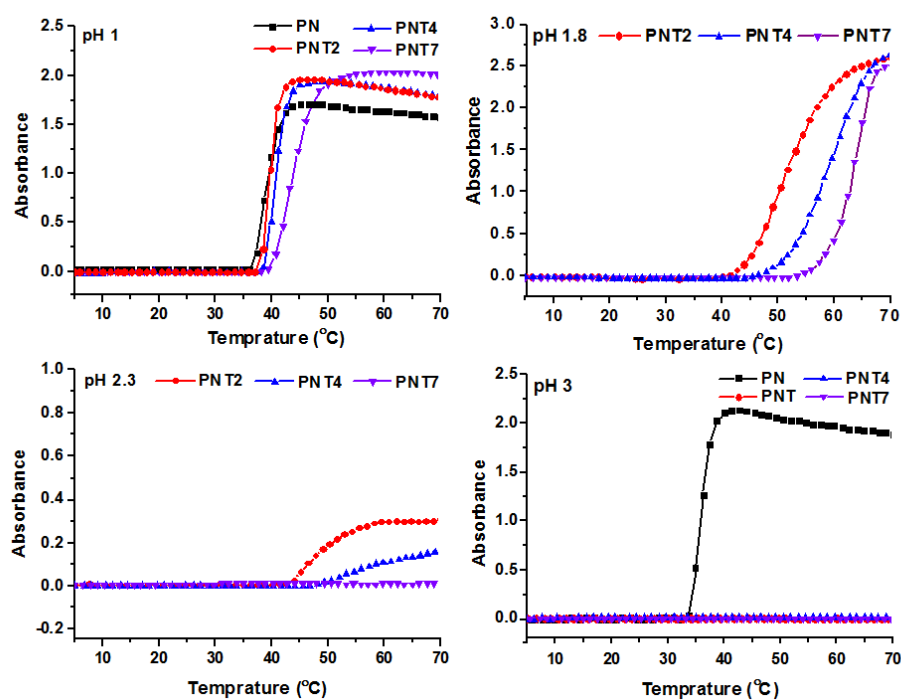


Figure 2-5. Absorbance dependence of temperature (5-70 °C) for PNT copolymers (1 mg/mL) at pH 1-3. His₆ binding behavior of trisNTA units from PNT copolymer.

2.2.3. Coordination of Cu²⁺ to PNT copolymers

It has already been reported that Cu²⁺ can coordinate to trisNTA pockets and the binding stoichiometry between trisNTA and Cu²⁺ is 1:3.[18] To investigate whether the conjugation of trisNTA to the polymers influences its coordination with Cu²⁺, FTIR experiments were first performed (Figure 2-6). The absorption band at 1723 cm⁻¹ assigned to C=O stretching vibration of carboxylic group on trisNTA, shifted to 1618 cm⁻¹ in the presence of Cu²⁺, indicating the coordination of Cu²⁺ to carboxylic groups.[28] The complete disappearance of the specific peak at 1723 cm⁻¹ showed that all the carboxylic groups chelated Cu²⁺. For the trisNTA functionalized copolymers such as PNT7, a total shift of specific absorption band from 1633 cm⁻¹ assigned to C=O stretching vibration of carboxylic group to 1627 cm⁻¹ was observed as well, which proved that all the trisNTA on the polymers involved in the binding of Cu²⁺.

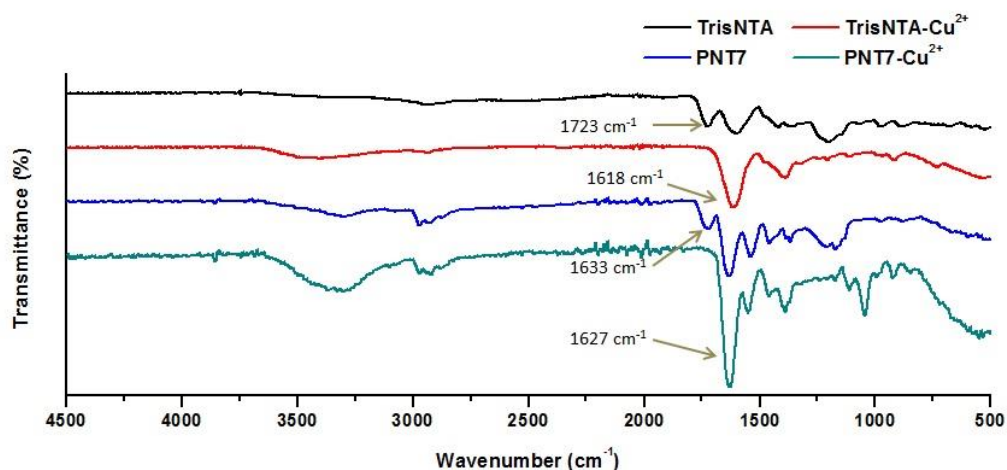


Figure 2-6. FTIR spectra of trisNTA (black), trisNTA-Cu²⁺ (red), PNT7 (blue) and PNT7-Cu²⁺ (green).

In addition, the binding of Cu²⁺ to the polymers was investigated by UV-vis spectroscopy (Figure 2-7). All copolymers showed similar UV-vis spectra and PNT2 was taken as a representative example. The coordination of PNT2 induced a shift of maximal absorbance of Cu²⁺ from 800 nm to 850 nm, in agreement with the data obtained from trisNTA-Cu²⁺ complex shown in Figure 2-7 as well. The absorbance intensity of Cu²⁺ increased as well after the coordination. The extinction coefficient of trisNTA-Cu²⁺ was determined as 143 M⁻¹cm⁻¹ by plotting the absorbance at 850 nm vs. its concentration. Because the polymer in low concentration doesn't have absorbance around 850 nm, the

concentration of trisNTA-Cu²⁺ on polymers in solutions was determined by the extinction coefficient of trisNTA-Cu²⁺. As shown in Figure 2-8, the actual amount of trisNTA-Cu²⁺ on polymers was in good agreement with the theoretical value, suggesting that the binding between trisNTA and Cu²⁺ strictly implemented as 1:3, and no influence of the conjugation of polymers was observed for all PNT copolymers.

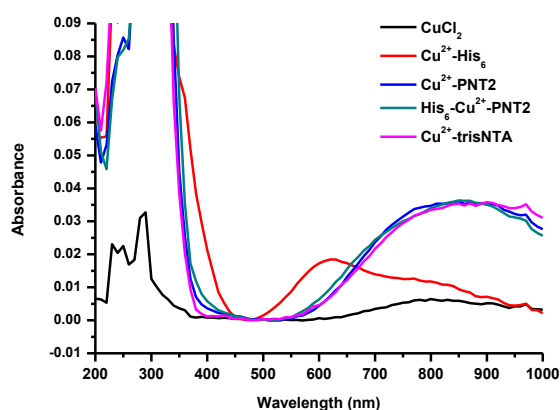


Figure 2-7. UV-vis spectra of CuCl₂ (black), CuCl₂-His₆ complex (red), PNT2-Cu²⁺ complex (blue), PNT2-Cu²⁺ - His₆ complex (green) and trisNTA-Cu²⁺ complex (pink) in water at pH 7. The concentration of CuCl₂ is 0.9mM for all the samples. The molar ratio between CuCl₂ and TrisNTA is 3:1.

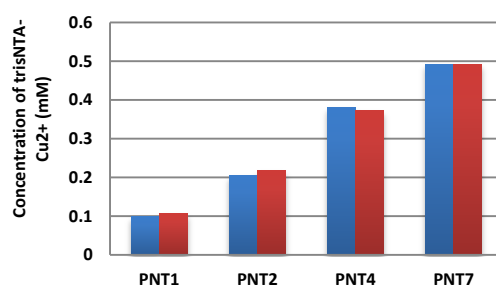


Figure 2-8. The theoretical (blue) and experimental (red) concentrations of trisNTA-Cu²⁺ in different trisNTA-containing copolymer aqueous solutions. The concentration of copolymers is 1.5 mg mL⁻¹. The theoretical concentration was calculated by $1.5 \times (\text{polymer degree}) \times (\text{trisNTA molar ratio}) \times 3 \times 1000 / (\text{molecular weight of polymer})$.

2.2.4. Binding of His₆ to PNT copolymers

In order to evaluate the binding ability of Cu²⁺-loaded polymers to his-tagged molecules, His₆ was initially chosen as the appropriate model because of its smaller size. The binding of His₆ to the Cu²⁺-loaded polymers was first confirmed by FTIR (Figure 2-9). The absorption bands of His₆ at 1176 cm⁻¹ and 1124 cm⁻¹ relate to ring vibration of imidazole, which shift to 1189 cm⁻¹ and 1135 cm⁻¹ after the coordination of Cu²⁺, respectively.[29] First, the presence of His₆ was observed by its distinctive absorbance at 1176 cm⁻¹ and 1124 cm⁻¹ after the purification for both trisNTA-Cu²⁺ and PNT7-Cu²⁺ (Figure 2-9). The absorption bands of His₆ at 1176 cm⁻¹ and 1124 cm⁻¹ shifted upward as well after the presence of both trisNTA-Cu²⁺ and PNT7-Cu²⁺, indicating that His₆ coordinated to the polymers through the coordination of Cu²⁺ ions.

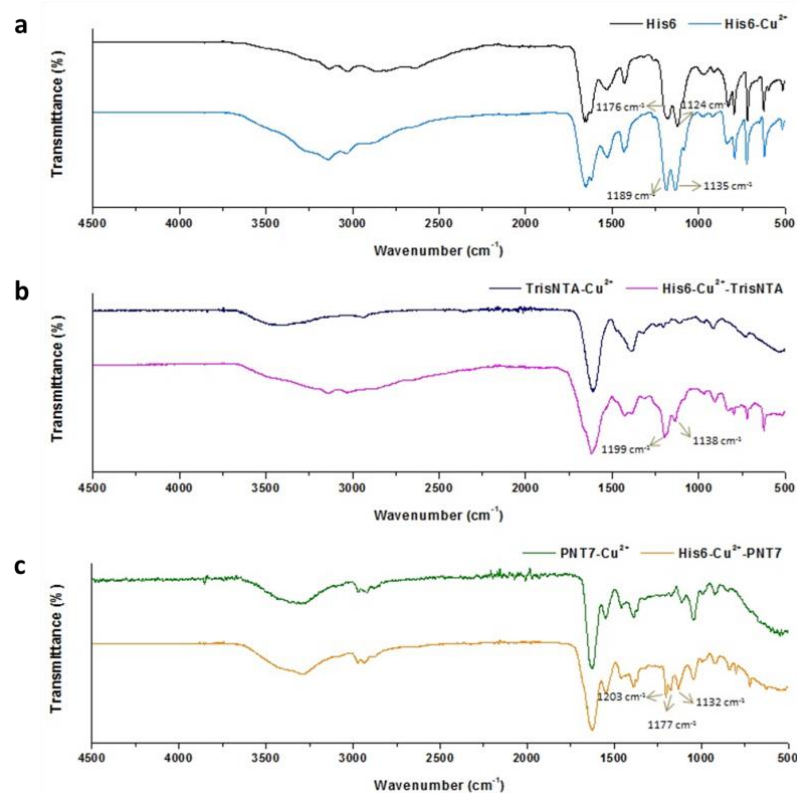


Figure 2-9. FTIR spectra of His₆ and His₆-Cu²⁺ (a), trisNTA-Cu²⁺ and His₆-Cu²⁺-trisNTA (b), PNT7-Cu²⁺ and His₆-Cu²⁺-PNT7 (c), respectively.

FPLC was performed to evaluate the binding ability of PNT copolymers to His₆ and identify whether there is an unspecific binding between his₆ and PNTs. Figure 2-10a showed a typically analytical chromatogram of Cu²⁺-loaded polymers. The polymer was

eluted after 1.5 mins and had almost no absorbance at 570 nm. The free sulforhodamine B-labeled His₆ (SRB-His₆) had a strong absorbance at 570 nm and was eluted later due to the smaller size comparing to PNTs (Figure 2-10c). After mixing Cu²⁺-PNT7 with SRB-His₆, the analytical chromatogram showed two peaks when detected at 570 nm by UV-detector, indicating that two SRB-His₆ fractions were present in the solution (Figure 2-10b). The first fraction is attributed to polymer-His₆ conjugates, indicating by the overlapped location of PNT7's elution peak alone (Figure 2-10a). The broad peak observed later belongs to the free SRB-His₆. Based on the integral area of the two peaks shown in Figure 2-10b, the binding stoichiometry between trisNTA-Cu²⁺ on PNT7 and His₆ was estimated at 1:0.8. The binding stoichiometry between His₆ and trisNTA-Cu²⁺ on PNT1, PNT2 and PNT4 were determined as well and the value remains close to 1:1 (Figure 2-11). The relative low binding stoichiometry between trisNTA-Cu²⁺ on PNT7 (1:0.8) and His₆ is due to the decrease of the distance between trisNTA binding sites, which sterically hampers the binding of His₆ to the polymer. The unspecific interaction between His₆ and polymers were investigated by a chromatography analysis of PolyNIPAM incubated with Cu²⁺ and fluorescein-labeled His₆ (FITC-His₆). As shown in Figure 2-10e, only one peak was observed after 7 mins at 490nm, which suggested that there is no unspecific binding between His₆ and the polymers. This proves that the binding of His₆ to the PNTs are achieved by the specific interaction between trisNTA-Cu²⁺ and His₆.

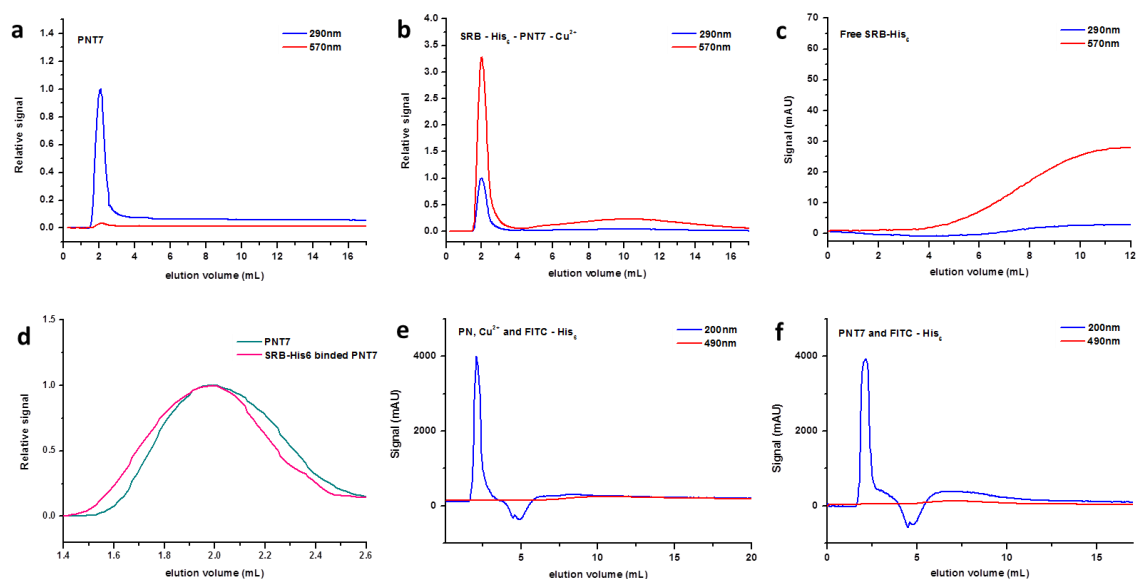


Figure 2-10. Chromatograms of PNT7-Cu²⁺ (a), PNT7-Cu²⁺ with 1.5-fold molar excess of SRB-His₆ (b), free SRB-His₆ (c), and the comparison of PNT7-Cu²⁺ with SRB-His₆-PNT7-Cu²⁺ complex(d). Control experiments including PolyNIPAM incubated with 2-fold molar excess of Cu²⁺ and FITC-His₆ (e) and PNT7 incubated with 2-fold molar excess of FITC-His₆ (f).

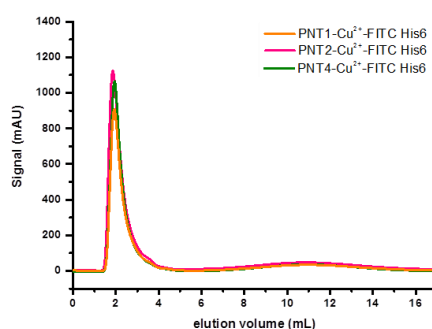


Figure 2-11. Chromatograms of PNT1-Cu²⁺ (yellow), PNT2-Cu²⁺ (pink) and PNT4-Cu²⁺ (green) with 1.2-fold molar excess of SRB-His₆.

As shown above, the decrease of the distance between trisNTA binding sites decreases the binding stoichiometry between trisNTA-Cu²⁺ and His₆. To confirm the influence of the distance between trisNTA binding sites to the binding stoichiometry and binding affinity, a series of ITC were performed (Figure 2-12). The complex formation is exothermic as expected for a reaction in which the coordination bonds are formed.[30] The stoichiometry between trisNTA-Cu²⁺ and His₆ is 1:1, which agrees with results reported previously (Table 2-2).[18] The conjugation of trisNTA to polymers doesn't show an obvious influence to the binding stoichiometry between trisNTA-Cu²⁺ and His₆ for PNT1, PNT2 and PNT4, but a decrease of the binding stoichiometry for PNT7 from 1:1 to 1:0.79. This result agrees with the one obtained from FPLC. The slightly decrease for PNT7-Cu²⁺-His₆ is due to steric hindrance determined by the decrease of the distance between trisNTA binding sites. The decrease of the distance between trisNTA binding sites reduces the distance among coordinated His₆ and polymers, which may increase the noncovalent interactions in the system. This is reflected by the change of enthalpy (ΔH°).[31, 32] For the PNT1-Cu²⁺-His₆ and PNT2-Cu²⁺-His₆ complexes, the value of ΔH° are basically the same with the ΔH° value obtained from trisNTA-Cu²⁺-His₆, which means ΔH° is only determined by the coordination of His₆ to trisNTA (Table 2-2). When the

distance between trisNTA binding sites is reduced, the enthalpy is decreasing and compensated by negative entropy (ΔS°). The decrease of enthalpy and the loss of the entropy value suggested there are other interactions except the coordination of His₆. A possible explanation is that the decrease of the distance between trisNTA binding sites increases the possibility of hydrogen bonding between His₆ and polymers, which contributes to the ΔH° value additionally.[33, 34] The hydrogen bond formation restricts the change of the conformation of the polymers, which may shield some of trisNTA binding sites and lead to a decrease of the binding stoichiometry. The binding affinity can be established by meaning dissociation constants (K_D). A low K_D suggests a strong non-covalent interaction. As shown in Table 2-2, the conjugation of trisNTA to the polymer doesn't influence the binding affinity. The decrease of the distance between trisNTA binding sites induces a decrease of K_D value, suggesting that the interaction between trisNTA-Cu²⁺ and His₆ is more stable. This agrees with the pervious conclusion and an extra interaction between His₆ and polymers enhances the stability between trisNTA-Cu²⁺ and His₆.

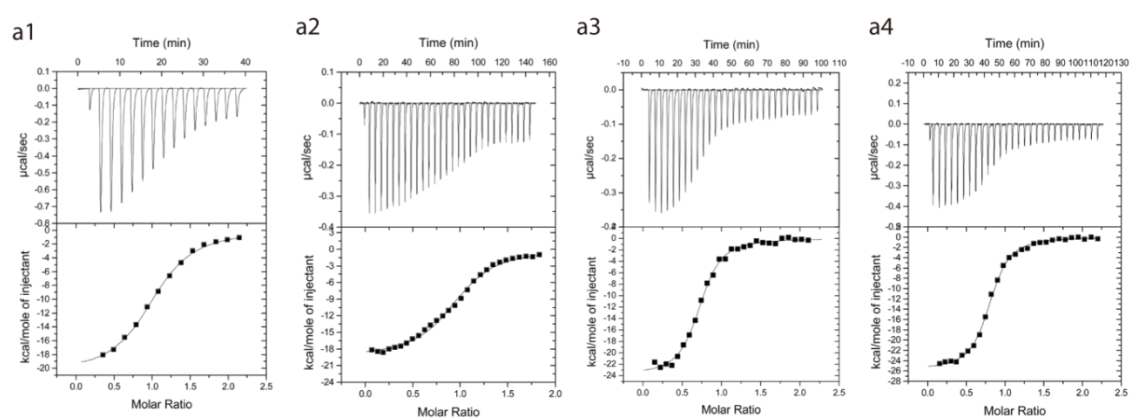


Figure 2-12. ITC thermograms (top) and titration curves (bottom) of TrisNTA-Cu²⁺ (a1), PNT1-Cu²⁺ (a2), PNT4-Cu²⁺ (a3), and PNT7-Cu²⁺ (a4) with His₆, respectively.

Table 2-2. Binding stoichiometry (N), K_D , ΔH° and ΔS° for the binding between trisNTA functionalized polymers and his-tagged molecules.

	N	K_D (μM) ^a	ΔH° (kcal/mol)	ΔS° (cal/mol/K)
TrisNTA-Cu ²⁺	1	0.39 ± 0.03	-20.7 ± 0.3	His ₆
PNT1-Cu ²⁺	0.98 ± 0.02	0.30 ± 0.02	-19.4 ± 0.2	-40.1
PNT2-Cu ²⁺	0.856 ± 0.01	0.17 ± 0.01	-19.8 ± 0.2	-35.3
PNT4-Cu ²⁺	1.01 ± 0.01	0.13 ± 0.01	-23.0 ± 0.1	-35.3
PNT7-Cu ²⁺	0.79 ± 0.01	0.10 ± 0.01	-25.8 ± 0.2	-45.5

A previous study reports that I28 immunoglobulin with two his tags was used to cross-link copolymers composed by acrylamide and NTA methacrylate into hybrid hydrogels through the binding between his tags of proteins and metal-coordinated NTA.[35] To investigate whether single His₆ can cross-link trisNTA functionalized copolymers, dynamic light scattering (DLS) was carried out with PNT1 and PNT7 before and after the complexation. As shown in Figure 2-13, the distribution of hydrodynamic radius of polymers are in the range of 3-4 nm, which agrees with the published value of polyNIPAM with similar degree of polymerization.[36] After complexation of Cu²⁺ and His₆, no obvious changes of the hydrodynamic radius were observed. This suggests that no cross-binding happened between trisNTA-Cu²⁺ and His₆, therefore no aggregation or self-assembled structure such as particles was observed.

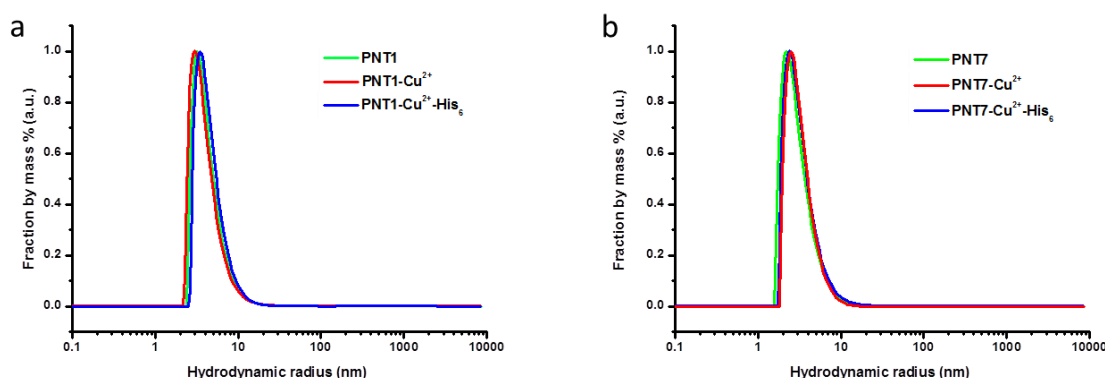


Figure 2-13. Distributions of the hydrodynamic radius of PNT1 (a), PNT7 (b) and the complexes in PBS buffer as measured by DLS at 25°C, scattering angle of 90°.

EPR spectroscopy was used to identify the Cu²⁺ coordination sphere when complexed to trisNTA on PNT polymers, and after addition of His₆, since the spectral parameters are known to change upon modification of the metal coordination sphere inside the NTA

pocket induced by complexation with His₆.^[37] Different model systems were studied and compared: CuCl₂ in solution (a), and mixtures of Cu²⁺ with PolyNIPAM, His₆, with trisNTA (c), with PNT1 (g) and with both PNT1 and His₆ (i) (Figure 2-14, and Table 2-3). The Cu²⁺ EPR spectrum in the presence of PolyNIPAM was similar to that of free Cu²⁺, which indicates that the metal is not coordinated by the polymer chain. In the presence of His₆ and trisNTA two species were detected: one similar to free Cu²⁺, and one with g_z and A_z values similar to those reported for the Cu²⁺ complexes of these molecules.^[23] In the case of Cu²⁺ complexation with PNT1 polymer only one species was detected (Figure 2-14(g)) with spectral parameters indicative of tetragonal symmetry^[38] and similar to those for the Cu²⁺ complexation of trisNTA;^[23] thus the Cu²⁺ coordination sphere involves three carboxyl groups and one amine group. The value of g and A tensors indicate a tetragonal symmetry.^[38] When His₆ was added to Cu²⁺: PNT1 the EPR spectrum changed significantly (Figure 2-14(i)). The signal was poorly resolved due to a significant broadening. The values of both g and hyperfine coupling differ from those observed for the Cu²⁺: PNT1 mixture, and are similar to the hyperfine coupling constants to those reported for Cu²⁺ dimers (A_x 27 G, A_y 38 G and A_z 82 G).^[39] The formation of the dimers is also supported by the signal recorded at half-field, which is typical for dimeric Cu²⁺ (Figure 2-15). A similar behavior was described for Cu²⁺: NTA: His₆ mixtures, where the formation of Cu²⁺ dimers was proposed.^[23]

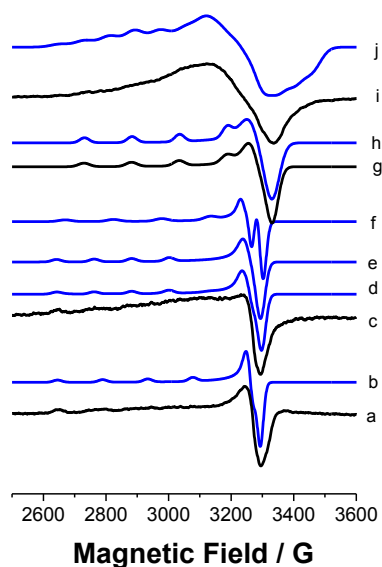


Figure 2-14. (a) X-band CW-EPR spectra of frozen solution in distilled water at 100 K together with their simulations using the EPR parameters indicated in Table 2-2: CuCl₂

solution (a), and the related simulation of its EPR spectrum (b), Cu²⁺-trisNTA mixture (c) with the related simulation of the EPR spectrum (d), Cu²⁺-PNT1 mixture (g) with the related simulation of EPR spectrum (h), Cu²⁺-PNT1: His₆ mixture (i) with the simulation of its EPR spectrum (j). (e) and (f) are individual contributions of paramagnetic species to the simulation (d). All EPR spectra are normalized for presentation means.

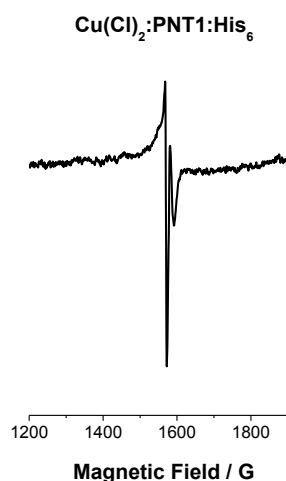


Figure 2-15. Experimental X-band CW-EPR spectrum of a frozen solution of Cu²⁺-PNT1:His₆ mixture in water at half-field.

Table 2-3. EPR spectral parameters for frozen solutions of Cu²⁺ in CuCl₂, Cu²⁺-trisNTA, Cu²⁺-His₆, Cu²⁺ mixing with PolyNIPAM, Cu²⁺-PNT1 and Cu²⁺-PNT1-His₆ complexes. The hyperfine values are given for the ⁶³Cu nucleus.

	g_x, g_y	g_z	$ A_x , A_y /G$	$ A_z /G$
CuCl ₂	2.080	2.38	5	140
Cu(Cl) ₂ :PolyNIPAM	2.083	2.38	5	142
Cu(Cl) ₂ :His ₆ (3:1)	2.082, 2.089	2.42	5	115
Cu(OTf) ₂ :His ₆ (1:5) ³⁴	2.082	2.28	5	120
	2.074	2.37	5	105
Cu(Cl) ₂ :trisNTA (3:1)	2.082, 2.090	2.41	10, 15	120
	2.089, 2.100	2.34	10, 5	154
Cu(OTf) ₂ :trisNTA (1:5) ³⁴	2.061	2.302	10	120
Cu(Cl) ₂ :PNT1	2.068	2.30	10	154
Cu(Cl) ₂ :PNT1: His ₆	2.062, 2.080	2.35	30, 35	80

2.3. Conclusion

We have designed and synthesized a library of novel poly (N-isopropylacrylamide-co-tris-nitrilotriacetic acid acrylamide)s bearing multi-trisNTA binding sites. PNT copolymers are

able to chelate with Cu^{2+} in a stoichiometry of 1 to 3 and further conjugate with His₆ with high binding affinity. One His₆ binding to one trisNTA on the polymers was observed for PNT1-PNT4 while a decrease of binding stoichiometry for PNT7 is due to the limited space and steric hindrance. The decrease of the distance between trisNTA bind sites favors the binding affinity of his₆ to the polymers due to the intermolecular interactions, and results in the increase of ΔH° and the decrease of ΔS° .

2.4. Experiment section

Materials

Materials. All chemicals were purchased from Sigma-Aldrich and used as received unless otherwise noted. N-isopropylacrylamide (NIPAM) and azobis(isobutyronitrile) (AIBN) was recrystallized twice from hexane and menthol, respectively. Hexahistidine was purchased from GenScript and his-tagged collagenase was purchased from Proteos Biotech.

Synthesis and characterization of *prot*-trisNTA and PNT copolymers

t-butyl ester protected tris-nitrilotriacetic acid acrylate (**2**). Chemical **1** was synthesized according to protocols published previously (Scheme 2-2).[40] Acryloyl chloride (335 mg, 3.7 mmol) was added to a solution of **1** (4.11 g, 2.64 mmol) and N,N-diisopropylethylamine (682 mg, 5.28 mmol) in 50 mL of dichloromethane, cooled in an ice bath, then purged with N₂ over night. The reaction mixture was washed with saturated NaHCO₃ and brine sequentially. The organic phase was dried in anhydrous MgSO₄. After removal of the solvent, the residue was isolated on silica gel using EtoAc/Hex (10/1) as eluent. A transparent oil was obtained in 91% yield. ¹H NMR (400 MHz, CDCl₃); δ = 6.26-6.09 (m, 2H, CH₂=CH-); 5.56-5.53 (d, 1H, CH₂=CH-); 3.84-3.40 (br, 15H, -N(CH₂COOC(CH₃)₃)₂ and -CHNCOOC(CH₃)₃); 3.4-3.3 (s, 16H, -CONCH₂CH₂CH₂NCO- and -CONCH₂CH₂NCO-); 3.30-3.13 (br, 2H, -CO(CH₂)₄CH₂NHCOCH=CH₂); 2.86-2.46 (m, 6H, -COCH₂CH₂CH-); 2.46-2.16 (m, 2H, -COCH₂(CH₂)₄NHCOCH=CH₂); 2.15-1.69 (br, 10H, -COCH₂CH₂CH- and -CONCH₂CH₂CH₂NCO-); 1.69-1.48 (m, 6H, -COCH₂(CH₂)₃CH₂NHCOCH=CH₂); 1.48-1.05 (d, 81H, -N(CH₂COOC(CH₃)₃)₂ and -CHNCOOC(CH₃)₃); ¹³C NMR (400 MHz, CDCl₃) δ = 24.5, 25.1, 26.3, 27.7, 28.0, 28.4, 28.7, 32.4, 38.9, 47.2, 53.3, 53.5, 64.0, 80.2, 80.3, 80.4, 80.9, 81.1, 125.4, 131.3, 165.5, 170.2,

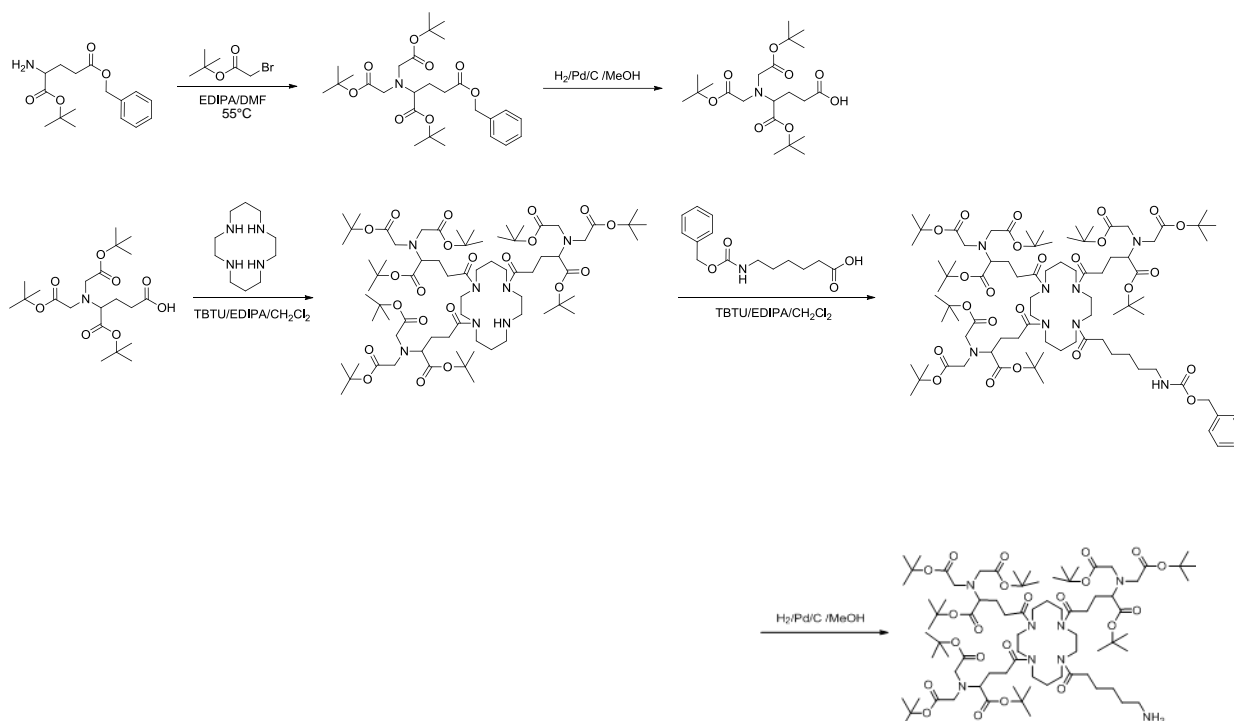
170.3, 171.7, 171.9, 173.0, 173.5; MS (ESI⁺, C₈₂H₁₄₂N₈O₂₃) Calculated mass: 1607.0
Observed mass: 1630.1 [MNa]⁺

t-butyl ester-protected PNTs (**3**). *t*-butyl ester-protected PNTs containing various trisNTA contents were synthesized by free radical polymerization initiated by AIBN under inert gas. All polymerizations were carried out in DMF at 65 °C. The concentration of monomers was 1mol/L and the concentrations of initiator for PolyNIPAM and PNTs are 2% based on the monomers ratio. The reaction time for PolyNIPAM, PNT1, PNT2 and PNT7 is 36 h, and PNT4 is 18 h. After cooling to room temperature, the polymer was dissolved in an excess of CHCl₃ and loaded on a silica column chromatography eluted by CHCl₃. A further purification was carried out by a precipitation from methanol solution into ether ester. ¹H NMR (400 MHz, CDCl₃); δ = 4.20-3.87 (br, -CONHCH(CH₃)₂ (NIPAM)); 3.84-3.43 (br, -N(CH₂COOC(CH₃)₃)₂ and -CHNCOOC(CH₃)₃); 3.43-3.30 (br, -CONCH₂CH₂CH₂NCO- and -CONCH₂CH₂NCO-); 3.30-3.01 (br, -CO(CH₂)₄CH₂NHCO-); 2.80-2.52 (br, COCH₂CH₂CH-); 2.52-2.41 (br, -COCH₂(CH₂)₄NHCO-); 2.41-1.79 (br, -COCH₂CH₂CH- and -CONCH₂CH₂CH₂NCO-); 1.79-1.66 (s, -CO(CH₂)₅NHCO-); 1.54-1.33 (d, N(CH₂COOC(CH₃)₃)₂ and -CHNCOOC(CH₃)₃); 1.27-0.94 (br, -CONHCH(CH₃)₂ (NIPAM)).

Deprotected PNT copolymers (**4**). *t*-butyl ester-protected polymers were deprotected by dissolving them in an excess of TFA at 0 °C. After stirring for 4 h at room temperature, excess amount of MeOH was added and the solvent was evaporated in vacuum. The copolymers were then dialyzed (MWCO 3500-5000) against double-distilled water for 2 days to remove small molecules. ¹H NMR (400 MHz, CDCl₃); δ = 4.33-3.98 (br, -N(CH₂COOC(CH₃)₃)₂ and -CHNCOOC(CH₃)₃); 3.98-3.79 (br, -CONHCH(CH₃)₂ (NIPAM)); 3.79-3.33 (br, -CONCH₂CH₂CH₂NCO- and -CONCH₂CH₂NCO-); 3.28-3.04 (br, -CO(CH₂)₄CH₂NHCO-); 2.96-2.65 (br, COCH₂CH₂CH-); 2.56-2.35 (br, -COCH₂(CH₂)₄NHCO-); 2.35-2.11 (br, -COCH₂CH₂CH-); 2.11-1.86 (br, -CONCH₂CH₂CH₂NCO-); 1.85-1.43 (br, -COCH₂(CH₂)₃CH₂NHCO-); 1.32-0.92 (br, -CONHCH(CH₃)₂ (NIPAM)).

¹H and ¹³C NMR spectra were recorded on Bruker DPX-NMR (400 MHz) instrument and chemical shifts are reported as δ values (ppm) relative to internal Me₄Si. The molecular weight and molecular weight distribution were analyzed by gel permeation chromatography (GPC), which was carried out on an Agilent 1100 Series instrument equipped with Viscotek I-columns (I-GUARD-0478 (40 mm x 7.8 mm), I-MBHMW-3078

(300 mm x 7.8 mm, exclusion limit > 10·10⁶ g mol⁻¹), and I-MBMMW-3078 (300 mm x 7.8 mm, exclusion limit > 10·10⁶ g mol⁻¹). N,N-Dimethylformamide (DMF) containing 20 mM lithium bromide was used as mobile phase with a flow rate of 1.0 mL min⁻¹ at 45 °C. Polystyrene standards were used for calibration. Acid-base titration was carried out to estimate the trisNTA content in polymers. The titration was performed by adding the 0.01 M standard NaOH solution with a microburet to 1 mg/mL polymer aqueous solution. The pH vs the amount of NaOH was recorded and the concentration of carboxylic group in 1 mg/mL polymer aqueous solution was estimated. The trisNTA content in each polymer was calculated.



Scheme 2-2. Synthesis of compound 15-[8,11-Bis-[4-(bis-tert-butoxycarbonylmethyl-amino)-4-tert-butoxycarbonyl-butyl]-4-(7-amino-hexanoyl)-1,4,8,11tetraaza-cyclotetradec-1-yl]-2-(bis-tert-butoxycarbonylmethyl-amino)-5-oxo-pentanoic acid *t*-butyl ester

Copper chelation of the copolymers

Respective polymers were incubated with a stoichiometric excess of copper chloride aqueous solution. The solution of polymer-Cu²⁺ complexes were adjusted to pH 7 and loaded onto an anion exchange column (HiTrap Q, GE Healthcare Life Sciences) to

remove the free Cu^{2+} . A gradient of 0-500mM sodium chloride was used as eluent. The obtained solutions were desalted using a 10-kDa-Ultrafree centrifugal filter unit (Millipore Corporation), lyophilized, and re-dissolved in bidistilled water at a given concentration. The final pH of the complex solution was adjusted to 7. FTIR spectra were recorded on a Bruker Alpha FTIR spectrometer (Bruker Optic GmbH, Ettlingen, Germany) to prove the chelation of copper to the polymers. A prior lyophilization was performed before the FTIR measurements. UV-vis spectroscopy was carried out on a SpectraMax M5e Multi-Mode Microplate Reader. A standard curve by plotting the 850 nm-absorbance of trisNTA-Cu^{2+} vs. its concentration was prepared. The concentration of trisNTA-Cu^{2+} in 1.5 mg mL^{-1} polymer aqueous solution was determined by the standard curve and the chelation efficiency was calculated. The concentration of bound Cu^{2+} was determined from the UV-vis spectra by using an extinction coefficient of $143 \text{ M}^{-1}\text{cm}^{-1}$ at 850 nm, determined experimentally.

Binding of hexahistidine to the polymer- Cu^{2+} complexes

Cu^{2+} -loaded polymers were equilibrated with 1.5-fold stoichiometric molar excess of SRB- His_6 in PBS buffer at pH 7.4. The free SRB- His_6 was removed by passing through a Hitrap desalting column (GE Healthcare Life Sciences), which was connected to a FPLC system. The elution was monitored at 290 nm and 570 nm, which are the maximal absorbance of polymers and SRB- His_6 , respectively.

Electron paramagnetic resonance

EPR measurements were performed on a Bruker CW EPR Elexsys-500 spectrometer equipped with a variable temperature unit. The spectra were recorded at 100 K with the following parameters: microwave power 10 mW, conversion time 61.12 ms, number of scans up to 100, resolution 2048 points, modulation amplitude in the range of 5 G, sweep width 1400 G. EPR spectra were simulated using the WINEPR Simphonia simulation package (Bruker); the fitting allowed the precise calculation of gyromagnetic tensor and hyperfine couplings values (with 5% standard error). The samples were prepared in distilled water at pH 7 keeping the copper concentration constant at 0.45 mM in the salt form and also in the corresponding mixtures. Before measuring the samples were purged with nitrogen and the tubes were sealed with parafilm, in order to avoid line broadening due to the oxygen presence.

Investigation of polymer structures in solution

The polymer structures in aqueous solution were investigated by DLS at 90° angle at room temperature with a commercial goniometer (ALV/CGS-8F, ALV Langen) equipped with a He:Ne linear polarized laser (JDS Uniphase, wavelength = 632.8 nm). An ALV-5000/60X0 correlator was used to calculate the correlation function of the scattered light intensity which was analyzed by the CONTIN method. The concentration of polymers and the complexes were kept as 2 mg/mL.

Microcalorimetry

ITC was carried out using a VP-ITC microcalorimeter from MicroCal. For each experiment, the same batch of buffer or distilled water was used for all the sample preparation and dilution. Interaction constants characterizing the Cu²⁺-loaded polymers and His₆ or his-tagged proteins were determined by direct titration of His₆ or his-tagged proteins to polymer solutions at pH 7.4 in PBS buffer at 25°C. The solution in the cell was stirred at 300 rpm to ensure rapid mixing. The volume of sample cell and syringe are 1.4 mL and 295 µL, respectively. Small aliquots of titrant (typically 10 µL) are successively injected into solution of the working cell with an adequate interval over 240 s to allow complete equilibration. The first injection is usually set to a volume of 2 µL because of possible dilution during the equilibration time preceding the measurement. The first injection was ignored in the analysis of the data. The heat change was monitored continuously upon addition of each injection of the titrant as a function of time.

The stoichiometry value is equal to the value of the molar ratio for which the slope of the plot is steepest. The slope of the plot at this point gives the value of the association constant, K_B , and the binding enthalpy ΔH° can be determined from the y-axis intercept of the curve. From the values for ΔH° and K_B found from the plot, K_D , ΔG° and ΔS° can be determined using the following equations:

$$K_D = 1/K_B \quad (2)$$

$$\Delta G^\circ = RT \ln K_D \quad (3)$$

$$\Delta S^\circ = (\Delta H^\circ - \Delta G^\circ)/T \quad (4)$$

R is the ideal gas constant and T is the temperature at which the experiment was performed.

2.5. References

- [1] Duncan R. Polymer conjugates as anticancer nanomedicines. *Nature Reviews Cancer*. 2006;6:688-701.
- [2] Wong LS, Khan F, Micklefield J. Selective covalent protein immobilization: strategies and applications. *Chemical Reviews*. 2009;109:4025-53.
- [3] Steen Redeker E, Ta DT, Cortens D, Billen B, Guedens W, Adriaensens P. Protein engineering for directed immobilization. *Bioconjugate Chemistry*. 2013;24:1761-77.
- [4] Harris JM, Chess RB. Effect of pegylation on pharmaceuticals. *Nature Reviews Drug Discovery*. 2003;2:214-21.
- [5] Kochendoerfer GG. Site-specific polymer modification of therapeutic proteins. *Current Opinion in Chemical Biology*. 2005;9:555-60.
- [6] Foley TL, Burkart MD. Site-specific protein modification: advances and applications. *Current Opinion in Chemical Biology*. 2007;11:12-9.
- [7] Heredia KL, Maynard HD. Synthesis of protein-polymer conjugates. *Organic & Biomolecular Chemistry*. 2007;5:45-53.
- [8] Gentle IE, De Souza DP, Baca M. Direct production of proteins with N-terminal cysteine for site-specific conjugation. *Bioconjugate Chemistry*. 2004;15:658-63.
- [9] Bontempo D, Heredia KL, Fish BA, Maynard HD. Cysteine-reactive polymers synthesized by atom transfer radical polymerization for conjugation to proteins. *Journal of the American Chemical Society*. 2004;126:15372-3.
- [10] Roberts MJ, Bentley MD, Harris JM. Chemistry for peptide and protein PEGylation. *Advanced Drug Delivery Reviews*. 2002;54:459-76.
- [11] Ding Z, Fong RB, Long CJ, Stayton PS, Hoffman AS. Size-dependent control of the binding of biotinylated proteins to streptavidin using a polymer shield. *Nature*. 2001;411:59-62.
- [12] Shao H, Chung J, Balaj L, Charest A, Bigner DD, Carter BS, et al. Protein typing of circulating microvesicles allows real-time monitoring of glioblastoma therapy. *Nature Medicine*. 2012;18:1835-40.
- [13] Schartner J, Güldenhaupt J, Mei B, Rögner M, Muhler M, Gerwert K, et al. Universal method for protein immobilization on chemically functionalized germanium investigated by ATR-FTIR difference spectroscopy. *Journal of the American Chemical Society*. 2013;135:4079-87.
- [14] Zhang Y, Yang Y, Ma W, Guo J, Lin Y, Wang C. Uniform magnetic core/shell microspheres functionalized with Ni²⁺-iminodiacetic acid for one step purification and immobilization of his-tagged enzymes. *ACS Applied Materials & Interfaces*. 2013;5:2626-33.
- [15] Dietrich C, Schmitt L, Tampé R. Molecular organization of histidine-tagged biomolecules at self-assembled lipid interfaces using a novel class of chelator lipids. *Proceedings of the National Academy of Sciences*. 1995;92:9014-8.
- [16] Schmitt J, Hess H, Stunnenberg H. Affinity purification of histidine-tagged proteins. *Molecular Biology Reports*. 1993;18:223-30.
- [17] Schmitt L, Dietrich C, Tampe R. Synthesis and characterization of chelator-lipids for reversible immobilization of engineered proteins at self-assembled lipid Interfaces. *Journal of the American Chemical Society*. 1994;116:8485-91.
- [18] Lata S, Reichel A, Brock R, Tampé R, Piehler J. High-affinity adaptors for switchable recognition of histidine-tagged proteins. *Journal of the American Chemical Society*. 2005;127:10205-15.

- [19] Lata S, Piehler J. Stable and functional immobilization of histidine-tagged proteins via multivalent chelator headgroups on a molecular poly (ethylene glycol) brush. *Analytical Chemistry*. 2005;77:1096-105.
- [20] Baldauf C, Schulze K, Lueders P, Bordignon E, Tampé R. In-Situ Spin Labeling of his-tagged proteins: distance measurements under in-cell conditions. *Chemistry – A European Journal*. 2013;19:13714-9.
- [21] Grunwald C, Schulze K, Giannone G, Cognet L, Lounis B, Choquet D, et al. Quantum-yield-optimized fluorophores for site-specific labeling and super-resolution imaging. *Journal of the American Chemical Society*. 2011;133:8090-3.
- [22] Wieneke R, Labòria N, Rajan M, Kollmannsperger A, Natale F, Cardoso MC, et al. Live-cell targeting of his-tagged proteins by multivalent nitrilotriacetic Acid carrier complexes. *Journal of the American Chemical Society*. 2014;136:13975-8.
- [23] Tanner P, Ezhevskaya M, Nehring R, Van Doorslaer S, Meier W, Palivan C. Specific His₆-tag attachment to metal-functionalized polymersomes relies on molecular recognition. *The Journal of Physical Chemistry B*. 2012;116:10113-24.
- [24] Yin X, Hoffman AS, Stayton PS. Poly(N-isopropylacrylamide-co-propylacrylic acid) copolymers that respond sharply to temperature and pH. *Biomacromolecules*. 2006;7:1381-5.
- [25] Cheng C, Schmidt M, Zhang A, Schlüter AD. Synthesis of thermally switchable poly(N-isopropylacrylamide-block-dendronized methacrylate)s. *Macromolecules*. 2006;40:220-7.
- [26] Mi Kyong Y, Yong Kiel S, Chong SC, Young ML. Effect of polymer complex formation on the cloud-point of poly(N-isopropyl acrylamide) (PNIPAAm) in the poly(NIPAAm-co-acrylic acid): polyelectrolyte complex between poly(acrylic acid) and poly(allylamine). *Polymer*. 1997;38:2759-65.
- [27] Sellers RM, Williams WJ. High-temperature dissolution of nickel chromium ferrites by oxalic acid and nitrilotriacetic acid. *Faraday Discussions of the Chemical Society*. 1984;77:265-74.
- [28] Veeraraj A, Sami P, Raman N. Copper(II) complex of 3-cinnamalideneacetylacetone: Synthesis and characterisation. *Journal of Chemical Sciences*. 2000;112:515-21.
- [29] Saini GSS, Kaur S, Tripathi SK, Dogra SD, Abbas JM, Mahajan CG. Vibrational spectroscopic and density functional theory studies of chloranil–imidazole interaction. *Vibrational Spectroscopy*. 2011;56:66-73.
- [30] Stadlbauer S, Riechers A, Späth A, König B. Utilizing reversible copper(II) peptide coordination in a sequence-selective luminescent receptor. *Chemistry – A European Journal*. 2008;14:2536-41.
- [31] Zaitseva KV, Varfolomeev MA, Novikov VB, Solomonov BN. Enthalpy of cooperative hydrogen bonding in complexes of tertiary amines with aliphatic alcohols: Calorimetric study. *The Journal of Chemical Thermodynamics*. 2011;43:1083-90.
- [32] Zweep N, Hopkinson A, Meetsma A, Browne WR, Feringa BL, van Esch JH. Balancing hydrogen bonding and van der Waals interactions in cyclohexane-based bisamide and bisurea organogelators. *Langmuir*. 2009;25:8802-9.
- [33] Grünberg R, Nilges M, Leckner J. Flexibility and conformational entropy in protein-protein binding. *Structure*. 2006;14:683-93.
- [34] Baldwin RL. In Search of the Energetic role of peptide hydrogen bonds. *Journal of Biological Chemistry*. 2003;278:17581-8.

- [35] Chen L, Kopeček J, Stewart RJ. Responsive hybrid hydrogels with volume transitions modulated by a titin immunoglobulin module. *Bioconjugate Chemistry*. 2000;11:734-40.
- [36] Zhou S, Fan S, Au-yeung SCF, Wu C. Light-scattering studies of poly(N-isopropylacrylamide) in tetrahydrofuran and aqueous solution. *Polymer*. 1995;36:1341-6.
- [37] Nehring R, Palivan C, Casse O, Tanner P, Tu xen J, Meier W. Amphiphilic diblock copolymers for molecular recognition: metal-nitrilotriacetic acid functionalized vesicles. *Langmuir*. 2008;25:1122-30.
- [38] Nishida Y, Takahashi K. Unusual changes in hyperfine coupling constants observed for copper(II) complexes with N,N-bis(benzimidazol-2-ylmethyl)amine and its homologues; X-ray crystal structure determinations of [CuLPr(NO₃)(MeOH)]NO₃, [CuLbu(NO₃)(MeOH)]NO₃, [CuLbu(NO₃)]NO₃, and [CuLbu(NO₃)]NO₃. *Journal of the Chemical Society, Dalton Transactions*. 1988:691-9.
- [39] Ellena J, Kremer E, Facchin G, Baran EJ, Nascimento OR, Costa-Filho AJ, et al. X-ray structure and EPR behavior of a new dimeric copper(II) complex with 4-amino-N-(5-methoxy-2-pyrimidinyl)benzenesulfonamide. *Polyhedron*. 2007;26:3277-85.
- [40] Heeres JT, Kim S-H, Leslie BJ, Lidstone EA, Cunningham BT, Hergenrother PJ. Identifying modulators of protein-protein interactions using photonic crystal biosensors. *Journal of the American Chemical Society*. 2009;131:18202-3.

3. Combined study of molecular recognition and spatial constraints in protein binding and interactions using a polymer module

Adapted with permission from *J. Am. Chem. Soc.*, 2014, 136 (36), 12607–12614.

Copyright 2014 American Chemical Society.

3.1. Introduction

Association and dissociation interactions/processes are fundamental to almost all the biological processes, such as DNA replication and transcription,[1-3] signaling transduction,[4, 5] and molecular production,[6] simultaneously involving multiple molecules. The precise regulation of biological processes and the achievement of biological functions is based on accurate molecular recognition interactions and spatial constraints between molecules.[7-9] Molecular recognition, determined by the exact geometric match between interacting molecules and the formation of complementary noncovalent bonds,[10] plays an important role in specific interactions between molecules.[11, 12] In addition, the simultaneous interaction of multiple molecules is strongly dependent on spatial constraints when diverse binding sites of various ligands are located in the vicinity of each other. In nature, a large number of proteins work together in pairs, and the inter-protein distance influences their synergy.[13-15] An example is the synergy between TATA-binding protein and initiator elements. Decrease the distance induces stronger synergy and consequently higher activity.[16]

Currently, the interactions and synergy of proteins can be successfully predicted by computer simulations,[17-19] while the influence of distance constraints on binding and activity of biomolecules has been reported in only very few cases.[16] In addition, current computer simulations do not account for variation of physical properties, such as entropy, that are known to be crucial for molecular recognition.[20-23] Nanostructures based on self-assembled DNA have been used to study inter-ligand distances resulting from the simultaneous binding of multiple ligands.[24, 25] However, DNA self-assembled structures behave as rigid scaffolds, which induce a decrease in binding due to spatial mismatches.[25] To the best of our knowledge, there are very few

model scaffolds that can specifically bind multiple proteins with controlled distances between binding sites, and none has used polymer-based scaffolds.

Various polymers have been used for protein conjugation through different approaches, such as covalent bond formation,[26-28] or non-covalent interactions attributed to molecular recognition.[29-33] In particular, trisNTA functionalized polymers have been used to bind his-tagged proteins with multiple metal-NTA coordination pockets due to the high binding affinity.[34-44] As his tag normally is expressed on either the N- or C-terminus of proteins, far away from their active centers, the binding does not influence their activities.[38, 45-47] For example, trisNTA functionalized poly(butadiene)-*block*-poly(ethylene oxide) binds to his-tagged enhanced green fluorescent protein (His₆-eGFP) without affecting its fluorescence,[38, 47] and his-tagged laccase preserved its activity when interacting with Ni²⁺-NTA functionalized surface.[46] However, to the best of our knowledge, the functionalization of polymers by trisNTA is limited to the terminal ends of the polymers.[47, 48] Therefore, polymer-his tagged protein interactions have been studied only in relation to their binding affinity via molecular recognition interactions at a single, specific metal-NTA pocket. An influence of distance between the NTA pockets on his-tagged proteins binding was only considered when NTA pockets were exposed at the surface of polymer vesicles.[38]

Here, we have synthesized a library of novel PNT copolymers, and complexed them with Cu²⁺ as shown before. In the next step, PNTs is used to serve as flexible models to assess the combined effect of molecular recognition and spatial constraints in binding his-tagged molecules ranging from small molecular mass molecules (< 1kDa) up to proteins (Figure 3-1). This library of PNTs provides different average distances between trisNTA sites, which can modulate the binding of multiple molecules as a function of their size. We selected His₆, his-tagged enhanced yellow fluorescent protein (His₆-eYFP) and his-tagged collagenase G (His₆-ColG) as model molecules because they provide a large range of sizes (from 1 to 11 nm). The binding of his-tagged molecules to trisNTA was analyzed by ITC. We investigated the binding affinity, and inter-molecular interactions of his-tagged molecules bound to the polymers as a function of the specific local topology. Our polymers provide a dual topologic match at the molecular level involving both molecular recognition at trisNTA pockets, and steric effects regulated by the distance between the

trisNTA sites. In this way it is possible to get an insight into the fine details of binding affinities of molecules, which are regulated not only by attachment to a specific target, but also by spatial constraints.

The concept of polymers serving as models for combined geometric topology with size requirements is expected to show the real binding capacity of molecules to a complex targeting configuration, which mimics biological systems in important details.

PNT copolymers with high trisNTA mol% have a short average distance between trisNTA binding sites, and are expected to influence the binding ability and binding affinity between his-tagged molecules and trisNTA pockets, whereas PNT copolymers with low trisNTA mol% are expected to not influence the binding of His-tagged molecules.

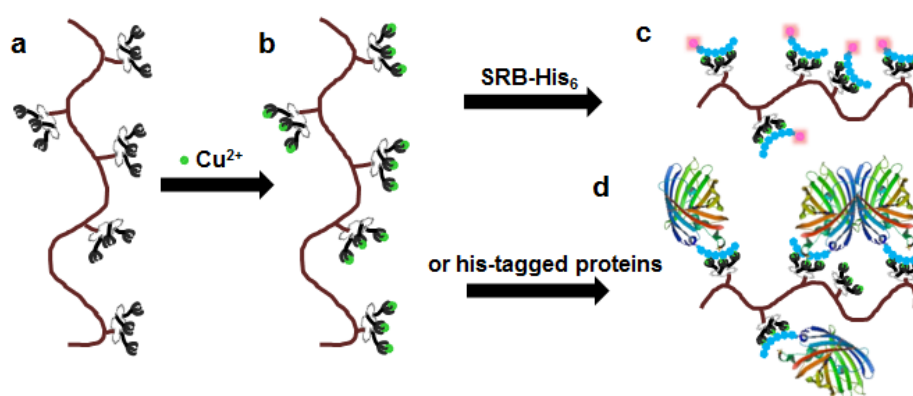


Figure 3-1. Schematic representation of PNTs, which coordinate Cu^{2+} , and further bind to SRB-His_6 , $\text{His}_6\text{-eYFP}$, and $\text{His}_6\text{-ColG}$.

3.2. Results and Discussion

Reactivity ratio of comonomers and average distance between trisNTA binding sites

Based on the monomer feed ratios and copolymer compositions (Table 3-1), the monomer reactivity ratio of trisNTA (r_{trisNTA}) and NIPAM (r_{NIPAM}) were determined by Fineman-Ross method using ^1H NMR data (Figure 3-2, 3-3, Equation 1).[67] The conversions of all copolymers were controlled below 18% and the copolymers compositions were calculated from the ratios between the integrals of the peaks at $\delta=3.44$ ppm and $\delta=3.50$ ppm (from trisNTA), and the peak at $\delta=4.00$ ppm (from $-\text{CH}-$ of NIPAM) from ^1H NMR spectra (Figure 3-2). G values were plotted against H values to

yield a straight line with r_{trisNTA} as its slope and $-r_{\text{NIPAM}}$ as the intercept (Figure 3-3). The reactivity ratio of trisNTA and NIPAM were determined as 0.8 and 1.35, respectively.

$$G = r_{\text{trisNTA}}H - r_{\text{NIPAM}} \quad (1)$$

The variation of trisNTA mol% in polymer/in feed with the degree of conversion is shown in Figure S13. Even though r_{NIPAM} is higher than r_{trisNTA} , trisNTA mol% in feeds only varied from 10 mol% to 13% when the degree of conversion increased from 0 to 0.62. Therefore, the difference of reactivity ratios of comonomers can't obviously influence the trisNTA mol% in copolymers in our experimental conditions as also observed in Figure 3-4.

As expected, trisNTA groups are statistically distributed on the polymer chains. We considered a homogeneous distribution of trisNTA groups on the polymer chain, and neglected possible statistical agglomeration due to the random character of polymerization.[53-55]

Table 3-1. trisNTA mol% in feed and in copolymers, parameters of equations for copolymerization of trisNTA and NIPAM.

Sample code	f_{trisNTA}^a (mol%)	F_{trisNTA}^b (mol%)	f_{NIPAM} (mol%)	F_{NIPAM} (mol%)	f^c	F^d	G^e	H^f
S1	5	4	95	96	0.053	0.042	-1.211	0.066
S2	10	8	90	92	0.111	0.087	-1.167	0.142
S3	30	25	70	75	0.429	0.333	-0.857	0.551
S4	50	39	50	61	1.000	0.639	-0.564	1.564
S5	70	66	30	34	2.333	1.941	1.131	2.805

^a trisNTA mol% in feed, ^b trisNTA mol% in copolymers, ^c $f=f_{\text{trisNTA}}/f_{\text{NIPAM}}$, ^d $F=F_{\text{trisNTA}}/F_{\text{NIPAM}}$, ^e $G=f(F-1)/F$, ^f $H=f^2/F$

A gas phase geometry of the PNT copolymers with the arrangement based on minimum energy conformation was built using the visualization program Avogadro. The yielded upper bound to the polymer length varying from 94.4 nm to 43.3 nm for PNT1-PNT7 (Table 3-2).[68] Hence the upper bound to the distance between two successive trisNTA binding sites varies from 31.5 nm to 4.3 nm.

3.2.1. Influences to the protein binding ability

To understand the influence of spatial constraints on the binding ability of molecules with high MW, we investigated the binding of two his-tagged proteins, His₆-eYFP and His₆-ColG to the PNT copolymers with different distance between the trisNTA binding sites. Binding of proteins to Cu²⁺-trisNTA sites was assessed in physiologic conditions in order to preserve the natural conformation of proteins.[49, 50] The dimensions of monomeric eYFP and monomeric ColG are 3 × 4 nm and 7 × 11.5 nm, respectively.[51, 52] The average distances between the trisNTA-Cu²⁺ binding sites of PNTs was calculated by molecular dynamic calculations based on a minimum energy conformation. This 3D model describes in a first approximation the average distance between the trisNTA sites because repulsive forces associated to the trisNTA sites are expected to favor a Langevin dependence of elongation on force, and favor a stretch chain conformation. Compared to a normal random coil model of the polymer chain, the charges on PNTs associated to trisNTA sites determine that different chain conformations are no longer equally probable because they correspond to a different energy of the chain in the field produced by the electrical charges (Langevin dependence). Indeed, Zeta potential measurements proved the charged character of polymers in PBS buffer, due to the presence of metal-trisNTA sites (Table 3-3). Theoretical average distance values varied from 31.5 nm to 4.3 nm for PNT1-7 (Table 3-2). Note that the calculated average distance values are larger than the real distance between two neighboring trisNTA sites in solution due to the 3D conformation of PNTs. The average distance approaches the real distance value only when the trisNTA sites are close to each other, as in the case of PNT4 and PNT7.

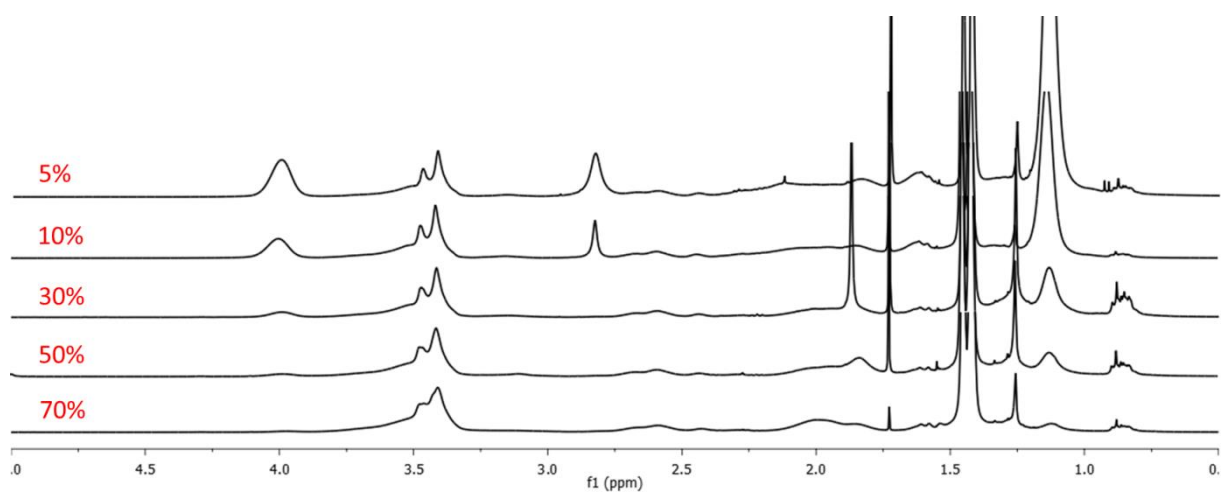


Figure 3-2. ^1H NMR spectra of copolymers composited with trisNTA and NIPAM. The trisNTA mol% in feed varied from 5% to 70%.

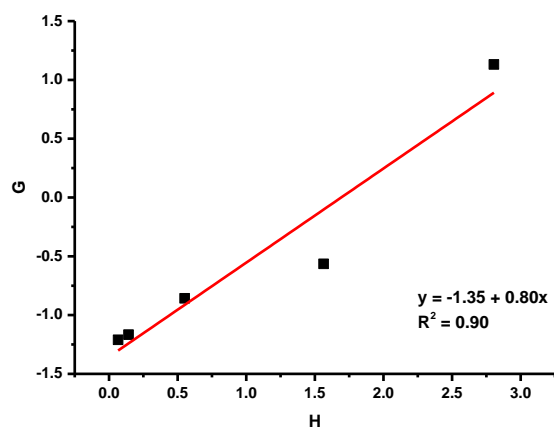


Figure 3-3. Fineman-Ross plots for copolymerization of trisNTA and NIPAM.

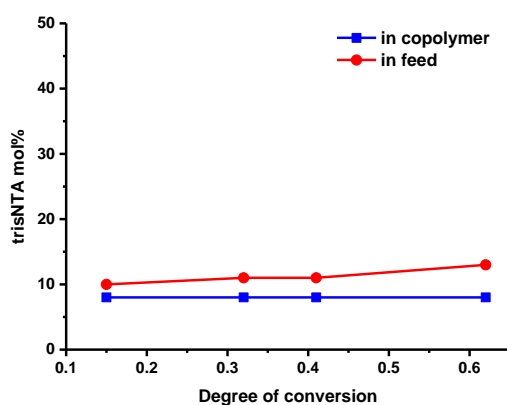


Figure 3-4. The variation of trisNTA mol% in copolymer/in feed with the degree of conversion.

Table 3-2. Length of polymer chain, trisNTA number per polymers and distances between trisNTA binding sites.

	PNT1	PNT2	PNT4	PNT7
polymer degree	276	182	168	127
chain length ^a (nm)	94.4	65.9	41.4	43.4
triNTA number per polymer	2.2	3.5	6.9	8.6
distances between binding sites ^a (nm)	31.5	13.2	5.2	4.3

^a (distances between binding sites) (nm)= (chain length) (nm)/ (triNTA number per polymer+1)

Table 3-3. ζ potential of PNTs and Cu²⁺-PNTs in PBS buffer.

ζ potential (mV)			
PNT1-Cu ²⁺	PNT2-Cu ²⁺	PNT4-Cu ²⁺	PNT7-Cu ²⁺
-4.4±0.3	-6.2±0.4	-8.3±0.7	-13.6±1.5

To investigate the influence of spatial constraints on binding ability of his-tagged proteins to PNTs, we used ITC (Figure 3-5, 3-6). The highest binding stoichiometry for both His₆-eYFP and His₆-ColG (0.87 and 0.47) was determined for PNT1, which has the largest distance between trisNTA sites. Decreasing the distance between triNTA-Cu²⁺ groups had no influence on the binding stoichiometry of His₆-eYFP, due to its relatively small size (3 × 4 nm), but evidently reduced the binding stoichiometry of His₆-ColG from 0.47 to 0.36. For PNT7, which has the smallest distance between trisNTA, a dramatic decrease in binding stoichiometry was observed for both His₆-eYFP and His₆-ColG (0.51 and 0.18, respectively). This significant decrease was expected because of the inaccessibility of trisNTA-Cu²⁺ binding sites due to their close packing, which prevents coordination of high MW molecules. The low binding stoichiometry of His₆-ColG to PNTs could be the consequence of His₆-ColG dimer formation, which inhibits the binding to PNTs (Figure 3-7). An interesting observation is that proteins and polymers are able to arrange themselves to achieve maximal binding. When the average distance between trisNTA binding sites is decreased to 5.2 nm (PNT4), which is closer to the size of eYFP, the binding stoichiometry of the protein does not change. We attribute the binding stoichiometry, in the case of PNT4, to the flexibility of the polymer chain and a 3-D structure rearrangement, which allow the binding of eYFP even though their size is close

to the maximal average distance between the trisNTA sites. This is in agreement with previous reports, which indicated that polymers with multiple ligands are able to bind multiple proteins on each polymer chain.[45, 56] When the average distance decreases to the size of eYFP, as in the case of PNT7, the number of proteins bound to the polymer chain is not increased, as would have been expected by the increased number of trisNTA's/polymer chain. We suppose that in this case the 3D conformation of PNT7 in solution induces spatial limitations, which do not favor a topologic match between trisNTA sites and eYFP. The binding stoichiometry of His₆-ColG to PNT2 is only slightly higher than that to PNT4, due to the low number of ColG proteins/polymer chain, which prevents the distance constraints from playing a role in protein binding.

PNTs copolymers possess higher binding capacity to small MW molecules than to large molecules, as expected. Although PNT7 has the highest trisNTA mol%, the binding capacity to his-tagged proteins is not higher than for PNT4 because of the spatial constraint (Table 3-4).

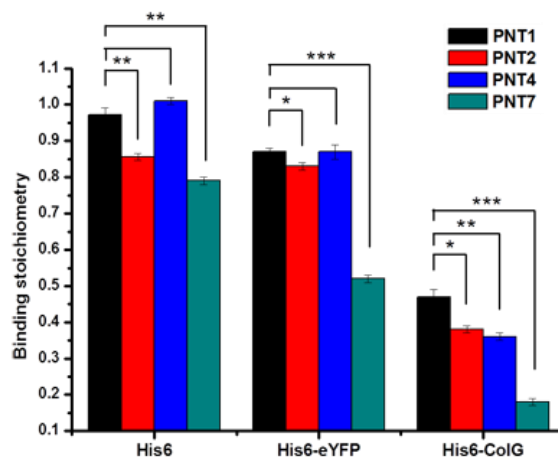


Figure 3-5. Binding stoichiometry between trisNTA-Cu²⁺ groups in PNTs and His₆, His₆-eYFP and His₆-ColG. Stars indicate significance in two-tailed Student's t-test; *P<0.05, **P<0.005, ***P<0.0005.

Table 3-4. Average binding capacities of PNTs copolymers (per 100 repeat units).

	His ₆	his-tagged eYFP	his-tagged ColG
PNT1	1	1	0
PNT2	2	2	1
PNT4	4	4	2
PNT7	5	4	1

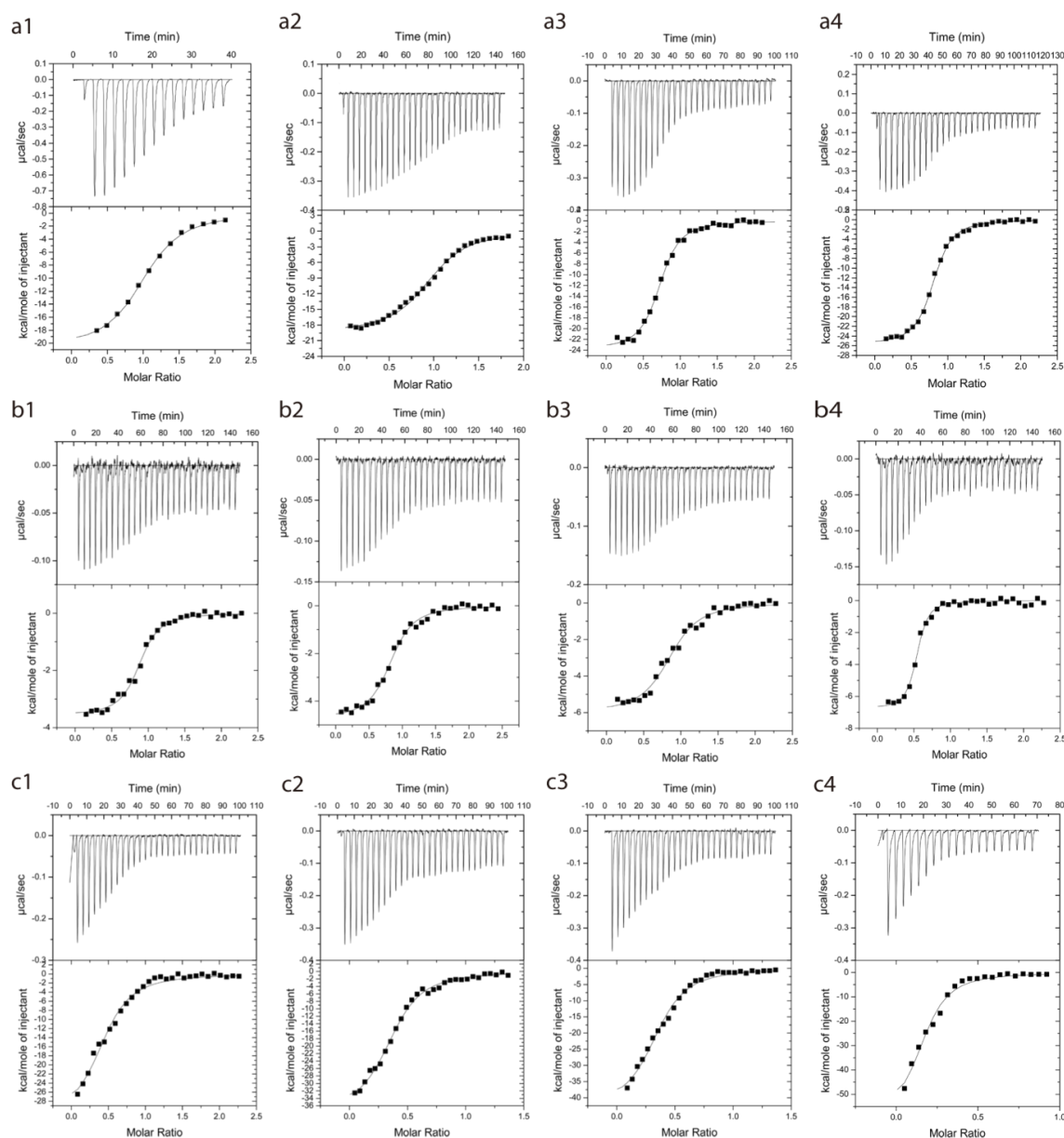


Figure 3-6. ITC thermograms (top) and titration curves (bottom) of TrisNTA-Cu²⁺ (a1), PNT1-Cu²⁺ (a2), PNT4-Cu²⁺ (a3), and PNT7-Cu²⁺ (a4) with His₆, respectively. Row b and row c represent the thermograms and titration curves of PNT1, PNT2, PNT4 and PNT7

with His₆-eYFP and His₆-ColG, respectively. The plots were fitted using the standard interaction model assuming a single type of binding sites.

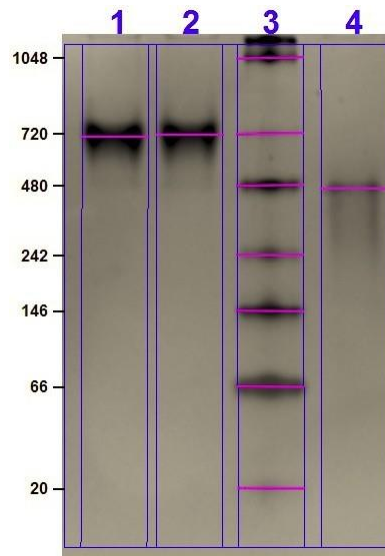


Figure 3-7. Native PAGE analysis of ColG (1, 2), NativeMark™ Unstained Protein Standard (Novex) and atto488-ColG.

3.2.2. Influences to the protein binding affinity

High binding affinity is crucial in nature for the binding of multiple proteins. For example, Bcd protein is able to position at a distance close to 10 base pairs on DNA when the binding affinity is high, whereas the binding site arrangements of the Bcd protein decreases rapidly when the binding affinity is decreased.[53] Therefore, the binding affinity is an essential parameter for indicating the binding of multiple proteins, and for studying the effect of spatial constraints. We chose trisNTA for protein binding because of its high binding affinity for his tag and his-tagged proteins.[38, 45, 48, 54, 57] To investigate whether conjugation of trisNTA to polymers and the spatial constraint between the trisNTA sites affect the binding affinity of his-tagged molecules, we determined the K_D values. The K_D values obtained for His₆ bound to trisNTA on PNTs are similar to that obtained for trisNTA-Cu²⁺-His₆ (Table 3-5), which suggests that the conjugation of polymer to trisNTA does not influence the binding affinity to His₆. A higher K_D ($0.6 \pm 0.2 \mu\text{M}$) value was reported for His₆ bound to trisNTA-modified polymer vesicles, due to the presence of surrounding polyethylene oxide brushes at the surface of the polymer vesicles.[38] Interestingly, the binding affinity of different his-tagged molecules to PNT1 was not affected by the structure or the size of his-tagged molecules,

but spatial constraint played an active role in the binding affinity between trisNTA and his-tagged molecules. When the distance between the binding sites was reduced, a decrease in K_D was observed for all his-tagged molecules. This suggests hydrogen bond formation between his-tagged molecules which decreases their separation, and thus influences their binding.[45] It has been reported that the binding affinity of proteins can be enhanced when they are located closer to each other on a surface.[55, 58] PNTs have a higher binding affinity to his-tagged proteins compared to other trisNTA-functionalized polymers,[47, 54] because Cu^{2+} was used as coordination ion instead of Ni^{2+} , and it is known to favor stronger binding than Ni^{2+} .[38]

Table 3-5. K_D for the binding between trisNTA functionalized polymers and his-tagged molecules.

	K_D (μM) ^a		
	His ₆	His ₆ -eYFP	His ₆ -ColG
PNT1-Cu ²⁺	0.30±0.02	0.15±0.02	0.35±0.06
PNT2-Cu ²⁺	0.17±0.01	0.26±0.03	0.26±0.03
PNT4-Cu ²⁺	0.13±0.01	0.33±0.06	0.20±0.04
PNT7-Cu ²⁺	0.10±0.01	0.07±0.01	0.20±0.04
TrisNTA-Cu ²⁺	0.39±0.03		

^a K_D values presented in this paper were determined by ITC measurements.

3.2.3. Spatial Constraints induce protein-protein interactions

To get more information on the interactions between his-tagged molecules and PNTs, we assessed the change of ΔH° and ΔS° (Table 4).[59, 60] For PNT1-Cu²⁺-His₆ and PNT2-Cu²⁺-His₆ complexes, the value of ΔH° is similar to that obtained for trisNTA-Cu²⁺-His₆ (Table 3-6), suggesting that the coordination between trisNTA-Cu²⁺ and His₆ is the only interaction when His₆ binds PNTs copolymers. With decreasing distance between trisNTA binding sites, ΔH° increases, and ΔS° decreases, due to formation of hydrogen bonds between neighboring His₆ units, and a conformation restriction of the polymer chain.[61, 62] Short distances and hydrogen bond formation between His₆ units inhibit access to several trisNTA binding sites, and lead to decreases in binding stoichiometry for the case of PNT7 (as shown both by ITC and FPLC).

The binding behavior between PNTs and his-tagged proteins is more complicated. When His₆-eYFP was bound to PNTs, low ΔH° (3.6 kcal/mol), and positive ΔS° values (19.3

cal/mol/K) were obtained. No influence of the secondary structure of His₆-eYFP was observed by circular dichroism (CD) spectroscopy after the coordination of PNTs (Figure 3-8). A possible explanation to the positive ΔS° values is that His₆ was not freely exposed, but interacted with eYFPs.[63, 64] The binding of His₆ to PNTs affected the interaction between His₆ and eYFP, and caused a total increase of ΔS° . The decrease in distance between trisNTA sites induced a decrease in ΔS° , due to restrictions in rotation and translation of the binding proteins.[65] When the distance between tris-NTA sites was further decreased (PNT7), the number of proteins bound to PNTs copolymers was unchanged (Table 3-4), and therefore ΔS° remained constant (Table 3-6). This indicates that no additional proteins are able to bind to the polymer due to the limited space, even though the number of trisNTA sites is increased.

In contrast to PNT-Cu²⁺-eYFP complexes, His₆-ColG binding to PNT1 is accompanied by an increase in ΔH° to a value of 31.7 kcal/mol, due to the formation of hydrogen bonds between PNTs and the protein molecules. The decrease in space between trisNTA sites induced an increase in ΔH° from 31.7 kcal/mol to 60.0 kcal/mol, which was compensated by a large decrease in ΔS° from -87.6 cal/mol/K to -177 cal/mol/K. The decrease in ΔS° is possibly the result of oligomerization of the proteins, as has been shown for the fibroblast growth factor 8b.[45] Oligomerization of proteins reduces the translational and rotational degrees of freedom, and induces a reduction in ΔS° .

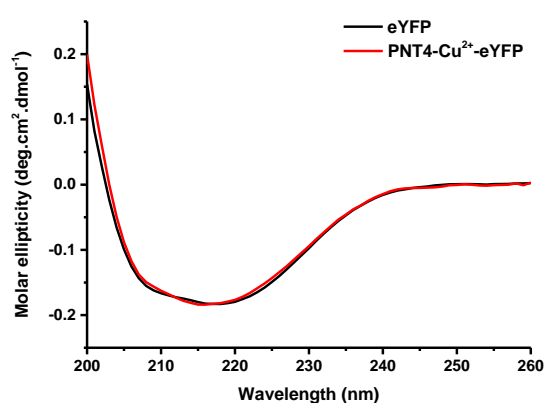


Figure 3-8. CD-spectra of eYFP and PNT4-Cu²⁺- eYFP in PBS buffer.

Table 3-6. ΔH° and ΔS° of interactions between trisNTA on PNTs and his-tagged molecules.

	ΔH° (kcal/mol) ^a			ΔS° (cal/mol/K) ^a		
	His ₆	His ₆ -eYFP	His ₆ -ColG	His ₆	His ₆ -eYFP	His ₆ -ColG
TrisNTA-Cu ²⁺	-20.7±0.3			-40.1		
PNT1-Cu ²⁺	-19.4±0.2	-3.6±0.1	-31.7±1.8	-35.3	19.3	-87.7
PNT2-Cu ²⁺	-19.8±0.2	-4.7±0.1	-37.6±1	-35.3	14.3	-89.5
PNT4-Cu ²⁺	-23.0±0.1	-6.0±0.1	-42.9±1.7	-45.5	9.5	-123.0
PNT7-Cu ²⁺	-25.8±0.2	-6.8±0.1	-60.0±5.0	-54.4	9.9	-177.0

3.3. Conclusion

A library of PNT copolymers containing multi-trisNTA binding sites with different average distances between them were complexed with copper, and used as models to assess the combined effect of molecular recognition and spatial constraints on the binding of molecules ranging from small molecular mass compounds up to proteins. Small molecular mass molecules (His₆) can easily access and bind to trisNTA sites of the polymers: a high binding ability of all PNT polymers was obtained, independent of the average distance between the tris-NTA sites. A different situation was found in the case of protein binding. His₆-eYFP binds efficiently to PNTs only when the average distance between the trisNTA sites is larger than the protein size. The lowest binding stoichiometry was determined for interaction of His₆-ColG with PNTs, due to the protein size (11 nm) and its possible dimerization. By controlling the amount of trisNTA on PNT polymers, we have efficiently controlled the binding stoichiometry, their affinity for selected his-tagged molecules, and their interactions in real conditions mimicking those encountered in biology.

These novel polymers containing multi-trisNTA binding sites with different average spaces between them open a wide field of possible applications as scaffolds for multi-binding of his-tagged proteins, or combination therapy. By selecting an appropriate PNT with a known average distance between the trisNTA sites and his-tagged proteins with a specific size, it is possible to predict the number of proteins bound per PNT chain, as well as their binding affinity. In addition, PNTs can be used to preorganize proteins to favor encapsulation of proteins inside polymeric vesicles and cellular uptake.

3.4. Experiment section

Materials

All chemicals were purchased from Sigma-Aldrich and used as received unless otherwise noted. His-tagged collagenase was purchased from Proteos Biotech.

Protein expression and analysis

eYFP expression. The expression of enhanced yellow fluorescent protein (eYFP) followed a previous publication.[66] The concentration was determined by UV-Vis spectroscopy, using an extinction coefficient $\epsilon(\text{eYFP})_{513\text{nm}} = 36500\text{M}^{-1}\text{cm}^{-1}$. The expressed eYFP has one His₆ on N-terminal.

PAGE analysis. Native PAGE was carried out using 4-12% Novex Tris-Glycine gels (Invitrogen) at 100V for 2h, using Tris-Glycine as running buffer. The gels were Coomassie stained with Simply Blue Safe Stain (Innitrogen). Gels were scanned by Gel Doc™ EZ Imager (BIO-RAD).

CD spectra were recorded using a spectral bandwidth of 1.5nm (AVIV) and 1nm (Chirascan) respectively, at 25 °C with a time constant of 5 s and a step resolution of 1 nm. CD data are given as mean residual molar ellipticities ($\text{deg cm}^2 \text{dmol}^{-1}$). The spectra are the result of 2-4 accumulations. A quartz cell with a path length of 1 mm was used with solutions containing constant 4 μM of eYFP protein in PBS buffer. For the spectra in buffer the blank spectrum of the solution was subtracted.

Collagenase G analysis. The structure of His₆-ColG was confirmed by Native PAGE and the concentration of His₆-ColG was determined by BCA protein assay. His₆-ColG was fluorescently labeled by NHS-atto488 for the confirmation of structures. As shown in Figure 3-7, atto488-labeled His₆-ColG has only one band, but His₆-ColG presents two bands. The band showing the same position as atto488-labeled His₆-ColG is very small and negligible. The molecular weight of His₆-ColG shown on the gel is approximately double comparing to atto488-labeled His₆-ColG, which suggests His₆-ColG mainly stays as a dimer in the solution and the fluorescent-labeled His₆-ColG is monomeric due to the change of the chemical structure.

ζ potential measurements of Cu²⁺-PNTs

The ζ potential of Cu^{2+} -PNTs in PBS buffer was determined by measuring the direction and velocity of polymer movement in an applied electrical field using a Zetasizer Nano ZSP (Malvern Instrument). The zeta potential measured was reported as the average calculated from three readings. The concentration of Cu^{2+} -PNTs is 1mg/mL.

3.5. References

- [1] Chagin VO, Stear JH, Cardoso MC. Organization of DNA replication. *Cold Spring Harbor Perspectives in Biology*. 2010;2.
- [2] Costa A, Hood IV, Berger JM. Mechanisms for initiating cellular DNA replication. *Annual Review of Biochemistry*. 2013;82:25-54.
- [3] Falkenberg M, Larsson N-G, Gustafsson CM. DNA replication and transcription in mammalian mitochondria. *Annual Review of Biochemistry*. 2007;76:679-99.
- [4] Bailly-Bechet M, Borgs C, Braunstein A, Chayes J, Dagkessamanskaia A, François J-M, et al. Finding undetected protein associations in cell signaling by belief propagation. *Proceedings of the National Academy of Sciences*. 2011;108:882-7.
- [5] Scott JD, Pawson T. Cell signaling in space and time: where proteins come together and when they're apart. *Science*. 2009;326:1220-4.
- [6] Benkovic SJ, Hammes-Schiffer S. A perspective on enzyme catalysis. *Science*. 2003;301:1196-202.
- [7] Baron R, McCammon JA. Molecular recognition and ligand association. *Annual Review of Physical Chemistry*. 2013;64:151-75.
- [8] Mammen M, Choi S-K, Whitesides GM. Polyvalent interactions in biological systems: implications for design and use of multivalent ligands and inhibitors. *Angewandte Chemie International Edition*. 1998;37:2754-94.
- [9] Zhu X, Gerstein M, Snyder M. Getting connected: analysis and principles of biological networks. *Genes & Development*. 2007;21:1010-24.
- [10] Fersht AR. The hydrogen bond in molecular recognition. *Trends in biochemical sciences*. 1987;12:301-4.
- [11] Eck MJ, Pluskey S, Trub T, Harrison SC, Shoelson SE. Spatial constraints on the recognition of phosphoproteins by the tandem SH2 domains of the phosphatase SH-PTP2. *Nature*. 1996;379:277-80.
- [12] Katchalski-Katzir E, Shariv I, Eisenstein M, Friesem AA, Aflalo C, Vakser IA. Molecular surface recognition: determination of geometric fit between proteins and their ligands by correlation techniques. *Proceedings of the National Academy of Sciences*. 1992;89:2195-9.
- [13] Vardhanabhuti S, Wang J, Hannenhalli S. Position and distance specificity are important determinants of cis-regulatory motifs in addition to evolutionary conservation. *Nucleic Acids Research*. 2007;35:3203-13.
- [14] Chiang D, Nix D, Shultzaberger R, Gasch A, Eisen M. Flexible promoter architecture requirements for coactivator recruitment. *BMC Molecular Biology*. 2006;7:16.
- [15] Yu X, Lin J, Masuda T, Esumi N, Zack DJ, Qian J. Genome-wide prediction and characterization of interactions between transcription factors in *Saccharomyces cerevisiae*. *Nucleic Acids Research*. 2006;34:917-27.
- [16] Emami KH, Jain A, Smale ST. Mechanism of synergy between TATA and initiator: synergistic binding of TFIID following a putative TFIIA-induced isomerization. *Genes & Development*. 1997;11:3007-19.
- [17] Pedersen AG, Baldi P, Chauvin Y, Brunak S. The biology of eukaryotic promoter prediction—a review. *Computers & Chemistry*. 1999;23:191-207.
- [18] Qi Y, Bar-Joseph Z, Klein-Seetharaman J. Evaluation of different biological data and computational classification methods for use in protein interaction prediction. *Proteins: Structure, Function, and Bioinformatics*. 2006;63:490-500.

- [19] Kortemme T, Baker D. Computational design of protein–protein interactions. *Current Opinion in Chemical Biology*. 2004;8:91-7.
- [20] Sousa SF, Fernandes PA, Ramos MJ. Protein–ligand docking: Current status and future challenges. *Proteins: Structure, Function, and Bioinformatics*. 2006;65:15-26.
- [21] Kitchen DB, Decornez H, Furr JR, Bajorath J. Docking and scoring in virtual screening for drug discovery: methods and applications. *Nature Reviews Drug Discovery*. 2004;3:935-49.
- [22] Frederick KK, Marlow MS, Valentine KG, Wand AJ. Conformational entropy in molecular recognition by proteins. *Nature*. 2007;448:325-9.
- [23] Marlow MS, Dogan J, Frederick KK, Valentine KG, Wand AJ. The role of conformational entropy in molecular recognition by calmodulin. *Nature Chemical Biology*. 2010;6:352-8.
- [24] Rinker S, Ke Y, Liu Y, Chhabra R, Yan H. Self-assembled DNA nanostructures for distance-dependent multivalent ligand-protein binding. *Nature Nanotechnology*. 2008;3:418-22.
- [25] Andersen CS, Knudsen MM, Chhabra R, Liu Y, Yan H, Gothelf KV. Distance dependent interhelical couplings of organic rods incorporated in DNA 4-helix bundles. *Bioconjugate Chemistry*. 2009;20:1538-46.
- [26] Gauthier MA, Klok H-A. Polymer-protein conjugates: an enzymatic activity perspective. *Polymer Chemistry*. 2010;1:1352-73.
- [27] Heredia KL, Maynard HD. Synthesis of protein-polymer conjugates. *Organic & Biomolecular Chemistry*. 2007;5:45-53.
- [28] Shakya AK, Sami H, Srivastava A, Kumar A. Stability of responsive polymer–protein bioconjugates. *Progress in Polymer Science*. 2010;35:459-86.
- [29] Maheshwari R, Levenson EA, Kiick KL. Manipulation of electrostatic and saccharide linker interactions in the design of efficient glycopolyptide-based cholera toxin inhibitors. *Macromolecular bioscience*. 2010;10:68-81.
- [30] Polizzotti BD, Maheshwari R, Vinkenburg J, Kiick KL. Effects of saccharide spacing and chain extension on toxin inhibition by glycopolyptides of well-defined architecture. *Macromolecules*. 2007;40:7103-10.
- [31] Hoffman AS, Stayton PS, Bulmus V, Chen G, Chen J, Cheung C, et al. Really smart bioconjugates of smart polymers and receptor proteins. *Journal of Biomedical Materials Research*. 2000;52:577-86.
- [32] Bontempo D, Maynard HD. Streptavidin as a macroinitiator for Polymerization: In Situ Protein–Polymer Conjugate Formation. *Journal of the American Chemical Society*. 2005;127:6508-9.
- [33] Alconcel SNS, Kim SH, Tao L, Maynard HD. Synthesis of biotinylated aldehyde polymers for biomolecule conjugation. *Macromolecular Rapid Communications*. 2013;34:983-9.
- [34] Platt V, Huang Z, Cao L, Tiffany M, Riviere K, Szoka FC. Influence of multivalent nitrilotriacetic acid lipid–ligand affinity on the circulation half-life in mice of a liposome-attached His₆-protein. *Bioconjugate Chemistry*. 2010;21:892-902.
- [35] Huang Z, Hwang P, Watson DS, Cao L, Szoka FC. Tris-Nitrilotriacetic acids of subnanomolar affinity toward hexahistidine tagged molecules. *Bioconjugate Chemistry*. 2009;20:1667-72.

- [36] Grunwald C, Schulze K, Reichel A, Weiss V, Blaas D, Piehler J, et al. In situ assembly of macromolecular complexes triggered by light. *Proceedings of the National Academy of Sciences*. 2010;107:6146.
- [37] Lata S, Piehler J. Stable and functional immobilization of histidine-tagged proteins via multivalent chelator headgroups on a molecular poly (ethylene glycol) brush. *Analytical Chemistry*. 2005;77:1096-105.
- [38] Tanner P, Ezhevskaya M, Nehring R, Van Doorslaer S, Meier W, Palivan C. Specific His₆-tag attachment to metal-functionalized polymersomes relies on molecular recognition. *The Journal of Physical Chemistry B*. 2012;116:10113-24.
- [39] Rakickas T, Gavutis M, Reichel A, Piehler J, Liedberg B, Valiokas Rn. Protein–protein interactions in reversibly assembled nanopatterns. *Nano Letters*. 2008;8:3369-75.
- [40] Beutel O, Nikolaus J, Birkholz O, You C, Schmidt T, Herrmann A, et al. High-fidelity protein targeting into membrane lipid microdomains in living cells. *Angewandte Chemie International Edition*. 2014;126:1335-9.
- [41] Roullier V, Clarke S, You C, Pinaud F, Gouzer Gr, Schaible D, et al. High-affinity labeling and tracking of individual histidine-tagged proteins in Live Cells Using Ni²⁺ tris-nitrilotriacetic acid quantum dot conjugates. *Nano Letters*. 2009;9:1228-34.
- [42] Lata S, Gavutis M, Tampé R, Piehler J. Specific and stable fluorescence labeling of histidine-tagged proteins for dissecting multi-protein complex formation. *Journal of the American Chemical Society*. 2006;128:2365-72.
- [43] Bhagawati M, Ghosh S, Reichel A, Froehner K, Surrey T, Piehler J. Organization of motor proteins into functional micropatterns fabricated by a photoinduced fenton reaction. *Angewandte Chemie International Edition*. 2009;48:9188-91.
- [44] Grunwald C, Schulze K, Giannone G, Cognet L, Lounis B, Choquet D, et al. Quantum-yield-optimized fluorophores for site-specific labeling and super-resolution imaging. *Journal of the American Chemical Society*. 2011;133:8090-3.
- [45] Griffith BR, Allen BL, Rapraeger AC, Kiessling LL. A polymer scaffold for protein oligomerization. *Journal of the American Chemical Society*. 2004;126:1608-9.
- [46] Balland V, Hureau C, Cusano AM, Liu Y, Tron T, Limoges B. Oriented immobilization of a fully active monolayer of histidine-Tagged recombinant laccase on modified gold electrodes. *Chemistry – A European Journal*. 2008;14:7186-92.
- [47] Nehring R, Palivan C, Casse O, Tanner P, Tu xen J, Meier W. Amphiphilic diblock copolymers for molecular recognition: metal-nitrilotriacetic acid functionalized vesicles. *Langmuir*. 2008;25:1122-30.
- [48] Lata S, Reichel A, Brock R, Tampé R, Piehler J. High-affinity adaptors for switchable recognition of histidine-tagged proteins. *Journal of the American Chemical Society*. 2005;127:10205-15.
- [49] Hsu S-TD, Blaser G, Behrens C, Cabrita LD, Dobson CM, Jackson SE. Folding study of venus reveals a strong ion dependence of its yellow fluorescence under mildly acidic conditions. *Journal of Biological Chemistry*. 2010;285:4859-69.
- [50] Anderson DE, Becktel WJ, Dahlquist FW. pH-Induced denaturation of proteins: a single salt bridge contributes 3-5 kcal/mol to the free energy of folding of T4 lysozyme. *Biochemistry*. 1990;29:2403-8.
- [51] Wang YM, Tegenfeldt JO, Reisner W, Riehn R, Guan X-J, Guo L, et al. Single-molecule studies of repressor–DNA interactions show long-range interactions. *Proceedings of the National Academy of Sciences of the United States of America*. 2005;102:9796-801.

- [52] Eckhard U, Schönauer E, Nüss D, Brandstetter H. Structure of collagenase G reveals a chew-and-digest mechanism of bacterial collagenolysis. *Nature Structural & Molecular Biology*. 2011;18:1109-14.
- [53] Makeev VJ, Lifanov AP, Nazina AG, Papatsenko DA. Distance preferences in the arrangement of binding motifs and hierarchical levels in organization of transcription regulatory information. *Nucleic Acids Research*. 2003;31:6016-26.
- [54] Nehring R, Palivan C, Moreno-Flores S, Mantion A, Tanner P, Toca-Herrera J, et al. Protein decorated membranes by specific molecular interactions. *Soft Matter*. 2010;6:2815-24.
- [55] Li L, Klim JR, Derda R, Courtney AH, Kiessling LL. Spatial control of cell fate using synthetic surfaces to potentiate TGF- β signaling. *Proceedings of the National Academy of Sciences*. 2011;108:11745-50.
- [56] Cairo CW, Gestwicki JE, Kanai M, Kiessling LL. Control of multivalent interactions by binding epitope density. *Journal of the American Chemical Society*. 2002;124:1615-9.
- [57] Sellers RM, Williams WJ. High-temperature dissolution of nickel chromium ferrites by oxalic acid and nitrilotriacetic acid. *Faraday Discussions of the Chemical Society*. 1984;77:265-74.
- [58] De Crescenzo G, Pham PL, Durocher Y, O'Connor-McCourt MD. Transforming growth factor-beta (TGF- β) binding to the extracellular domain of the type II TGF- β receptor: receptor capture on a biosensor surface using a new coiled-coil capture system demonstrates that avidity contributes significantly to high affinity binding. *Journal of Molecular Biology*. 2003;328:1173-83.
- [59] Zaitseva KV, Varfolomeev MA, Novikov VB, Solomonov BN. Enthalpy of cooperative hydrogen bonding in complexes of tertiary amines with aliphatic alcohols: Calorimetric study. *The Journal of Chemical Thermodynamics*. 2011;43:1083-90.
- [60] Zweep N, Hopkinson A, Meetsma A, Browne WR, Feringa BL, van Esch JH. Balancing hydrogen bonding and van der Waals interactions in cyclohexane-based bisamide and bisurea Organogelators. *Langmuir*. 2009;25:8802-9.
- [61] Grünberg R, Nilges M, Leckner J. Flexibility and conformational entropy in protein-protein binding. *Structure*. 2006;14:683-93.
- [62] Baldwin RL. In search of the energetic role of peptide hydrogen bonds. *Journal of Biological Chemistry*. 2003;278:17581-8.
- [63] Liao S-M, Du Q-S, Meng J-Z, Pang Z-W, Huang R-B. The multiple roles of histidine in protein interactions. *Chemistry Central Journal*. 2013;7:1-12.
- [64] Cauët E, Rooman M, Wintjens R, Liévin J, Biot C. Histidine–aromatic interactions in proteins and protein–ligand complexes: quantum chemical study of X-ray and model structures. *Journal of Chemical Theory and Computation*. 2005;1:472-83.
- [65] Grasberger B, Minton AP, DeLisi C, Metzger H. Interaction between proteins localized in membranes. *Proceedings of the National Academy of Sciences*. 1986;83:6258-62.
- [66] Bruns N, Pustelny K, Bergeron LM, Whitehead TA, Clark DS. Mechanical nanosensor based on FRET within a thermosome: damage-reporting polymeric materials. *Angewandte Chemie International Edition*. 2009;48:5666-9.
- [67] Kelen T, Tüd s F. Analysis of the linear methods for determining copolymerization reactivity ratios. I. A new improved linear graphic method. *Journal of Macromolecular Science—Chemistry*. 1975;9:1-27.

[68] Hanwell M, Curtis D, Lonie D, Vandermeersch T, Zurek E, Hutchison G. Avogadro: an advanced semantic chemical editor, visualization, and analysis platform. *Journal of Cheminformatics*. 2012;4:1-17.

4. A single polymer chain as a nanocarrier for multiple protein delivery with regulated pH responsiveness

4.1. Introduction

Protein therapeutics is of high importance in almost every field of medicine.[1] However, its functional applications are still in their infancy, as new applications are still being discovered. The high interest raised by protein therapeutics is mainly due to the highly specific actions of proteins, and their ability to regulate natural cell processes.[1, 2] There are still a number of challenges in the application of protein therapeutics that have to be overcome.[1, 3] Therapeutic proteins exhibit low stability, fast renal clearance, enzymatic degradation, and are frequently immunogenic.[4]

In order to overcome these drawbacks, a combination of polymer science and protein therapeutics has been developed. One approach is the application of polymeric nanocarriers, such as polymersomes, for the delivery of proteins.[5-9] These nanocarriers have exhibited good protection and improved half-life of encapsulated proteins,[10] but unfortunately they often exhibit a low loading efficiency,[11, 12] and are often not rapidly eliminated from the body.[13]

The most well-known approach for protein therapy is the conjugation of polymers, such as poly(ethylene glycol), to protect the protein and improve their stability, half-life, solubility, and reduce immunogenicity.[14-18] Polymer-protein conjugation for therapeutics has been developed for more than 40 years, and has led to several poly(ethylene glycol) conjugated proteins that are already on the market such as Pegloticase (Krystexxa®)[19] and Pegfilgrastim (Neulasta®)[20] for the treatments of chronic gout refractory and febrile neutropenia respectively. However, a number of deficiencies still exist that must be elegantly solved to create effective therapeutics. On one hand, the flexible polymer chains presented on the proteins generate a “conformational cloud”, which prevents interactions with blood components, enzymatic degradation, and fast renal clearance.[15, 21] On the other hand, this “conformational cloud” can obstruct normal protein-protein interactions, decreasing, or completely inhibiting the activity of the protein.[22, 23] To overcome this deficiency, stimuli-responsive linkers are implemented to enable cleavage of the protein from the polymer

conjugate by a specific stimulus, reducing the influence of the “conformation cloud effect” created by the polymer chains.[24, 25] However, the toxicity of the linker must be kept in mind when designing the nanoparticle.[26, 27]

Another disadvantage is that proteins are often covalently conjugated to polymers via lysine or cysteine residues. This results in random modification and heterogeneous conjugates.[28, 29] Site-specific modification of proteins is possible, but unfortunately often involves complicated modifications to achieve reactive sites on both the protein and polymer chains.[26, 30-32] Ultimately, an ideal polymer-protein conjugate needs to fulfill several requirements: 1) easy and versatile modification and conjugation 2) a linker that is stable in the bloodstream but cleavable in specific environments 3) polymers with a molecular weight lower than 40kDa, or biodegradable polymers that degrade to avoid accumulation after repeated administrations.[33]

Currently, the main source of therapeutic proteins is the recombinant expression by E.coli, most commonly incorporating a His tag (His₆) for easier purification. His₆ also gives the benefit of site specific, and pH responsive binding to the metal-coordinated nitrilotriacetic acid (NTA-Meⁿ⁺).[34-36] Unfortunately, using NTA-Meⁿ⁺-His₆ is still limited. Most systems are based on the presence of heavy metals, such as Cu²⁺ or Ni²⁺, in the NTA pocket to induce binding.[37] Repeated administrations of heavy metals can lead to their accumulation in the liver, kidney and spleen, and leading to organ damage.[38-41] In addition, neither of these two metals shows a high enough binding affinity for efficient polymer-protein conjugation (NTA-Cu²⁺-His₆: $\log_{10}K$ of 4.59 M⁻¹, NTA-Ni²⁺-His₆: $\log_{10}K$ of 3.76 M⁻¹).[42] To the best of our knowledge, there is only one study published recently using bisNTA-Ni²⁺-His₆ for improved polymer-protein conjugation due to the increase of binding affinity compared with NTA-Ni²⁺-His₆. [43] In addition, NTA-Meⁿ⁺ is capable of releasing His-tagged molecules when the pH is lower than 6,[44] but unfortunately, very few publications applied this chemistry for specific applications.[34]

It is intrinsically difficult for non-covalent interactions, such as the chelation between NTA-Me²⁺ and His₆-tagged proteins, to possess triggerable binding/release under mild biological conditions, but still exhibit high binding affinity and stability. Therefore, the successful design of a system combining both attributes would greatly advance protein therapeutics.

In previous chapters, we introduced poly (N-isopropylacrylamide-co-tris-nitrilotriacetic acid acrylamide)s (PNTn, where n represents the mol% of trisNTA on the polymer) containing Cu^{2+} for specific binding of His-tagged molecules. By increasing the trisNTA content in the polymer, (reducing the space between possible His-tagged binding sites) intermolecular interactions between bound His-tagged molecules were enhanced. Increasing the number of inter-protein interactions could stabilize the self-assembled structure, similar to many natural stabilized protein assemblies.[46-48]

Here, PNTs are employed for a novel concept using single polymer chains as a nanocarrier for the simultaneous binding of multiple proteins with regulated pH responsiveness. Low molecular weight polymers were tested to ensure their full elimination from the body after pH-triggered release of a bound His-tagged protein.[14] For this study, His₆-eYFP was chosen as a model molecule. PNTs with different average distances between trisNTA- Me^{n+} binding sites were tested to incorporate the natural concept of increasing protein-protein interactions between His-tagged proteins to improve the stability of the conjugate. Three metal cations, Cu^{2+} , Zn^{2+} , Fe^{3+} , were chosen as the coordination center in the trisNTA pocket to modulate the binding affinity of His-tagged proteins to the polymer, and were assessed by ITC. Then their ability to reversibly bind based on changes in pH was analyzed by FPLC. Zn^{2+} and Fe^{3+} offer the possibility to reduce the inherent toxicity of the conjugated delivery system compared to Cu^{2+} . By manipulating these two main factors, the distance between trisNTA- Me^{n+} and the nature of the coordinated metal, the binding affinity between PNTs and His-tagged proteins and their pH responsiveness could be controlled. The protein stability before and after conjugation, as well as after pH mediated release, were measured by CD and fluorescence spectroscopy. The delivery of His-tagged molecules including His₆-eYFP and His₆ into living cells was investigated.

4.2. Results and Discussion

4.2.1. Binding stoichiometry of His₆-eYFP to PNTs coordinated with different metal cations

PNT copolymers were coordinated with three different metal cations, Cu²⁺, Zn²⁺, or Fe³⁺, and the binding stoichiometry of His₆-eYFP to the PNT-Meⁿ⁺ were assessed by ITC (Figure 4-1).

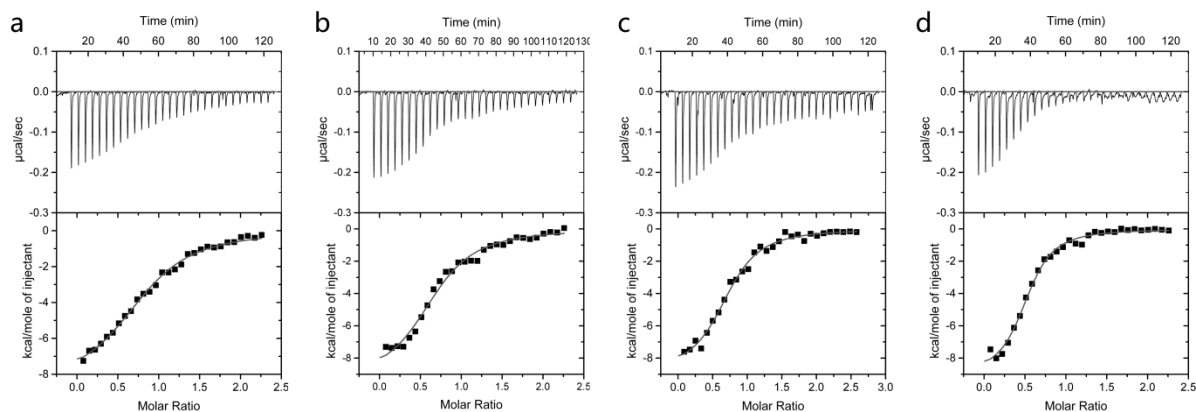


Figure 4-1. ITC thermograms (top) and titration curves (bottom) of PNT1-Zn²⁺ (a), PNT2-Zn²⁺ (b), PNT4-Zn²⁺ (c), and PNT7-Zn²⁺ (d) with His₆-eYFP, respectively. The plots were fitted using the standard interaction model assuming a single type of binding sites.

trisNTA-Zn²⁺ on PNT copolymers efficiently bound to His₆-eYFP with a binding stoichiometry approaching 1:1, when the average distance between trisNTA binding sites is larger than the size of His₆-eYFP, as was the case for PNT1-PNT4, agreeing with previously published results for trisNTA-Cu²⁺ (Figure 4-2).[45] This stoichiometry is crucial for a well-defined polymer-protein conjugation and holds benefits over the heterogeneous conjugates often seen with modifying lysines as previously described.[28, 49] trisNTA-Zn²⁺ showed the same binding stoichiometry to His₆-eYFP as trisNTA-Cu²⁺ copolymers, exemplified by both PNT4 polymers where a maximal 4 His₆-eYFPs were able to bind per 100 repeat units of polymers (Table 4-1). However, even though PNT7 has a higher content of trisNTA-Me²⁺ sites, a lower binding stoichiometry was observed (0.53 His₆-eYFP to trisNTA-Me²⁺ sites) due to steric hindrance.[45]

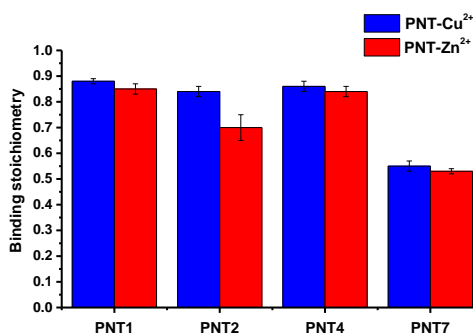


Figure 4-2. Binding stoichiometry between trisNTA-Me²⁺ in PNTn and His₆-eYFP.

Table 4-1. Average binding number of His₆-eYFP per polymer chain.

PNT1-Zn ²⁺	PNT2-Zn ²⁺	PNT4-Zn ²⁺	PNT7-Zn ²⁺
1	2	4	4

In the case of PNTs containing trisNTA-Fe³⁺, no binding of His₆-eYFP to the copolymers was observed by ITC even when high concentrations of His₆-eYFP (180 μM) were added (data not shown). This suggests the interaction between trisNTA-Fe³⁺ and His₆-eYFP is too weak for conjugating polymers with his-tagged proteins.

4.2.2. Binding affinity of His₆-eYFP to PNT-Me²⁺ copolymers

In addition to calculating the binding stoichiometry, the binding affinity of His₆-eYFP to PNTs containing trisNTA-Zn²⁺ was determined. Similar to PNT-Cu²⁺ (0.09-0.39 μM), K_D values for PNT-Zn²⁺-His₆-eYFP depended on the average distance between trisNTA binding sites. When the distance was decreased from 31.5 nm to 4.3 nm (PNT1-Zn²⁺-His₆-eYFP and PNT7-Zn²⁺-His₆-eYFP, respectively), the K_D values decreased from 1.35 ± 0.12 μM to 0.46 ± 0.06 μM. Smaller binding site separation led to a higher local concentration of proteins which increased inter-protein interactions such as hydrogen bond formation and protein oligomerization.[50-52] These interactions can promote the stabilization of the whole polymer-protein conjugate. Thus, by controlling the coordination metal and distance between trisNTA binding sites, the amount of inter-protein interactions and the K_D of PNT-Me²⁺-His₆-eYFP can be regulated (1.35 ± 0.12 μM to 0.09 ± 0.03 μM, Figure 4-3).[50]

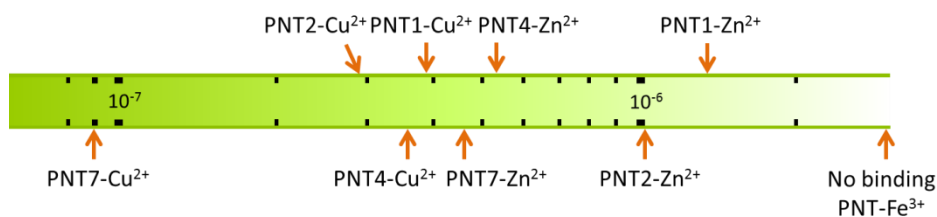


Figure 4-3. K_D (M) for the binding between PNT- Zn^{2+}/Cu^{2+} and His₆-eYFP.

The binding affinity of NTA- Me^{2+} towards His-tagged proteins varies in the order $Cu^{2+} > Ni^{2+} > Zn^{2+}$. [37] Therefore, Zn^{2+} is rarely used for NTA applications due to its poor binding affinity ($\log_{10}K = 3.25 M^{-1}$). [42] However, due to the multivalent interactions of trisNTA, the affinity of His₆-eYFP for PNTn- Zn^{2+} copolymers is greatly increased. This is exemplified by, at least, a 20, 130, and 420 fold decrease in K_D for PNT containing trisNTA- Zn^{2+} -His₆-eYFP ($1.35 \pm 0.12 \mu M$ for PNT1- Zn^{2+}) compared to NTA- Cu^{2+} -His₆, NTA- Ni^{2+} -His₆ and NTA- Zn^{2+} -His₆, respectively. [42] The enhanced binding affinity between trisNTA- Me^{2+} and His₆-eYFP suggested a higher stability of the protein-polymer conjugates compared with previously reported His₆ and NTA- Ni^{2+} ($K_D=41.6 \mu M$) or bisNTA- Ni^{2+} ($17.7 \mu M$) conjugates. [43]

4.2.3. Structure of PNT- Me^{2+} -His₆-eYFP conjugates and protein stability

The structure of PNT- Me^{2+} -His₆-eYFP was first characterized by DLS. PNT1- Cu^{2+}/Zn^{2+} and PNT4- Cu^{2+}/Zn^{2+} were chosen as representative polymers. The molar ratio between trisNTA and His₆-eYFP was fixed at 2.2:1 for both PNT1 and PNT4. The average number of His₆-eYFP per polymer chain on PNT1/PNT4 at this ratio was calculated as 1 and 3, respectively, and was independent of the metal used. The inter-protein interactions of His₆-eYFP for the case of PNT1- Me^{2+} , at this binding molar ratio, can be neglected considering the low average number of His₆-eYFP per PNT1- Me^{2+} , which is similar with conventional site-specific protein-polymer conjugate, binding one protein per polymer chain. [53-55]

The D_H of His₆-eYFP and PNT4- Zn^{2+} determined by DLS were 5.0 ± 0.9 nm and 5.8 ± 1.8 nm, respectively (Figure 4-4). After binding, the diameter shifted to 13.1 ± 2.8 nm, similar to PNT4- Cu^{2+} -His₆-eYFP (data not shown). For His₆-eYFP bound to PNT1- Zn^{2+} , the D_H increased from 8.1 ± 2.5 nm for PNT1 alone to 9.7 ± 2.4 nm (Figure 4-5). The change in size between PNT1- Zn^{2+} and PNT4- Zn^{2+} after binding His₆-eYFP can be explained by

the increased average number of proteins per polymer chain (3 for PNT4 and only 1 for PNT1). This data was supported by TEM, revealing structures with a diameter of 11.6 ± 2.7 nm for PNT4-Zn²⁺-His₆-eYFP (Figure 4-6).

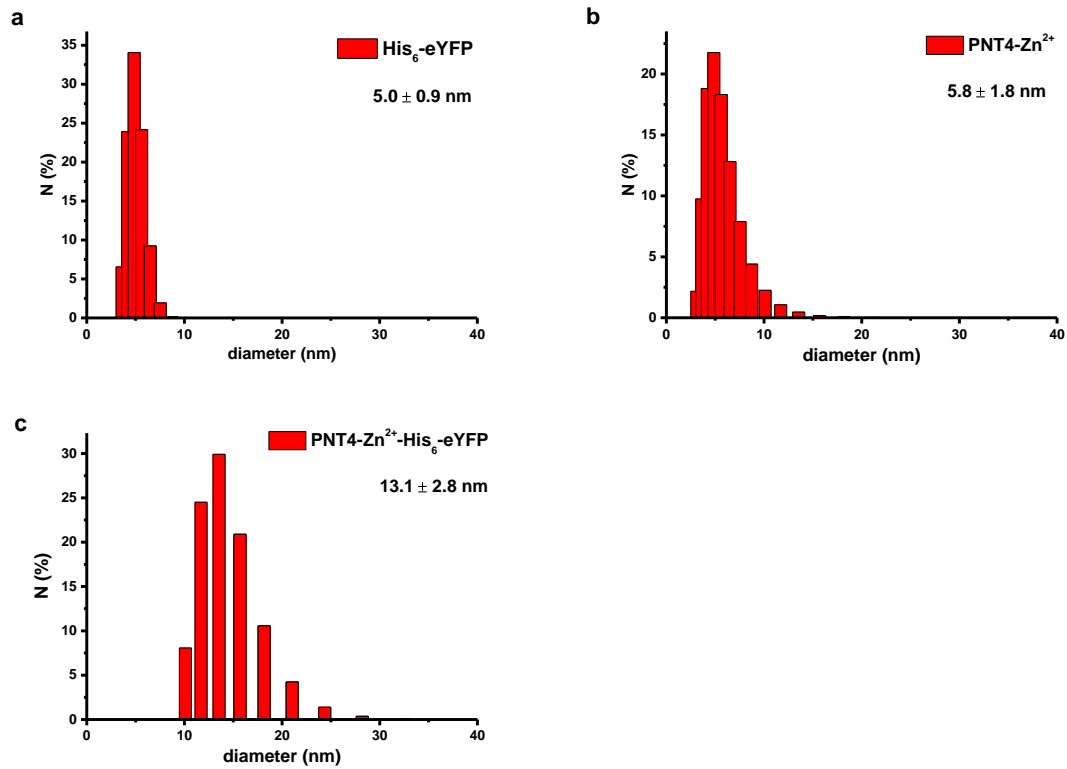


Figure 4-4. Size distribution of His₆-eYFP (a), PNT4-Zn²⁺ (b) and PNT4-Zn²⁺-His₆-eYFP (c).

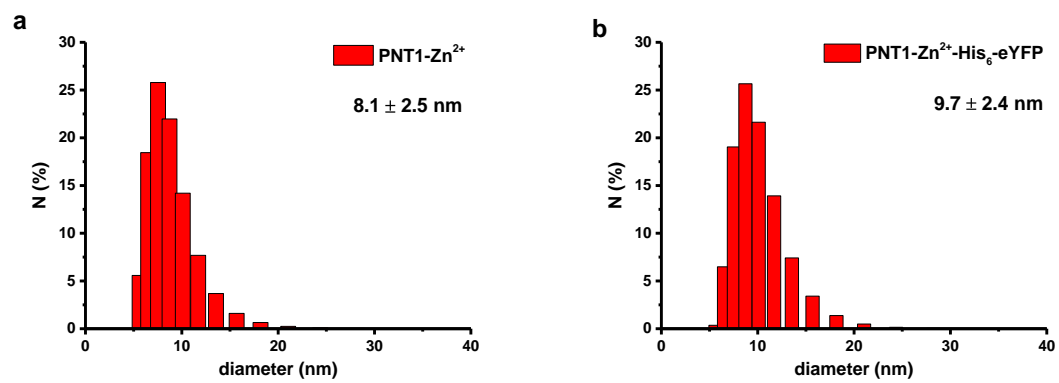


Figure 4-5. Size distribution of PNT1-Zn²⁺ (a) and PNT1-Zn²⁺-His₆-eYFP (b).

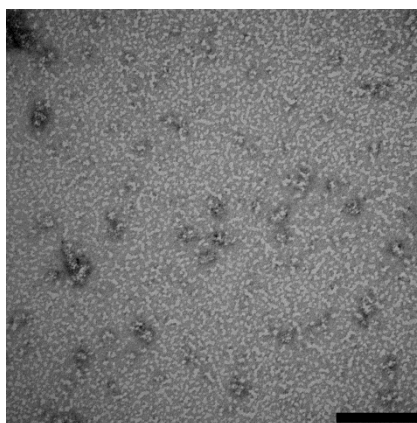


Figure 4-6. TEM image of PNT4-Zn²⁺-His₆-eYFP. The scale bar is 100 nm.

To address the question of whether the conjugation of polymers to proteins causes alterations in their secondary structure, His₆-eYFP was characterized before and after polymer conjugation by CD spectroscopy. The far-UV CD spectrum of His₆-eYFP and PNT4-Zn²⁺-His₆-eYFP, showed that conjugation did not alter the protein structure (Figure 4-7), agreeing with the previous published PNT-Cu²⁺ results. Also, the binding of PNT1-Zn²⁺ to His₆-eYFP did not alter the protein structure.

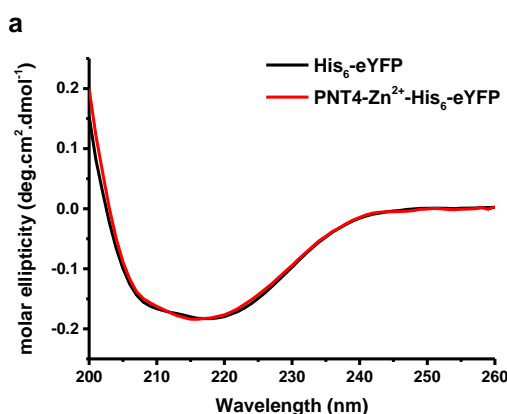


Figure 4-7. The far-UV CD spectra of His₆-eYFP and PNT4-Zn²⁺-His₆-eYFP.

4.2.4. PNT-Me²⁺-His₆-eYFP stability in varying pH

The stability of PNT-Me²⁺-His₆-eYFP conjugates under various pH's were investigated by FPLC. As shown in Figure 4-8, PNT4-Cu²⁺-His₆-eYFP showed a higher stability than PNT1-Cu²⁺-His₆-eYFP at pH 7.4. The difference between PNT1-Zn²⁺-His₆-eYFP and PNT4-Zn²⁺-His₆-eYFP was even more significant with 80.2% of His₆-eYFP remaining complexed with PNT4-Zn²⁺, while only 46.6% of His₆-eYFP remained bound with PNT1-Zn²⁺. The higher stability of PNT4-Me²⁺-His₆-eYFP compared to PNT1-Me²⁺-His₆-eYFP could be attributed

to a higher density of proteins per polymer chain that increased intermolecular interactions preventing the disassociation of the complex. This strategy is seen in nature to stabilize self-assembled structures by inter-protein interactions [46-48] and was used to compensate for the lower binding affinity of Zn^{2+} for His_6 than Cu^{2+} (Figure 4-8). By optimizing inter-protein interactions through decreasing space between trisNTA- Me^{2+} binding sites, PNT4- Zn^{2+} - His_6 -eYFP remains more stable than PNT1- Cu^{2+} - His_6 -eYFP.

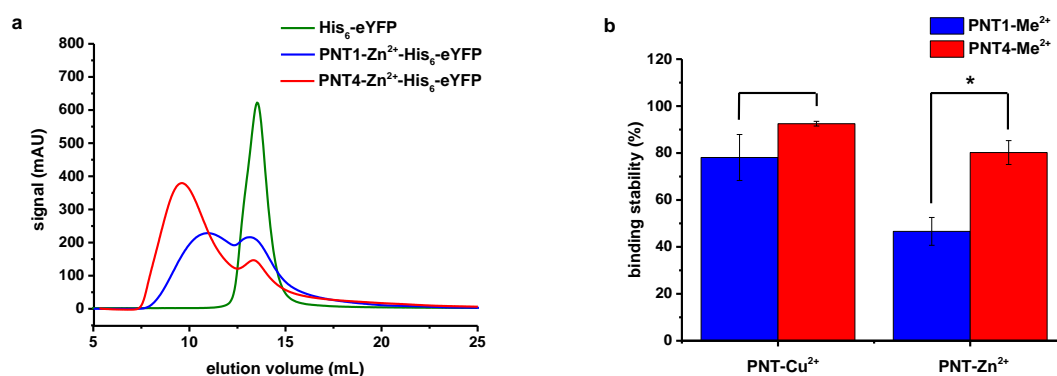


Figure 4-8. Stability of PNT- Me^{2+} - His_6 -eYFP conjugates at pH 7.4. (a) FPLC chromatograms of His_6 -eYFP and PNT1/4- Zn^{2+} - His_6 -eYFP. (b) The percentage of His_6 -eYFP bound with PNT1/4- Me^{2+} . Stars indicate significance in two-tailed Student's t-test; * $P < 0.05$, $n = 3$.

An attractive property of NTA- Me^{2+} - His_6 molecular recognition is the reversible binding at pH 6 [34]. Currently, no pH responsive investigations of trisNTA- Me^{2+} - His_6 have been shown. In order to investigate this, rhodamine B-labelled His_6 (RB- His_6) (which is strongly quenched when bound to Cu^{2+} , and more stable than eYFP at lower pH)[56] was used. As shown in Figure 4-9c, the binding of trisNTA- Cu^{2+} to RB- His_6 resulted in a significant decrease of fluorescent intensity from 570 to 60, remaining unchanged at pH values > 3.3 . The quenching of RB- His_6 fluorescence after binding with trisNTA- Cu^{2+} at pH 3.8 (Figure 4-9c) is higher than the fluorescence shift of RB- His_6 alone at the same pH (Figure 4-9a), suggesting that RB- His_6 remained unchanged after binding with trisNTA- Cu^{2+} . When the pH value dropped to 2.8, a significant increase of the fluorescence was observed, indicating the release of SRB- His_6 from trisNTA- Cu^{2+} complexes. PNT4- Cu^{2+} - His_6 exhibited the same pH tolerance at pH > 3.5 , suggesting that the presence of polymers does not significantly influence the binding stabilities at various pH values.

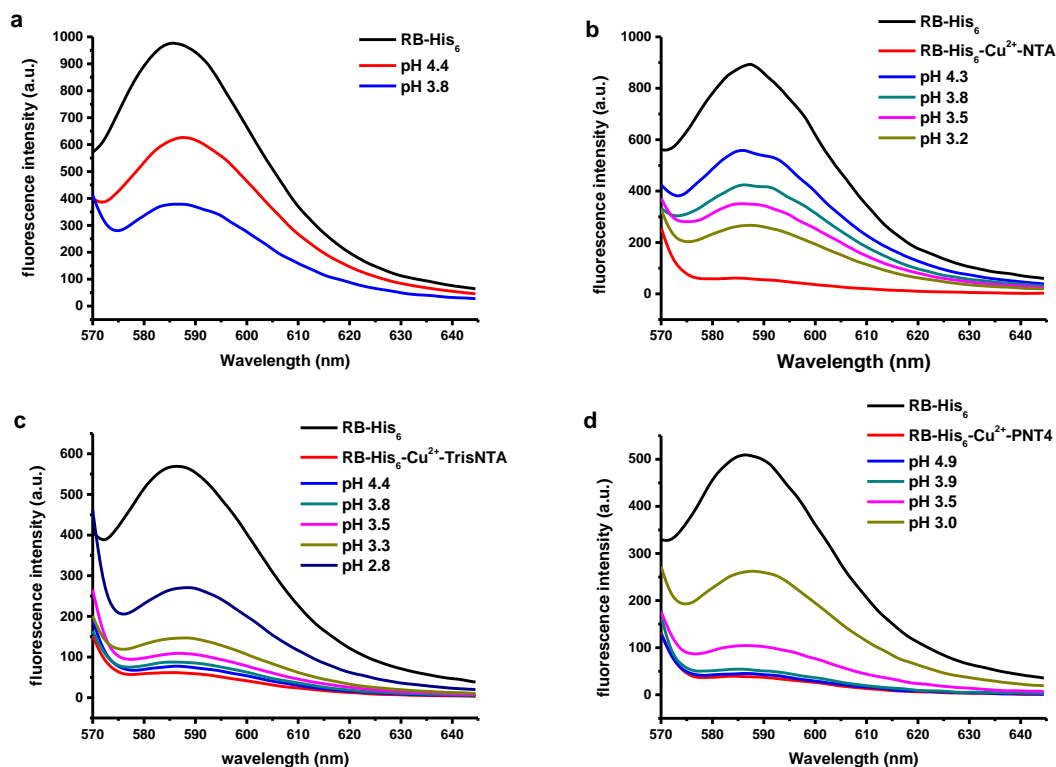


Figure 4-9. Fluorescence emission spectra of RB-His₆ (a) conjugated with NTA-Cu²⁺ (b), trisNTA-Cu²⁺ (c) and PNT4-Cu²⁺ (d) at different pH values.

With the stability of PNT4-Cu²⁺-RB-His₆ determined, pH stability of PNT_n-Me²⁺-His₆-eYFP was investigated. PNT1-Cu²⁺ and PNT4-Cu²⁺ did not show a significant release of His₆-eYFP when the pH was changed from 7.4 to 6, but 53% and 52% of the conjugates dissociated at pH 5 (Figure 4-10). The higher percent of pH-triggered dissociation of PNT4-Cu²⁺-His₆-eYFP compared with PNT4-Cu²⁺-His₆ ($K_D=0.13 \mu\text{M}$)[45] was due to the higher K_D . In contrast with PNT-Cu²⁺, both PNT1-Zn²⁺ and PNT4-Zn²⁺ exhibited a more rapid dissociation. At pH 7.4 PNT1-Zn²⁺ had 53.4% dissociated while PNT4-Zn²⁺ remained bound. Decreasing the pH to 6.0 increased dissociation to 92% and 76%, respectively, with both being completely unbound at pH 5.0. The higher dissociation of PNT-Zn²⁺-His₆-eYFP compared with PNT-Cu²⁺-His₆-eYFP at lower pH is attributed to the lower binding affinity (0.53-1.02 μM , 0.09-0.35 respectively). PNT-Cu²⁺ and His₆-eYFP creates a stable conjugate, which is hard to protonate and dissociate. However, the affinity of PNT-Zn²⁺-His₆-eYFP is comparable to the acid dissociation constant of His₆ (1 μM of K_a)[44] resulting in direct competition between protonation of the imidazole nitrogen and coordination with the conjugate, resulting in a higher rate of dissociation when the

proton concentration is increased. This can also explain the different pH responsiveness of His₆-tagged molecules bound to NTA-Me²⁺ or PNT-Me²⁺.

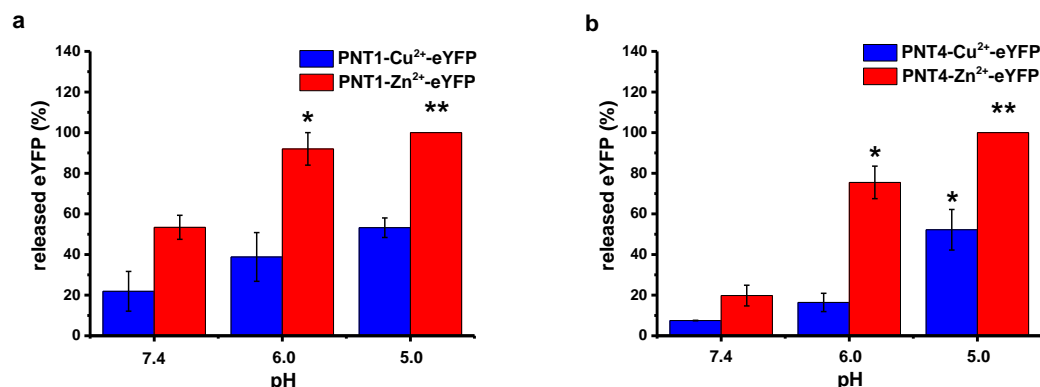


Figure 4-10. Release of His₆-eYFP from PNT1-Me²⁺ (a) and PNT4-Me²⁺ (b) at different pH values. All statistics were analysed by comparing samples to their respective protein-polymer conjugate at pH 7.4. Stars indicate significance in two-tailed Student's t-test; *P<0.05, **P<0.005.

To address the question of whether the reversible binding of PNT copolymers to His₆-eYFP influence its fluorescent property, His₆-eYFP was characterized by fluorescence spectroscopy before and after polymer conjugation (Figure 4-11). When His₆-eYFP was conjugated with PNT4-Zn²⁺, a decrease in fluorescence intensity was observed due to the chelation with Zn²⁺. After dissociation from PNT4-Zn²⁺ in acidic conditions (pH = 5 or 6) and then buffered back to pH 7.4, the fluorescence of His₆-eYFP recovered almost to its original value. The slight decrease of fluorescence intensity was due to short-term exposure to acidic condition which corresponds to literature precedence.[57] These results indicate that PNT copolymers are able to bind His₆-eYFP at physiological pH causing a decrease in fluorescence, and release the loaded protein in acidic conditions.

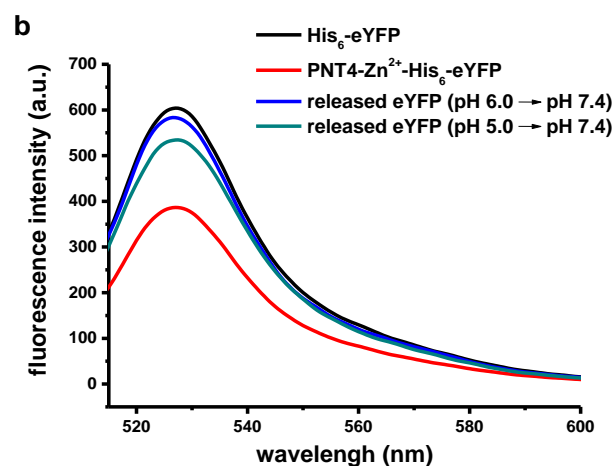


Figure 4-11. The fluorescence emission spectra of His₆-eYFP and PNT4-Zn²⁺-His₆-eYFP before and after release in acidic conditions. While reactions were run in acidic conditions, all samples were analysed at pH 7.4 in PBS.

4.2.5. Delivery of PNT-Zn²⁺-His₆-tagged molecules conjugates into living cells

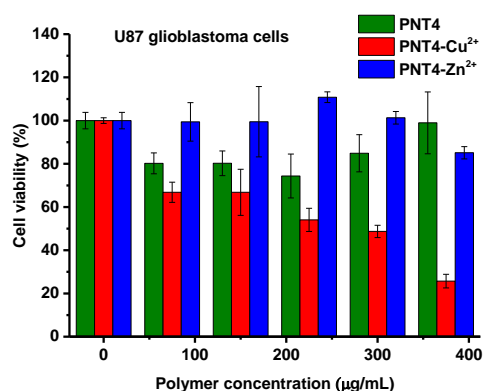


Figure 4-12. Toxicity evaluation of PNT4-Meⁿ⁺ copolymers on U87 cells using MTS assay. Errors bars represent the standard deviation (n=3).

The cytotoxicity of PNT4-Meⁿ⁺ copolymers was evaluated by using the 3-(4,5-dimethylthiazol-2-yl)-5-(3-carboxymethoxyphenyl)-2-(4-sulfophenyl)-2H-tetrazolium (MTS) assay. While PNT4 copolymer showed low cytotoxicity (Figure 4-12), PNT4 coordinated with Cu²⁺ led to an increase of the cytotoxicity with increasing PNT4-Cu²⁺ concentration. In contrast to PNT4-Cu²⁺, low toxicity was observed for PNT4-Zn²⁺ in all tested concentrations, suggesting that PNT4-Zn²⁺ can be used for *in-vitro* or *in-vivo* applications.

The cellular uptake of PNT4-Zn²⁺-His₆-RB was first investigated. After incubating PNT4-Zn²⁺-His₆-RB with U87 glioblastoma cells for 24 hs, a significant cellular uptake of PNT4-Zn²⁺-His₆-RB was observed compared with His₆-RB alone (Figure 4-13, red channel). To determine the cellular localization of PNT4-Zn²⁺-His₆-RB, z-stack confocal images of PNT4-Zn²⁺-His₆-RB treated U87 cells were obtained (Figure 4-14). Based on confocal fluorescence images it is apparent that His₆-RB was distributed in the interior not on the surface of cells.

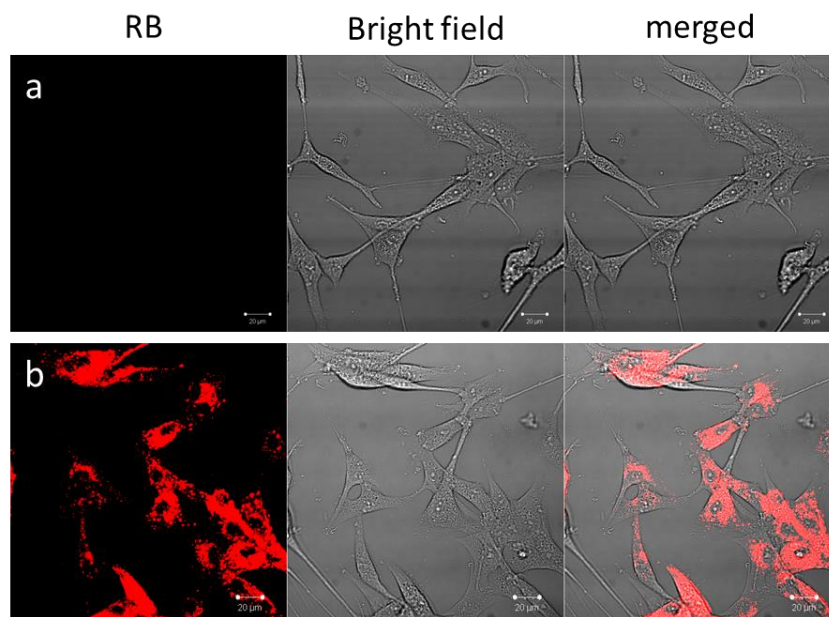


Figure 4-13. CLSM images of U87 cells incubated with a) His₆-RB and b) PNT4-Zn²⁺-His₆-RB (scale bar = 20 μm).

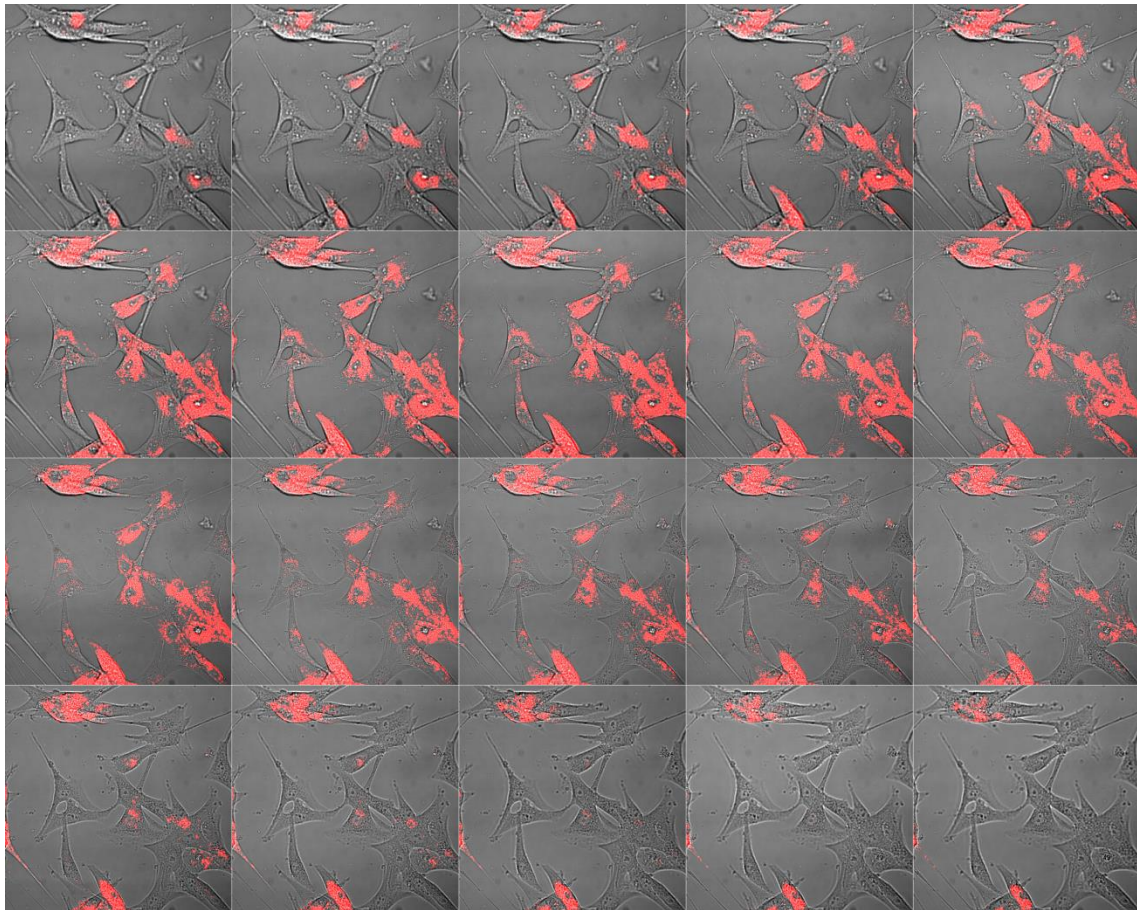


Figure 4-14. Confocal fluorescence microscopy Z-stack montage for living U87 cells incubated with PNT4-Zn²⁺-His₆-RB.

In the next step, the cellular internalization of PNT4-Zn²⁺-His₆-eYFP was investigated. No obvious cellular uptake of PNT4-Zn²⁺-His₆-eYFP was observed compared with His₆-eYFP alone (Figure 4-15). The distinct results comparing with PNT4-Zn²⁺-His₆-RB can be due to the negative charged His₆-eYFP (-6.3 ± 3.0 mV). We are trying to conjugate targeting molecules such as TAT peptides on the PNT copolymers to promote the cellular uptake of proteins. It's still on the process.

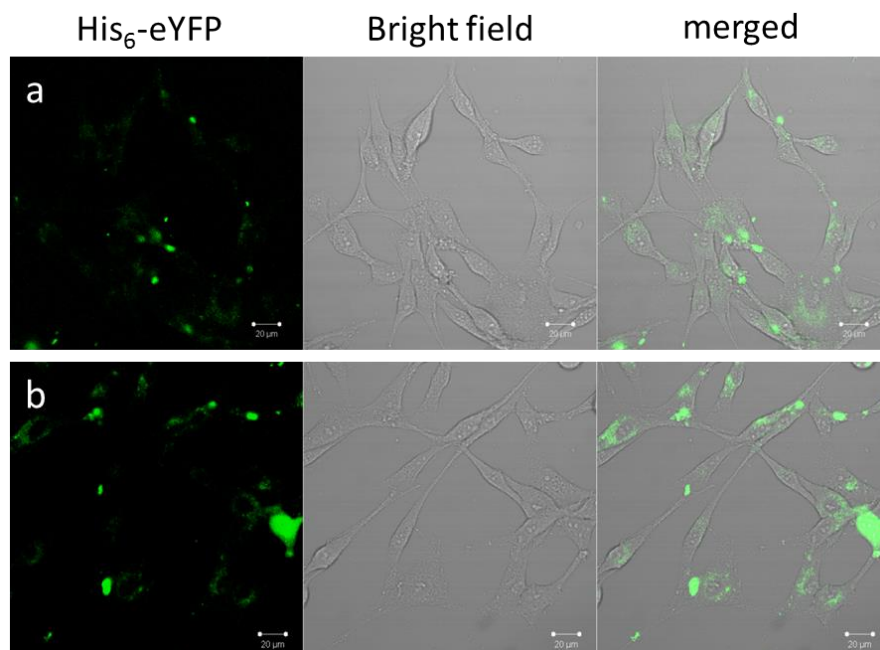


Figure 4-15. CLSM images of U87 cells incubated with a) His₆-eYFP and b) PNT4-Zn²⁺-His₆-eYFP (scale bar = 20 μm).

4.3. Conclusion

A robust and efficient method to conjugate multiple proteins on a single polymer chain using trisNTA-Me²⁺-His₆ molecular recognition was designed. His₆-eYFP was used as a model protein for binding PNT-Meⁿ⁺ copolymers. It was demonstrated that the nature of the Meⁿ⁺, and the distance between trisNTA binding sites on PNT copolymers enable great selectivity for the binding affinity and inter-protein interactions, leading to control of the stability and pH triggered release of the protein from the polymer. After complete release of His₆-eYFP from PNT-Me²⁺ copolymers at selective pH, the return of fluorescence suggested that the protein was intact and maintained its properties.

The presented PNT copolymers in this work have many advantages as nanosystems for protein delivery because they: 1) have site-specific polymer conjugation to proteins; 2) have high stability of the conjugate in physiological condition while rapid dissociation in acid conditions (pH 6); 3) preserve protein structure and properties; 4) show low toxicity in vitro; 5) have low molecular weights and the polymers are expected to eliminate from the body; 6) allow the possibility to simultaneously bind multiple different proteins (combination of therapeutic, detection, and targeting proteins). In addition, the toxicity problem of NTA and its derivatives, which often incorporate toxic metals such as Ni²⁺

and Cu^{2+} due to their high binding affinity, has been improved by using less toxic Zn^{2+} . Moreover, PNT- Zn^{2+} -His₆-eYFP conjugates maintain high binding affinity (submicromolar) as well due to the multivalent binding (trisNTA) and inter-protein interactions.

However, the properties of His-tagged molecules might affect the cellular uptake ability of their conjugates with PNT- Zn^{2+} . More investigations are needed to fully understand the influence factors.

4.4. Experimental section

Materials. Copper(II) chloride, Zinc chloride, Iron(III) sulfate hydrate and Phosphate buffered saline (PBS) were purchased from Sigma-Aldrich and used as received. Rhodamine B labelled hexa-histidine was received as a gift from Dr. Pascal Tanner.

Chelation of metal cations to PNTn copolymers. Respective PNTn copolymers were dissolved in 1 mM PBS buffer (pH 7.4). A stoichiometric excess of CuCl_2 , ZnCl_2 , or $\text{Fe}_2(\text{SO}_4)_3$ was mixed with the respective PNTn solution and was purified on a HiTrap desalting column (5 mL, GE Healthcare Life Sciences) with PBS as the mobile phase.

Protein analysis. Fluorescence of His₆-eYFP ($\lambda_{\text{ex}} = 513 \text{ nm}$, $\lambda_{\text{em}} = 524 \text{ nm}$) and polymer-protein conjugates was investigated with a PerkinElmer LS55 fluorescence spectrometer (Waltham, Massachusetts, USA) at ambient temperature.

Stability and pH responsiveness of PNT- Me^{2+} -His₆-eYFP conjugates. Fast protein liquid chromatography (FPLC) was used for the analysis of the stability and the pH responsiveness of PNT- Me^{2+} -His₆-eYFP conjugates. 250 μM His₆-eYFP was incubated with a metal cation-coordinated PNT in PBS buffer with a molar ratio of 1:2.2 His₆-eYFP:trisNTA. The solution (500 μL) was loaded onto a Superdex 200 10/300 GL (Akta Prime system, Amersham Biosciences, measuring @ 513 nm), and eluted with a PBS mobile phase. For the investigation of pH responsiveness, the column was equilibrated with buffering power of PBS solution at pH 5.0 or 6.0. The sample was prepared in the same way as previously described, loaded onto the column and eluted with PBS solution at pH 5.0 or 6.0. The data were analyzed by Fityk software to calculate the integral area of the individual peaks.

Structure of PNT- Me^{2+} -His₆-eYFP conjugates. The size of PNT- Me^{2+} -His₆-eYFP conjugates were investigated by DLS with a Zetasizer Nano ZSP (Malvern Instruments Ltd., UK) at

25 °C in PBS buffer. The data were fit based on number distribution. The concentration of His₆-eYFP was 20 μM and 1mL of solution was used for measurements.

The negatively stained image of PNT4-Zn²⁺-His₆-eYFP conjugates stained with 2% uranyl acetate was performed on a transmission electron microscope (Philips CM100) at an acceleration voltage of 80 kV. The size of the conjugates was analyzed using ImageJ software.

Cell culture. HeLa cells or U87 glioblastoma cells were maintained at 37 °C in a 5% CO₂ humidified atmosphere and were grown in Dulbecco's modified eagle medium (DMEM) with 10% fetal bovine serum (FBS), 100 units/mL penicillin, 100 μg/mL streptomycin and 2 mM L-glutamine.

Cell viability. Cytotoxicity testing was performed using the Promega CellTiter 96 Aqueous Non-Radioactive Cell Proliferation (MTS) assay (Promega, USA) to determine the number of viable cells in culture. HeLa and U87 cells were seeded in a 96-well plate the night before experiments at 0.5×10^4 and 1×10^4 cells/well in 100 μl, respectively. The day of the experiment, samples (10μL) containing different amount of PNT4-Me²⁺ (0-400 μg/mL), were added to the cells. Twenty-four hours later, 20 μL of MTS solution were added to each well and incubated for 3h at 37 °C. Cell viability was calculated by measuring the absorbance at 490 nm using a 96-well plate reader and plotted relative to untreated cells that were grown the same day in the same plate and assays were performed in triplicate.

Cellular uptake. The U87 cells (3×10^4 cells in 0.3 mL medium) were seeded in 8-well ibidi chamber. After an overnight incubation, the cell culture medium was replaced with serum-free medium (0.14 mL). The PNT4-Zn²⁺-His₆-eYFP conjugate, containing 30 μg of protein, or PNT4-Zn²⁺-RB-His₆ with the same molar concentration were then added by dilution to the cell culture medium. After 4h incubation, the serum-free medium was carefully removed and replaced with medium containing 10% FBS (0.3 mL). The cells were incubated for 20 h more. Right before live cell imaging, the cell culture medium was replaced with an Opti-MEM solution. The imaging was performed on Zeiss microscope. Images were taken using a 40x water-immersion objective. Excitation was at 514 nm for YFP fluorescence and 543 nm for RB-His₆.

4.5. References

- [1] Leader B, Baca QJ, Golan DE. Protein therapeutics: a summary and pharmacological classification. *Nature Review Drug Discovery*. 2008;7:21-39.
- [2] Swinney DC, Anthony J. How were new medicines discovered? *Nature Review Drug Discovery*. 2011;10:507-19.
- [3] Frokjaer S, Otzen DE. Protein drug stability: a formulation challenge. *Nature Review Drug Discovery*. 2005;4:298-306.
- [4] De Groot AS, Scott DW. Immunogenicity of protein therapeutics. *Trends in Immunology*. 2007;28:482-90.
- [5] Christian DA, Cai S, Bowen DM, Kim Y, Pajeroski JD, Discher DE. Polymersome carriers: From self-assembly to siRNA and protein therapeutics. *European Journal of Pharmaceutics and Biopharmaceutics*. 2009;71:463-74.
- [6] Lee KY, Yuk SH. Polymeric protein delivery systems. *Progress in Polymer Science*. 2007;32:669-97.
- [7] Vermonden T, Censi R, Hennink WE. Hydrogels for protein delivery. *Chemical Reviews*. 2012;112:2853-88.
- [8] Zhao M, Hu B, Gu Z, Joo K-I, Wang P, Tang Y. Degradable polymeric nanocapsule for efficient intracellular delivery of a high molecular weight tumor-selective protein complex. *Nano Today*. 2013;8:11-20.
- [9] Balasubramanian V, Onaca O, Enea R, Hughes DW, Palivan CG. Protein delivery: from conventional drug delivery carriers to polymeric nanoreactors. *Expert Opinion on Drug Delivery*. 2010;7:63-78.
- [10] Palivan CG, Fischer-Onaca O, Delcea M, Itef F, Meier W. Protein-polymer nanoreactors for medical applications. *Chemical Society Reviews*. 2012;41:2800-23.
- [11] Baumann P, Balasubramanian V, Onaca-Fischer O, Sienkiewicz A, Palivan CG. Light-responsive polymer nanoreactors: a source of reactive oxygen species on demand. *Nanoscale*. 2013;5:217-24.
- [12] Langowska K, Palivan CG, Meier W. Polymer nanoreactors shown to produce and release antibiotics locally. *Chemical Communications*. 2013;49:128-30.
- [13] Lee JS, Feijen J. Polymersomes for drug delivery: Design, formation and characterization. *Journal of Controlled Release*. 2012;161:473-83.
- [14] Duncan R. Polymer conjugates as anticancer nanomedicines. *Nat Rev Cancer*. 2006;6:688-701.
- [15] Knop K, Hoogenboom R, Fischer D, Schubert US. Poly(ethylene glycol) in drug delivery: pros and cons as well as potential alternatives. *Angewandte Chemie International Edition*. 2010;49:6288-308.
- [16] Kolata A, Baradia D, Patil S, Vhora I, Kore G, Misra A. PEG — A versatile conjugating ligand for drugs and drug delivery systems. *Journal of Controlled Release*. 2014;192:67-81.
- [17] Pelegri-O'Day EM, Lin E-W, Maynard HD. Therapeutic protein-polymer conjugates: advancing beyond PEGylation. *Journal of the American Chemical Society*. 2014;136:14323-32.
- [18] Harris JM, Chess RB. Effect of pegylation on pharmaceuticals. *Nature Review Drug Discovery*. 2003;2:214-21.
- [19] Hershfield M, Sundry J, Ganson N, Kelly S. Development of PEGylated mammalian urate oxidase as a therapy for patients with refractory gout. In: Veronese F, editor.

PEGylated Protein Drugs: Basic Science and Clinical Applications: Birkhäuser Basel; 2009. p. 217-27.

[20] Welte K, Gabrilove J, Bronchud M, Platzer E, Morstyn G. Filgrastim (r-metHuG-CSF): the first 10 years 1996.

[21] Caliceti P, Veronese FM. Pharmacokinetic and biodistribution properties of poly(ethylene glycol)-protein conjugates. *Advanced Drug Delivery Reviews*. 2003;55:1261-77.

[22] Gauthier MA, Klok H-A. Polymer-protein conjugates: an enzymatic activity perspective. *Polymer Chemistry*. 2010;1:1352-73.

[23] Secundo F. Conformational changes of enzymes upon immobilisation. *Chemical Society Reviews*. 2013;42:6250-61.

[24] Filpula D, Zhao H. Releasable PEGylation of proteins with customized linkers. *Advanced Drug Delivery Reviews*. 2008;60:29-49.

[25] Tao L, Liu J, Xu J, Davis TP. Bio-reversible polyPEGylation. *Chemical Communications*. 2009:6560-2.

[26] Kochendoerfer GG. Site-specific polymer modification of therapeutic proteins. *Current Opinion in Chemical Biology*. 2005;9:555-60.

[27] Delgado C, Francis GE, Fisher D. The uses and properties of PEG-linked proteins. *Critical reviews in therapeutic drug carrier systems*. 1991;9:249-304.

[28] Broyer RM, Grover GN, Maynard HD. Emerging synthetic approaches for protein-polymer conjugations. *Chemical Communications*. 2011;47:2212-26.

[29] Roberts MJ, Bentley MD, Harris JM. Chemistry for peptide and protein PEGylation. *Advanced Drug Delivery Reviews*. 2002;54:459-76.

[30] Cong Y, Pawlisz E, Bryant P, Balan S, Laurine E, Tommasi R, et al. Site-specific PEGylation at histidine tags. *Bioconjugate Chemistry*. 2012;23:248-63.

[31] Xia Y, Tang S, Olsen BD. Site-specific conjugation of RAFT polymers to proteins via expressed protein ligation. *Chemical Communications*. 2013;49:2566-8.

[32] Deiters A, Cropp TA, Summerer D, Mukherji M, Schultz PG. Site-specific PEGylation of proteins containing unnatural amino acids. *Bioorganic & Medicinal Chemistry Letters*. 2004;14:5743-5.

[33] Haag R, Kratz F. Polymer therapeutics: concepts and applications. *Angewandte Chemie International Edition*. 2006;45:1198-215.

[34] June RK, Gogoi K, Eguchi A, Cui X-S, Dowdy SF. Synthesis of a pH-Sensitive nitrilotriacetic linker to peptide transduction domains to enable intracellular delivery of histidine imidazole ring-containing macromolecules. *Journal of the American Chemical Society*. 2010;132:10680-2.

[35] Lata S, Reichel A, Brock R, Tampé R, Piehler J. High-affinity adaptors for switchable recognition of histidine-tagged proteins. *Journal of the American Chemical Society*. 2005;127:10205-15.

[36] Reichel A, Schaible D, Al Furoukh N, Cohen M, Schreiber G, Piehler J. Noncovalent, Site-specific biotinylation of histidine-tagged proteins. *Analytical Chemistry*. 2007;79:8590-600.

[37] Choe W-S, Clemmitt RH, Chase HA, Middelberg APJ. Comparison of histidine-tag capture chemistries for purification following chemical extraction. *Journal of Chromatography A*. 2002;953:111-21.

[38] Turnlund JR. Human whole-body copper metabolism. *The American Journal of Clinical Nutrition*. 1998;67:960S-4S.

- [39] Pereira MC, Pereira ML, Sousa JP. Evaluation of nickel toxicity on liver, spleen, and kidney of mice after administration of high-dose metal ion. *Journal of Biomedical Materials Research*. 1998;40:40-7.
- [40] Gupta S. Cell therapy to remove excess copper in Wilson's disease. *Annals of the New York Academy of Sciences*. 2014;1315:70-80.
- [41] Guo H, Wu B, Cui H, Peng X, Fang J, Zuo Z, et al. NiCl₂-down-regulated antioxidant enzyme mRNA expression causes oxidative damage in the broiler's kidney. *Biological Trace Element Research*. 2014;162:288-95.
- [42] Stadlbauer S. *Coordination chemistry in molecular recognition*. Regensburg: University of Regensburg; 2009.
- [43] Kim TH, Swierczewska M, Oh Y, Kim A, Jo DG, Park JH, et al. Mix to validate: a facile, reversible PEGylation for fast screening of potential therapeutic proteins *In vivo*. *Angewandte Chemie International Edition*. 2013;52:6880-4.
- [44] Lee ES, Shin HJ, Na K, Bae YH. Poly(l-histidine)-PEG block copolymer micelles and pH-induced destabilization. *Journal of Controlled Release*. 2003;90:363-74.
- [45] Liu J, Spulber M, Wu D, Talom RM, Palivan CG, Meier W. Poly(N-isopropylacrylamide-co-tris-nitilotriacetic acid acrylamide) for a Combined Study of Molecular Recognition and Spatial Constraints in Protein Binding and Interactions. *Journal of the American Chemical Society*. 2014;136:12607-14.
- [46] Bolanos-Garcia VM, Wu Q, Ochi T, Chirgadze DY, Sibanda BL, Blundell TL. Spatial and temporal organization of multi-protein assemblies: achieving sensitive control in information-rich cell-regulatory systems. *Philosophical Transactions of the Royal Society A: Mathematical, Physical and Engineering Sciences*. 2012;370:3023-39.
- [47] Nussinov R, Jang H. Dynamic multiprotein assemblies shape the spatial structure of cell signaling. *Progress in Biophysics and Molecular Biology*. 2014;116:158-64.
- [48] Saka SK, Honigsmann A, Eggeling C, Hell SW, Lang T, Rizzoli SO. Multi-protein assemblies underlie the mesoscale organization of the plasma membrane. *Nat Communication*. 2014;5.
- [49] Duncan R. The dawning era of polymer therapeutics. *Nature Review Drug Discovery*. 2003;2:347-60.
- [50] Griffith BR, Allen BL, Rapraeger AC, Kiessling LL. A polymer scaffold for protein oligomerization. *Journal of the American Chemical Society*. 2004;126:1608-9.
- [51] Saluja A, Kalonia DS. Nature and consequences of protein-protein interactions in high protein concentration solutions. *International Journal of Pharmaceutics*. 2008;358:1-15.
- [52] Van Rijn P. Polymer directed protein assemblies. *Polymers*. 2013;5:576-99.
- [53] Gao W, Liu W, Mackay JA, Zalutsky MR, Toone EJ, Chilkoti A. In situ growth of a stoichiometric PEG-like conjugate at a protein's N-terminus with significantly improved pharmacokinetics. *Proceedings of the National Academy of Sciences*. 2009;106:15231-6.
- [54] Heredia KL, Bontempo D, Ly T, Byers JT, Halstenberg S, Maynard HD. In situ preparation of protein-"smart" polymer conjugates with retention of bioactivity. *Journal of the American Chemical Society*. 2005;127:16955-60.
- [55] Chilkoti A, Chen G, Stayton PS, Hoffman AS. Site-specific conjugation of a temperature-sensitive polymer to a genetically engineered protein. *Bioconjugate Chemistry*. 1994;5:504-7.

[56] Lata S, Gavutis M, Tampé R, Piehler J. Specific and stable fluorescence labeling of histidine-tagged proteins for dissecting multi-protein complex formation. *Journal of the American Chemical Society*. 2006;128:2365-72.

[57] Anderson DE, Becktel WJ, Dahlquist FW. pH-induced denaturation of proteins: a single salt bridge contributes 3-5 kcal/mol to the free energy of folding of T4 lysozyme. *Biochemistry*. 1990;29:2403-8.

5. Design and construct of DNA-functionalized polymersomes

5.1. Introduction

In 1996, spherical nucleic acids (SNAs) were first introduced by Prof. Chad Mirkin and defined as nanostructures typically synthesized from inorganic nanoparticle templates and DNA shells, which are immobilized on the surface with high orientation.[1, 2] SNAs not only possess the unique properties from both inorganic nanoparticle (e.g., electronic, luminescent, magnetic, plasmonic, catalytic, quenching) and DNA (e.g., information storage, molecular recognition), but also generate novel properties that are distinct from both sides. For example, linear nucleic acids do not enter cell without transfection agents such as cationic polymers, dendrimers, peptides, or viruses, while SNAs are able to overcome this limitation and be rapidly taken up by 60 different cell types without any additional requirements.[3, 4] In addition, the densely packed DNA on the surface of the particle prevents their digestion by cellular nucleases.[5-7] SNAs have proven their potential in many important applications including intracellular detection, gene transfection, and therapeutic and gene regulation via antisense or siRNA pathways.[2, 8-11] In addition, these well-defined nanoparticles are able to create structures with high regulation in large scale by bottom-up nanofabrication for different purposes such as colloid crystallization,[12, 13] which opens a new way to programmably assemble the nanoparticles into microscopic materials.[14-18]

One of many advantages for SNAs is that they are synthesized from readily available starting materials, which is ideal for applications requiring specific shape and structures. Moreover, all SNAs seem like they share the common properties and features such as rapid cellular uptake, independent of the structure and composition. Liposomal SNAs have been recently reported that they are able to enter ovarian adenocarcinoma cells in high quantities even after a short 1 h incubation time.[11] However, no significant uptake of free DNA with the same sequence was observed after 36 h incubation. In addition, liposomal SNAs exhibit high efficiency for both cellular transfection and gene regulation.[11] Even though liposomal SNAs show higher stability compared with naked liposomes, the stability is still unsatisfactory for *in vivo* applications. Polymersomes can be ideal replacements of liposomes due to their mechanical stability and

adaptability.[19-21] However, until now, studies combining DNA and polymersomes has been rarely performed,[28] even though they are important for both theoretical developments and practical applications.

In this chapter, different approaches for the construction of DNA-functionalized polymersomes are described. First, we tried to modify triblock copolymer, PMOXA-*b*-PDMS-*b*-PMOXA, with DNA by both solution coupling and solid-phase coupling methods. The modification was investigated by gel electrophoresis and anion exchange chromatography. Second, DNA-functionalized polymersomes were self-assembled by a mixture of naked and DNA modified PMOXA-*b*-PDMS-*b*-PMOXA and the structure was characterized by TEM. The presence of DNA on the surface of the vesicle was evaluated by fluorescent correlation spectroscopy (FCS).

In addition, we tried to construct DNA-functionalized polymersomes by in situ modification. Polymersomes were first pre-formed containing a mixture of PMOXA-*b*-PDMS-*b*-PMOXA and PDMS-*b*-PMOXA with azide groups in different molar ratio. The structures of the vesicles were characterized by TEM and DLS. DNA-dibenzylcyclooctyne was subsequently used in order to couple DNA on the surface of the vesicle through strain-promoted azide-alkyne cycloaddition. The obtained DNA-functionalized polymersomes were analyzed by gel electrophoresis and the number of DNAs per vesicle was quantified by FCS.

5.2. Results and discussion

5.2.1. Coupling DNA to the end of triblock copolymer by solid support synthesis

We selected PMOXA-*b*-PDMS-*b*-PMOXA triblock copolymers as the constituent material for the polymersomes because it is capable of self-assembling into nanometer sized vesicular structures with high mechanical stability, good biocompatibility, and minimum toxicity.[22, 23] Compared to diblock copolymers, vesicles formed by triblock copolymers show an enhanced mechanical stability due to the stronger interdigitation and entanglement of the chains within the membranes.[23] PMOXA-*b*-PDMS-*b*-PMOXA (Mn: 6800 g/mol) was synthesized as previously published and the block ratio was calculated as 8:49:8 based on the ¹H NMR results.[23] First, a 22 nucleotide-long sequence (5'-CCT CGC TCT GCT AAT CCT GTT A-3', named as ssDNAa) was coupled to the

polymer by amide bond formation on a solid support (Scheme 5-1). We chose the solid-phase coupling method because it shows higher reaction efficiency for non-hydrophilic polymers compared with the coupling reaction in solution.[24, 25] Hydroxyl-terminated PMOXA₈-*b*-PDMS₄₉-*b*-PMOXA₈ was first reacted with maleic anhydride for the incorporation of the carboxyl group. The carboxyl terminal group of the polymers was further converted to a NHS ester then reacted with the amino group on the 5'-end of DNA, with the 3'-end anchored on a controlled pore glass (CpG) phosphoramidite solid support. After cleavage from the CpG solid support and analysis by agarose gel electrophoresis, only one band was observed corresponding to the free ssDNAa, suggesting the coupling reaction wasn't successful (Figure 5-1). Increasing the reaction time and the concentration didn't show any improvement to the reaction (Data not shown).

Scheme 5-1. Synthesis route of polymer-ssDNAa conjugate by amide bond formation on solid support.

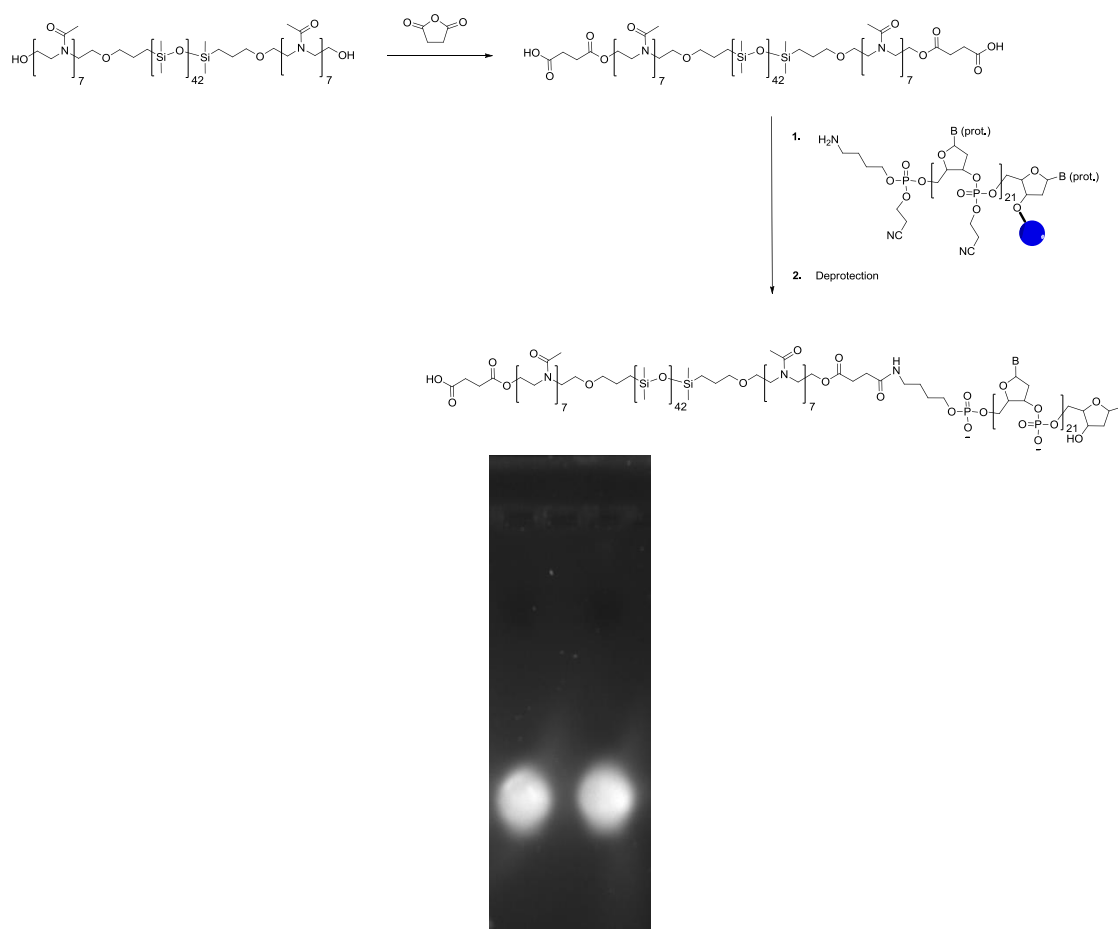
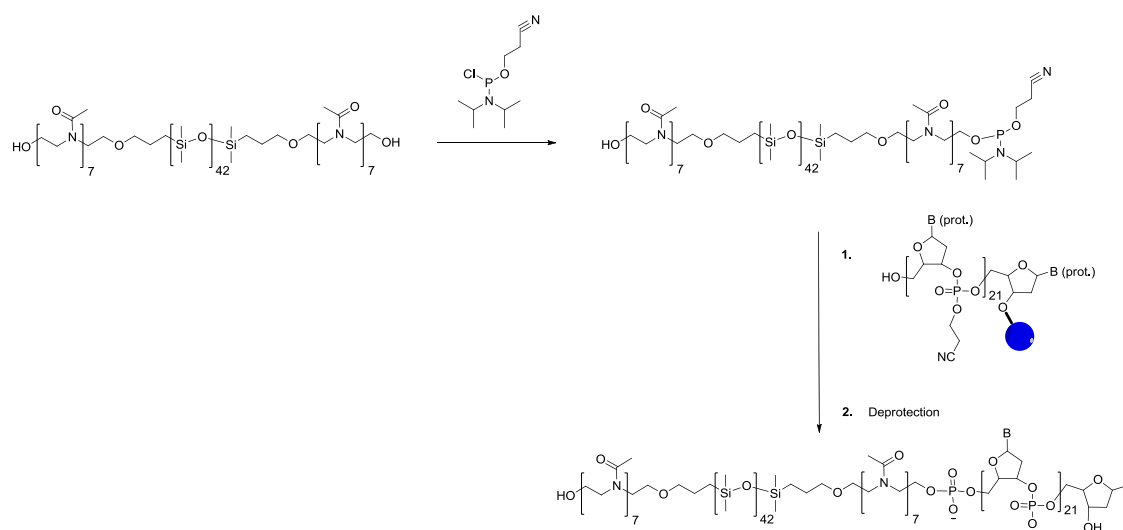


Figure 5-1. Gel analysis of polymer-ssDNAa conjugate (left) and ssDNAa (right).

Next, we tried to couple polymers to ssDNAa by phosphoramidite method, which showed a higher efficiency compared with amide bond formation method and no modification of DNA is required.[26, 27] Hydroxyl-terminated PMOXA₈-*b*-PDMS₄₉-*b*-PMOXA₈ was reacted with phosphoramidite chloride to yield the corresponding phosphoramidite-PMOXA₈-*b*-PDMS₄₉-*b*-PMOXA₈-phosphoramidite derivatives (Scheme 5-2). The presence of phosphoramidite on polymers is proved by the typical peak at 147 ppm by ³¹P NMR (Figure 5-2). The activated polymers were then coupled to the 5' end of the ssDNAa on a CpG solid support in dichloromethane (Scheme 5-2). However, no DNA-polymer conjugate was detected by agarose gel after deprotection in the concentrated ammonia solution (data not shown). A possible reason is that the obtained ssDNAa-polymer conjugates cannot dissolve in any solutions including aqueous solution, organic solvents and the mixtures, due to the huge difference between the polarity of polymer block and the one of DNA block, so no method can prove the presence.

Scheme 5-2. Synthesis route of polymer-ssDNAa conjugate by phosphoramidite method on solid support.



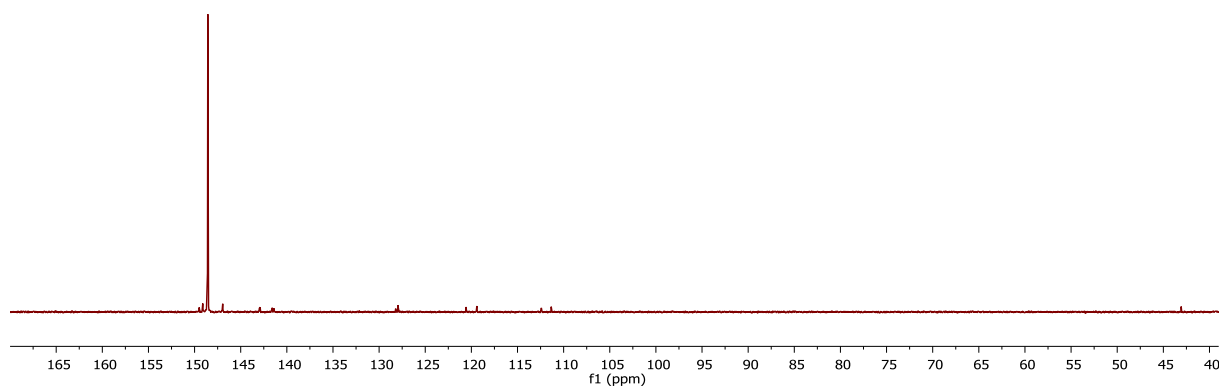
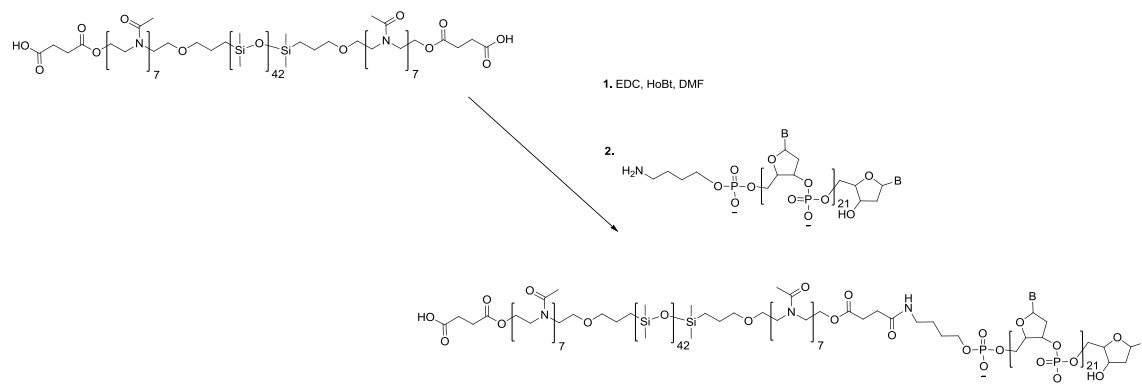


Figure 5-2. ^{31}P NMR spectrum of phosphoramidite-PMOXA₈-*b*-PDMS₄₉-*b*-PMOXA₈-phosphoramidite.

5.2.2. Coupling DNA to the end of triblock copolymer in solution

As discussed above, ssDNA-polymer conjugates might precipitate during the cleavage process in the concentrated ammonia solution and cannot be identified in the presence of CpG beads. To avoid this, coupling reactions were carried out in solution. The amide bond formation method was chosen because it has good efficiency in aqueous solution (Scheme 5-3). Carboxyl-end-functionalized PMOXA₈-*b*-PDMS₄₉-*b*-PMOXA₈ was first dissolved in dimethylformamide (DMF) and activated by EDC and 1-hydroxybenzotriazole hydrate (HoBt). ssDNA aqueous solution was added subsequently and 2/1 of DMF/H₂O (V/V) was used for to dissolve both polymers and DNA. The resulting conjugate was analyzed by agarose gel electrophoresis and anion exchange chromatography. The DNA coupled PMOXA₈-*b*-PDMS₄₉-*b*-PMOXA₈ appeared as a discrete band in the gel and the electrophoretic mobility differed significantly from that of the DNA starting material (Figure 5-3a). Further structural analysis was performed by anion exchange chromatography (Figure 5-3b). A significantly different retention time was observed after the polymer conjugation due to the increase of the molecular weight and size. A 100% reaction yield was calculated based on gel analysis. To be sure that the polymer is covalently bound to ssDNA, the conjugate was incubated in formamide solution or 2% triton solution at 95 °C for 10 mins in order to prevent hydrogen bond formation or hydrophobic interactions. The ssDNA-polymer conjugate was then precipitated in cold isopropanol to remove the free polymer. The resulting conjugates were analyzed by electrophoresis and no change of the migration on the gel was observed (data not shown). As a control experiment, PMOXA₈-*b*-PDMS₄₉-*b*-PMOXA₈

without a carboxyl group was used and reacted following the same procedure. Only free ssDNAa was observed after purification (Figure 5-4). Based on these results, we suppose that ssDNAa has been successfully conjugated to PMOXA₈-*b*-PDMS₄₉-*b*-PMOXA₈. Complementary single-stranded DNA with a sequence (5'-TAA CAG GAT TAG CAG AGC GAG G-3', named as ssDNAb) was conjugated to PMOXA₈-*b*-PDMS₄₉-*b*-PMOXA₈ by the same procedure and the characterizations are shown in Figure 5-5.



Scheme 5-3. Synthesis route of polymer-ssDNAa conjugate by amide bond formation in solution.

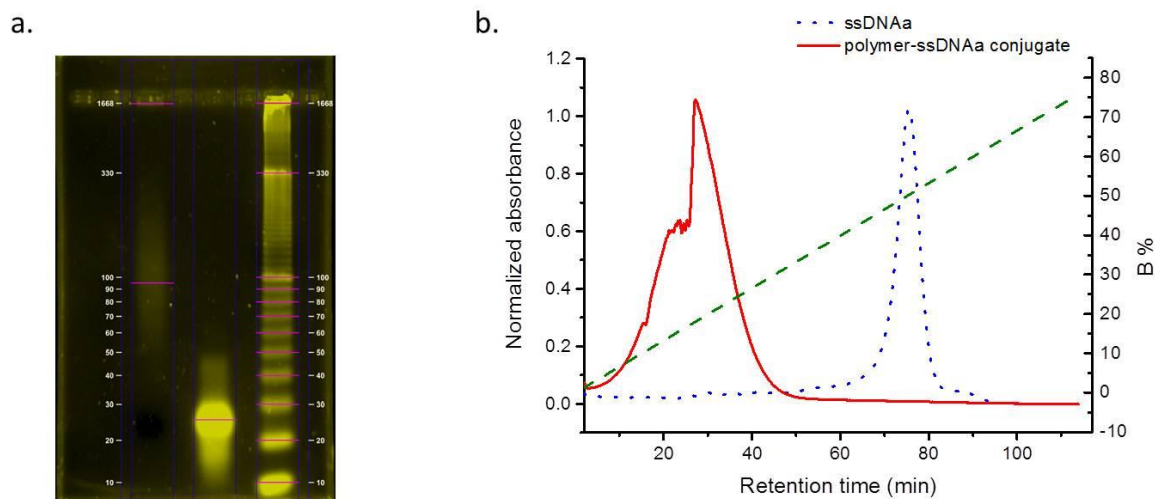


Figure 5-3. Characterization of polymer-ssDNAa conjugate. (a) Gel analysis of polymer-ssDNAa conjugate (left) and free ssDNAa (right); (b) chromatogram from analytical anion exchange chromatography: polymer-ssDNAa conjugate (red line) and free ssDNAa (blue dot). Buffer A: Tris-HCl (25mM). Buffer B: Tris-HCl (25mM)+NaCl (1M)

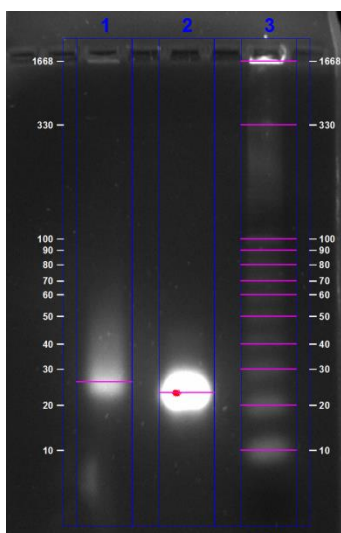
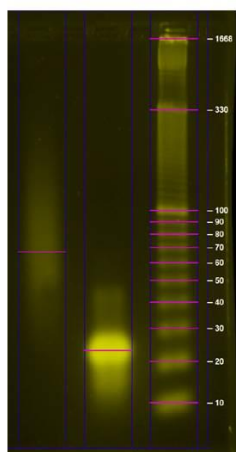


Figure 5-4. Gel analysis of a mixture of PMOXA₈-*b*-PDMS₄₉-*b*-PMOXA₈ and ssDNAa (left) and ssDNAa (right).

a.



b.

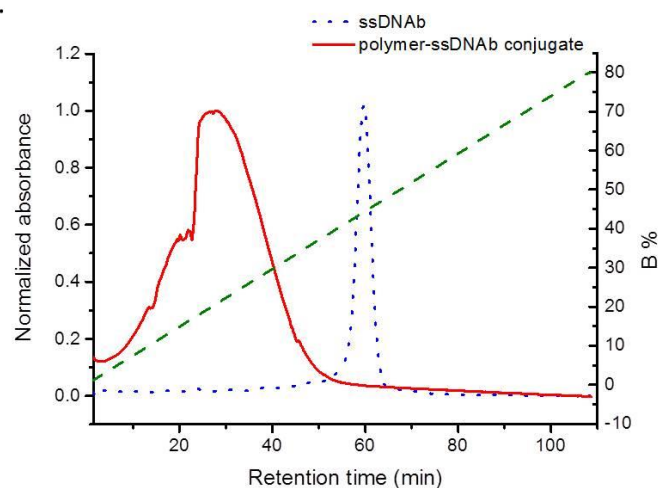


Figure 5-5. Characterization of polymer-ssDNAb conjugate. (a) gel analysis of polymer-ssDNAb conjugate (left) and free ssDNAb (right); (b) chromatogram from analytical anion exchange chromatography: polymer-ssDNAb conjugate (red line) and free ssDNAb (blue dot). Buffer A: Tris-HCl (25mM). Buffer B: Tris-HCl (25mM)+NaCl (1M)

5.2.3. Self-assembly of blended triblock copolymers with DNA-polymer conjugates

The formation of polymersomes was achieved by the bulk film rehydration method using three different mixtures of PMOXA₇-PDMS₄₂-PMOXA₇ with 2, 5, and 10 mol % of PMOXA₈-*b*-PDMS₄₉-*b*-PMOXA₈-ssDNAa (polymer-ssDNAa conjugate). The self-assembled structures were investigated by TEM (Figure 5-6). Nice vesicular structures are observed

when the molar ratio of polymer-ssDNAa conjugate is lower than 10 % and the sample with 5 % of polymer-ssDNAa conjugate was used for further investigation. Two approaches were used to prove and quantify the ssDNAa on the polymersomes. First, atto550-labelled complementary single-stranded DNA (atto550-ssDNAb) was hybridized to the ssDNAa on the polymersomes at 37 °C. The binding of atto550-ssDNAb on the polymersomes can be detected by FCS due to the change of the diffusion time. The number of ssDNAas per vesicle is determined by dividing the value of the molecular brightness of atto550-ssDNAb hybridized vesicles, expressed as counts per molecule (CPM), by the CPM of freely diffusing atto550-ssDNAb. No change of the diffusion time was observed by FCS after the hybridization and only free atto550-ssDNAb ($\tau_D = 120 \mu\text{s}$) was detected, suggesting no ssDNAa on the polymersomes is available for hybridization.

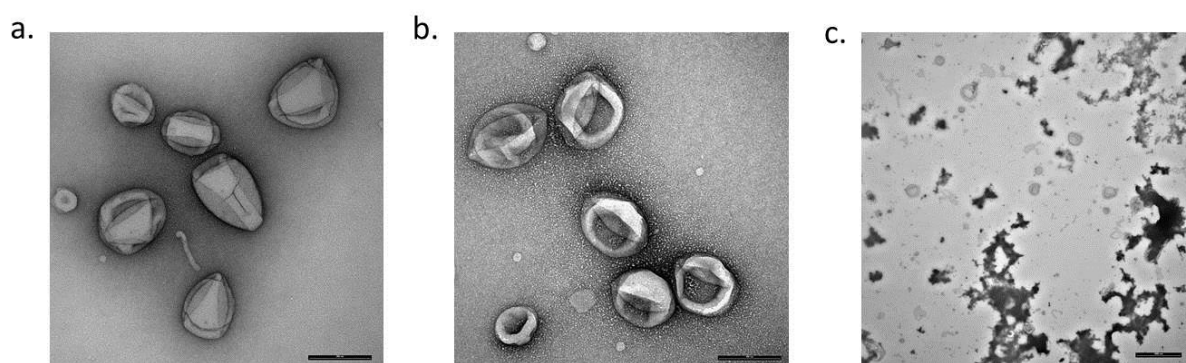


Figure 5-6. TEM images of polymersomes self-assembled by PMOXA₇-PDMS₄₂-PMOXA₇ mixed with 2 (a), 5 (b) and 10 % (c) of PMOXA₈-*b*-PDMS₄₉-*b*-PMOXA₈-ssDNAa. The scale bar is 200 nm, 200nm, and 1000 nm, respectively.

In another approach, we tried to fluorescently label ssDNAa on the polymersome by TdT. TdT is a template independent polymerase that catalyzes the addition of fluorescent-labelled deoxynucleotides to the 3'-hydroxyl terminus of DNA molecules. The activity of TdT was first investigated and analyzed by agarose gel. As shown in Figure 5-7, the base pairs (bp) of DNA increased from 22 to 100 after 15 mins catalyzed by TdT. When polymer-ssDNAa conjugates were mixed with TdT, the migration immediately shifted to 22 bp, the same position with free ssDNAa, suggesting that ssDNAa was cleaved from the polymers. To avoid the influence of the other components in the TdT stock solution and TdT buffer, TdT was purified by centrifugal ultrafiltration and PBS was used for the reaction. However, the shift of the migration of polymer-ssDNAa conjugate to 22 bp was

still observed (Data not shown). We suppose that TdT can break the amide bond or some unknown interactions, which connect $\text{PMOXA}_8\text{-}b\text{-PDMS}_{49}\text{-}b\text{-PMOXA}_8$ and ssDNAa together. The reason is still not clear up to now.

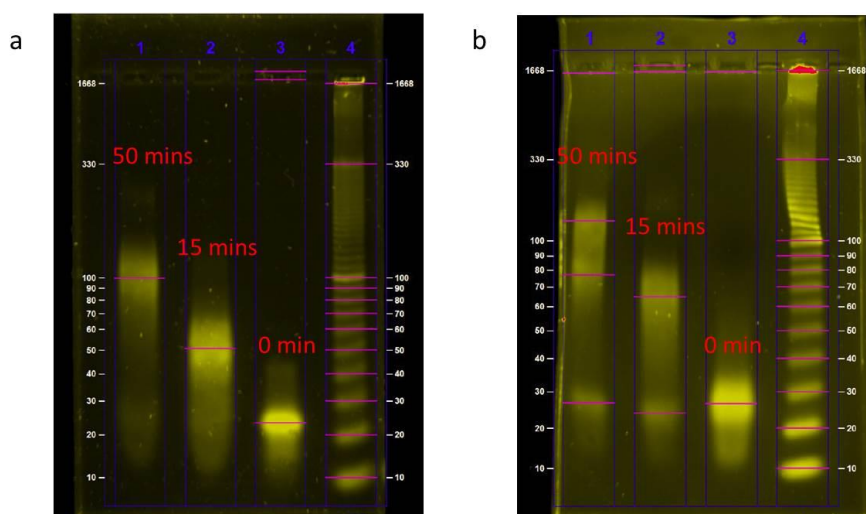


Figure 5-7. TdT activity assessment by gel analysis. Polymerization of free ssDNAa (a) and polymer- ssDNAa conjugate (b) catalyzed by TdT after 15 mins and 50 mins.

5.2.4. Construction of DNA-functionalized polymersomes by in situ modification

As discussed above, the solubility of DNA-polymer conjugates cannot be predicted and some unknown interactions might exist between DNA and polymers. In order to avoid these problems, we were the first to apply in situ coupling of DNA on pre-formed polymersomes. A $\text{PMOXA}\text{-}b\text{-PDMS}\text{-}b\text{-PMOXA}$ triblock polymer with a block ratio of 7:42:7 [23] was selected as the constituent material for the polymersomes because it is capable of self-assembling into nanometer sized vesicular structures. Linking component poly(dimethylsiloxane)-*b*-poly(2-methyloxazoline) diblock copolymers modified with an azide group ($\text{PDMS}\text{-}b\text{-PMOXA}\text{-N}_3$) at a block ratio of 65:32 [22] was used for further functionalization with DNA. $\text{PDMS}_{65}\text{-PMOXA}_{32}\text{-OH}$ was converted to $\text{PDMS}_{65}\text{-PMOXA}_{32}\text{-N}_3$ by a two-step reaction (Scheme 5-4). As shown in Figure 5-8b, $\text{PDMS}_{65}\text{-PMOXA}_{32}\text{-N}_3$ has a longer hydrophilic PMOXA block compared to $\text{PMOXA}_7\text{-PDMS}_{42}\text{-PMOXA}_7$. In this manner, the exposure of the azide group outside of the membrane for further reactions is promoted.

Scheme 5-4. Synthesis route of PDMS₆₅-PMOXA₃₂-N₃.

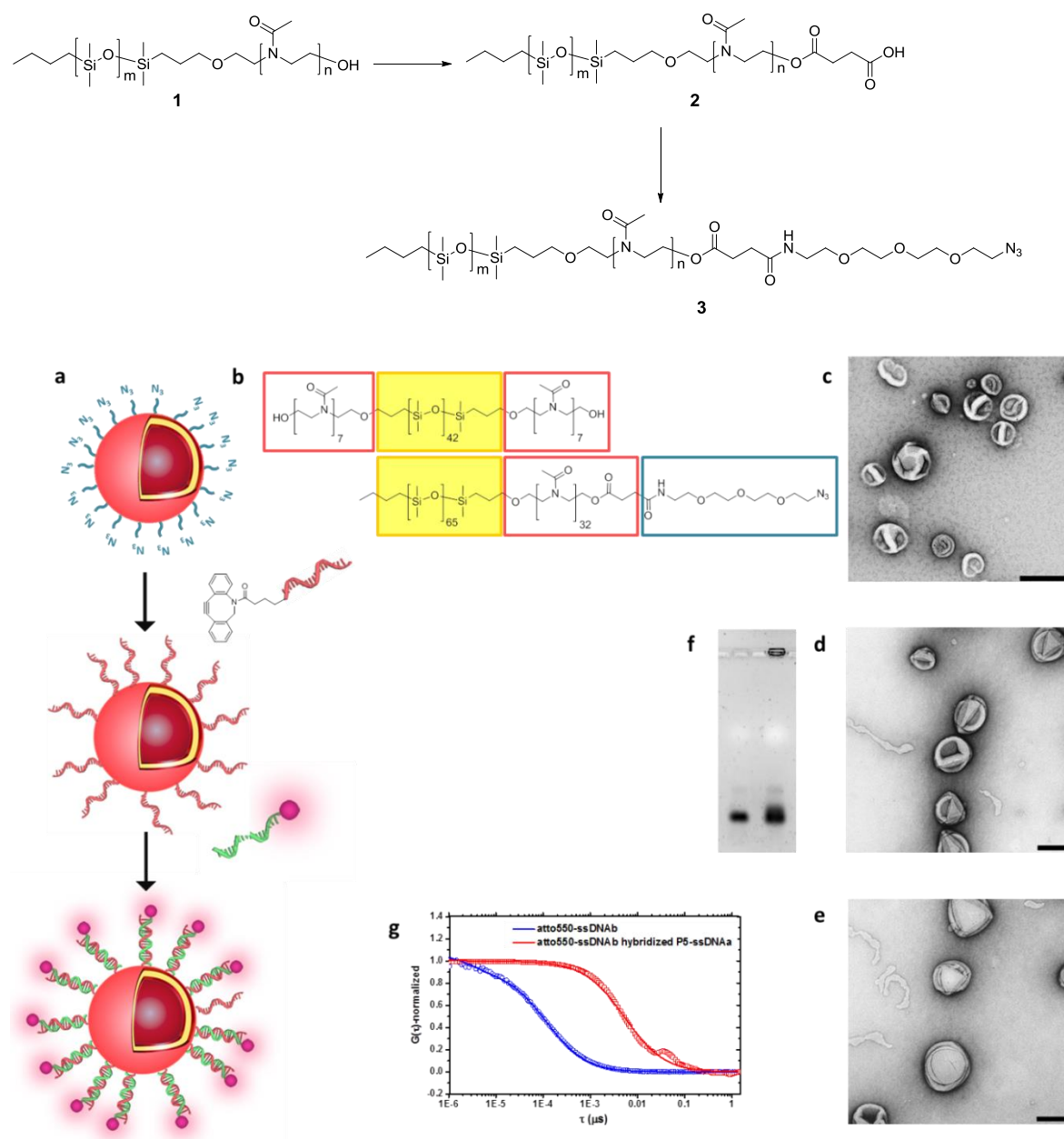


Figure 5-8. Construct DNA-functionalized polymersomes. (a) Schematic representation of polymersomes with azide groups on the surface, anchored with DBCO-ssDNAa and further hybridized with atto550-ssDNAb; (b) chemical structures of PMOXA₇-*b*-PDMS₄₂-*b*-PMOXA₇ and PDMS₆₅-*b*-PMOXA₃₂-N₃; TEM images of P5-N₃ (c), which was modified with ssDNAa (d) and subsequently hybridized with atto550-ssDNAb (e); (f) gel analysis of free ssDNAa (left) and P5-ssDNAa (right); (g) normalized autocorrelation curves from FCS data in PBS: free atto550-ssDNAb (blue) and atto550-ssDNAb hybridized P5-ssDNAa (red).

Polymersomes were obtained by the bulk rehydration approach using three different mixtures of PMOXA₇-*b*-PDMS₄₂-*b*-PMOXA₇ with 0.25, 1, and 5 mol % of PDMS₆₅-*b*-PMOXA₃₂-N₃ (coded as P0.25-N₃, P1-N₃, P5-N₃). TEM confirmed the formation of polymersomes (Figure 5-9). A morphology transition to micelles was observed when higher amounts of PDMS₆₅-PMOXA₃₂-N₃ (>5 %) was used (Figure 5-9). The formed P5-N₃ have a D_H of 180 ± 60 nm and no changes of D_H were observed when the molar ratio of PDMS₆₅-PMOXA₃₂-N₃ was decreased (Table 5-1). A larger diameter of 230 ± 60 nm for P5-N₃ was determined from TEM images due to the collapse of polymersomes during the measurements.

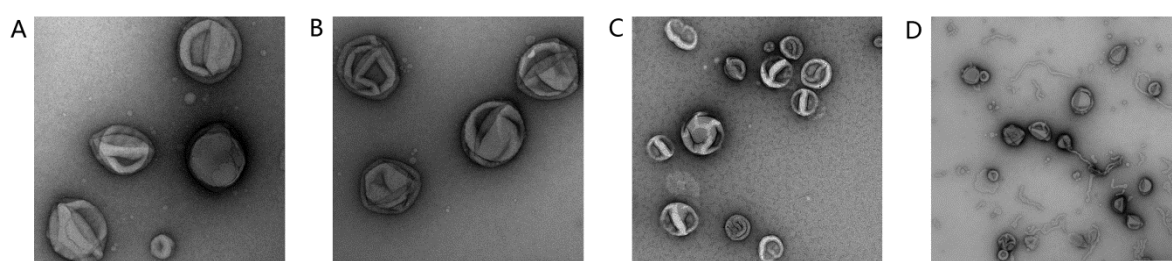


Figure 5-9. TEM images of polymersomes self-assembled by a mixture of PMOXA₇-PDMS₄₂-PMOXA₇ and PDMS₆₅-PMOXA₃₂-N₃ with a molar ratio of 0.25% (A), 1% (B) 5% (C) and 10% (D). The scale bar is 200 nm, 200nm, 500 nm and 500 nm, respectively.

Table 5-1. Reaction yields and sample characteristics: D_H from DLS measurements, diameters (D) from TEM images and ξ potential.

Sample code	Yields (%)	DLS D_H (nm)	TEM D (nm)	ξ potential (mV)
P5-N ₃	--	180 ± 60	230 ± 60	-3.4 ± 1.1
P5-ssDNAa	28	180 ± 60	220 ± 50	-9.2 ± 1.3
P5-ssDNAb	27	180 ± 70	230 ± 50	-9.3 ± 0.7
P1-N ₃	--	180 ± 50	200 ± 40	-2.2 ± 2.3
P1-ssDNAa	45	180 ± 60	220 ± 50	-6.0 ± 0.5
P1-ssDNAb	59	170 ± 50	220 ± 50	-7.2 ± 0.4
P0.25-N ₃	--	180 ± 50	190 ± 40	-2.3 ± 2.1
P0.25-ssDNAa	68	180 ± 60	180 ± 60	-3.7 ± 1.0
P0.25-ssDNAb	96	180 ± 60	190 ± 40	-4.6 ± 1.5

After the formation of polymersomes, a 22mer dibenzocyclooctyl-terminated DNA oligonucleotide (5'-CCT CGC TCT GCT AAT CCT GTT A-3', named as DBCO-ssDNAa) was post-functionalized to the polymersomes through strain-promoted azide-alkyne

cycloaddition. The conjugation of ssDNAa to the polymersomes was proven by agarose electrophoresis analysis (Figure 5-8f). After the click reaction, two DNA bands could be distinguished. The band that did not migrate corresponded to the fraction of ssDNAa anchored on polymersomes. No influence of the polymersome structure and size was observed after DNA functionalization both by TEM and DLS (Figure 5-8d and Table 5-1). The coupling reaction of ssDNAa to polymersomes had a yield of 68 % for P0.25-N₃, determined from DNA absorbance at 260 nm, decreased to 45 % for P1-N₃ and 28 % for P5-N₃. The lower yield obtained for P5-N₃ is due to the higher density of azide groups at the surface leading to higher electrostatic and steric repulsion generated by coupled ssDNAa on the polymersomes (Table 5-1). The increasing electrostatic repulsion is indicated by a decrease of ξ potential value from -3.7 ± 1.0 mV for ssDNAa modified P0.25 (P0.25-ssDNAa) to -9.2 ± 1.3 mV for P5-ssDNAa in PBS buffer (Table 5-1). The reaction yield increased with the reaction time up to 3 days, and no increase in reaction yield could be observed over longer reaction times up to 10 days (Figure 5-10). In a similar manner, the complementary stranded ssDNA with DBCO group on 5'-end (5'-TAA CAG GAT TAG CAG AGC GAG G-3', named DBCO-ssDNAb) was coupled to pre-formed polymersomes. The reaction yield ranged from 96 % for P0.25-N₃, to 59 % and 27 % for P1-N₃ and P5-N₃.

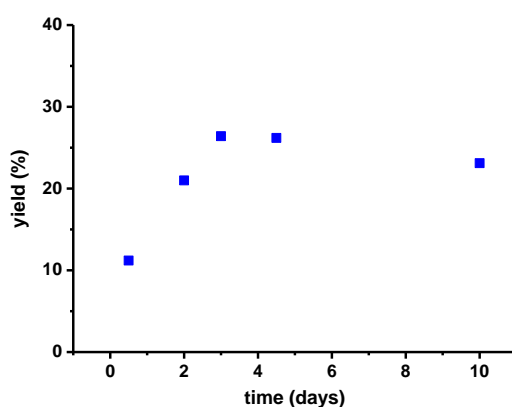


Figure 5-10. The kinetics of the reaction between ssDNAa and azido-polymersomes.

Table 5-2. Characterization of DNA-functionalized polymersomes: diffusion time, number of DNA per vesicle and average surface coverage (σ).

Sample code	Diffusion time (μ s)	Count per molecule (kHz)	Number of DNA per vesicle ^c	σ^d (10^{-3} nm ⁻²)
Atto550-ssDNAb	120 \pm 0	20 \pm 2	--	--
P5-ssDNAa-ssDNAb-Atto550 ^a	5270 \pm 780	1905 \pm 42	93 \pm 2	0.9
P1-ssDNAa-ssDNAb-Atto550	3990 \pm 590	690 \pm 33	34 \pm 2	0.3
P0.25-ssDNAa-ssDNAb-Atto550	3970 \pm 320	280 \pm 16	14 \pm 1	0.1
Atto647N-ssDNAa	140 \pm 0	15 \pm 2	--	--
P5-ssDNAb-ssDNAa-Atto647N ^b	5090 \pm 200	1844 \pm 131	127 \pm 9	1.2
P1-ssDNAb-ssDNAa-Atto647N	3650 \pm 530	579 \pm 41	40 \pm 3	0.4
P0.25-ssDNAb-ssDNAa-Atto647N	4070 \pm 780	267 \pm 29	18 \pm 2	0.2
P5-ssDNAa mixing with Atto647N-ssDNAa	6980 \pm 1860	6 \pm 2	0	0
P5-N ₃ mixing with Atto550-ssDNAb	3440 \pm 1060	2 \pm 0	0	0
Liposomes [29]			39	1.2

^a Polymersomes with ssDNAa were hybridized by Atto550-ssDNAb.

^b Polymersomes with ssDNAb were hybridized by Atto647N-ssDNAa.

^c The number of DNA per vesicle was calculated by count per molecule of atto-DNA hybridizing vesicles divided by count per molecule of free atto-DNA molecules.

^d The σ value was calculated by number of DNA per vesicle/ $\{4 \times 3.14 \times (\text{radius of vesicle})^2\} \times 1000$

In the next step, atto550-labelled complementary single-stranded DNA (atto550-ssDNAb) was hybridized to the ssDNAa on the polymersomes at 37 °C. The number of ssDNAa per vesicle was determined by FCS. The change in the diffusion time, from the value characteristic for free atto550-ssDNAb ($\tau_D = 120 \mu$ s) to a value of 5.3 ± 0.8 ms for atto550-ssDNAb hybridized P5-ssDNAa, indicated the successful hybridization of atto550-ssDNAb to ssDNAa on the polymersomes (Figure 5-8g). Assuming most of

ssDNAa on the polymersomes is involved in the hybridization, the average number of ssDNAa per polymersome of P5-ssDNAa, P1-ssDNAa, and P0.25-ssDNAa was determined as 93 ± 2 , 34 ± 2 and 14 ± 1 , corresponding to an average surface coverage density (σ) of ≈ 0.9 , 0.3 , 0.1 strands per 1000 nm^2 (Table 5-2). The σ value of polymersomes anchored with ssDNAb was determined as 1.2 , 0.4 and 0.2 for P5-ssDNAb, P1-ssDNAb and P0.25-ssDNAb using the same procedure. In control experiments, fluorescence-labelled DNA was incubated with non-functionalized polymersomes and polymersomes with non-complementary stranded DNA. No nonspecific adhesion of DNA to the polymersomes was detected by FCS (Table 5-2). Considering the low amount of diblock copolymers used for polymersome formation and the similar chemical structure of diblock and triblock copolymers, no phase separation on the polymer membrane was taken into account and homogeneous distribution of DNA on the polymersome surface was expected.

5.3. Conclusion

In this chapter, three different strategies were used to construct DNA-functionalized polymersomes. First, the conjugation of PMOXA₈-*b*-PDMS₄₉-*b*-PMOXA₈ with DNA was attempted by the solid-phase coupling method; however, no polymer-DNA conjugates were obtained. Polymer-DNA conjugation carried out in solution showed high reaction yield (100 %). However, it's still not clear whether the polymer and DNA are conjugated covalently. These results indicate that the conventional methods are not suitable for constructing DNA-functionalized polymersomes, because the solubility of DNA-polymer conjugates cannot be predicted and some unknown interactions might exist between DNA and polymers.

In addition, in situ coupling of DNA on formed polymersomes was achieved for the first time. The reaction yield was 28% - 96%, which decreased with the increase of DNA surface coverage on polymersomes due to electrostatic and steric repulsion. No change to the vesicle structures was observed after DNA conjugation to the vesicle surface. This method is able to extend to other structures for their DNA modifications.

5.4. Experimental section

Materials

All chemicals were purchased from Sigma-Aldrich and used as received unless otherwise noted. 50X TAE buffer was purchased from Applichem. All ODNs were purchased from Microsynth.

Synthesis of HOOC-PMOXA₈-*b*-PDMS₄₉-*b*-PMOXA₈-COOH

HO-PMOXA₈-*b*-PDMS₄₉-*b*-PMOXA₈-OH (150 mg, 0.022 mmol) synthesized according to the published procedure was first dissolved into 5 mL anhydrous chloroform, then succinic anhydride (6.5 mg, 0.066 mmol), 4-dimethylaminopyridine (1.32 mg, 0.011 mmol) and triethylamine (8.7 mg, 0.088 mmol) were added. After deoxygenation by vacuum argon cycles, the mixture was further stirred for another 72 hs at RT. Finally, 140 mg colorless solid product was obtained after the ultrafiltration with a yield of 93%. ¹H NMR (400 MHz, δ , CDCl₃): 0 ppm (m, -Si(CH₃)₂), 0.54 ppm (m, -SiCH₂), 1.31 ppm (m, -SiCH₂-CH₂-CH₂O-), 2.08-2.21 ppm (m, CH₃-C=O), 3.40-3.60 ppm (m, -N-CH₂-CH₂-), 3.75 ppm (t, -CH₂-CH₂-COOH).

Coupling of ssDNAa to HOOC-PMOXA₈-*b*-PDMS₄₉-*b*-PMOXA₈-COOH

HOOC-PMOXA₈-*b*-PDMS₄₉-*b*-PMOXA₈-COOH (170 mg, 0.025 mmol) was first reacted with EDC (9.6 mg, 0.05 mmol), HoBt (8.1 mg, 0.06 mmol) and N,N'-Diisopropylethylamine (DIPEA, 15.5 mg, 0.12 mmol) in dichloromethane (DCM) at RT under argon atmosphere for 3 h to obtain PMOXA₈-*b*-PDMS₄₉-*b*-PMOXA₈ with NHS ester groups. ssDNAa, which 5'-end is modified with amino group and the 3'-end is bound to CpG solid support, was subsequently added to the solution and the reaction was carried out for three days. EDC (4.8 mg, 0.025 mmol), HoBt (4 mg, 0.03 mmol) and DIPEA (8 mg, 0.06 mmol) were added three times per day to promote the reaction yield. The solid phase was purified by centrifuge and washed with DCM, ethanol and H₂O for at least three times, respectively. Finally, the solid support and protecting groups were removed by treatment with concentrated ammonia for 16 h at 55 °C. The solid support was removed by centrifuge. After evaporation of ammonia, the conjugate was analyzed by gel electrophoresis.

Synthesis of phosphoramidite-PMOXA₈-*b*-PDMS₄₉-*b*-PMOXA₈-phosphoramidite

HO-PMOXA₈-*b*-PDMS₄₉-*b*-PMOXA₈-OH (300 mg, 0.08 mmol) was dissolved in dry DCM and reacted with N-diisopropyl-2-cyanoethyl-chlorophosphoramidite (189 mg, 0.8 mmol) in the presence of DIPEA (207 mg, 1.6 mmol) at RT under argon atmosphere for 2 h. The

crude product was dried and dissolved in ethyl acetate and extracted with Na₂CO₃ solution, water (3x) and brine (3x). The solution was dried over MgSO₄. After evaporation of the solvent the product was dried under high vacuum. (Yield: 99%) ³¹P NMR (400 MHz, CDCl₃): 147 ppm. ¹H NMR (400 MHz, δ, CDCl₃): 0 ppm (m, -Si(CH₃)₂), 0.54 ppm (m, -SiCH₂), 1.31 ppm (m, -SiCH₂-CH₂-CH₂O-), 2.08-2.21 ppm (m, CH₃-C=O), 2.62 ppm (NC-CH₂-), 2.85 ppm ((CH₃)₂-CH-), 3.40-3.60 ppm (m, -N-CH₂-CH₂-), 3.75 ppm (t, -CH₂-CH₂-CO(O)-), 3.92 ppm (NC-CH₂-CH₂-).

Coupling of ssDNAa to phosphoramidite-PMOXA₈-*b*-PDMS₄₉-*b*-PMOXA₈-phosphoramidite

Phosphoramidite-PMOXA₈-*b*-PDMS₄₉-*b*-PMOXA₈-phosphoramidite (1.1 mg, 0.16 mmol), ssDNAa anchored CpG solid support (0.001 mmol) and 0.3 M 5-(Ethylthiol)-1H-tetrazole was dissolved in DCM (4 mL) at RT under argon atmosphere for three days. The solid phase was purified by centrifuge and washed with DCM, ethanol and H₂O for at least three times, respectively. Finally, the solid support and protecting groups were removed by treatment with concentrated ammonia for 16 h at 55 °C. The solid support was removed by centrifuge. After evaporation of ammonia, the conjugate was analyzed by gel electrophoresis.

Synthesis of PDMS₆₅-PMOXA₃₂-N₃

Poly(dimethylsiloxane)-*block*-poly(2-methyl-2-oxazoline)-COOH. PDMS-*b*-PMOXA-OH (200 mg, 0.022 mmol) synthesized according to the published procedure was first dissolved into 5 mL anhydrous chloroform, then succinic anhydride (6.5 mg, 0.066 mmol), 4-Dimethylaminopyridine (1.32 mg, 0.011 mmol) and triethylamine (8.7 mg, 0.088 mmol) were added. After deoxygenation by vacuum argon cycles, the mixture was further stirred for another 72 hs at RT. Finally, 180 mg colorless solid product was obtained after the ultrafiltration with a yield of 90%. ¹H NMR (400 MHz, δ, CDCl₃): 0 ppm (m, -Si(CH₃)₂), 0.45 ppm (m, -SiCH₂), 0.80 ppm (t, -CH₃), 1.20 ppm (m, -CH₂-CH₂-), 1.50 ppm (m, -SiCH₂-CH₂-CH₂O-), 1.90-2.10 ppm (m, CH₃-C=O), 2.40-2.60 ppm (m, -CH₂-CH₂-COOH), 3.20-3.60 ppm (m, -CH₂-O-CH₂-CH₂-N-CH₂-CH₂-).

Poly(dimethylsiloxane)-*block*-poly(2-methyl-2-oxazoline)-N₃. PDMS-*b*-PMOXA-COOH (100 mg, 0.011 mmol) was first dissolved into anhydrous chloroform, then 11-Azido-3, 6,

9-trioxaundecan-1-amine (11.80 mg, 0.055 mmol), N, N'-Dicyclohexylcarbodiimide (15.6 mg, 0.078 mmol) and 4-Dimethylaminopyridine (1.2 mg, 0.01 mmol) were added. After deoxygenation, the mixture was stirred for another 48 h at RT. Finally, 86 mg colorless solid product was obtained after the ultrafiltration with a yield of 86%. ^1H NMR (400 MHz, δ , CDCl_3): 0 ppm (m, $-\text{Si}(\text{CH}_3)_2$), 0.45 ppm (m, $-\text{SiCH}_2$), 0.80 ppm (t, $-\text{CH}_3$), 1.20 ppm (m, $-\text{CH}_2-\text{CH}_2-$), 1.50 ppm (b, $-\text{SiCH}_2-\text{CH}_2-\text{CH}_2\text{O}-$), 2.0-2.20 ppm (m, $\text{CH}_3-\text{C}=\text{O}$, $\text{OOC}-\text{CH}_2-\text{CH}_2-\text{C}(\text{O})\text{NH}$), 3.20-3.60 ppm (m, $-\text{CH}_2-\text{O}-\text{CH}_2-\text{CH}_2-\text{N}-\text{CH}_2-\text{CH}_2-$, $-\text{C}(\text{O})\text{NH}-\text{CH}_2-\text{CH}_2-\text{O}-\text{C}_2\text{H}_4-\text{O}-\text{C}_2\text{H}_4-\text{O}-\text{C}_2\text{H}_4-\text{N}_3$).

Preparation of polymeric nanocompartments

4 mg $\text{PMOXA}_7\text{-PDMS}_{42}\text{-PMOXA}_7$ was dissolved with 427 μg , 85 μg , and 21 μg of $\text{PDMS}_{65}\text{-PMOXA}_{32}\text{-N}_3$ in 1 mL ethanol in a 5 mL round-bottom flask, and ethanol was removed on a rotary evaporator (100 mbar, 40 °C, 120 rpm). The thin polymer film was then rehydrated by adding 1 mL PBS buffer and stirred overnight. The yielded solution was extruded with an Avanti mini-extruder (Avanti Polar Lipids, Alabama, USA) through a 200 nm or 50 nm diameter pore-size polycarbonate (PC) membrane for 15 times.

Conjugation of ssDNA to the nanocompartments

400 μL of 4 mg/ml azido-vesicles (45 μM azide moieties), corresponding to the sample P5- N_3 , was mixed with dibenzocyclooctyl-terminated DNA oligonucleotide (DBCO-ssDNAa, 45 μM , 1 equivalent per azide moiety) in PBS buffer at 37 °C for 0.5, 2, 3, 4.5 and 10 days. The sequences of all presented DNA oligonucleotides are supplied in supplementary Table S2. The unreacted DBCO-ssDNA was removed by size exclusion chromatography (Sephacrose 2B column; 10 cm length). The yield of the reaction was determined based on the concentration of unreacted DBCO-ssDNAa measured by the UV absorbance at 260 nm (Figure S3). The conjugation of DBCO-ssDNAb to the azido-vesicles (45 μM azide moieties) was performed following the above procedure and the reaction was carried out for 3 days.

400 μL of 4 mg/ml azido-vesicles with lower amount of azide moieties (9 μM and 1.8 μM), P1 and P0.25, were mixed with DBCO-ssDNAa/DBCO-ssDNAb (18 μM and 7.2 μM) at 37 °C for 3 days, respectively. The purification was carried out as mentioned above.

Agarose electrophoresis analysis

Electrophoresis analysis was carried out using 5% agarose gel at 170 V for 34 mins, using TAE buffer as running buffer. The gels were stained with SYBR Gold nucleic acid gel staining (Invitrogen) and scanned by Gel Doc™ EZ Imager (BIO-RAD).

Fluorescence correlation spectroscopy (FCS)

FCS measurements were performed on a confocal laser scanning microscope (Zeiss LSM 510-META/Confocor2, Carl Zeiss, Jena, Germany). An Ar+ laser was used for 488 nm wavelength, a HeNe laser for 543 nm and a HeNe laser for 633 nm. The laser light was focused through a 40x C-Apochromat water immersion objective with a numeric aperture of 1.2 onto the sample and using the appropriate filter sets depending on the wavelength used. The fluorescent signal was recorded on an avalanche photodiode (APD). For each measurement and each fluorescent probe, the pinhole was calibrated for maximum count rate using free dye in PBS.

The sample volumes were typically 5 µL. Fluorescent fluctuations over time were recorded for 30 x 10 s. The raw data was processed and analysed using ConfoCor3 software. Autocorrelation curves were fitted by using a two-component model (equation 1). The diffusion times obtained for free atto550-ssDNAa and atto550-ssDNAa hybridized polymersomes were fixed in the fitting procedure.

$$G_{2comp}(\tau) = 1 + \frac{1}{N} \cdot \left(1 + \frac{T_{trip}}{1-T_{trip}} e^{-\frac{\tau}{\tau_{trip}}} \right) \cdot \left[\frac{f_1}{\left(1 + \frac{\tau}{\tau_{D1}}\right) \left(1 + \frac{\tau}{S^2 \tau_{D1}}\right)^{1/2}} + \frac{f_2}{\left(1 + \frac{\tau}{\tau_{D2}}\right) \left(1 + \frac{\tau}{S^2 \tau_{D2}}\right)^{1/2}} \right] \quad (1)$$

Where $G_{2comp}(\tau)$ is the two-component autocorrelation function, N is the number of particles, S the structural parameter, T_{trip} is the fraction of fluorophores in the triplet state, τ_{trip} is the corresponding triplet time, f_1 and f_2 are the fraction of the particles of the corresponding component 1 or 2, τ_{D1} and τ_{D2} are the diffusion times of the corresponding component 1 or 2.

5.5. References

- [1] Mirkin CA, Letsinger RL, Mucic RC, Storhoff JJ. A DNA-based method for rationally assembling nanoparticles into macroscopic materials. *Nature*. 1996;382:607-9.
- [2] Cutler JI, Auyeung E, Mirkin CA. Spherical nucleic acids. *Journal of the American Chemical Society*. 2012;134:1376-91.
- [3] Choi CHJ, Hao L, Narayan SP, Auyeung E, Mirkin CA. Mechanism for the endocytosis of spherical nucleic acid nanoparticle conjugates. *Proceedings of the National Academy of Sciences*. 2013;110:7625-30.
- [4] Giljohann DA, Seferos DS, Patel PC, Millstone JE, Rosi NL, Mirkin CA. Oligonucleotide loading determines cellular uptake of DNA-modified gold nanoparticles. *Nano Letters*. 2007;7:3818-21.
- [5] Prigodich AE, Alhasan AH, Mirkin CA. Selective enhancement of nucleases by polyvalent DNA-functionalized gold nanoparticles. *Journal of the American Chemical Society*. 2011;133:2120-3.
- [6] Seferos DS, Prigodich AE, Giljohann DA, Patel PC, Mirkin CA. Polyvalent DNA nanoparticle conjugates stabilize nucleic acids. *Nano Letters*. 2008;9:308-11.
- [7] Rush AM, Thompson MP, Tatro ET, Gianneschi NC. Nuclease-resistant DNA via high-density packing in polymeric micellar nanoparticle coronas. *ACS Nano*. 2013;7:1379-87.
- [8] Zheng D, Giljohann DA, Chen DL, Massich MD, Wang X-Q, Iordanov H, et al. Topical delivery of siRNA-based spherical nucleic acid nanoparticle conjugates for gene regulation. *Proceedings of the National Academy of Sciences*. 2012;109:11975-80.
- [9] Medley CD, Smith JE, Tang Z, Wu Y, Bamrungsap S, Tan W. Gold nanoparticle-based colorimetric assay for the direct detection of cancerous cells. *Analytical Chemistry*. 2008;80:1067-72.
- [10] Song Y, Xu X, MacRenaris KW, Zhang X-Q, Mirkin CA, Meade TJ. Multimodal gadolinium-enriched DNA-gold nanoparticle conjugates for cellular imaging. *Angewandte Chemie International Edition*. 2009;48:9143-7.
- [11] Banga RJ, Chernyak N, Narayan SP, Nguyen ST, Mirkin CA. Liposomal spherical nucleic acids. *Journal of the American Chemical Society*. 2014;136:9866-9.
- [12] Park SY, Lytton-Jean AKR, Lee B, Weigand S, Schatz GC, Mirkin CA. DNA-programmable nanoparticle crystallization. *Nature*. 2008;451:553-6.
- [13] Nykypanchuk D, Maye MM, van der Lelie D, Gang O. DNA-guided crystallization of colloidal nanoparticles. *Nature*. 2008;451:549-52.
- [14] Auyeung E, Li TING, Senesi AJ, Schmucker AL, Pals BC, de la Cruz MO, et al. DNA-mediated nanoparticle crystallization into Wulff polyhedra. *Nature*. 2014;505:73-7.
- [15] Cheng W, Campolongo MJ, Cha JJ, Tan SJ, Umbach CC, Muller DA, et al. Free-standing nanoparticle superlattice sheets controlled by DNA. *Nat Materials*. 2009;8:519-25.
- [16] Macfarlane RJ, Lee B, Jones MR, Harris N, Schatz GC, Mirkin CA. Nanoparticle superlattice engineering with DNA. *Science*. 2011;334:204-8.
- [17] Tan SJ, Campolongo MJ, Luo D, Cheng W. Building plasmonic nanostructures with DNA. *Nat Nanotechnology*. 2011;6:268-76.
- [18] Zhang C, Macfarlane RJ, Young KL, Choi CHJ, Hao L, Auyeung E, et al. A general approach to DNA-programmable atom equivalents. *Nat Materials*. 2013;12:741-6.
- [19] Lee JS, Feijen J. Polymersomes for drug delivery: Design, formation and characterization. *Journal of Controlled Release*. 2012;161:473-83.

- [20] Peters RJRW, Marguet M, Marais S, Fraaije MW, van Hest JCM, Lecommandoux S. Cascade reactions in multicompartimentalized polymersomes. *Angewandte Chemie International Edition*. 2014;53:146-50.
- [21] Onaca O, Enea R, Hughes DW, Meier W. Stimuli-responsive polymersomes as nanocarriers for drug and gene delivery. *Macromolecular bioscience*. 2009;9:129-39.
- [22] Wu D, Spulber M, Itef F, Chami M, Pfohl T, Palivan CG, et al. Effect of molecular parameters on the architecture and membrane properties of 3D assemblies of amphiphilic copolymers. *Macromolecules*. 2014;47:5060-9.
- [23] Itef F, Chami M, Najer A, Lörcher S, Wu D, Dinu IA, et al. Molecular organization and dynamics in polymersome membranes: A lateral diffusion study. *Macromolecules*. 2014;47:7588-96.
- [24] Alemdaroglu FE, Ding K, Berger R, Herrmann A. DNA-templated synthesis in three dimensions: introducing a micellar scaffold for organic reactions. *Angewandte Chemie International Edition*. 2006;45:4206-10.
- [25] Schnitzler T, Herrmann A. DNA block copolymers: functional materials for nanoscience and biomedicine. *Accounts of Chemical Research*. 2012;45:1419-30.
- [26] Rodríguez-Pulido A, Kondrachuk AI, Prusty DK, Gao J, Loi MA, Herrmann A. Light-triggered sequence-specific cargo release from DNA block copolymer–lipid vesicles. *Angewandte Chemie International Edition*. 2013;125:1042-6.
- [27] Alemdaroglu FE, Alemdaroglu NC, Langguth P, Herrmann A. DNA block copolymer micelles – a combinatorial tool for cancer nanotechnology. *Advanced Materials*. 2008;20:899-902.
- [28] Cottenye N, Syga M-I, Nosov S, Muller AHE, Ploux L, Vebert-Nardin C. Biological-like vesicular structures self-assembled from DNA-block copolymers. *Chemical Communications*. 2012;48:2615-7.
- [29] Beales PA, Vanderlick TK. Specific Binding of Different Vesicle Populations by the Hybridization of Membrane-Anchored DNA[†]. *The Journal of Physical Chemistry A*. 2007;111:12372-80.

6. Spatially organizing polymersomes into multicompartmental systems

6.1. Introduction

The evolution of single or multicellular organisms benefited from the formation of membrane boundaries, separating life processes from non-living matter. The isolated compartments separated by intracellular membranes, called organelles, ensure not only the specificity, but also the efficiency of multiple reactions for each individual organelle to maintain all of the cell's metabolism.[1] Mimicking the biological processes to design artificial cells and/or organelles is essential for synthetic biology and therapeutic/diagnostic applications.[2-7] Several outstanding achievements related to artificial cells/organelles have previously been reported. Artificial cells or organelles based on lipid or polymer vesicles were endowed with cell-like functions, such as transport,[8] molecule synthesis,[9] self-replication,[10] signaling,[11] or energy production,[6] and were used as implants to compensate for defects in cellular functions. In most cases, artificial organelles are synthesized via 'one-pot' processes leading to vesicles capable of performing the basic function as the natural ones.[12] In the case of artificial cells the design approach is more complicated due to compartmentalization that represents the basic requirement for multi-step reaction process systems. The most common method to achieve compartmentalization is to encapsulate small vesicles into larger ones.[3, 13] However, organelles in living cells often have their characteristic positions and spatial connections for molecular transport, such as proteins and lipids, to maintain and fulfill their functions.[14] Therefore, spatial organization and arrangement of compartments with different functions in a defined order is of great significance for mimicking the organization and metabolic pathway of living cells, even though it hasn't been achieved yet so far.

Bottom-up nanofabrication is an indispensable approach to position and organize diverse components into complex structures at the nanoscale level.[15, 16] Its realization is based on molecular recognition of individual building blocks (molecules, nanoparticles, or self-assembled structures) as found in nature.[15-18] Through the appropriate design of the molecular information stored in the building blocks, which determines the specificity, robustness, and stimuli-responsiveness of the interactions,

direct and programmable control of the assembly process with minimal defects can be achieved.[19-21] DNA is the top choice for this target due to its unique molecular recognition properties, high information storage capacity, structural features, and ease of manipulation.[20-23] Building blocks with hollow structures are more promising for nanofabrication, because they are able to accommodate active entities (such as enzymes, DNA, etc)[24-26] to create hybrid systems with novel functions. Moreover, they are suitable to mimic cells and organelles, to replicate biological functions and/or processes.[10, 12, 27] Protein cages, such as ferritin and some bacteriophages have been used for nanofabrication,[28-30] but they act more as templates than as building blocks due to their smaller size, leading to low encapsulation efficiency of specific molecules.[31] Lipid-based vesicular structures (liposomes) represent better candidates for nanofabrication, because they can be manipulated to have a certain size,[32] entrapment of active molecules,[33] and permeability (controlled by surface modification or by insertion of membrane proteins)[34]. Liposomes have been functionalized with DNA[35] or peptides[36] to induce aggregation by molecular recognition. Nevertheless, the aggregation scale is hard to control[35] and the stability of the structures is reduced due to membrane fusion occurring during the aggregation process.[36-38]

In the previous chapter, we described the construction of DNA functionalized polymersomes. Here, we applied DNA as the algorithm to regulate the course of self-organization of binary polymersomes (two distinct polymeric vesicles) to construct compartmentalized structures with spatial organization and connection. Polymersomes supply a robust and shielded encapsulation of active entities, while DNA is capable of controlling the spatial organization and distance between compartments due to the rigid nature of double-helix DNA (< 50 nm).[39] Opposed to aggregated lipid-based systems, the self-assembly scale can be modulated by tailoring the attractive forces between the DNA complementary strands and the repulsive steric and hydration forces between polymer chains in proximity. The size of the polymersomes, as the second algorithm, plays an important role in their assembly behavior and spatial organization due to the modulation of repulsive forces. In addition, the presence of DNA on polymer networks is expected to facilitate cellular uptake, promoting their *in-vitro* applications. The

polymeric compartmentalized network system described in this work offers a new perspective into the evolution from unitary to binary systems, with collective properties greater than the individual building blocks, which serve as a platform for the generation of novel, multi-functional, intelligent and complex systems and biodevices.

6.2. Results and discussions

6.2.1. Controllable self-assembly of DNA-functionalized polymeric nanocompartments

After the functionalization of polymersomes with ssDNA, the potential to assemble the polymersomes into a network using DNA recognition was explored. The nanocompartments with complementary DNA strands were mixed in equal mass ratio. The formation of double-stranded DNA (dsDNA) resulted in an increase in particle size, which was monitored by DLS (Figure 6-1c,d). All the polymersomes with different σ value (average surface coverage density of ssDNA) undergo a rapid assembly based on the DNA recognition, and the network expands in time till reaching equilibrium. The D_H of particles increased from 190 ± 60 nm (P5-ssDNAa alone) to 290 ± 90 nm (P5-ssDNAa-P5-ssDNAb network) (Figure 6-1c). TEM images reveal the initiation and at equilibrium of the polymersome networks after 20 min and 6 h (Figure 6-1a,b). The formed networks were composed, in general, of 3 polymersomes, counted from TEM images. The small D_H of the polymersome network compared to the expected value from aggregation number is due to the deformation and spatial rearrangement of polymersomes induced by the strong DNA interaction as observed in cryo-TEM images (Figure 6-2), which reveal the real structure of linked polymersomes in solution. Interestingly, the neutral liposomes (100 nm in diameter) with 39 single stranded DNAs (ssDNA) per polymersome and an σ value similar with the one of P5-ssDNAa or P5-ssDNAb (P5-ssDNAa/b), showed a continuous aggregation until precipitating from solution.[35] The distinct behavior of the polymersome assemblies compared with neutral liposomes is caused by the strong steric repulsion between polymer chains when in proximity of each other, hindering DNA hybridization. This strategy has been used to control the assembly of DNA-modified gold nanoparticles by grafting polymers on the surface.[40] The size of polymer network at equilibrium decreases with the σ value of polymersomes due to the weakening of attractive forces.

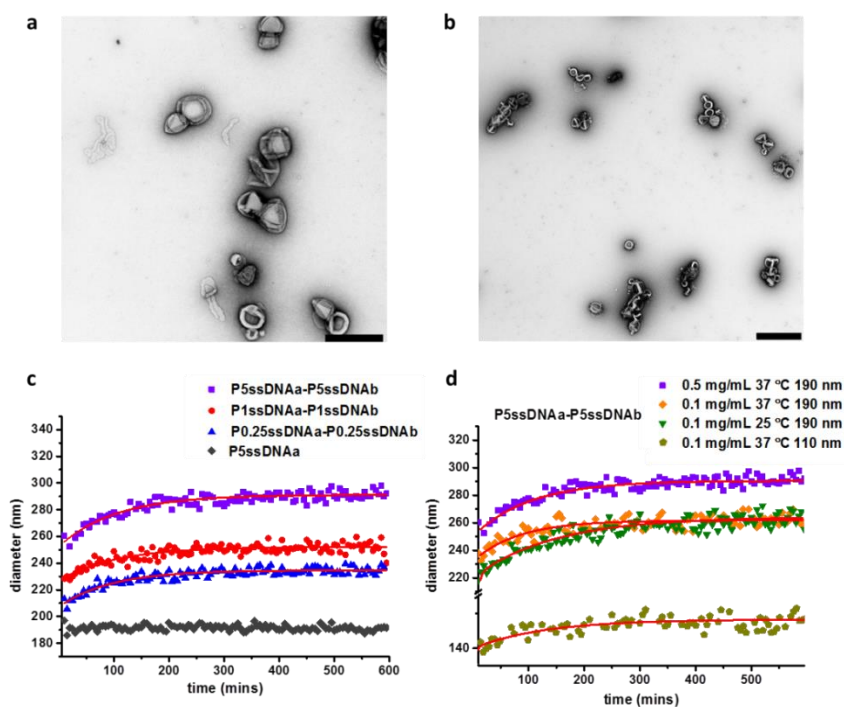


Figure 6-1. Self-assembly of DNA-functionalized polymersomes into network. The networking of polymersomes was monitored by TEM after 20 mins (a) and 6 hs (b). The scale bars are 500 nm and 1000 nm, respectively. The influence of σ value to the assembly process was investigated by recording the size change as a function of the time by DLS (c). P5ssDNAa-P5ssDNAb network was chosen as the model system for the evaluation of the influence of concentration, temperature and polymersome size to the polymersome assembly (d).

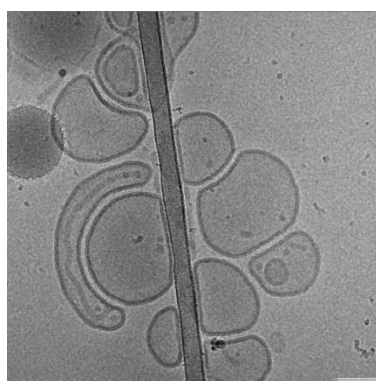


Figure 6-2. Cryo-TEM image of polymersome network (P5-ssDNAa-P5-ssDNAb). The scale bar is 100 nm.

The time course of polymersome assembly was well described by a double-exponential function ($y = A_1(1 - e^{-k_1t}) + A_2(1 - e^{-k_2t})$) with a fast k_1 and a slow k_2 rate constants (Table

6-1), indicating two different periods existing in the assembly process. k_1 corresponds to the rate constant for the initial period of the assembly, when ssDNA is free on the polymersome's surface and the attractive force generated by the complementary ssDNAs is dominant. Both internal (σ value and size) and external factors (concentration and temperature) decide the k_1 value. Increasing the σ value of polymersomes from P0.25-ssDNAa/b to P5-ssDNAa/b induced an increase of the k_2 value from $5.0 \pm 0.1 \text{ s}^{-1}$ to $10.0 \pm 0.1 \text{ s}^{-1}$ due to the rising of dsDNA duplex formation. By decreasing the polymersome diameter from 190 nm to 110 nm for P5-ssDNAa/b, k_1 value dropped from $5.0 \pm 0.1 \text{ s}^{-1}$ to $0.3 \pm 0.1 \text{ s}^{-1}$, even though the σ value was the same. The reduction of contact area between small polymersomes is the reason for a decreased number of ssDNA available for the dsDNA duplex formation. Lowering the concentration of polymers from 0.5 mg/mL to 0.1 mg/mL led to a decrease of both k_1 and the aggregation size at equilibrium, while temperature influenced only the k_1 , but not the aggregation size. When the assembly entered the later period, a much lower rate constant of k_2 was generated due to the reduction of the available number of ssDNA for hybridization. k_2 didn't show a significant correlation with σ value, size, concentration, and temperature.

Table 6-1. Rate constants for the growth of polymersome network.

	$k_1 \text{ (s}^{-1}\text{)}$	$k_2 \text{ (10}^{-3} \text{ s}^{-1}\text{)}$
P5-ssDNAa-P5-ssDNAb, 0.5 mg/mL, 37 °C, 190 nm	10.0 ± 0.1	9.7 ± 0.8
P1-ssDNAa-P1-ssDNAb, 0.5 mg/mL, 37 °C, 190 nm	5.0 ± 0.1	9.6 ± 1.2
P0.25-ssDNAa-P0.25-ssDNAb, 0.5 mg/mL, 37 °C, 190 nm	5.0 ± 0.1	10.7 ± 1.0
P5-ssDNAa-P5-ssDNAb, 0.1 mg/mL, 37 °C, 190 nm	10.0 ± 0.1	10.6 ± 1.5
P5-ssDNAa-P5-ssDNAb, 0.1 mg/mL, 25 °C, 190 nm	0.4 ± 0.4	6.1 ± 0.7
P5-ssDNAa-P5-ssDNAb, 0.1 mg/mL, 37 °C, 110 nm	0.3 ± 0.1	7.8 ± 1.3

6.2.2. Spatial organization of DNA-functionalized polymeric nanocompartments

In general, the organization of nanoparticles into nano-objects and nanomaterials is templated by various molecules or structures, which determines the sequence and spatial distance between individual blocks and the final geometrical structure.[17, 41]

Elaborate modulation of interparticle forces is possible to direct the assembly of nanoparticles,[42] while achieving well-defined spatial organization for individual blocks is still challenging. First, we tried to control the size of nanocompartments and aimed to regulate the assembled architectures dominated by the steric and repulsion forces generated by DNA-functionalized polymersomes.

In order to investigate the influence of the size of polymersomes to their spatial organization, P5-ssDNAa/b were prepared with a diameter of either 230 ± 60 nm or 90 ± 20 nm (determined by TEM). Atto488 and dy633 dyes were encapsulated in P5-ssDNAb and P5-ssDNAa (P5-ssDNAb-atto488, P5-ssDNAa-dy633) for the visualization. Two distinct spatial organizations were observed by TEM and CLSM, based on the size combinations of polymersomes (Figure 6-3). An almost linear arrangement was obtained when 230 nm complementary polymersomes were mixed (Figure 6-3b,c). However, when nonequivalent sized polymersomes were combined, several 90 nm polymersomes hybridized onto the surface of each 230 nm polymersome resulting in a “satellite structure”, observed by TEM, CLSM (Figure 6-3d,e) and cryo-TEM (Figure 6-4). The diverse structures resulted by the different combination of various sized polymersomes is due to the effect of steric hinderance and charge repulsion between proximate polymersomes. Larger repulsion force generated between linked 230 nm polymersomes, causing them to distribute further apart. This leads to the reduction of available space for binding and results in a linear-like structure. Multiple small polymersomes can bind the surface of the large polymersome without being close enough in proximity to increase the repulsive energy. In addition, the electrostatic repulsive forces generated by the small polymersomes resulted in large separations between individual satellite structures, increasing the stability of multicompartmental structures. No large aggregation was observed by DLS for both linear-like and satellite-like structures (Figure 6-5).

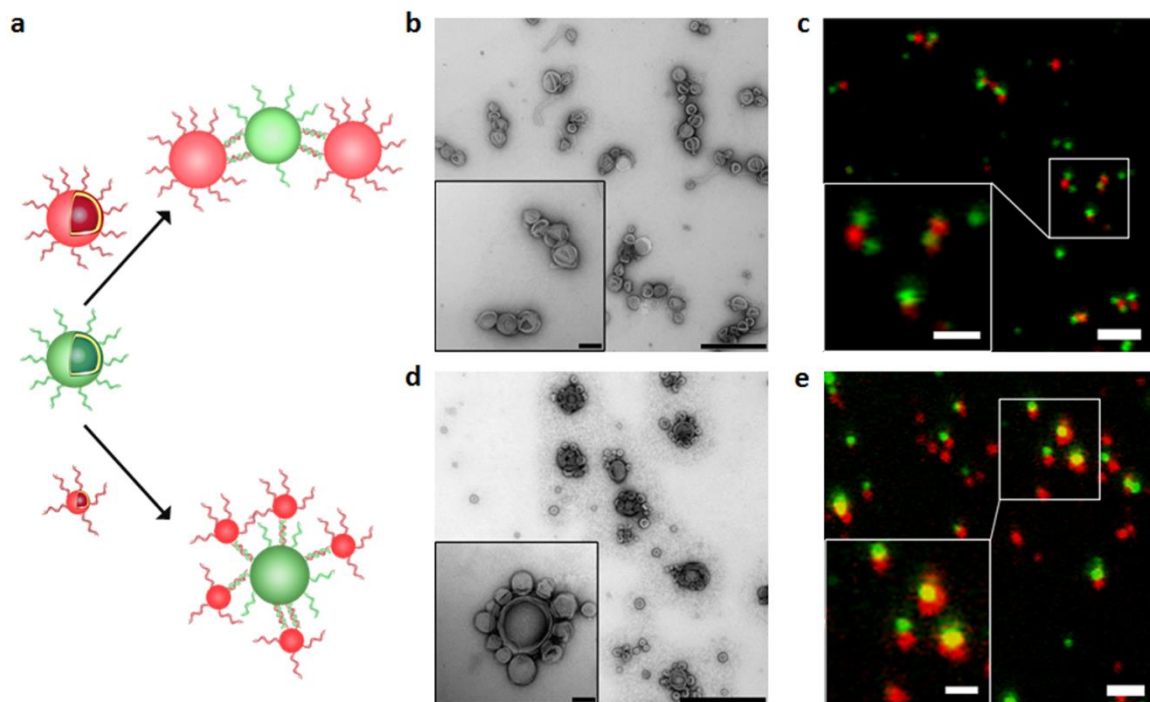


Figure 6-3. Self-organization of DNA-functionalized polymeric nanocompartments directed by the size of polymersomes. (a) Schematic presentation of distinct spatial organizations directed by the size of the polymersomes. TEM and CLSM images of linear structure (b and c) and satellite structure (d and e) self-organized by polymersomes. The scale bar for b image is 1000 nm, inset - 200 nm, for c - 2000 nm, inset -1000 nm, for d - 1000 nm, inset - 100 nm and for e - 2000 nm, inset - 1000 nm.

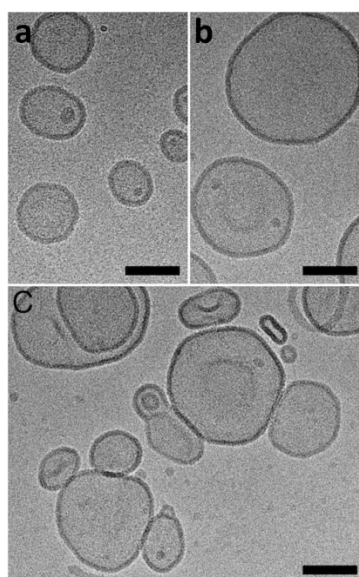


Figure 6-4. Cryo-TEM images of small polymersomes (a), big polymersomes (b) and the formed satellite-like structures.

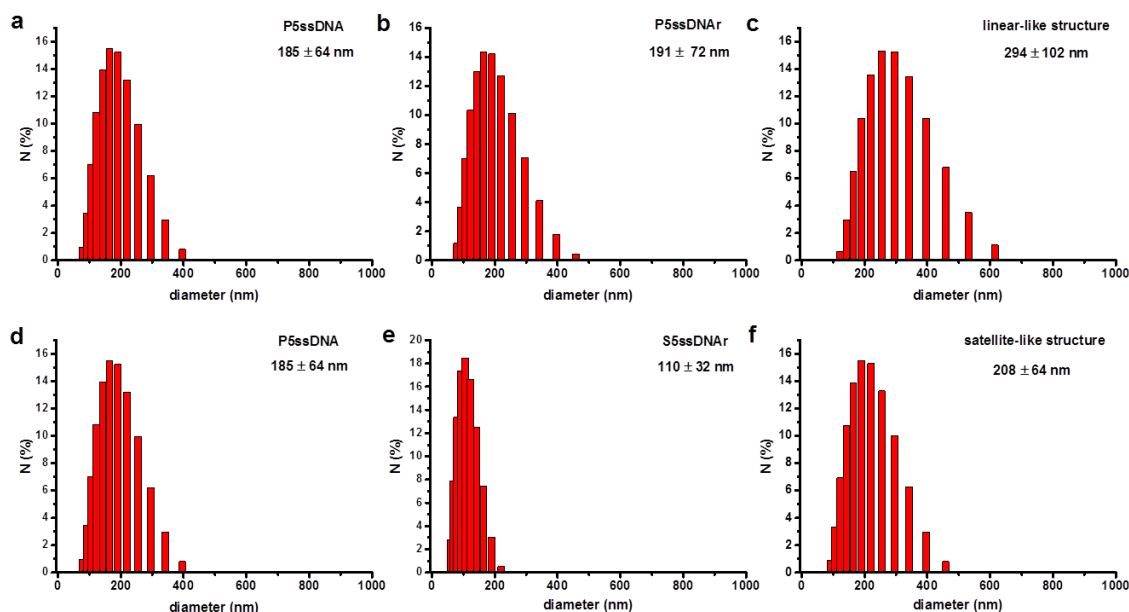


Figure 6-5. Size distribution of linear-like structures (c) assembled by equivalent sized polymersomes (a, b) and satellite-like structures (f) assembled by larger polymersomes and smaller ones (d, e).

In addition, we tried to control the spatial distance between compartments by the length of DNA on the polymersomes. P5 was modified with complimentary sequences of either 22 or 44 nucleotides and used for the construction of polymersome networks. Cryo-TEM was performed for the determination of the spatial distance between polymersomes (Figure 6-6). Cryo-TEM images showed polymersomes interacting via a gap with constant distance, corresponding to the formed dsDNA between polymersomes. The black spots between two connecting membranes are due to the phosphorous of DNA molecules, which have a stronger contrast.[43] The deformation of the membranes indicates a strong interaction between polymersomes.

The distances between polymersomes sustained by 22mer dsDNA and 44mer dsDNA were determined as 8 ± 2 nm and 14 ± 2 nm by the analysis of cryo-TEM images (Figure 6-6), which are slightly different with the theoretical values of 7.5 nm and 15 nm, respectively. These results suggest that the actual distance between polymersomes is not only decided by the length of DNA, but also influenced by interparticle forces. When polymersomes are located close to each other, repulsive forces including electrostatic, steric, and hydration repulsions dominate, and resulted in a larger distance compared with the theatrical value. In contrast, when the polymersomes are separated by a larger

distance, the influence of repulsive forces decreased. The observed lower distance compared with the theoretical dsDNA length can be due to the compression from polymersomes.

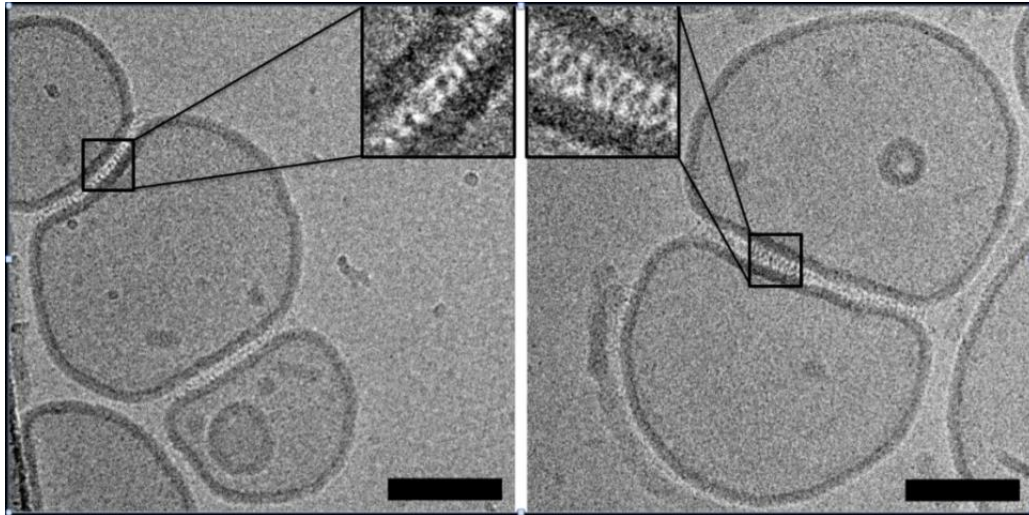


Figure 6-6. Cryo-TEM images of polymersome networks sustained by 22mer (left) and 44mer (right) dsDNA. The scale bar is 100 nm.

In addition, intact polymersomes observed by cryo-TEM suggests that no membrane fusion occurs during the networking of polymersomes. To prove it, we probed the mixing of the aqueous vesicles content and leakage by employing a conventional membrane fusion assay using sulforhodamine B (SRB). In brief, 25 mM SRB was encapsulated in one vesicle population and PBS buffer alone was used for another vesicle population. SRB is self-quenched at 25 mM. Membrane fusion or the leakage of polymersomes leads to a decrease of SRB's concentration, which can be observed by an increase of the fluorescence. As shown in Figure 6-7, no increase of the fluorescence was observed after polymersome networking after 5 days, suggesting polymersomes are highly stable during the assembly process.

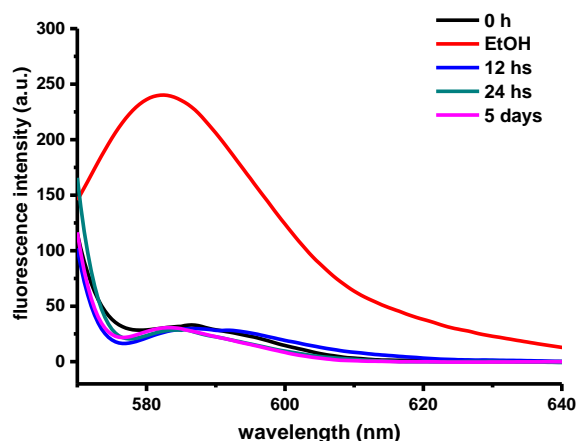


Figure 6-7. Fluorescence spectroscopy of SRB encapsulated polymersomes after networking.

6.2.3. Cellular internalization of polymersome network

The 3D arrangement of DNA on spherical inorganic nanoparticles[44] and liposomes[45] was reported to significantly promote their cellular uptake due to the extracellular protein association on the particle surface,[46] inducing endocytosis.[47, 48] To examine the cellular uptake efficiency of DNA functionalized polymersomes and the polymersome network, a series of investigations were performed.

First, the toxicity of P5 functionalized with complementary ssDNA strands and the formed polymer network was evaluated by a MTS assay in U87 glioblastoma cells (Figure 6-8). Minimal in vitro cytotoxicity was observed for both P5-ssDNAa/b and polymersome networks after 24 h. This agrees with the reported lack in toxicity of PMOXA-*b*-PDMS-*b*-PMOXA-based copolymers with different block lengths, as studied in various cell lines.[12, 49]

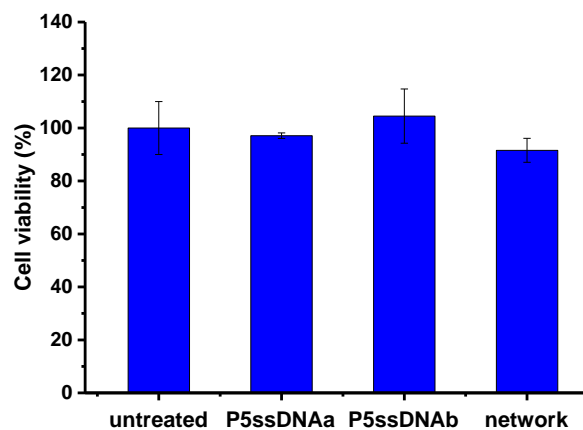


Figure 6-8. Cellular toxicity evaluation of 80 $\mu\text{g/ml}$ DNA functionalized polymersomes and polymersome network on U87 cells using MTS assay. Errors bars represent the standard deviation ($n=3$).

Second, the stability of polymersome networks in cell media and in PBS as a control was assessed by DLS and FCS (Figure 6-9a, Table 6-2). After 24h of incubation, no significant difference in the size was observed by either technique, suggesting that the polymersome networks remain intact in cell culture media. This result was confirmed by TEM (Figure 6-9b).

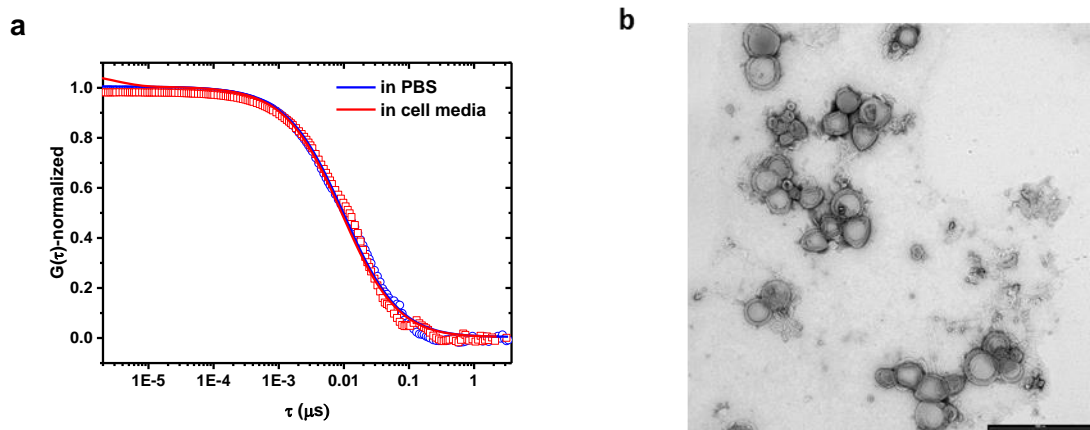


Figure 6-9. a) Normalized autocorrelation curves from FCS data: polymersome network formed by P5-ssDNAa/b in PBS (blue) and in cell media (red) after incubating for 24 h at 37 $^{\circ}\text{C}$; b) TEM image of polymersome network formed by P5-ssDNAa/b in cell media after incubating for 24 h at 37 $^{\circ}\text{C}$.

Table 6-2. D_H of polymersome network formed by P5-ssDNAa/b. The samples were incubated in PBS or cell media for 24 h at 37 °C before measurements.

	D_H (nm, FCS)	D_H (nm, DLS)
In PBS	330 ± 30	250 ± 120
in cell media	310 ± 70	290 ± 100

Typically, high density of DNA on the surface of nanostructures is required to ensure the efficient cellular uptake.[44] The surface coverage of DNA on the presented polymersomes is much lower than for other reported systems.[46, 50] In order to examine the cellular uptake efficiency of DNA-functionalized polymersomes with different σ values (180 nm in diameter), dy633 encapsulated polymersomes were prepared. The extent of uptake of individual DNA functionalized polymersomes was measured by flow cytometry (Figure 6-10).

After incubation of 40 $\mu\text{g/ml}$ naked polymersomes (P0) and DNA-functionalized polymersomes (P0.25-ssDNAb, P1-ssDNAb and P5-ssDNAb) with U87 cells for 24 h, flow cytometry revealed that the cellular internalization of polymersomes is highly dependent on their σ values. The cells treated with P0 showed low uptake efficiency. Functionalization of polymersomes with DNA for the case of P0.25-ssDNAb (σ : $0.1 \times 10^{-3} \text{ nm}^{-2}$) did not increase the uptake efficiency compared with P0. However, ~6-fold increase in fluorescent intensity for the case of P1-ssDNAb with σ value of $0.3 \times 10^{-3} \text{ nm}^{-2}$ was observed compared with P0. Increasing the σ value to $0.9 \times 10^{-3} \text{ nm}^{-2}$ for P5-ssDNAb did not further enhance the cellular uptake. These results suggest that a low DNA surface coverage (σ : $0.3 \times 10^{-3} \text{ nm}^{-2}$) is sufficient to benefit the cellular uptake of nanostructures.

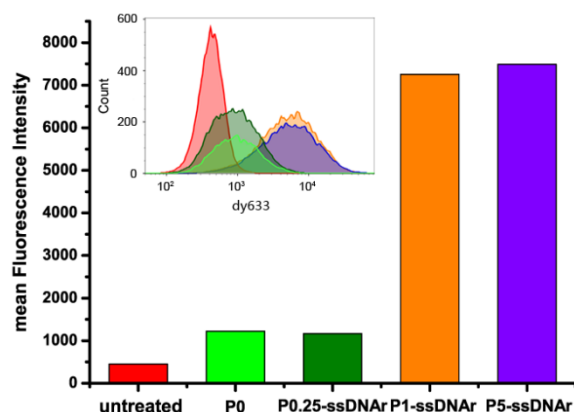


Figure 6-10. Flow cytometry results of U87 cells treated with naked polymersomes and DNA-functionalized polymersomes with different σ values, using untreated U87 cells as a control.

In the next step, the cellular internalization of polymersome networks formed by P5-ssDNAa/b was assessed by CLSM (Figure 6-11). P5-ssDNAa-dy633 and P5-ssDNAb-atto488 were used for these experiments. Different combinations of polymersomes were added to the U87 cells and incubated for 24h. Low cellular internalization was observed for the mixture of P0-dy633 and P0-atto488 polymersomes (data not shown). Atto488 and dy633 contained polymersomes functionalized with ssDNA strands showed significantly higher uptake compared to P0. The confocal images of polymersome networks show internalization of both P5-ssDNAa-dy633 and P5-ssDNAb-atto488 (Figure 6-11c, red and green channels) inside the cell cytoplasm with their evident colocalization. In contrast, polymersomes functionalized with non-complementary strands were randomly distributed and no evident colocalization was observed (Figure 6-11b). As a control P5ssDNAa-dy633 were mixed with P0-atto488 and incubated with cells resulting in significant uptake of P5ssDNAa-dy633 compared to P0-atto488 as shown in Figure 6-11a. Flow cytometry confirmed the results obtained from CLSM (data not shown).

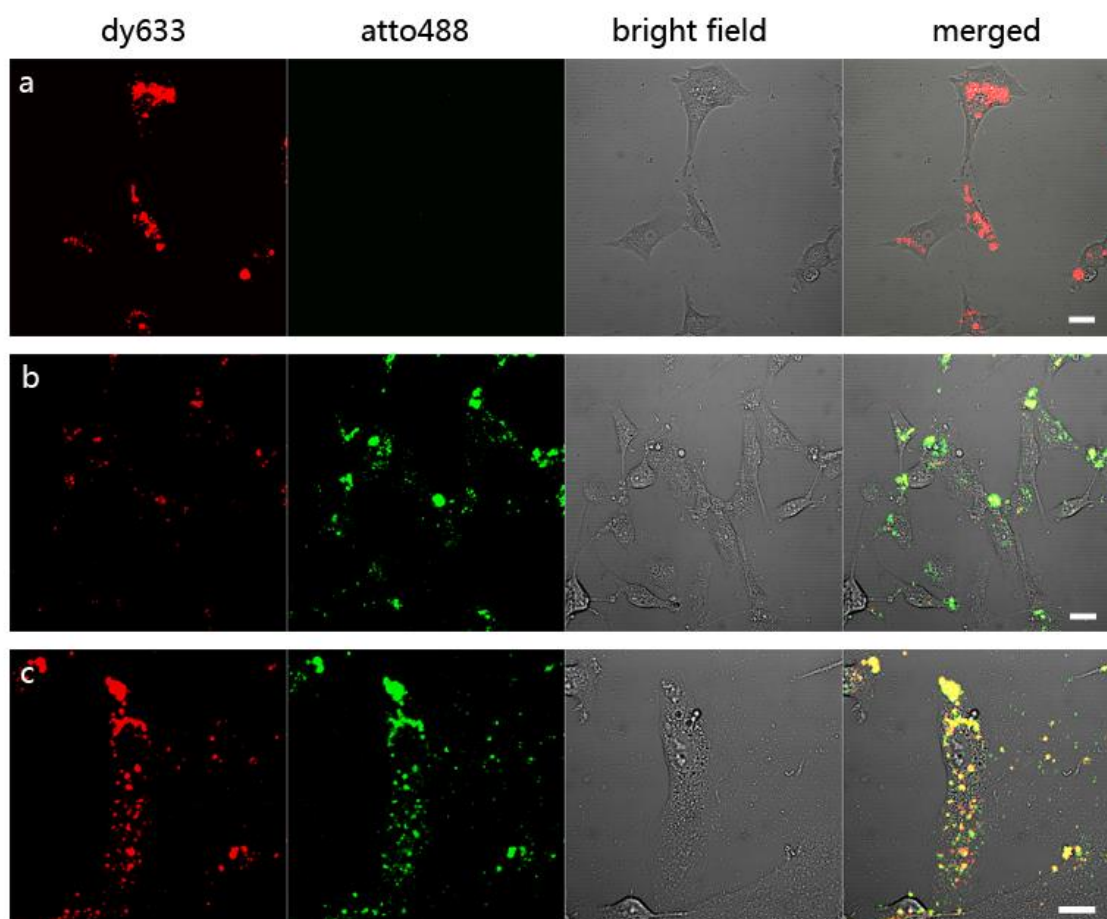


Figure 6-11. CLSM images of U87 cells incubated with a) P5ssDNAa-dy633 and P0-atto488, b) P5ssDNAa-dy633 and P5ssDNAa-atto488, c) P5ssDNAa-dy633 and P5ssDNAb-atto488 (scale bar = 20 μm).

6.3. Conclusion

We described, for the first time, polymersome networks formed by DNA hybridization. The kinetics and the self-assembly scale of polymersomes can be well controlled by both internal (σ value and size) and external factors (concentration and temperature). Spatial organization of polymersomes into linear- or satellite-like structures has been achieved by combining different sized polymersomes. The spatial distance between compartments was modulated as well by controlling the length of ssDNA on polymersomes.

The presented polymersome network is highly promising for the fabrication of novel multi-functional, intelligent, and complex nanosystems because it supplies isolated multicompartments for individual active molecules with defined connections. In addition,

polymersome networks exhibit high cellular uptake abilities and stability, promoting their *in-vitro* applications.

6.4. Experimental section

Materials

atto488 and dy633 were purchased from ATTO-TEC GmbH and Dyomics GmbH, respectively. 3-(4,5-dimethylthiazol-2-yl)-5-(3-carboxymethoxyphenyl)-2-(4-sulfophenyl)-2H-tetrazolium was purchased from Promega, USA.

Preparation of DNA-functionalized polymeric nanocompartments

Polymersomes was prepared as described previously. In order to encapsulate fluorescent probes in the vesicles, atto488 and DY-633 (2 mM in 1 mL PBS buffer) individually, were added for film rehydration. Non-encapsulated fluorescent dyes were separated from the encapsulated ones by size exclusion chromatography (Sephacrose 2B column; 37 cm length).

The functionalization of polymersomes with ssDNA was performed as described previously. The sequences for 44mer ssDNAa and 44mer ssDNAb are 5'-CCT CGC TCT GCT AAT CCT GTT ACC TCG CTC TGC TAA TCC TGT TA-3' and 5'-TAA CAG GAT TAG CAG AGC GAG GTA ACA GGA TTA GCA GAG CGA GG-3', respectively.

Kinetic analysis of vesicle assembly

The measurements of D_H of nanostructures were performed on a Zetasizer Nano ZSP (Malvern Instruments Ltd., UK) at 20 °C. The investigation of the kinetic of vesicle assembly was carried out by recoding the D_H of particles as a function of time at 20°C and 37 °C. Then, D_H of the nanostructures were plotted as a function of time by OriginPro 9.1G and the data was fitted by double-exponential function as shown in eq. 1,2.

$$y = y_0 + A_1 \left(1 - e^{-\frac{x}{t_1}}\right) + A_2 \left(1 - e^{-\frac{x}{t_2}}\right) \quad (1)$$

$$k_1 = \frac{1}{t_1} \quad k_2 = 1/t_2 \quad (2)$$

y_0 is the average D_H of P5-ssDNAa and P5-ssDNAb. A_1 and A_2 are the corresponding number of traces. t_1 and t_2 represents the dwell times. k_1 and k_2 are the rate constant.

FCS and CLSM

FCS measurements were performed on a confocal laser scanning microscope (Zeiss LSM 510-META/Confocor2, Carl Zeiss, Jena, Germany). An Ar+ laser was used for 488 nm wavelength, and a HeNe laser for 633 nm. The laser light was focused through a 40x C-Apochromat water immersion objective with a numeric aperture of 1.2 onto the sample and using the appropriate filter sets depending on the wavelength used. The fluorescent signal was recorded on an avalanche photodiode (APD). For each measurement and each fluorescent probe, the pinhole was calibrated for maximum count rate using free dye in PBS.

The sample volumes were 5 μ L. Fluorescent fluctuations over time were recorded for 10 x 10 s. The raw data was processed and analysed using ConfoCor3 software. Autocorrelation curves were fitted by using a two-component model (equation 1). The diffusion times obtained for free dyes (atto488 and dy633) were fixed in the fitting procedure.

$$G_{2comp}(\tau) = 1 + \frac{1}{N} \cdot \left(1 + \frac{T_{trip}}{1-T_{trip}} e^{-\frac{\tau}{\tau_{trip}}} \right) \cdot \left[\frac{f_1}{\left(\left(1 + \frac{\tau}{\tau_{D1}} \right) \left(1 + \frac{\tau}{S^2 \tau_{D1}} \right) \right)^{1/2}} + \frac{f_2}{\left(\left(1 + \frac{\tau}{\tau_{D2}} \right) \left(1 + \frac{\tau}{S^2 \tau_{D2}} \right) \right)^{1/2}} \right] \quad (1)$$

Where $G_{2comp}(\tau)$ is the two-component autocorrelation function, N is the number of particles, S the structural parameter, T_{trip} is the fraction of fluorophores in the triplet state, τ_{trip} is the corresponding triplet time, f_1 and f_2 are the fraction of the particles of the corresponding component 1 or 2, τ_{D1} and τ_{D2} are the diffusion times of the corresponding component 1 or 2.

CLSM experiments were performed on a confocal laser scanning microscope (Zeiss LSM 510-META/Confocor2, Carl Zeiss, Jena, Germany). For atto488 and dy633 containing polymersomes, a Argon-2 laser with $\lambda = 488$ nm (15 mW output), and a He-Ne laser with $\lambda = 633$ nm (15 mW output) was used. The laser output intensity was adjusted by changing the transmission in order to keep the laser intensity low. A main dichromatic beam splitter (HFT 488/543/633), a secondary dichroic beam splitter (NFT 545) and a low pass filter (LP 505) were used for 488 nm laser and a low pass filter (LP 650) in case

of the 633 laser. The light was focused on the sample using a C-Apochromat 40x water immersion objective (NA=1.2).

Cell culture

U87 glioblastoma cells were maintained at 37 °C in a 5% CO₂ humidified atmosphere and were grown in DMEM with 10% FBS, 100 units/mL penicillin, 100 µg/mL streptomycin and 2 mM L-glutamine.

Cell viability assay

Cytotoxicity testing was performed using the Promega CellTiter 96 AQueous Non-Radioactive Cell Proliferation MTS assay to determine the number of viable cells in culture. 10⁴ U87 cells were cultured in a 96-well plate for 24 h prior to the experiment. P5-ssDNAa/b and polymersome networks (10 µl of 0.8 mg/ml) were added to the cells and incubated for 24h at 37°C with 5% CO₂. Next, a MTS mixture (20 µL/well) was added to the cells and then incubated for 3 h. Cell viability was calculated by measuring the absorbance at 490 nm using a 96-well plate reader (Spectramax). Two internal controls were set up for each experiment: cells alone and medium alone. Background absorbance due to the non-specific reaction between test compounds and the MTS reagent was deducted from exposed cell values. Each experiment was performed in triplicate.

Cellular uptake

Freshly trypsinized U87 cells (3x10⁴ cells in 300 µL cell culture medium) were seeded into 8-wells chamber 24h prior to the experiment. The cell culture medium was replaced with a cell culture medium without serum (130 µL) followed by addition of the polymer-DNA conjugates prepared as described above (20 µl of 0.2 mg/ml). After 4h incubation, the cell culture medium was carefully removed and replaced with serum-containing medium (300 µL). The cells were incubated for 20 hs more. Right before live cell imaging, the cell culture medium was replaced with an Opti-MEM. The imaging was performed on Zeiss LSM 510-META/Confocor2, Carl Zeiss, Jena, Germany. Images were taken using a 40x water-immersion objective. Excitations were at 488 nm and 633 nm for atto488 and dy633, respectively. Images were taken with the same acquisition settings for comparison purpose.

Flow cytometry analysis

The U87 cells (10^5 cells/well) were plated into 24-well tissue culture plates 24 hours prior to treatment and subsequent flow cytometry analysis. After an overnight incubation, the cell culture medium was replaced with serum-free medium (0.44 mL) and the polymer-DNA conjugates prepared as described above (57 μ l of 0.35 mg/ml), were added. After 4h incubation, the serum-free medium was carefully removed and replaced with 1 ml of medium containing 10% FBS. The cells were then let to grow 20h more in the incubator. The cells were then trypsinized with 200 μ l of trypsin for 10 minutes at 37 °C and 5% CO₂. Following trypsinization, 800 μ l PBS was added to the cells, gently mixed by pipetting and transferred in 1.5 mL microcentrifuge tubes. Cells were then pelleted by centrifugation at 300 RCF for five minutes. Subsequently, the media was aspirated and the pellet was resuspended in 200 μ l cold PBS and put on ice until flow cytometry analysis. Cells were vortexed gently immediately prior to flow cytometry analysis. Flow cytometry analyses were carried out using a Canto II flow cytometer.

6.5. References

- [1] Lodish H, Berk A, Zipursky SL, Matsudaira P, Baltimore D, Darnell J. *Organelles of the Eukaryotic Cell*. 2000.
- [2] Miller D, Booth PJ, Seddon JM, Templer RH, Law RV, Woscholski R, et al. *Procell design through modular compartmentalization* 2013.
- [3] Peters RJRW, Marguet M, Marais S, Fraaije MW, van Hest JCM, Lecommandoux S. *Cascade Reactions in Multicompartmentalized Polymersomes*. *Angewandte Chemie International Edition*. 2014;53:146-50.
- [4] Pohorille A, Deamer D. *Artificial cells: prospects for biotechnology*. *Trends in Biotechnology*. 2002;20:123-8.
- [5] Chang TMS. *Therapeutic applications of polymeric artificial cells*. *Nat Rev Drug Discov*. 2005;4:221-35.
- [6] Choi H-J, Montemagno CD. *Artificial Organelle: ATP Synthesis from Cellular Mimetic Polymersomes*. *Nano Letters*. 2005;5:2538-42.
- [7] Ben-Haim N, Broz P, Marsch S, Meier W, Hunziker P. *Cell-Specific Integration of Artificial Organelles Based on Functionalized Polymer Vesicles*. *Nano Letters*. 2008;8:1368-73.
- [8] Kumar M, Grzelakowski M, Zilles J, Clark M, Meier W. *Highly permeable polymeric membranes based on the incorporation of the functional water channel protein Aquaporin Z*. *Proceedings of the National Academy of Sciences*. 2007;104:20719-24.
- [9] Langowska K, Palivan CG, Meier W. *Polymer nanoreactors shown to produce and release antibiotics locally*. *Chemical Communications*. 2013;49:128-30.
- [10] Kurihara K, Tamura M, Shohda K-i, Toyota T, Suzuki K, Sugawara T. *Self-reproduction of supramolecular giant vesicles combined with the amplification of encapsulated DNA*. *Nat Chem*. 2011;3:775-81.
- [11] Charalambous K, Booth PJ, Woscholski R, Seddon JM, Templer RH, Law RV, et al. *Engineering de Novo Membrane-Mediated Protein-Protein Communication Networks*. *Journal of the American Chemical Society*. 2012;134:5746-9.
- [12] Tanner P, Balasubramanian V, Palivan CG. *Aiding Nature's Organelles: Artificial Peroxisomes Play Their Role*. *Nano Letters*. 2013;13:2875-83.
- [13] Fu Z, Ochsner MA, de Hoog H-PM, Tomczak N, Nallani M. *Multicompartmentalized polymersomes for selective encapsulation of biomacromolecules*. *Chemical Communications*. 2011;47:2862-4.
- [14] Alberts B, Johnson A, Lewis J, Raff M, Roberts K, Walter P. *The compartmentalization of cells*. 2002.
- [15] Ozin GA, Hou K, Lotsch BV, Cademartiri L, Puzzo DP, Scotognella F, et al. *Nanofabrication by self-assembly*. *Materials Today*. 2009;12:12-23.
- [16] Zhang S. *Fabrication of novel biomaterials through molecular self-assembly*. *Nat Biotech*. 2003;21:1171-8.
- [17] Grzelczak M, Vermant J, Furst EM, Liz-Marzán LM. *Directed Self-Assembly of Nanoparticles*. *ACS Nano*. 2010;4:3591-605.
- [18] Mann S. *Self-assembly and transformation of hybrid nano-objects and nanostructures under equilibrium and non-equilibrium conditions*. *Nat Mater*. 2009;8:781-92.
- [19] Lehn J-M. *Toward Self-Organization and Complex Matter*. *Science*. 2002;295:2400-3.
- [20] Nykypanchuk D, Maye MM, van der Lelie D, Gang O. *DNA-guided crystallization of colloidal nanoparticles*. *Nature*. 2008;451:549-52.

- [21] Park SY, Lytton-Jean AKR, Lee B, Weigand S, Schatz GC, Mirkin CA. DNA-programmable nanoparticle crystallization. *Nature*. 2008;451:553-6.
- [22] Li H, Carter JD, LaBean TH. Nanofabrication by DNA self-assembly. *Materials Today*. 2009;12:24-32.
- [23] Zhang C, Macfarlane RJ, Young KL, Choi CHJ, Hao L, Auyeung E, et al. A general approach to DNA-programmable atom equivalents. *Nat Mater*. 2013;12:741-6.
- [24] Tanner P, Baumann P, Enea R, Onaca O, Palivan C, Meier W. Polymeric Vesicles: From Drug Carriers to Nanoreactors and Artificial Organelles. *Accounts of Chemical Research*. 2011;44:1039-49.
- [25] Vriezema DM, Garcia PML, Sancho Oltra N, Hatzakis NS, Kuiper SM, Nolte RJM, et al. Positional Assembly of Enzymes in Polymersome Nanoreactors for Cascade Reactions. *Angewandte Chemie*. 2007;119:7522-6.
- [26] Oberholzer T, Albrizio M, Luisi PL. Polymerase chain reaction in liposomes. *Chemistry & Biology*. 1995;2:677-82.
- [27] Schoffelen S, van Hest JCM. Multi-enzyme systems: bringing enzymes together in vitro. *Soft Matter*. 2012;8:1736-46.
- [28] Lee LA, Niu Z, Wang Q. Viruses and virus-like protein assemblies—Chemically programmable nanoscale building blocks. *Nano Res*. 2009;2:349-64.
- [29] Uchida M, Klem MT, Allen M, Suci P, Flenniken M, Gillitzer E, et al. Biological Containers: Protein Cages as Multifunctional Nanoplatfoms. *Advanced Materials*. 2007;19:1025-42.
- [30] Flenniken ML, Uchida M, Liepold LO, Kang S, Young MJ, Douglas T. A Library of Protein Cage Architectures as Nanomaterials. In: Manchester M, Steinmetz N, editors. *Viruses and Nanotechnology*: Springer Berlin Heidelberg; 2009. p. 71-93.
- [31] Jutz G, Böker A. Bionanoparticles as functional macromolecular building blocks – A new class of nanomaterials. *Polymer*. 2011;52:211-32.
- [32] Olson F, Hunt CA, Szoka FC, Vail WJ, Papahadjopoulos D. Preparation of liposomes of defined size distribution by extrusion through polycarbonate membranes. *Biochimica et Biophysica Acta (BBA) - Biomembranes*. 1979;557:9-23.
- [33] Lian T, Ho RJY. Trends and developments in liposome drug delivery systems. *Journal of Pharmaceutical Sciences*. 2001;90:667-80.
- [34] Rigaud J-L, Pitard B, Levy D. Reconstitution of membrane proteins into liposomes: application to energy-transducing membrane proteins. *Biochimica et Biophysica Acta (BBA) - Bioenergetics*. 1995;1231:223-46.
- [35] Beales PA, Vanderlick TK. Specific Binding of Different Vesicle Populations by the Hybridization of Membrane-Anchored DNA[†]. *The Journal of Physical Chemistry A*. 2007;111:12372-80.
- [36] Versluis F, Voskuhl J, van Kolck B, Zope H, Bremmer M, Albrechtse T, et al. In Situ Modification of Plain Liposomes with Lipidated Coiled Coil Forming Peptides Induces Membrane Fusion. *Journal of the American Chemical Society*. 2013;135:8057-62.
- [37] Kuvichkin V, Danev R, Shigematsu H, Nagayama K. DNA-Induced Aggregation and Fusion of Phosphatidylcholine Liposomes in the Presence of Multivalent Cations Observed by the Cryo-TEM Technique. *J Membrane Biol*. 2009;227:95-103.
- [38] Stengel G, Zahn R, Höök F. DNA-Induced Programmable Fusion of Phospholipid Vesicles. *Journal of the American Chemical Society*. 2007;129:9584-5.
- [39] Stein IH, Schüller V, Böhm P, Tinnefeld P, Liedl T. Single-Molecule FRET Ruler Based on Rigid DNA Origami Blocks. *ChemPhysChem*. 2011;12:689-95.

- [40] Valignat M-P, Theodoly O, Crocker JC, Russel WB, Chaikin PM. Reversible self-assembly and directed assembly of DNA-linked micrometer-sized colloids. *Proceedings of the National Academy of Sciences of the United States of America*. 2005;102:4225-9.
- [41] Le JD, Pinto Y, Seeman NC, Musier-Forsyth K, Taton TA, Kiehl RA. DNA-Templated Self-Assembly of Metallic Nanocomponent Arrays on a Surface. *Nano Letters*. 2004;4:2343-7.
- [42] Groschel AH, Walther A, Lobling TI, Schacher FH, Schmalz H, Muller AHE. Guided hierarchical co-assembly of soft patchy nanoparticles. *Nature*. 2013;503:247-51.
- [43] Li S-Y, Millstone J, Mirkin C, Dravid V. Detection of Phosphorus in Biological Samples with Analytical Electron Microscopy. *Microscopy and Microanalysis*. 2007;13:456-7.
- [44] Cutler JI, Auyeung E, Mirkin CA. Spherical Nucleic Acids. *Journal of the American Chemical Society*. 2012;134:1376-91.
- [45] Banga RJ, Chernyak N, Narayan SP, Nguyen ST, Mirkin CA. Liposomal Spherical Nucleic Acids. *Journal of the American Chemical Society*. 2014;136:9866-9.
- [46] Giljohann DA, Seferos DS, Patel PC, Millstone JE, Rosi NL, Mirkin CA. Oligonucleotide Loading Determines Cellular Uptake of DNA-Modified Gold Nanoparticles. *Nano Letters*. 2007;7:3818-21.
- [47] Wu XA, Choi CHJ, Zhang C, Hao L, Mirkin CA. Intracellular Fate of Spherical Nucleic Acid Nanoparticle Conjugates. *Journal of the American Chemical Society*. 2014;136:7726-33.
- [48] Choi CHJ, Hao L, Narayan SP, Auyeung E, Mirkin CA. Mechanism for the endocytosis of spherical nucleic acid nanoparticle conjugates. *Proceedings of the National Academy of Sciences*. 2013;110:7625-30.
- [49] Najer A, Wu D, Bieri A, Brand F, Palivan CG, Beck H-P, et al. Nanomimics of Host Cell Membranes Block Invasion and Expose Invasive Malaria Parasites. *ACS Nano*. 2014;8:12560-71.
- [50] Maye MM, Nykypanchuk D, van der Lelie D, Gang O. DNA-Regulated Micro- and Nanoparticle Assembly. *Small*. 2007;3:1678-82.
- [51] Stoneham CA, Hollinshead M, Hajitou A. Clathrin-mediated Endocytosis and Subsequent Endo-Lysosomal Trafficking of Adeno-associated Virus/Phage. *Journal of Biological Chemistry*. 2012;287:35849-59.

7. Summary and perspectives

Hybrid nanosystems advance the developments of biochemistry, polymer chemistry and material science. Intelligent organization of diverse materials together brings the opportunities to combine all their properties and design new nanomaterials for as many as possible applications, such as diagnostic or therapeutic agents, sensing devices or nanotechnology.

In this thesis, we described two hybrid nanosystems constructed by molecular recognition. First, we designed and synthesized novel trisNTA functionalized polymers for the binding of His-tagged molecules through the specific interaction between trisNTA-Me²⁺ and His₆. PNT copolymers were used as models to mimic the complex targeting configuration in nature, and to investigate the correlation between geometric limitation and binding capacity in details. PNT copolymers exhibited many advantages for protein delivery. They site-specifically bound to multiple His-tagged protein per chain without the requirements for any modifications, and rapidly released the bound proteins in acid conditions. Low toxicity and no obvious influence to the properties of proteins were observed.

In the second system, we designed and constructed multicompartmental systems self-organized by binary polymersomes. The self-organization was achieved by the hybridization of ssDNA on the surface of polymersomes. The combination of different sized polymersomes resulted in linear-like or satellite-like structures. The length of ssDNA on the surface of polymersomes controlled the spatial distance between compartments. In addition, the multicompartmental systems exhibited high cellular uptake and stability.

Afterward, these two hybrid nanosystems are expected to be promising in many interdisciplinary applications at the border between different research areas and technologies. PNT copolymers are able to combine various His-tagged proteins into one nanosystem with controllable distances, useful for the study of protein-protein interactions, protein synergy, as well as combination therapy. The design and the construction of polymeric multicompartmental systems with specific spatial organization will be promisingly used for complex nanobiomaterials.

8. Acknowledgements

First of all, I want to thank Prof. Wolfgang Meier for the opportunity to perform my work from the Ph.D. thesis in his group, under his supervision. I appreciate his patience, trust and freedom of mind he offered me during my time in Basel. I am much obliged to Prof. Cornelia Palivan for her supervision and help during this time. I admire her passion, her attitude and dedication toward work.

I thank my co-referee, Prof. Dr. Corinne Nardin (University Geneva) for accepting to be my co referee and for all her time invested in my thesis.

I affectionately thank my husband, Dr. Dalin Wu for all the support he gave to me. He is also my main collaborator and spent many hours working on various polymer synthesis and modification.

I cordially thank Dr. Mariana Spulber for all her efforts during our scientific collaboration in the group and not only, beyond that in our private lives.

I thank Dr. Viktoriia Postupalenko for all her help and fruitful discussions, especially for her involvement in all the cell experiments presented in this thesis.

Many thanks go to Samuel Lörcher and Fabian Itel for their participation and fruitful discussions. I am much obliged to Dr. Mohamed Chami for the amazing Cryo-TEM images. I also thank Dr. Jason Duskey and Ian Rouse for their dedication in the correction of this thesis.

I am grateful to all present and former colleagues, Adrian Najer, Patric Baumann, Dr. Gesine Gunkel-Grabole, Tomaz Einfalt, Justyna Kowal, Dr. Martin Nussbaumer, Martin Rother, Dr. Vimalkumar Balasubramanian and Dr. Dominik Dobrunz for their friendly help and discussions. Especially, I want to thank Dr. Karolina Langowska and Sven Kasper for the efficient organization and management of the chemistry laboratories.

Last but not the least, I'm grateful for the scholarship from CMC (China Scholarship Council) and the supports from my families and friends.

9. Curriculum Vitae, List of Contributions

Personal Information

Name: Juan Liu

Date of Birth: 15.02.1985

Private Address: Ryffstrasse 22, 4056 Basel

Phone Number: +41 (0)76 61 78 395

E-Mail: juan.liu@unibas.ch



Hobbies: Dancing, listening to music, play musical instruments and cooking

Education

10/2010-present: **University of Basel, Department of Chemistry, Switzerland**

- PhD in Polymer Chemistry and Physics

09/2007-07/2010: **Zhengzhou University, School of Material Science and Engineering, China**

- Master in Materials Science

04/2009-04/2010: **Institute of Materials Science and Technology, Nagaoka University of Technology, Japan**

- Guest Master Student in Polymer Chemistry

09/2003-07/2007: **Zhengzhou University, School of Material Science and Engineering, China**

- Bachelor in Polymer Science and Engineering

Research Experience

09/2010-present: **Scientific Associate** with Prof. Dr. Wolfgang Meier and Prof. Dr. Cornelia Palivan.

- Synthesis of poly (N-isopropylacrylamide-co-tris-nitrilotriacetic acid acrylamide) and combined study of the influence of molecular recognition and distance constraints in protein binding and interactions; Evaluate their applications as nanocarriers for protein delivery.
- Fabricate polyersome networks by specific DNA recognition.

09/2007-07/2010: **Scientific Associate** with Prof. Kobayashi Takaomi in Japan.

- Preparation and development of conducting polymer membranes based on polyfuran.

Spring/2007: **Scientific Associate** with Prof. Hongying Wang in China.

- Synthesis and characterization of molecular imprinted copolymer membranes for uracil recognition.

Skills and additional information

Polymer synthesis chemistry: living free-radical polymerization and polymer functionalization.

DNA chemistry: DNA reactions with small molecules, polymers and nano particles, DNA hybridization, DNA ligation, DNA polymerization, PCR, DNA characterization.

Cell biology experience: expression, purification and characterization of proteins, bacterial cell culture, protein labelling.

Polymer and nanoparticle characterization techniques: nuclear magnetic resonance (NMR), MALDI-TOF-MS, gel permeation chromatography, fourier transform infrared spectroscopy, UV-Vis spectroscopy, fluorometer, zeta-potential, electrophoresis, transmission electron microscopy, fluorescence correlation spectroscopy, dynamic light scattering and static light scattering.

Management skills: As one of the executive members of Chinese Association of Materials Science and Technology in Switzerland, scheme, organize and actualize different academic and social activities.

Languages: English –fluent, Japanese-mediate, Chinese- native

Communication skills: Scientific writing, conference presentation, scientific reports and proposal writing.

IT skills: Microsoft Office, Origin, EndNote, Photoshop, ChemBioDraw, SciFinder, Reaxys, OmniSEC, MestReNove, LSM image browser and ALV/Static & Dynamic FIT.

Publications

- **Juan Liu**, Mariana Spulber, Dalin Wu, Renee M. Talom, Cornelia G. Palivan*, Wolfgang Meier*. Poly (N-isopropylacrylamide-co-tris-nitrilotriacetic acid acrylamide) for a combined study of molecular recognition and distance constraints in protein binding and interactions. *J. Am. Chem. Soc.* , 2014, 136, 12607.
- **Juan Liu**, Viktoriia Postupalenko, Dalin Wu, Mariana Spulber, Cornelia G. Palivan*, Wolfgang Meier*. A single polymer chain as a nanocarrier for multiple proteins delivery with regulated pH responsibility. In preparation.
- **Juan Liu**, Dalin Wu, Viktoriia Postupalenko, Mariana Spulber, Samuel Lörcher, Fabian IteI, Cornelia G. Palivan*, Wolfgang Meier*. Fabrication of binary polymersome networks by DNA recognition. In preparation.
- Mariana Spulber; Patric Baumnn; **Juan Liu**; Cornelia G. Palivan*. Ceria loaded nanoreactors: a nontoxic superantioxidant system with high stability and efficacy. *Nanoscale*, 2015, 7, 1411.

- Ozana Onaca-Fischer; **Juan Liu**; Mark Inglin; Cornelia G. Palivan*. Polymeric Nanocarriers and Nanoreactors: A Survey of Possible Therapeutic Applications. *Curr. Pharm. Des.* , 2012, 18, 2622.

10. Abbreviations

α RlgG-biotin	biotinylated goat antirabbit immunoglobulin
ΔH°	standard enthalpy change
ΔS°	standard entropy change
τ_D	diffusion time
ϵ	extinction coefficient
σ	average surface coverage density
ABPs	amphiphilic block polymers
ADPCs	amphiphilic DNA–polymer conjugates
AIBN	azobisisobutyronitrile
APD	avalanche photodiode
AqpZ	water-channel protein Aquaporin Z
ATP	adenosine triphosphate
ATRP	atom transfer radical polymerization
APD	avalanche photodiode
BME	2-mercaptoethanol
bp	base pairs
BSA	bovine serum albumin
CB[8]	macrocyclic cucurbit[8]uril
CCMV	cowpea Chlorotic Mottle Virus
CD	circular dichroism
cmc	critical micelle concentration
DMEM	Dulbecco's modified eagle medium
CpG	controlled pore glass
CPM	counts per molecule
Cryo-TEM	cryogenic transmission electron microscopy
D	diameter
DBCO	dibenzocyclooctyl group
DCC	<i>N,N'</i> -dicyclohexylcarbodiimide
DCM	dichloromethane
D_H	hydrodynamic diameter
DIC	<i>N,N'</i> -diisopropylcarbodiimide
DIPEA	<i>N,N'</i> -Diisopropylethylamine
DLS	dynamic light scattering
DMF	dimethylformamide
DNA- <i>b</i> -PEG	DNA- <i>block</i> -poly (ethylene glycol)
DNA- <i>b</i> -PPO	DNA- <i>block</i> -polypropylene
ds	double-stranded
Dox	doxorubicin

DPCs	DNA-polymer conjugates
dsDNA	double-stranded DNA
DTT	dithiothreitol
EDC	1-ethyl-3-(3-dimethylaminopropyl) carbodiimide
EDTA	ethylenediaminetetraacetic acid
EPR	electron paramagnetic resonance
EPR effect	enhanced permeability and retention effect
ESI-MS	electrospray ionisation mass spectrometry
FBS	fetal bovine serum
FCS	fluorescent correlation spectroscopy
FDA	Food and Drug Administration
FITC-His ₆	fluorescein-labeled His ₆
FPLC	fast protein liquid chromatography
FTIR	fourier transform infrared spectroscopy
F-Type ATPase	ATP synthase
GAPDH	endogenous glyceraldehyde 3-phosphate dehydrogenase
GPC	gel permeation chromatography
His ₆	His tag
His ₆ -eGFP	his-tagged enhanced green fluorescent protein
His ₆ -eYFP	his-tagged enhanced yellow fluorescent protein
His ₆ -ColG	his-tagged collagenase G
HoBt	1-hydroxybenzotriazole hydrate
IDA	iminodiacetic acid
ITC	isothermal titration calorimetry
IgG	immunoglobulin G
k_1	fast rate constant
k_2	slow rate constant
K_D	dissociation constant
LNA	locked nucleic acid
LPA	nanoparticles Locked nucleic acid-polymer nanoparticles
LPO	lactoperoxidase
Me ²⁺	metal cations
MTS	3-(4,5-dimethylthiazol-2-yl)-5-(3-carboxymethoxyphenyl)-2-(4-sulfophenyl)-2H-tetrazolium
MV7	viologen
MW	molecular weight

NCS	neocarzinostatin
NHS	N-hydroxysuccinimide
NIPAM	N-isopropylacrylamide
Np8	naphthalene
NTA	nitrilotriacetic acid
NTA-Me ⁿ⁺	metal-coordinated nitrilotriacetic acid
ODNs	oligonucleotides
OmpF	outer membrane protein F
PB	poly (butadiene)
PBS buffer	phosphate buffered saline
PC	pore&size polycarbonate
PCR	polymerase chain reaction
PDIs	polydispersities
PEG	poly(ethyleneglycol)
PEG- <i>b</i> -PPO- <i>b</i> -PEG	poly(polyethylene glycol)- <i>block</i> -poly (propylene)- <i>block</i> -poly(ethylene glycol)
PEGMA	poly(ethylene glycol) methyl ether methacrylate
PEI	polyethylenimine
PEO	poly (ethylene oxide)
PGA	poly(glutamic acid)
PHPMA	poly(<i>N</i> -(2-hydroxypropyl)methacrylamide)
PIB	poly (isobutylene)
pK _a	acid dissociation constant
PMOXA- <i>b</i> -PDMS- <i>b</i> -PMOXA	poly(2-methyloxazoline)- <i>block</i> -poly(dimethylsiloxane)- <i>block</i> -poly(2-methyloxazoline)
PNTs	poly (N-isopropylacrylamide- <i>co</i> -tris-nitrilotriacetic acid acrylamide)s
PolyNIPAM	poly(N-isopropylacrylamide)
PNTs	poly (N-isopropylacrylamide- <i>co</i> -tris-nitrilotriacetic acid acrylamide)s polymers
prot-trisNTA	<i>tert</i> -butyl ester protected tris-nitrilotriacetic acid acrylate

PS	polystyrene
RAFT	reversible addition–fragmentation chain-transfer
RB-His ₆	rhodamine B-labelled His ₆
RT	room temperature
SMA	styrene-co-maleic anhydride
SNAs	spherical nucleic acids
SRB-His ₆	sulforhodamine B labelled His ₆
SOD	superoxide dismutase
ssDNA	single stranded DNA
ssDNAa	5'-CCT CGC TCT GCT AAT CCT GTT A-3'
ssDNAb	5'-TAA CAG GAT TAG CAG AGC GAG G-3'
TEM	transmission electron microscopy
TdT	terminal deoxynucleotidyl transferase
TNF- α	tumor necrosis factor- α
TRAIL	tumor necrosis factor-related apoptosis inducing ligand
Tris-HCl	tris hydrochloride
trisNTA	tris-nitrilotriacetic acid